2008

Solid-state NMR studies of the interactions between cationic membrane peptides and lipid bilayers

Ming Tang
Iowa State University

Solid-state NMR studies of the interactions between cationic membrane peptides and lipid bilayers

by

Ming Tang

A dissertation submitted to the graduate faculty

in partial fulfillment of the requirements for the degree of

DOCTOR OF PHILOSOPHY

Major: Chemistry

Program of Study Committee:
Mei Hong, Major Professor
Klaus Schmidt-Rohr
Victor Lin
Nicola Pohl
Edward Yu

Iowa State University

Ames, Iowa

2008

Table of Contents

Acknowledgement

I am sincerely grateful to all those who have guided me and supported me through the last five amazing years. The person I would like to thank most is my major professor Dr. Mei Hong. She is an excellent mentor who teaches me the knowledge about solid-state NMR and supports my PhD studies. She makes me realize that solid-state NMR is such a wonderful tool that I would pursue my academic career with it. I hope our scientific discussion and collaboration continue in future.

I would like to thank Prof. Klaus Schmidt-Rohr for his enlightening lectures and insightful discussion. I also want to thank my colleagues: Dr. Rajeswari Mani, Wenbin Luo, Sarah Cady, Tim Doherty, Dr. Evgenii Levin, Dr. Aditya Rawal, Dr. Qiang Chen, Xiaowen Fang, Yongchao Su, Yuan Zhang, Xueqian Kong, Yanyan Hu. They give me tremendous help and provide such a good working environment. The works in my thesis cannot be done without the peptides provided by our collaborators, Dr. Alan Waring and Dr. Robert Lehrer in University of California in Los Angeles. I want to express my deep appreciation to them. I would like to thank Prof. Victor Lin, Prof. Nicola Pohl, Prof. Yeon-Kyun Shin and Prof. Edward Yu for serving on my Program of Study committee. I am very thankful to Prof. James Espenson and Prof. Keith Woo for their instructions on my work as a teaching assistant. I also want to thank the department office, especially Renee, Beverly, Carlene, Nancy and Carolyn for their continuous help. My life in Ames would not be fun without all the friends I met here. I appreciate their help and advice.

The special person I want to thank is my wife Po Hu. She has given me so much joy and marvelous support. She makes my life in Ames full of delight and warmth. I owe her a lot of thanks for her care and patience. I would like to thank my family, especially my mother, for their unconditional love and considerateness. To them I sincerely dedicate this thesis.

Abstract

Solid-state NMR is a powerful and versatile spectroscopic method for analyzing the sophisticated structure of biological systems, especially the non-crystalline and insoluble systems that are difficult for solution NMR and X-ray diffraction to study. In this thesis, we used solid-state NMR to elucidate the structures of complex systems, such as peptide aggregates, and membrane peptides in oriented and unoriented lipid bilayers. Various NMR techniques have been used to study the peptide-peptide and peptide-lipid interactions, which have a great influence on the topology of these systems.

The peptides we are interested in are antimicrobial peptides (AMP), which can kill microbes at micromolar concentration by disrupting the microbial cell membrane. These peptides usually contain cationic residues and have an amphipathic structure. Understanding the peptide-peptide and peptide-lipid interactions will shed light on the antimicrobial mechanism of AMP. To determine the oligomeric structure of the aggregates of an antimicrobial beta-hairpin peptide, Protegrin-1 (PG-1), we used 2D ^{1}H-driven ^{13}C spin diffusion and other correlation methods. We found that PG-1 aggregates in a parallel fashion with like strands lining the intermolecular interface. In an oriented membrane system, we applied a method for determining the orientation of β-sheet membrane peptides using 2D separated local-field spectroscopy. Retrocyclin-2, an antibacterial and antiviral β-hairpin peptide, was found to adopt a transmembrane orientation in short-chain lipids (DLPC) and a more in-plane orientation in long-chain lipids (POPC), which indicates that the membrane thickness affects the peptide orientation. In unoriented membrane systems, we utilized a variety of methods under magic-angle spinning (MAS), such as ^{13}C{^{31}P} REDOR, ^{13}C DIPSHIFT, LGCP and ^{1}H spin diffusion, to study the interaction of PG-1 with lipid bilayers. The experimental results led to the toroidal pore model as the mechanism of action of PG-1. Moreover, we found that the guanidinium-phosphate complexation is the driving force for pore formation. Both ionic interaction and hydrogen-bonding play a significant role in stabilizing the guanidinium-phosphate complex, because altering either one of the two factors would affect the antimicrobial activity and membrane topology of PG-1 dramatically. By mutating the Arg sidechain with methylation, we showed that without sufficient hydrogen-bonding, the mutant adopts an in-plane orientation and undergoes fast uniaxially rotation.

Chapter 1

Introduction

1.1 Antimicrobial Peptides

Antimicrobial peptides are small polypeptides (usually containing less than 50 amino acids) found in animals and plants, which possess potent and broad-spectrum antimicrobial activity. They can kill a wide range of microbes, such as bacteria, fungi, viruses and protozoa, thus these peptides serve multicellular organisms as advanced protective weapons against unicellular organisms. Unlike antibiotics produced or isolated from microbial sources, which are categorized by common chemical structure [1], antimicrobial peptides have such a great diversity that they can only be categorized generally based on their secondary structures. For instances, magainin from the African clawed frog [2] and LL-37 from human [3] are α-helical peptides; Tachyplesin from the horseshoe crab [4] and protegrin-1 in porcine leukocytes [5] are anti-parallel β-sheet peptides constrained by disulfide bonds; The tryptophan-rich indolicidin found in the cow [6] and the proline-arginine-rich PR39 in the pig [7] are non-helical linear peptides. Despite this great structural diversity, all classes of antimicrobial peptides contain hydrophobic, hydrophilic and cationic residues with the underlying structural principle that polar and non-polar regions in the molecule are spatially separated (‘amphipathic’ structure) [8].

How do antimicrobial peptides target microbes in the major presence of host cells? These small peptides utilize a surprisingly fundamental difference between membranes of microbes and multicellular organisms. Microbial membranes are rich in anionic phospholipids, especially in the outer leaflet, rendering the cells susceptible to the antimicrobial peptides with cationic residues. In contrast, the outer leaflet of membranes of animals and plants consist of zwitterionic phospholipids and most anionic lipids are present in the inner leaflet [9]. The cholesterol present in most mammalian cell membranes further reduces the peptide activity by either rigidifying the lipid bilayer or interacting with the peptides [10].

In general, antimicrobial peptides kill microbes by disrupting their cell membranes. Various models have been proposed for this membrane disruption. The first is the "barrel-stave" model (Fig. 1.1a), where the peptides aggregate as a transmembrane helical bundle that inserts into the bilayer to form transmembrane pores that cause lysis of the cell substances. This model has been used to explain pore formation and step-wise conductivity increases in single-channel measurements on alamethicin [11]. The second is the carpet model (Fig. 1.1b), where the peptides accumulate on the surface with the hydrophobic face embedded relatively shallowly within the hydrophobic region of the membrane and its positive charges directed toward the hydrophilic region. When the peptide concentration reaches a threshold, the peptides would cause bilayer disruption and lead to the leakage of the cellular contents. This model is proposed based on observations with the antimicrobial peptide dermaseptin [12]. The third model is the toroidal pore model (Fig. 1.1c), where the peptides aggregate and induce disorder of lipids and the two leaflets of the bilayer merge to form a toroidal pore. This model can explain the larger water-filled cavities [13] and enhanced lipid flip-flop rate [14] caused by magainin in the membrane.

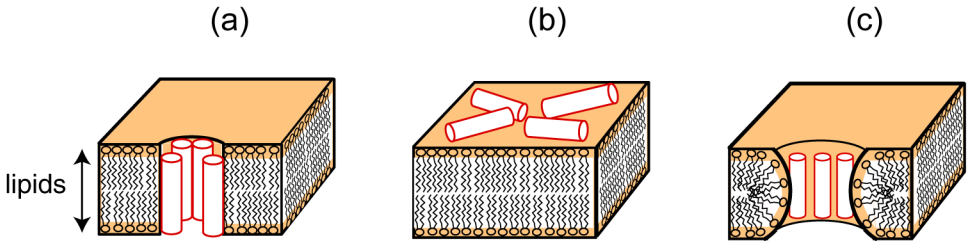

Figure 1.1. Three models of membrane disruption mechanism of antimicrobial peptides: Barrel-stave model (a), Carpet model (b) and Toroidal Pore model (c).

Microbes tend to develop resistance against conventional antibiotics like penicillin by mutating the target protein with a sensitive microbial strain. However, antimicrobial peptides target microbial membrane, whose composition and design are very difficult to change, and thus microbes have not been successful in resisting antimicrobial peptides. In a few rare cases, some microbes express an outer membrane with less anionic lipids for peptides to bind, and other resistant species use destructive proteases to digest peptides [15].

1.2 Protegrin-1: A β-Hairpin Antimicrobial Peptide

Protegrin-1 (PG-1) is one of a family of protegrin peptides isolated from porcine neutrophils [16]. It possesses an unusually broad spectrum of antimicrobial activity against gram-positive and gram-negative bacteria, fungi and some enveloped viruses [5]. Its minimum inhibitory concentrations are in the range of a few micrograms per millilitre [17]. PG-1 (**R**GG**R**LCYC**RRR**FCVCVG**R**) has eighteen amino acids and six of them are Arg. It also has two disulfide bonds to constrain the structure to be a β-hairpin, which can be separated into a β-strand region (residue 4–8 and 13–17) and a β-turn region (residue 9–12). An extensive structure–activity relationship (SAR) study has been conducted on several hundred protegrin analogues to conclude that overall structural features such as amphiphilicity, charge density, intermolecular hydrogen-bonding capability and hairpin shape are more important to activity than the presence of specific amino acids and stereochemistry [18]. PG-1 carries out its antimicrobial function by forming pores in the microbial cell membrane, thus disrupting the membrane's barrier function. These pores were observed from lipid vesicle leakage assays [19, 20] and neutron diffraction [21]. However, the detailed mechanism of membrane disruption at the atomic level is still unclear for PG-1. Solid-state NMR spectroscopy is an excellent technique to provide high-resolution information about intermolecular interaction and dynamics in amorphous and insoluble systems such as lipid membranes for which solution NMR and X-ray diffraction are not suitable. In order to distinguish which one of the three models mentioned above explains the antimicrobial activity of PG-1 and to further elucidate the interaction between PG-1 and lipid bilayers, the following aspects of the complex system consisting of PG-1 and lipid bilayers have to be investigated:

Peptide Oligomerization

Both the barrel-stave model and the toroidal pore model involve peptide oligomerization. SAR studies of PG-1 showed that linearized analogues or analogues that have amino acid mutations that eliminate hydrogen bonding between PG-1 β-sheets have

reduced activity [18]. Therefore, understanding the oligomerization of PG-1 in the lipid bilayers should shed light on its antimicrobial mechanism. Previous work in our group using ^{1}H and ^{19}F spin diffusion NMR showed that PG-1 self-assembles into a transmembrane β-barrel in bacteria-mimetic POPE/POPG membranes [22]. A solution NMR study of PG-1 in DPC micelles [23] showed that the peptide forms antiparallel dimers with the C-strand lining the dimer interface. Since micelles are known to impose curvature strains onto peptides due to spatial constraint, it is possible that the oligomeric state of PG-1 in micelles may not be the same as that in the biologically more relevant lipid bilayers.

Depth of Insertion

In general, the insertion of membrane proteins is interesting because of the amphipathic nature of the bilayers. The concepts of "hydrophobic matching" and "interfacial anchoring" have been used in various studies to determine the alignments of α-helical peptides in the membrane [24-27]. Nevertheless, few studies have been conducted on the insertion of β-sheet membrane peptides. The paramagnetic relaxation enhancement (PRE) effect had been used by Buffy, et al. in our laboratory to determine the insertion of PG-1 in DLPC bilayers [28]. The Mn^{2+} ions on the surface of the bilayer induce distance-dependent T_2 decrease and corresponding signal loss. The results showed that residues G2 at the N-terminus and F12 at the β-turn of the peptide reside near the membrane surface, whereas L5 and V16 are embedded in the acyl chain region, which indicates that PG-1 is fully inserted in DLPC bilayers. Compared with the hydrophobic matching conditions of α-helical peptides, PG-1 shows hydrophobic mismatch of 8–10 Å in DLPC bilayers and possibly induces membrane thinning [28], but the case of PG-1 insertion in long-chain lipid bilayers had still been unclear and can not be explained by hydrophobic mismatch.

Peptide-Lipid Contact

Revealing the contact between the peptide and the lipids helps to explain how the peptide binds the lipid bilayer. Indirect methods such as ^{1}H spin diffusion have been used to study the contacts between the peptides and different parts of the membrane. ^{13}C and ^{31}P detected ^{1}H spin diffusion from lipid to a colicin Ia channel domain was used to prove the

existence of membrane-embedded domain [29]. As for the β-hairpin PG-1, ^{1}H spin diffusion experiments showed that PG-1 contacts both the surface and the hydrophobic center of the POPC bilayer [30]. More direct methods such as distance measurement from peptide to lipid have been utilized in discerning the model for an α-helical antimicrobial peptide, K3, in lipid bilayers [31, 32]. Short peptide-headgroup distances, short peptide-lipid chain distances, and enhanced lipid headgroup-chain contacts were obtained, though only 30% of peptides have contact with lipids. Combined with the distances measured within K3 aggregates and K3 alignment obtained by oriented-sample ^{19}F NMR, a toroidal pore model was proposed for the mode of action of K3 [32]. Compared to Lys-containing K3, Arg-containing PG-1 is more potent and may have closer contact with lipids, especially the headgroups.

Peptide Dynamics

Lipid membranes consist of water and lipids and are highly fluid. Lipids undergo fast lateral diffusion and uniaxial rotational diffusion, thus molecular motion for membrane proteins is very common and is often related to the function and lipid-interaction of proteins. For small membrane peptides, whole-body motion has been observed for both α-helical [33] and β-sheet peptides [34]. In some cases, if the motion of the peptides is uniaxial rotation, then the motionally averaged dipolar coupling and chemical shift anisotropy can provide valuable information about peptide orientation [35-38]. For large membrane proteins, large-amplitude segmental motion has been reported. For instance, membrane-induced mobility increase was found in the colicin Ia channel domain [39], suggesting that the mobile lipids interact with protein and thus increase the protein internal motion. Versatile dynamics of segmental fluctuations and axially symmetric overall motions were shown for the C-terminus of membrane-associated full-length lipidated Ras protein [40]. The dynamics of PG-1 serves as an indicator of the interaction between PG-1 and lipids. Particularly, the motion of Arg residues of PG-1 poses a special interest, because cationic Arg residues may bind anionic lipid headgroups, and their dynamics should be affected.

Peptide Orientation

The orientation of membrane peptides and protein domains in lipid bilayers is an important aspect of the three-dimensional structure of these molecules. 2D separated-local field (SLF) spectroscopy correlating the ^{15}N chemical shift with ^{15}N-^{1}H dipolar coupling has been well established to determine the orientation of α-helical peptides and protein domains in macroscopically aligned membranes [41]. Although the preparation of well-oriented membrane samples is a limiting factor to the success of this type of experiment, recent developments of new aligned sample systems such as bicelles [42-45] and nanopore-supported lipid nanotube arrays [46-48] have greatly improved the stability and surface accessibility of aligned bilayers. Despite the advances in the orientation determination of α-helical membrane peptides, information about the orientation of β-sheet peptides in lipid bilayers is still scarce, due to the complexity of the pattern analysis of 2D SLF spectra. Recently, the orientation of the β-barrel domain of the bacterial outer membrane protein OmpX has been investigated in the membrane [49]. The resolved peaks in 2D SLF spectra agreed well with the spectra calculated from the crystal structure of OmpX with 5˚ tilt angle. Compared to large β-barrel proteins, small disulfide-stabilized β-hairpin peptides are promising systems both for understanding β-sheet peptide binding to lipid membranes and for testing the applicability of the solid-state NMR method. The orientation of PG-1 in DLPC bilayers has been determined by fitting the experimental results with calculated orientation-dependent ^{13}C and ^{15}N chemical shifts [34]. Whether the orientation of the peptide is in-plane or transmembrane implicates which model is likely to explain its antimicrobial action.

1.3 Guanidinium-Phosphate Complexation

The guanidinium group on the side chain of Arg is a very stable cation and is responsible for most of Arg's noncovalent interactions, among which particularly important interactions are those formed by guanidinium with anions such as phosphates, sulfates and carboxylates. These interactions are often used in molecular recognition since ion-pairing can be versatile and combined with other interactions to develop unique schemes, both for biological mimetics and for the purpose of drug developments [50].

Generally, the insertion of the charged and polar residues into the hydrophobic part of the bilayer is energetically unfavorable. Yet charged and polar residues are surprisingly common in a diverse range of membrane proteins, such as antimicrobial peptides, cell-penetrating peptides and ion channel domains. The hydrophobicity scale [51] has been established in detail by measuring, for examples, the free energies of transferring peptides from water to lipid bilayer interface [52] and octanol [53]. The whole-residue hydrophobicity scale appears to be a good measure of the partitioning of hydrophobic α-helices into the bilayer interior. Recently, the scale was modified "biologically" by utilizing an endoplasmic reticulum translocon system mutated with designed α-helical strain. The study found that the free energy of insertion not only depends on the polarity of the residues, but also depends sensitively on the position of the polar residues in the membrane [54]. The resulting biological hydrophobicity scale was then used to predict transmembrane helices based on the amino acid sequence and overall length [55]. In addition to taking into account the protein-lipid hydrophobic interaction, hydrophilic interactions such as ionic interaction and hydrogen bonding need to be considered for charged and polar amino acids. A similar translocon system with the S4 helix of the voltage-gated potassium channel KvAP inserts into the membrane despite the presence of four Arg's [56]. Molecular dynamics simulations showed that the effective lipid bilayer thickness was reduced to an astonishingly small ~10 Å near the inserted single S4 helix so that water and phosphate groups stabilize the Arg residues in the middle of the helix through hydrogen bonding [57].

Indirect evidence about anion-mediated insertion of cationic charged residues has been reported. Fluorescently labeled oligoarginines, which are among the most active cell-penetrating peptides, was found to phase-transfer from water into bulk chloroform and anionic lipid membranes with the mediation of amphiphilic lipid and reverse-phase transfer from bulk chloroform and lipids into water with the mediation of hydrophilic heparin [58]. The cellular uptake mechanism of guanidinium-rich transporters conjugated to small molecules has been studied by testing the partition of a fluoresceinated arginine octamer in a bilayer of octanol and water [59]. With the help of a fatty acid salt, the polyarginines transfer from water into octanol. But the uptake was greatly reduced when the guanidinium group of each arginine was methylated. This reduction can be explained by the weakened hydrogen

bonding in the guanidinium-anion bidentate complex. Therefore, hydrogen bonding plays an important role in the cellular uptake of cell-penetrating peptides.

1.4 Thesis Organization

Solid-state NMR studies of β-sheet antimicrobial peptides are presented in this thesis. Chapter 2 describes the procedures for synthesizing protected amino acids, preparing various types of samples (oriented and unoriented samples), NMR techniques which have been used in the experiments, and methods for simulating experimental data. Various input codes for numerical simulations are included in the Appendices.

Chapter 3 shows the investigation of the oligomeric structure of lipid-free PG-1 aggregates. Using 2D ^{1}H-driven spin diffusion (PDSD) and other correlation methods, we determined that PG-1 molecules aggregate in a parallel fashion with like strands lining the intermolecular interface.

Chapter 4 demonstrates the method for determining the orientation of β-sheet membrane peptides using 2D separated local-field spectroscopy. Retrocyclin-2 (RC100b), an antibacterial and antiviral β-hairpin peptide, was found to adopt a transmembrane orientation in short-chain lipids (DLPC) and a more in-plane orientation in long-chain lipids (POPC), which indicates that the membrane thickness affects the peptide orientation.

Chapter 5 demonstrates that the cryoprotectant trehalose retains the lipid bilayer structure during dehydration by comparing the lipid conformation and dynamics between trehalose-protected lyophilized membranes and hydrated membranes. The trehalose-incorporated membrane is a promising matrix for membrane protein structure determination without the interference of motion.

Solid-state NMR studies on various aspects of the interaction of PG-1 with lipid bilayers are described in chapter 6, 7, and 8. In chapter 6, the depth of insertion of Arg residues of PG-1 is studied in anionic and zwitterionic membranes by measuring the ^{13}C-^{31}P distances between Arg and lipid headgroups. Short peptide-lipid distances and transmembrane orientation of PG-1 led to the toroidal pore model as the mechanism of action of PG-1. It also suggests that guanidinium-phosphate complexation to be the driving force for

pore formation. In chapter 7, the effects of membrane insertion on Arg dynamics were studied by measuring C-H bond order parameters, chemical shift anisotropy (CSA) scaling factors and ^{1}H rotating-frame spin-lattice relaxation times ($T_{1\rho}$). Different dynamics were observed between the β-strand region and the β-turn region, which is attributed to PG-1 aggregation and peptide-lipid interaction. Finally, chapter 8 examines the effects of guanidinium-phosphate hydrogen-bonding on the membrane bound structure and antimicrobial activity of PG-1 by studying the insertion and dynamics of an Arg-dimethylated PG-1 mutant in anionic lipid bilayers. The mutant was found to adopt an in-plane orientation and undergo fast uniaxial rotation, which differs dramatically from the rigid transmembrane wild-type PG-1. The weakened guanidinium-phosphate hydrogen bonding prevent PG-1 insertion and oligomerization, and thus change the membrane-disruptive mechanism of the mutant to an in-plane diffusion model, which is less potent than the toroidal pore mechanism.

1.5 Copyright Permission

Chapters 3, 4, 5, 6, 7 and 8 are reprints of published papers. Permissions have been obtained from the following publishing groups.

Chapter 3 and 6	American Chemical Society
Chapter 4	the Biophysical Society
Chapter 5	Elsevier Inc.
Chapter 7 and 8	Wiley-VCH Verlag GmbH & Co. KGaA, Weinheim

References

[1] J. Berdy, Recent developments of antibiotic research and classification of antibiotics according to chemical structure, Adv. Appl. Microbiol. 18 (1974) 309-406.

[2] M. Zasloff, Magainins, a Class of Antimicrobial Peptides from Xenopus Skin - Isolation, Characterization of 2 Active Forms, and Partial Cdna Sequence of a Precursor, Proc. Natl. Acad. Sci. U. S. A. 84 (1987) 5449-5453.

[3] G.H. Gudmundsson, B. Agerberth, J. Odeberg, T. Bergman, B. Olsson, R. Salcedo, The human gene FALL39 and processing of the cathelin precursor to the antibacterial peptide LL-37 in granulocytes, Eur. J. Biochem. 238 (1996) 325-332.

[4] T. Nakamura, H. Furunaka, T. Miyata, F. Tokunaga, T. Muta, S. Iwanaga, M. Niwa, T. Takao, Y. Shimonishi, Tachyplesin, a Class of Antimicrobial Peptide from the Hemocytes of the Horseshoe-Crab (Tachypleus-Tridentatus) - Isolation and Chemical-Structure, J. Biol. Chem. 263 (1988) 16709-16713.

[5] L. Bellm, R.I. Lehrer, T. Ganz, Protegrins: new antibiotics of mammalian origin, Expert Opin. Investig. Drugs 9 (2000) 1731-1742.

[6] M.E. Selsted, M.J. Novotny, W.L. Morris, Y.Q. Tang, W. Smith, J.S. Cullor, Indolicidin, a Novel Bactericidal Tridecapeptide Amide from Neutrophils, J. Biol. Chem. 267 (1992) 4292-4295.

[7] B. Agerberth, J.Y. Lee, T. Bergman, M. Carlquist, H.G. Boman, V. Mutt, H. Jornvall, Amino-Acid-Sequence of Pr-39 - Isolation from Pig Intestine of a New Member of the Family of Proline-Arginine-Rich Antibacterial Peptides, Eur. J. Biochem. 202 (1991) 849-854.

[8] W.L. Maloy, U.P. Kari, Structure-Activity Studies on Magainins and Other Host-Defense Peptides, Biopolymers 37 (1995) 105-122.

[9] K. Matsuzaki, Why and how are peptide-lipid interactions utilized for self-defense? Magainins and tachyplesins as archetypes, Biochim. Biophys. Acta 1462 (1999) 1-10.

[10] Y. Shai, Mechanism of the binding, insertion and destabilization of phospholipid bilayer membranes by alpha-helical antimicrobial and cell non-selective membrane-lytic peptides, Biochim. Biophys. Acta 1462 (1999) 55-70.

[11] G. Baumann, P. Mueller, A molecular model of membrane excitability, J. Supramol. Struct. 2 (1974) 538-557.

[12] Y. Pouny, D. Rapaport, A. Mor, P. Nicolas, Y. Shai, Interaction of Antimicrobial Dermaseptin and Its Fluorescently Labeled Analogs with Phospholipid-Membranes, Biochemistry 31 (1992) 12416-12423.

[13] S.J. Ludtke, K. He, W.T. Heller, T.A. Harroun, L. Yang, H.W. Huang, Membrane pores induced by magainin, Biochemistry 35 (1996) 13723-13728.

[14] K. Matsuzaki, O. Murase, N. Fujii, K. Miyajima, An antimicrobial peptide, magainin 2, induced rapid flip-flop of phospholipids coupled with pore formation and peptide translocation, Biochemistry 35 (1996) 11361-11368.

[15] M. Zasloff, Antimicrobial peptides of multicellular organisms, Nature 415 (2002) 389-395.

[16] V.N. Kokryakov, S.S. Harwig, E.A. Panyutich, A.A. Shevchenko, G.M. Aleshina, O.V. Shamova, H.A. Korneva, R.I. Lehrer, Protegrins: leukocyte antimicrobial peptides that combine features of corticostatic defensins and tachyplesins, FEBS Lett. 327 (1993) 231-236.

[17] X.D. Qu, S.S.L. Harwig, A. Oren, W.M. Shafer, R.I. Lehrer, Susceptibility of Neisseria gonorrhoeae to protegrins, Infect. Immun. 64 (1996) 1240-1245.

[18] J. Chen, T.J. Falla, H.J. Liu, M.A. Hurst, C.A. Fujii, D.A. Mosca, J.R. Embree, D.J. Loury, P.A. Radel, C.C. Chang, L. Gu, J.C. Fiddes, Development of protegrins for the treatment and prevention of oral mucositis: Structure-activity relationships of synthetic protegrin analogues, Biopolymers 55 (2000) 88-98.

[19] R.I. Lehrer, A. Barton, T. Ganz, Concurrent assessment of inner and outer membrane permeabilization and bacteriolysis in E. coli by multiple-wavelength spectrophotometry, J. Immunol. Methods 108 (1988) 153-158.

[20] V.I. Ternovsky, Y. Okada, R.Z. Sabirov, Sizing the pore of the volume-sensitive anion channel by differential polymer partitioning, FEBS Lett. 576 (2004) 433-436.

[21] L. Yang, T.M. Weiss, R.I. Lehrer, H.W. Huang, Crystallization of antimicrobial pores in membranes: magainin and protegrin, Biophys. J. 79 (2000) 2002-2009.

[22] R. Mani, S.D. Cady, M. Tang, A.J. Waring, R.I. Lehrert, M. Hong, Membrane-dependent oligomeric structure and pore formation of beta-hairpin antimicrobial peptide in lipid bilayers from solid-state NMR, Proc. Natl. Acad. Sci. U. S. A. 103 (2006) 16242-16247.

[23] C. Roumestand, V. Louis, A. Aumelas, G. Grassy, B. Calas, A. Chavanieu, Oligomerization of protegrin-1 in the presence of DPC micelles. A proton high-resolution NMR study., FEBS Lett. 421 (1998) 263-267.

[24] U. Harzer, B. Bechinger, Alignment of lysine-anchored membrane peptides under conditions of hydrophobic mismatch: a CD, 15N and 31P solid-state NMR spectroscopy investigation., Biochemistry 39 (2000) 13106-13114.

[25] S.H. Park, S.J. Opella, Tilt angle of a trans-membrane helix is determined by hydrophobic mismatch, J. Mol. Biol. 350 (2005) 310-318.

[26] M.R.R. de Planque, J.A. Killian, Protein-lipid interactions studied with designed transmembrane peptides: role of hydrophobic matching and interfacial anchoring (Review), Mol. Membr. Biol. 20 (2003) 271-284.

[27] M.R.R. de Planque, B.B. Bonev, J.A.A. Demmers, D.V. Greathouse, R.E. Koeppe, F. Separovic, A. Watts, J.A. Killian, Interfacial anchor properties of tryptophan residues in transmembrane peptides can dominate over hydrophobic matching effects in peptide-lipid interactions, Biochemistry 42 (2003) 5341-5348.

[28] J.J. Buffy, T. Hong, S. Yamaguchi, A. Waring, R.I. Lehrer, M. Hong, Solid-State NMR Investigation of the Depth of Insertion of Protegin-1 in Lipid Bilayers Using Paramagnetic Mn2+, Biophys. J. 85 (2003) 2363-2373.

[29] D. Huster, X.L. Yao, M. Hong, Membrane protein topology probed by H-1 spin diffusion from lipids using solid-state NMR spectroscopy, J. Am. Chem. Soc. 124 (2002) 874-883.

[30] J.J. Buffy, A.J. Waring, R.I. Lehrer, M. Hong, Immobilization and Aggregation of the Antimicrobial Peptide Protegrin-1 in Lipid Bilayers Investigated by Solid-State NMR, Biochemistry 42 (2003) 13725-13734.

[31] O. Toke, W.L. Maloy, S.J. Kim, J. Blazyk, J. Schaefer, Secondary structure and lipid contact of a peptide antibiotic in phospholipid bilayers by REDOR, Biophys. J. 87 (2004) 662-674.

[32] O. Toke, R.D. O'Connor, T.K. Weldeghiorghis, W.L. Maloy, R.W. Glaser, A.S. Ulrich, J. Schaefer, Structure of (KIAGKIA)3 aggregates in phospholipid bilayers by solid-state NMR, Biophys. J. 87 (2004) 675-687.

[33] S.H. Park, A.A. Mrse, A.A. Nevzorov, A.A. De Angelis, S.J. Opella, Rotational diffusion of membrane proteins in aligned phospholipid bilayers by solid-state NMR spectroscopy, J. Magn. Reson. 178 (2006) 162-165.

[34] S. Yamaguchi, T. Hong, A. Waring, R.I. Lehrer, M. Hong, Solid-state NMR investigations of peptide-lipid interaction and orientation of a beta-sheet antimicrobial peptide, protegrin, Biochemistry 41 (2002) 9852-9862.

[35] M. Hong, T. Doherty, Orientation determination of membrane-disruptive proteins using powder samples and rotational diffusion: A simple solid-state NMR approach, Chem. Phys. Lett. 432 (2006) 296-300.

[36] S.D. Cady, C. Goodman, C.D. Tatko, W.F. DeGrado, M. Hong, Determining the orientation of uniaxially rotating membrane proteins using unoriented samples: A H-2, C-13, and N-15 solid-state NMR investigation of the dynamics and orientation of a transmembrane helical bundle, J. Am. Chem. Soc. 129 (2007) 5719-5729.

[37] S.D. Cady, M. Hong, Simultaneous extraction of multiple orientational constraints of membrane proteins by C-13-detected N-H dipolar couplings under magic angle spinning, J. Magn. Reson. 191 (2008) 219-225.

[38] S.D. Cady, M. Hong, Amantadine-induced conformational and dynamical changes of the influenza M2 transmembrane proton channel, Proc. Natl. Acad. Sci. U. S. A. 105 (2008) 1483-1488.

[39] D. Huster, L.S. Xiao, M. Hong, Solid-state NMR investigation of the dynamics of the soluble and membrane-bound colicin Ia channel-forming domain, Biochemistry 40 (2001) 7662-7674.

[40] G. Reuther, K.T. Tan, A. Vogel, C. Nowak, K. Arnold, J. Kuhlmann, H. Waldmann, D. Huster, The lipidated membrane anchor of full length N-Ras protein shows an extensive dynamics as revealed by solid-state NMR spectroscopy, J. Am. Chem. Soc. 128 (2006) 13840-13846.

[41] S.J. Opella, F.M. Marassi, Structure determination of membrane proteins by NMR spectroscopy, Chem. Rev. 104 (2004) 3587-3606.

[42] S.H. Park, A.A. De Angelis, A.A. Nevzorov, C.H. Wu, S.J. Opella, Three-dimensional structure of the transmembrane domain of Vpu from HIV-1 in aligned phospholipid bicelles, Biophys. J. 91 (2006) 3032-3042.

[43] A.A. De Angelis, S.C. Howell, A.A. Nevzorov, S.J. Opella, Structure determination of a membrane protein with two trans-membrane helices in aligned phospholipid bicelles by solid-state NMR spectroscopy, J. Am. Chem. Soc. 128 (2006) 12256-12267.

[44] S.H. Park, S. Prytulla, A.A. De Angelis, J.M. Brown, H. Kiefer, S.J. Opella, High-resolution NMR spectroscopy of a GPCR in aligned bicelles, J. Am. Chem. Soc. 128 (2006) 7402-7403.

[45] A.A. De Angelis, A.A. Nevzorov, S.H. Park, S.C. Howell, A.A. Mrse, S.J. Opella, High-resolution NMR spectroscopy of membrane proteins in aligned bicelles, J. Am. Chem. Soc. 126 (2004) 15340-15341.

[46] E.Y. Chekmenev, P.L. Gor'kov, T.A. Cross, A.M. Alaouie, A.I. Smirnov, Flow-through lipid nanotube arrays for structure-function studies of membrane proteins by solid-state NMR spectroscopy, Biophys. J. 91 (2006) 3076-3084.

[47] E.Y. Chekmenev, J. Hu, P.L. Gor'kov, W.W. Brey, T.A. Cross, A. Ruuge, A.I. Smirnov, N-15 and P-31 solid-state NMR study of transmembrane domain alignment of M2 protein of influenza A virus in hydrated cylindrical lipid bilayers confined to anodic aluminum oxide nanopores, J. Magn. Reson. 173 (2005) 322-327.

[48] A.I. Smirnov, O.G. Poluektov, Substrate-supported lipid nanotube arrays, J. Am. Chem. Soc. 125 (2003) 8434-8435.

[49] R. Mahalakshmi, C.M. Franzin, J. Choi, F.M. Marassi, NMR structural studies of the bacterial outer membrane protein OmpX in oriented lipid bilayer membranes, Biochim. Biophys. Acta 1768 (2007) 3216-3224.

[50] K.A. Schug, W. Lindner, Noncovalent binding between guanidinium and anionic groups: focus on biological- and synthetic-based arginine/guanidinium interactions with phosph[on]ate and sulf[on]ate residues, Chem. Rev. 105 (2005) 67-114.

[51] S.H. White, W.C. Wimley, Membrane protein folding and stability: Physical principles, Annu. Rev. Biophys. Biomol. Struct. 28 (1999) 319-365.

[52] W.C. Wimley, S.H. White, Experimentally determined hydrophobicity scale for proteins at membrane interfaces, Nature Structural Biology 3 (1996) 842-848.

[53] W.C. Wimley, T.P. Creamer, S.H. White, Solvation energies of amino acid side chains and backbone in a family of host-guest pentapeptides, Biochemistry 35 (1996) 5109-5124.

[54] T. Hessa, H. Kim, K. Bihlmaier, C. Lundin, J. Boekel, H. Andersson, I. Nilsson, S.H. White, G. von Heijne, Recognition of transmembrane helices by the endoplasmic reticulum translocon, Nature 433 (2005) 377-381.

[55] T. Hessa, N.M. Meindl-Beinker, A. Bernsel, H. Kim, Y. Sato, M. Lerch-Bader, I. Nilsson, S.H. White, G. von Heijne, Molecular code for transmembrane-helix recognition by the Sec61 translocon, Nature 450 (2007) 1026-1030.

[56] T. Hessa, S.H. White, G. von Heijne, Membrane insertion of a potassium-channel voltage sensor, Science 307 (2005) 1427.

[57] J.A. Freites, D.J. Tobias, G. von Heijne, S.H. White, Interface connections of a transmembrane voltage sensor, Proc. Natl. Acad. Sci. U.S.A. 102 (2005) 15059-15064.

[58] N. Sakai, T. Takeuchi, S. Futaki, S. Matile, Direct observation of anion-mediated translocation of fluorescent oligoarginine carriers into and across bulk liquid and anionic bilayer membranes, ChemBioChem 6 (2005) 114-122.

[59] J.B. Rothbard, T.C. Jessop, R.S. Lewis, B.A. Murray, P.A. Wender, Role of membrane potential and hydrogen bonding in the mechanism of translocation of guanidinium-rich peptides into cells, J. Am. Chem. Soc. 126 (2004) 9506-9507.

Chapter 2
Material and Methods

2.1 Sample Preparation

2.1.1 Amino Acid Protection

Procedures for Fmocing Amino Acid

In a 250 ml flask, 2 mmol amino acid (Glycine, Valine or Leucine) with 30 mL dioxane was added. 3 eq. (0.64 g) of sodium carbonate dissolved in 25 mL water was added to the flask. The mixture was stirred in the ice bath. At around 5˚C, 1.1 eq (0.75 g) Fmoc-OSu in 30 mL 1:1 dioxane/acetone was added drop-wise over 15 minutes with a glass dropper. The mixture was kept stirring for 1 hour in the ice bath. After 1 hr, the ice bath was removed and reactants were allowed to warm to room temperature overnight while stirring. After overnight, water (~50 ml, enough to double the volume of the solution) was added and the residual Fmoc-OSu was extracted with ethyl ether (2×30 mL). To the aqueous layer 0.2 M HCl solution was added until the pH is ~2 as tested by pH paper. A large amount of white precipitates (Fmoc amino acid product) appeared. The product was extracted with ethyl acetate (3×50 mL) from the mixture. The organic layers (about ~150 mL) were combined and dried over sodium sulfate. The solution was filtered and the ethyl acetate solvent was removed in vacuo. The product was lyophilized for 12 h to remove any residual solvents. The purity was checked with ^{1}H solution NMR. The product was dissolved with $CDCl_3$ or d_6-DMSO. There was very little or no ^{1}H peak at ~ 2.7 ppm (Fmoc-OSu). The yield was around 80–90%. The products are white or slightly yellow powder. Fig. 2.1 shows the ^{1}H solution spectra of Fmoc-Val in $CDCl_3$, Fmoc-[U-^{13}C, ^{15}N]Gly and Fmoc-[U-^{13}C, ^{15}N]Leu in d_6-DMSO.

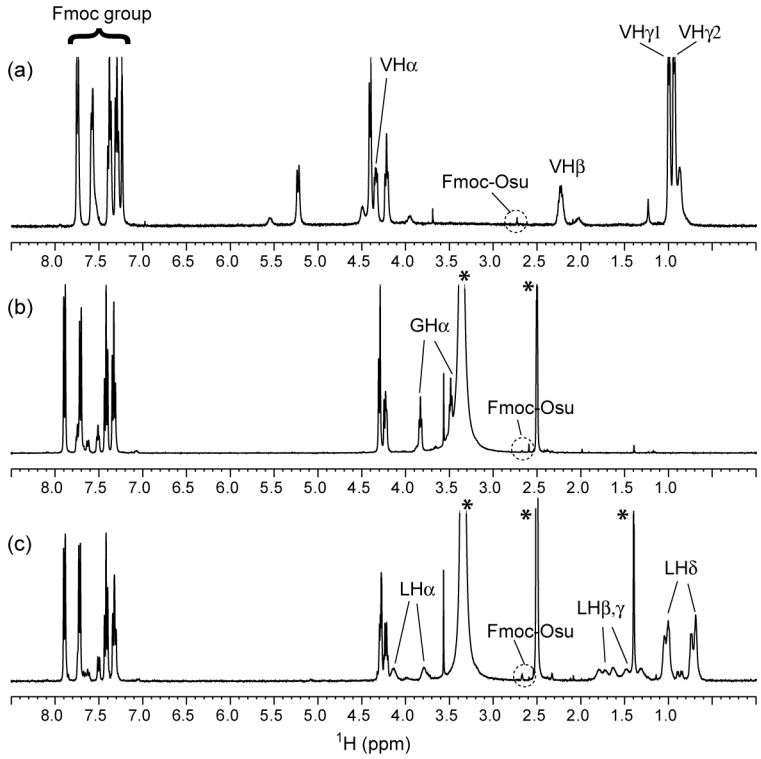

Figure 2.1. ^{1}H solution spectra of Fmoc-Val standard in $CDCl_3$ (a), Fmoc-[U-^{13}C, ^{15}N]Gly (b) and Fmoc-[U-^{13}C, ^{15}N]Leu (c) in d_6-DMSO. Asterisks (*) indicate solvent peaks. ^{1}H peaks (~2.7 ppm) of residual Fmoc-Osu are very small. ^{1}H peaks of Gly and Leu split into doublet due to the ^{1}H-^{13}C J-coupling from the uniform labeling.

Procedures for Trityl Protection of Histidine

Before the Fmoc protection, Histidine side chain has to be trityl (Trt) protected [1] to prevent the side chain Fmocing. 10 mmol (1.55 g) Histidine and 15 mL CH_2Cl_2 was added in a 100 mL three-neck flask and the suspension was stirred. The flask was connected with a water condenser, and the whole system was blown with N_2 for 15 min. A balloon was used on the top of the condenser to seal the system under N_2 atmosphere. All the open connectors were sealed with rubber stoppers. A glass syringe was used to add ~5 mL CH_2Cl_2 to compensate the loss during N_2 blowing. Then 10 mmol (1.21 mL) Me_2SiCl_2 was added to the flask. The system was refluxed for 4 h. Then 20 mmol (2.79 mL) Et_3N was added and the reflux continued for 15 min. The reflux was stopped and another 10 mmol (1.39 mL) Et_3N was added. A solution of 10 mmol (2.79 g) Trt-Cl in 10 mL of CH_2Cl_2 was added and the mixture was under stirring at the room temperature for 2 h. Then the N_2 protection was

released and an excess of MeOH was added. The solvent was removed in vacuo. Water was used to dissolve the residue and the pH was adjusted to 8–8.5 by dropwise addition of Et_3N (or 10% Na_2CO_3). Et_2O was added to the resulting slurry which was shaken well. The insoluble component was filtered off with suction, followed by further wash of the solid with water and Et_2O. An analytical sample was prepared by recrystallization from THF-water (1:1). Analytical thin-layer chromatography (TLC) was performed using the solvent mixture of 1-butanol, acetic acid and water (4:1:5, the organic phase at the top). R_f is 0.41.

2.1.2 Peptides and Lipids

1-palmitoyl-2-oleoyl-*sn*-glycero-3-phosphatidylcholine (POPC), 1-palmitoyl-2-oleoyl-*sn*-glycero-3-phosphatidylethanolamine (POPE), and 1-palmitoyl-2-oleoyl-*sn*-glycero-3-phosphatidylglycerol (POPG) were purchased from Avanti Polar Lipids (Alabaster, AL). PG-1 (NH_2-RGGRLCYCRRRFCVCVGR-$CONH_2$) was synthesized using Fmoc chemistry as previously described [2]. Fig. 2.2 shows schematic structures and the assignments for ^{13}C and ^{1}H spectra of three lipids.

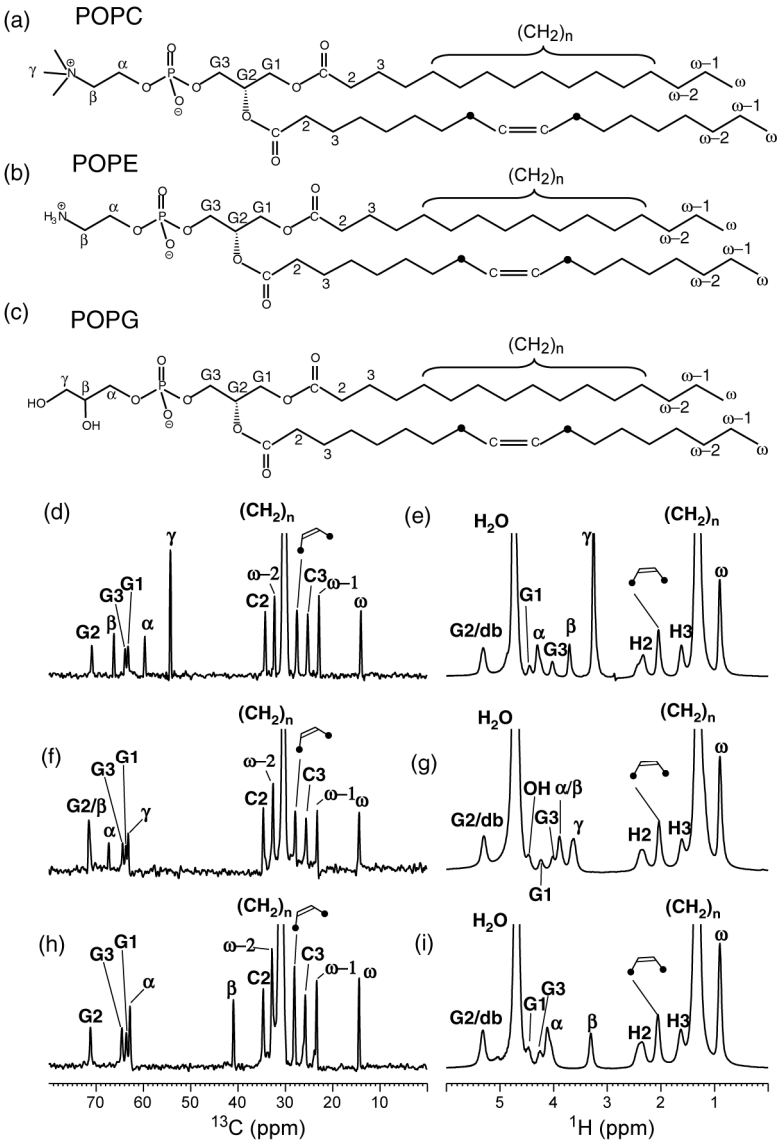

Figure 2.2. Schematic structures of three lipids: POPC (a), POPE (b) and POPG (c). ^{13}C and ^{1}H spectra of three lipids and peak assignments: POPC (d, e), POPG (f, g) and POPE (h, i), correspondingly.

2.1.3 Oriented Sample Preparation

Glass-plate oriented membrane mixtures were prepared using a naphthalene-incorporated procedure described recently [3]. The peptide was dissolved in TFE or methanol and mixed with a chloroform solution of the lipids with the desired molar ratio. The mixture was dried under a stream of N_2 gas and the dried film was redissolved in a 1:1 mixture of chloroform/TFE containing a two-fold excess of naphthalene with respect to the lipids. The

solution was deposited on 10 – 30 glass plates with an area concentration of 0.01 – 0.02 mg/mm^2, air-dried for 2 hours and then vacuum dried for 5 hours to remove all solvents and naphthalene. About 1 μL of water was added directly to each glass plate, then the sample was hydrated indirectly at a relative humidity of 98% over a saturated solution of K_2SO_4 or NaH_2PO_4 for 1 – 2 weeks. The glass plates were stacked, wrapped in parafilm and sealed in a polyethylene bag to prevent dehydration during the NMR experiments. Fig. 2.3 demonstrates how the alignment affects the quality of the spectra. Fig. 2.3a shows a ^{31}P static spectrum of a reasonable alignment, which provided a good separate-local-field (SLF) ^{15}N-^{1}H/^{15}N 2D correlation spectrum (Fig. 2.3c) of a peptide in the oriented sample with well resolved crosspeaks. Due to the heat generated by the long period of radio-frequency pulse irradiation (~ 18 h for the 2D experiment), the sample dehydrated and the alignment got worse. Fig. 2.3b shows a ^{31}P static spectrum after long 2D experiments. The intensity of 90˚ peak (~ 23 ppm) increased the linewidth of 0˚ peak (~ -17 ppm) got larger. The worse alignment resulted in less resolved crosspeaks in the corresponding 2D spectrum (Fig. 2.3d).

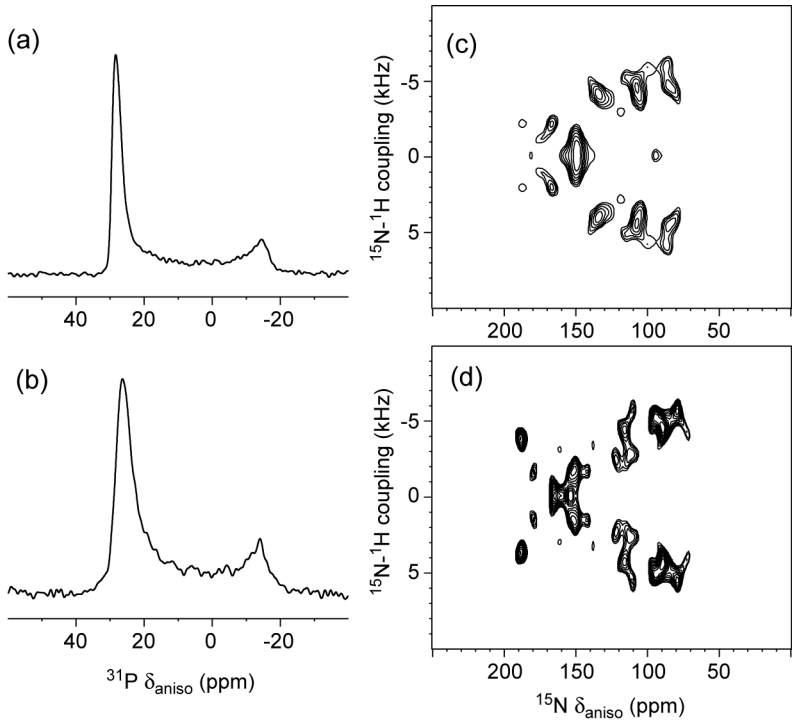

Figure 2.3. ^{31}P static spectra and ^{15}N-^{1}H/^{15}N 2D correlation spectra of retrocyclin-2 (RC100b) in DLPC bilayers. (a) ^{31}P static spectrum with a good alignment. (b) ^{31}P static spectrum with a poor alignment due to long time

pulsing of 2D experiments. (c) ^{15}N-$^{1}H/^{15}N$ 2D correlation spectrum of the well-oriented sample. (d) ^{15}N-$^{1}H/^{15}N$ 2D correlation spectrum of the same sample with a worse alignment after long 2D experiments.

2.1.4 Unoriented Sample Preparation

Lipids were mixed in chloroform and blown dry under N_2 gas. The mixture was then redissolved in cyclohexane and lyophilized. The dry lipid powder was dissolved in water and subjected to five cycles of freeze-thawing to form uniform vesicles. An appropriate amount of PG-1 to reach a desired peptide-lipid molar ratio (P/L) was dissolved in water and mixed with the lipid vesicle solution, let stand overnight, then centrifuged at 55,000 rpm for 2.5 hours. The pellet was packed into a MAS rotor, giving a fully hydrated membrane sample. For cryoprotected samples, trehalose equivalent to 20% of the dry weight of the lipids and peptide was added after the peptide bound to the vesicles. The mixture stood for overnight and was lyophilized to remove the water. The dry sample was packed into a MAS rotor and then lyophilized again to remove the residual moisture caught during packing.

2.2 NMR Methodology

2.2.1 Selective Rotational-Echo Dipolar Recoupling (REDOR)

A selective REDOR technique [4] was used to measure the ^{13}C-^{31}P distances between uniformly ^{13}C, ^{15}N-labeled Arg residues of PG-1 and lipid headgroups of the membrane. The central ^{13}C π pulse is a rotor-synchronized Gaussian pulse centered at the ^{13}C frequency of interest. This soft pulse recouples the desired ^{13}C-^{31}P dipolar coupling, but removes the ^{13}C-^{13}C J-coupling between the ^{13}C on resonance and its directly bonded ^{13}C. The selective pulse was divided into ~200 increments (the actual value depends on the spinning speed to make sure that the pulse length is a multiple of 50 ns times the number of increment) and the Gaussian profile is truncated at 5% at the maximum amplitude. Composite 90˚180˚90˚ pulses were applied on the ^{31}P channel to reduce the effect of flip angle errors and enhance the distance accuracy [5]. At each REDOR mixing time (t_m), a control experiment (S_0) with the ^{31}P pulses off and a dephasing experiment (S) with the ^{31}P pulses on were carried out. The

normalized dephasing, S/S_0, as a function of t_m gives the ^{13}C-^{31}P dipolar coupling. The CO data were corrected for the lipid natural-abundance CO signal.

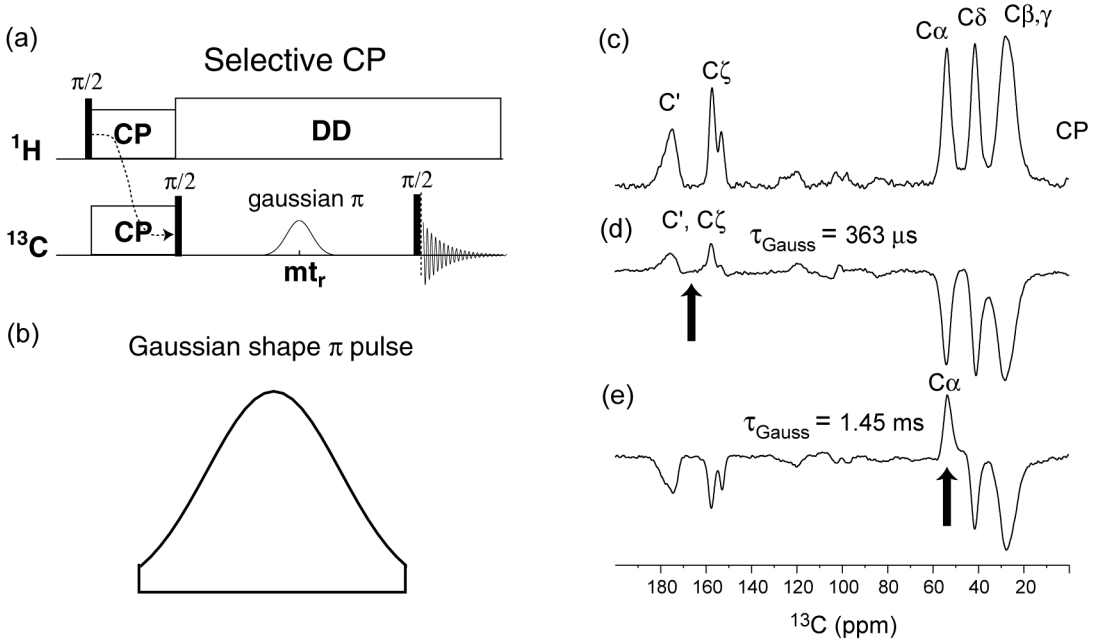

Figure 2.4. Selective CP pulse sequence and the spectra of Fmoc-[U-^{13}C, ^{15}N]Arg(MTR) under 5.5 kHz MAS. (a) Selective CP pulse sequence. (b) Gaussian pulse lineshape. The pulse is constructed by 200 steps of small square pulses. (c) ^{13}C CP spectrum and Arg assignments. (d) ^{13}C selective CP spectrum with a soft Gaussian π pulse on resonance with carbonyl region. The Gaussian pulse length is 363 μs. (e) ^{13}C selective CP spectrum with a soft Gaussian π pulse on resonance with Cα. The Gaussian pulse length is 1.45 ms.

A selective cross-polarization (CP) pulse program was used to test the efficiency of the Gaussian pulses and to choose the proper pulse length (Fig. 2.4a). After the normal Hartman-Hahn ^{1}H-^{13}C CP, ^{13}C magnetization is flipped to z direction by a hard π/2 pulse. Then a soft Gaussian π pulse flips only the ^{13}C magnetization on resonance to –z direction followed by another hard π/2 pulse to detect. So the resulting spectrum would show the on-resonance peak with positive intensity on resonance and the off-resonance peak with negative intensity. Fig. 2.4. shows the selective CP spectra of Fmoc-[U-^{13}C, ^{15}N]Arg(MTR). A relatively short Gaussian pulse (363 μs) inverts both C' and Cζ of Arg, while a relatively long Gaussian pulse (1.45 ms) inverts only Cα. Therefore, the Gaussian pulse can remove C'-Cα and Cα-Cβ J-coupling efficiently. The power of the Gaussian π pulses was directly

optimized in the REDOR S_0 experiment at a very short mixing time to achieve maximum intensity of the on-resonance peak of interest.

2.2.2 Dipolar-Chemical Shift Correlation (DIPSHIFT), Double-Quantum-Filtered DIPSHIFT (DQ-DIPSHIFT), and Lee-Goldburg Cross-Polarization (LG-CP)

Three techniques have been used to measure the motionally averaged dipolar couplings to get information about protein dynamics in the membrane: DIPSHIFT, DQ-DIPSHIFT and LG-CP. 2D DIPSHIFT experiment [6] with MREV-8 for ^{1}H homonuclear decoupling [6] is useful to measure small couplings at low MAS spinning speed (3~5 kHz). For very small couplings, DIPSHIFT experiment with dipolar doubling was used [7, 8] to increase the precision. The doubled version is only good for separated and specific labels, but not for uniform ^{13}C labels due to the interference of directly bonded ^{13}C-^{13}C dipolar couplings. For uniformly labeled samples, some ^{13}C sites overlap with lipid peaks. So the double-quantum-filtered (DQ) DIPSHIFT experiment [9] is used to suppress the natural abundance lipid ^{13}C signals while measuring the peptide dipolar couplings. The DQ filter used SPC5 homonuclear dipolar recoupling sequence [10] with typical spinning speed of 4 – 6 kHz. 2D LG-CP experiment [11, 12] is useful to measure large couplings at high MAS spinning speed (8~10 kHz). The scaling factors for the LG-CP sequence and the MREV-8 sequence are 0.57 and 0.47, respectively.

2.2.3 ^{1}H Spin Diffusion

^{1}H Spin Diffusion from Water in Gel-Phase Membrane

The gel-phase ^{1}H spin diffusion experiment [13] from water to peptide is useful to determine the depth of insertion of individual peptide residues. The signal intensities of the residues which are close to the surface water rise faster with ^{1}H mixing time. The experiments were carried out on PG-1 in DLPC membrane, which were used previously to measure the depths of PG-1 residues in the liquid-crystalline (LC) phase by Mn^{2+} paramagnetic relaxation enhancement [14]. The experiments were performed between 230 K

and 243 K, such that the water ^{1}H linewidth after a 200 μs T_2 filter is 330 Hz [15]. Fixed ^{1}H linewidth was chosen to ensure that ^{1}H spin diffusion rates are consistent throughout different samples. The pulse sequence is presented in Fig. 2.5a. After the T_2 filter, only the water ^{1}H magnetization and a small amount of headgroup γ proton signal remains, so that without spin diffusion, the ^{13}C spectrum suppresses all peptide and lipid signals except for the lipid Cγ signal (Fig. 2.5c). ^{1}H mixing times of 0.25 – 49 ms were then used to detect peptide signals that result from spin diffusion from the membrane surface water. Representative ^{1}H spin diffusion curves of G2 and $(CH_2)_n$ sites of DLPC are shown in Fig. 2.5d. G2 is much closer to surface water than $(CH_2)_n$, thus its signal intensity rises faster than $(CH_2)_n$. The criteria for the choice of temperature are that the ^{1}H T_2 of surface water is much longer than peptide and lipids, and that the spin diffusion through peptide and lipids occurs on the millisecond timescale at optimum temperature. As for the model lipid system, this method is good for PC lipids, but not applicable to PE and PG lipids due to the fact that the NH_3 group and OH groups on PE and PG form hydrogen bonds with water and reduce the ^{1}H T_2 of surface water.

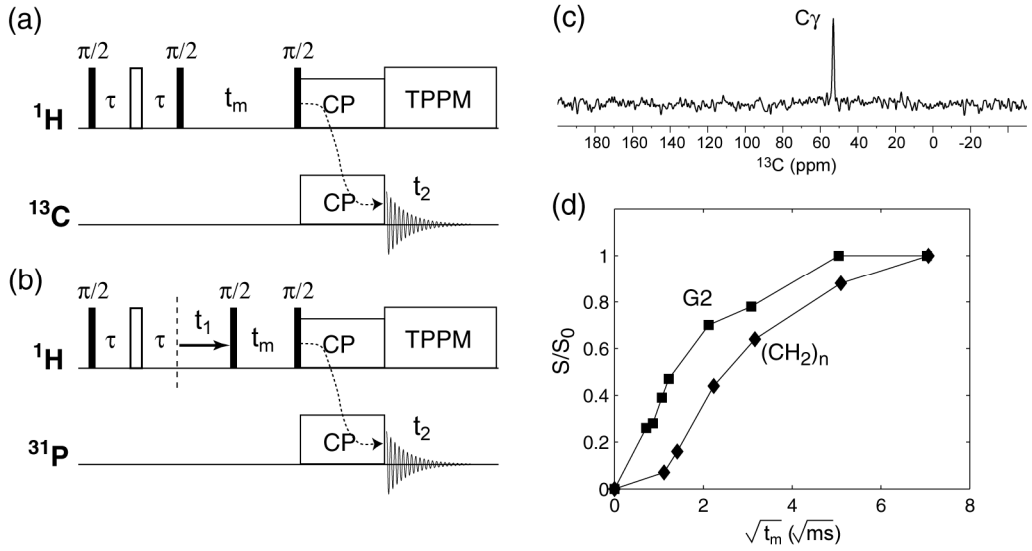

Figure 2.5. ^{1}H spin diffusion pulse sequences. (a) Gel-phase ^{1}H spin diffusion pulse program. The T_2 filter τ is 200 μs. The mixing time t_m is 0.25 – 49 ms. (b) Pulse sequence for ^{31}P-^{1}H correlation experiment with ^{1}H spin diffusion. The T_2 filter τ is 800 μs. The mixing time t_m is 64 – 225 ms. (c) ^{1}H spin diffusion spectrum at short mixing time of 1 μs. After the T2 filter, only Cγ signal remains. (d) Representative ^{1}H spin diffusion curves of G2 (squares) and $(CH_2)_n$ (diamonds) sites of DLPC.

2D ^{31}P-^{1}H Correlation with ^{1}H Spin Diffusion in the Liquid-Crystalline Membrane

The 2D ^{31}P-^{1}H correlation experiment with ^{1}H spin diffusion [16] determines the insertion state of the peptide. The pulse sequence is presented in Fig. 2.5b. If the crosspeak intensity of ^{31}P and lipid $(CH_2)_n$ rises much faster with ^{1}H mixing time in the membrane-bound peptide sample than in the pure lipids, it suggests that the peptide is rigid and inserted into the bilayers. The ^{1}H spin diffusion mixing time was 64 – 225 ms, and A pre-evolution ^{1}H T_2 filter (0.8 – 2 ms) was used to remove the magnetization on peptides. 1D ^{13}C detected ^{1}H spin diffusion experiment was conducted to test the effectiveness of the T_2 filter, which should be long enough to remove the methyl signals from the peptides. The ^{1}H-^{31}P CP contact time was 4 ms to get reasonable sensitivity because the lipids are quite mobile. The ^{1}H chemical shifts of the POPE/POPG membrane were assigned via the well-known ^{13}C chemical shifts by a ^{13}C-^{1}H 2D correlation experiment.

2.2.4 Dipolar Correlation Experiments for Measuring Backbone (ϕ, ψ) Torsion Angles (NCCN and HNCH)

NCCN and HNCH are robust methods for measuring the backbone torsion angles (ϕ, ψ) of proteins. The ψ angles of Arg_4 and Arg_{11} were measured using the NCCN technique, which correlates the $^{15}N_i$-$^{13}C\alpha_i$ and $^{13}CO_i$- $^{15}N_{i+1}$ dipolar couplings to obtain the relative orientation of the two bonds [17, 18]. $^{13}C\alpha$-^{13}CO double quantum coherence was excited using the SPC-5 sequence [10], and evolves under the REDOR-recoupled ^{13}C-^{15}N dipolar interaction [19]. A pair of ^{13}C spectra were collected at each C-N mixing time, and the S/S_0 values of the CO and Cα signals were averaged and plotted as a function of mixing time to yield the ψ-angle dependent curve. The ϕ angles were measured using the HNCH technique, which correlates the $^{1}H^{N}$-^{15}N and $^{13}C\alpha$-$^{1}H\alpha$ dipolar couplings [20]. The experiment yields H^{N}-N-Cα-Hα angle (ϕ_H), which is related to the ϕ-angle according to $\phi = \phi_H + 60^{\circ}$. The NCCN and HNCH experiments were conducted at 253 K on the trehalose-protected membrane samples and 233 K on the hydrated membrane samples to make sure backbones of the peptides are rigid. The typical spinning speed is slower than 6 kHz.

2.2.5 Separation of Undistorted Powder Patterns by Effortless Recoupling (SUPER) and Recoupling of Chemical Shift Anisotropy (ROCSA)

SUPER [21] and ROCSA [22] are useful techniques for directly obtaining chemical shift anisotropy (CSA) powder pattern under MAS. Both are 2D experiments correlating CSA powder pattern with isotropic chemical shift. Molecular motion in the membrane can reduce the CSA, so these experiments provide dynamic information of the proteins in the membrane. The SUPER experiment is suitable for sparsely labeled samples at slow MAS (< 4 kHz). The ROCSA experiment is suitable for uniformly ^{13}C-labeled samples under faster MAS (5 - 10 kHz). The recoupling field strengths are 12.12 times of the spinning speed (ν_r) for SUPER and 4.283 times for ROCSA. The CSA scaling factors are 0.155 and 0.272 for SUPER and ROCSA, respectively.

2.2.6 ^{1}H Rotating-Frame Spin-Lattice Relaxation Times ($T_{1\rho}$)

^{1}H $T_{1\rho}$ were measured using a ^{13}C-detected ^{1}H LG spin-lock (LGSL) experiment. The use of magic-angle spin lock suppresses ^{1}H spin diffusion so that only the $T_{1\rho}$ of protons directly attached to the ^{13}C is detected. $T_{1\rho}$ provides information on the rates of microsecond timescale motion. Fig. 2.6 shows the pulse sequence of $T_{1\rho}$ measurement.

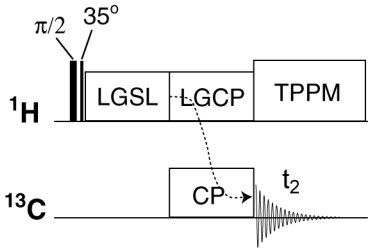

Figure 2.6. Pulse sequence for measuring ^{1}H $T_{1\rho}$.

2.3 Simulation

2.3.1 Orientation Calculations of Dipolar Couplings of ^{15}N-^{1}H, ^{13}Cα-^{1}H Vectors and CSA of ^{13}C' and ^{15}N in Rigid β-Sheet Peptides in the Membrane

The dipolar couplings of ^{15}N-^{1}H, ^{13}Cα-^{1}H vectors and the CSA of ^{13}C' and ^{15}N are calculated using in-house FORTRAN program. By fitting the experimental data, these simulations provide information on the orientation of the peptide in the membrane. The program defines a molecule-fixed coordinate system that reflects the β-strand axis and β-sheet plane geometry and calculates the anisotropic frequencies based on the orientation of the magnetic field ($\mathbf{B_0}$) in this coordinate system. The z-axis of this reference system, the β-strand axis, is defined and calculated as the average orientation of an even number of consecutive C'_{i-1}-N_i bonds. The local β-sheet plane is defined as the common plane containing the z-axis and a specific C=O vector. The tilt angle τ is the angle between this strand axis (z-axis) and the $\mathbf{B_0}$ field. The ρ angle was defined as the angle between the C=O bond of the specific residue and the common plane (y-z plane) formed by the strand axis and the $\mathbf{B_0}$ field. The molecular bonds necessary for defining the orientations of the ^{15}N and ^{13}C' chemical shift tensors and ^{15}N-^{1}H and ^{13}Cα-^{1}H dipolar tensors, including the N-H^N, Cα-H, C'-O, C'-N, and N-Cα bonds, were extracted from the PDB coordinates of the peptides of interest. We studied PG-1 (1PG1), RTD-1 (1HVZ) and an ideal antiparallel β-hairpin structure which was constructed using (ϕ, ψ) torsion angles of (-137˚, +135˚) for the strand residues, and (-45˚, +85˚) and (+155˚, -20˚) for the *i*+1 and *i*+2 residues of the β-turn. The chemical shifts and dipolar couplings were calculated from the scalar products between $\mathbf{B_0}$ and the respective tensors as $\mathbf{B_0}$ is rotated through all combinations of (τ, ρ) angles. The typical step size is 1˚. The unique angular range of τ is 0˚ to 180˚, while ρ is sampled over the entire 360˚ range. We refer to this β-sheet based program as the relative orientation program. Best fits to the experimental spectrum were determined by finding the minimum root-mean squared deviation (RMSD) between the experiment and the simulations.

To accurately visualize the results of the orientation calculation, and to determine the orientation of non-ideal β-hairpins, whose sheet axis and sheet plane orientations are ill defined, a second Fortran program without an internal β-sheet reference system was used.

The program defines the $\mathbf{B_0}$ orientation by a polar angle β and an azimuthal angle α in the default PDB coordinate system [2]. This program is referred to as the absolute orientation program. The best-fit (α, β) angles were converted into the Cartesian coordinates (sinβcosα, sinβsinα, cosβ) of a vector from the origin and added to the PDB file. This vector, the bilayer normal, was rotated together with the molecule until it was vertical on the screen, thus giving the exact orientation of the β-sheet peptide [2].

2.3.2 Simulations of REDOR curves and Gaussian Distribution of the Distances

REDOR curves were simulated using an in-house Fortran program. The distance distribution was assumed to consist of Gaussian functions $\exp(-(r - r_0)^2/2\sigma^2)$, where σ is the half-width-at-half-maximum and r_0 is the center of the Gaussian. The composite REDOR curve was the weighted average of the individual single-distance REDOR curves.

2.3.3 Multi-Spin Simulations of REDOR Curves by SIMPSON

The SIMPSON program [23] was used to simulate the REDOR curves considering multi-spin situation in ^{13}C-^{31}P distance measurement. Since the lipid-to-peptide ratio is much larger than one, it is relevant to consider how inclusion of multiple ^{31}P spins coupled to each ^{13}C affects the distance results. The input code is shown in Appendix A.

2.3.4 Simulations of DIPSHIFT Data of X-H, X-H_2 and X-H_3 Dipolar Tensors

DIPSHIFT curves were simulated using an in-house Fortran program. The input parameters are different for X-H, X-H_2 and X-H_3 dipolar tensors. The dipolar tensor is $(-\omega_{XH}/2, -\omega_{XH}/2, \omega_{XH})$ for X-H, $(-\omega_{XH}, 0, \omega_{XH})$ for X-H_2 and 1:3 weighted average of $(-\omega_{XH}/2, -\omega_{XH}/2, \omega_{XH})$ and $(-\omega_{XH}/6, -\omega_{XH}/6, \omega_{XH}/3)$ for X-H_3. The input codes are shown in Appendix B.

2.3.5 Simulations of HNCH and NCCN Data

HNCH and NCCN curves were simulated using in-house Fortran programs. The input parameters for HNCH are similar to the DIPSHIFT simulation. The input code for the HNCH program is shown in Appendix C. Best fits to the experimental data were evaluated by calculating the minimum root-mean squared deviation (RMSD) between the experiment and the simulation.

References

[1] K. Barlos, D. Papaioannou, D. Theodoropoulos, Efficient One-Pot Synthesis of N-Trityl Amino-Acids, J. Org. Chem. 47 (1982) 1324-1326.

[2] S. Yamaguchi, T. Hong, A. Waring, R.I. Lehrer, M. Hong, Solid-state NMR investigations of peptide-lipid interaction and orientation of a beta-sheet antimicrobial peptide, protegrin, Biochemistry 41 (2002) 9852-9862.

[3] K.J. Hallock, K. Henzler Wildman, D.K. Lee, A. Ramamoorthy, An innovative procedure using a sublimable solid to align lipid bilayers for solid-state NMR studies, Biophys. J. 82 (2002) 2499-2503.

[4] C.P. Jaroniec, B.A. Tounge, C.M. Rienstra, J. Herzfeld, R.G. Griffin, Measurement of C-13-N-15 distances in uniformly C-13 labeled biomolecules: J-decoupled REDOR, J. Am. Chem. Soc. 121 (1999) 10237-10238.

[5] N. Sinha, K. Schmidt-Rohr, M. Hong, Compensation for pulse imperfections in rotational-echo double-resonance NMR by composite pulses and EXORCYCLE, J. Magn. Reson. 168 (2004) 358-365.

[6] M.G. Munowitz, R.G. Griffin, G. Bodenhausen, T.H. Huang, Two-Dimensional Rotational Spin-Echo Nuclear Magnetic-Resonance in Solids - Correlation of Chemical-Shift and Dipolar Interactions, J. Am. Chem. Soc. 103 (1981) 2529-2533.

[7] M. Hong, J.D. Gross, C.M. Rienstra, R.G. Griffin, K.K. Kumashiro, K. Schmidt-Rohr, Coupling amplification in 2D MAS NMR and its application to torsion angle determination in peptides, J. Magn. Reson. 129 (1997) 85-92.

[8] D. Huster, S. Yamaguchi, M. Hong, Efficient beta-sheet identification in proteins by solid-state NMR spectroscopy, J. Am. Chem. Soc. 122 (2000) 11320-11327.

[9] D. Huster, L.S. Xiao, M. Hong, Solid-state NMR investigation of the dynamics of the soluble and membrane-bound colicin Ia channel-forming domain, Biochemistry 40 (2001) 7662-7674.

[10] M. Hohwy, C.M. Rienstra, C.P. Jaroniec, R.G. Griffin, Fivefold symmetric homonuclear dipolar recoupling in rotating solids: application to double-quantum spectroscopy., J. Chem. Phys. 110 (1999) 7983-7992.

[11] B.J. vanRossum, C.P. deGroot, V. Ladizhansky, S. Vega, H.J.M. deGroot, A method for measuring heteronuclear (1H-13C) distances in high speed MAS NMR, J. Am. Chem. Soc. 122 (2000) 3465-3472.

[12] M. Hong, X.L. Yao, K. Jakes, D. Huster, Investigation of molecular motions by Lee-Goldburg cross-polarization NMR Spectroscopy, J. Phys. Chem. B 106 (2002) 7355-7364.

[13] K.K. Kumashiro, K. Schmidt-Rohr, O.J. Murphy, K.L. Ouellette, W.A. Cramer, L.K. Thompson, A novel tool for probing membrane protein structure: solid-state NMR with proton spin diffusion and X-nucleus detection, J. Am. Chem. Soc. 120 (1998) 5043-5051.

[14] J.J. Buffy, T. Hong, S. Yamaguchi, A. Waring, R.I. Lehrer, M. Hong, Solid-State NMR Investigation of the Depth of Insertion of Protegin-1 in Lipid Bilayers Using Paramagnetic Mn2+, Biophys. J. 85 (2003) 2363-2373.

[15] G.J. Gallagher, M. Hong, L.K. Thompson, Solid-state NMR spin diffusion for measurement of membrane-bound peptide structure: gramicidin A, Biochemistry 43 (2004) 7899-7906.

[16] D. Huster, X.L. Yao, M. Hong, Membrane protein topology probed by H-1 spin diffusion from lipids using solid-state NMR spectroscopy, J. Am. Chem. Soc. 124 (2002) 874-883.

[17] P.R. Costa, J.D. Gross, M. Hong, R.G. Griffin, Solid-state NMR measurement of Psi in peptides: a NCCN 2Q-heteronuclear local field experiment, Chem. Phys. Lett. 280 (1997) 95-103.

[18] X. Feng, Y.K. Lee, D. Sandstroem, M. Eden, H. Maisel, A. Sebald, M.H. Levitt, Direct determination of a molecular torsional angle by solid-state NMR, Chem. Phys. Lett. 257 (1996) 314-320.

[19] T. Gullion, J. Schaefer, Rotational echo double resonance NMR, J. Magn. Reson. 81 (1989) 196-200.

[20] M. Hong, J.D. Gross, R.G. Griffin, Site-resolved determination of peptide torsion angle phi from the relative orientations of backbone N-H and C-H bonds by solid-state NMR, J. Phys. Chem. B 101 (1997) 5869-5874.

[21] S.F. Liu, J.D. Mao, K. Schmidt-Rohr, A robust technique for two-dimensional separation of undistorted chemical-shift anisotropy powder patterns in magic-angle-spinning NMR, J. Magn. Reson. 155 (2002) 15-28.

[22] J.C.C. Chan, R. Tycko, Recoupling of chemical shift anisotropies in solid-state NMR under high-speed magic-angle spinning and in uniformly 13C-labeled systems., J. Chem. Phys. 118 (2003) 8378-8389.

[23] M. Bak, J.T. Rasmussen, N.C. Nielsen, SIMPSON: a general simulation program for solid-state NMR spectroscopy, J. Magn. Reson. 147 (2000) 296-330.

Chapter 3

Intermolecular Packing and Alignment in an Ordered β-Hairpin Antimicrobial Peptide Aggregate from 2D Solid-State NMR

Published in J. Am. Chem. Soc.

2005, 127, 13919-13927

Ming Tang [a], Alan J. Waring [b], and Mei Hong [a]

[a] Department of Chemistry, Iowa State University, Ames, IA 50011

[b] Department of Medicine, University of California at Los Angeles School of Medicine, Los Angeles, California 90095

Abbreviations

PG-1: Protegrin-1

POPC: 1-palmitoyl-2-oleoyl-*sn*-glycerol-3-phosphatidylcholine

PBS: phosphate buffer saline

MAS: magic-angle spinning

LG: Lee-Goldburg

CP: cross polarization

PDSD: proton-driven spin diffusion

WISE: wideline separation

Abstract

The aggregation and packing of a membrane-disruptive β-hairpin antimicrobial peptide, protegrin-1 (PG-1), in the solid state is investigated to understand its oligomerization and hydrogen bonding propensity. Incubation of PG-1 in phosphate buffer saline produced well-ordered nanometer-scale aggregates, as indicated by ^{13}C and ^{15}N NMR linewidths,

chemical shifts and by electron microscopy. Two-dimensional ^{13}C and ^{1}H spin diffusion experiments using C-strand and N-strand labeled peptides indicate that the β-hairpin molecules in these ordered aggregates are oriented parallel to each other with like strands lining the intermolecular interface. In comparison, disordered and lyophilized peptide samples are randomly packed with both parallel and antiparallel alignments. The PG-1 aggregates show significant immobilization of the Phe ring near the β-turn, further supporting the structure ordering. The intermolecular packing of PG-1 found in the solid state is consistent with its oligomerization in lipid bilayers. This solid-state aggregation approach may be useful for determining the quaternary structure of peptides in general and for gaining insights into the oligomerization of antimicrobial peptides in lipid bilayers in particular.

Introduction

Protegrin-1 (PG-1) is a small β-hairpin peptide from porcine leukocytes that has potent and broad-spectrum antimicrobial activities [1]. Its minimum inhibitory concentrations lie in the range of a few micrograms per milliliter, more than two orders of magnitude stronger than existing antibiotics such as vancomysin [2]. PG-1 carries out this remarkably efficient microbicidal function by destroying the cell membranes of the target organisms. Yet how the peptide interacts with lipid bilayers on a molecular level, and what properties of the amino acid sequence of the peptide endow its potent and selective membrane-disruptive ability, remain a mystery. Understanding PG-1 structure can shed light on the structure-function relationships of a large class of similar β-sheet antimicrobial peptides [3].

Using solid-state NMR chemical shift anisotropy and dipolar coupling measurements, we recently found that PG-1 is immobilized in POPC bilayers, where the lipid acyl chains contain 16-18 carbons, but undergoes rigid-body uniaxial rotation in DLPC bilayers, where the lipid chains have only 12 carbons [4]. The immobilization in the biologically relevant membrane thickness of POPC bilayers suggests that the peptide is aggregated. Using ^{19}F spin diffusion NMR, we found that PG-1 is dimerized in POPC bilayers [5]. This prompted questions pertaining to the dimer structure: are the β-hairpins aligned parallel or antiparallel to each other? Which strand of the hairpin forms the dimer interface? Understanding the detailed membrane-bound dimer structure, which is essentially determined by intermolecular

hydrogen bonding, is important for deciphering the mechanism of action of the peptide. Since PG-1 is highly cationic, similar to most antimicrobial peptides [6], the dimer structure can also provide useful insights into the energetic driving force for the insertion of PG-1 into the hydrophobic membrane.

The crystal structures of two β-sheet antimicrobial peptides outside the lipid or detergent environments have been determined to understand the oligomerization and mechanisms of action of these peptides in the membrane [7,8]. It was found that these β-sheet peptides form dimers in the crystal, stabilized by a combination of hydrophobic interactions and hydrogen bonds. Since the crystal structure of PG-1 is not available, an alternative approach for gaining insights into the oligomerization of this peptide in the membrane is to create well-ordered and lipid-free peptide aggregates whose intermolecular packing can be determined by solid-state NMR. Studying the structure of lipid-free ordered aggregates has the practical advantages that it has high sensitivities due to the avoidance of lipid dilution and that it does not suffer from the dynamic disorder common to membrane systems. The solid-state aggregate structure can then be compared with independently determined membrane-bound oligomeric structure to shed light on the importance of various non-covalent interactions and the environment to peptide oligomerization.

In addition to antimicrobial peptides, other examples of β-strand peptide oligomerization include the amyloid peptide fibrils found in neurodegenerative diseases such as the Alzheimer's disease [9]. The packing and high-resolution structure of the Alzheimer's β-peptide $A\beta_{1-40}$ have recently been determined using solid-state NMR [10]. Whether PG-1 can form similar extended fibrils is not obvious, since the 18-residue disulfide-linked peptide has a much smaller shape anisotropy than typical amyloid-forming peptides, making the free energy reduction of oligomerization less significant than the longer β-strand peptides. The β-hairpin fold of PG-1 also presents an additional degree of complexity and novelty to the oligomerization: since the two strands of the hairpin share intramolecular hydrogen bonds in the plane of the β-sheet, aggregation can occur either with like strands or unlike strands lining the intermolecular interface.

Two general NMR strategies are available for determining the oligomeric structure of peptides. The first involves distance measurements on site-specifically labeled samples [11-13]. A

number of solid-state NMR techniques already exist for measuring site-specific distances with high accuracy [14,15]. However, the success of this approach depends crucially on the labeling positions, otherwise one may not be able to extract measurable distances even for well packed molecules. The second approach bypasses this difficulty by increasing the number of labeled sites in the peptide, and uses more qualitative methods such as spin diffusion [16] to determine the proximity of spins between different molecules [17,18].

In this work, we show that β-hairpin PG-1 can indeed form ordered aggregates on the tens-of-nanometer scale by suitable solution incubation, and we have determined the molecular packing and alignment in these aggregates using 2D ^{13}C and ^{1}H spin diffusion NMR. Several residues in PG-1 are uniformly labeled in ^{13}C and ^{15}N. Distance-dependent ^{13}C and ^{1}H spin diffusion produces cross peaks in the 2D spectra whose intensities provide semi-quantitative constraints on the intermolecular distances. In this way, we have determined both the identity of the β-strand lining the intermolecular interface and the mutual alignment of the strands.

Materials and Methods

Uniformly ^{13}C, ^{15}N-labeled Gly, Leu, Phe, and Val were purchased from Isotec (Miamisburg, OH) and Cambridge Isotope Laboratory (Andover, MA) and converted to Fmoc derivatives by Synpep Corp. (Dublin, CA). PG-1 (NH_2-RGGRLCYCRRRFCVCVGR-$CONH_2$) was synthesized using Fmoc solid-phase peptide synthesis protocols and purified by HPLC as described previously [19]. The labeled amino acids were incorporated at residues F_{12}, V_{14} and G_{17} on one sample, and G_3 and L_5 on another sample (Figure 3.1).

Preparation of PG-1 samples

Ordered PG-1 aggregates were prepared by dissolving the purified and lyophilized peptide in pH 7 phosphate buffer saline (PBS) containing 10 mM phosphates and 100 mM sodium chloride. The concentration of the peptide was typically 2-3 mM. The solution was incubated at room temperature for 2-3 weeks with gentle shaking. The solution was then centrifuged and the precipitate was collected and dried for ~8 hours before being packed into NMR rotors for magic-angle spinning (MAS) experiments. Mixed aggregates and 20%

diluted aggregate samples were prepared by co-incubating appropriate amounts of the starting compounds in the PBS solution. The untreated PG-1 samples were taken directly from the purified and lyophilized peptide without solution incubation.

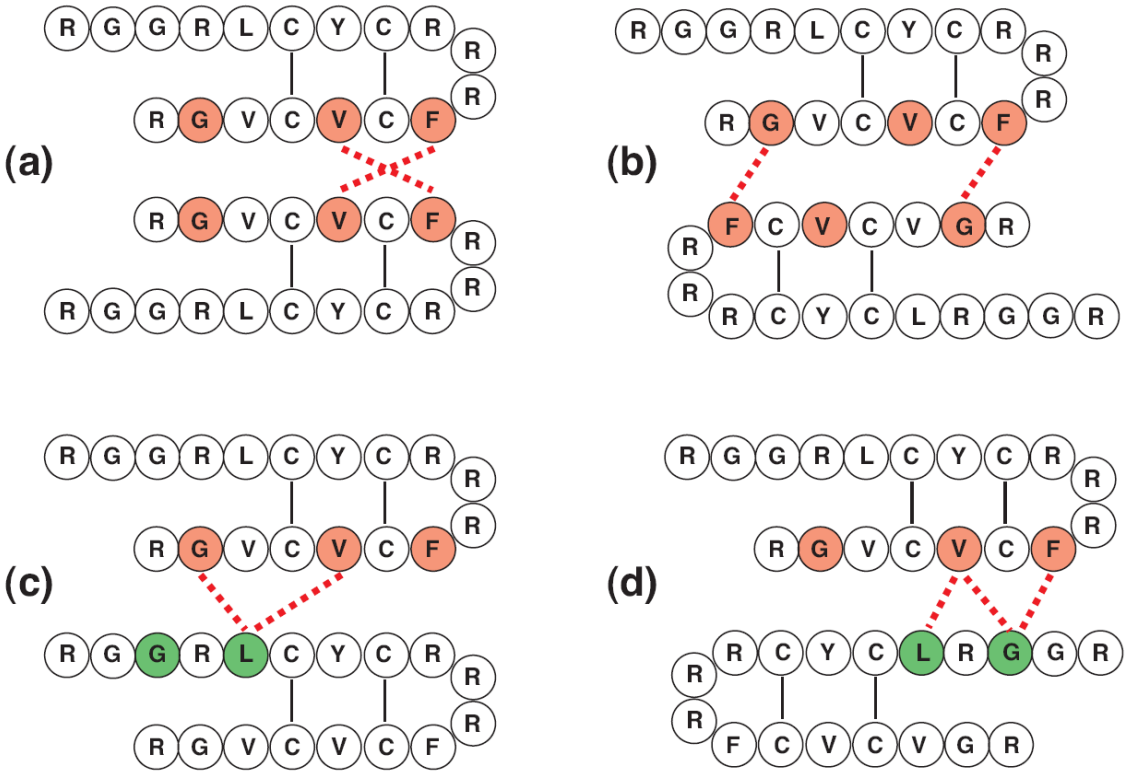

Figure 3.1. Schematics of possible modes of packing of the β-hairpin peptide PG-1. (a) NCCN parallel packing. (b) NCCN antiparallel packing. (c) NCNC parallel packing. (d) NCNC antiparallel packing. Colored residues indicate uniformly ^{13}C, ^{15}N-labeled residues used in this study. Dashed lines indicate expected short intermolecular distances.

Solid-state NMR experiments

NMR experiments were carried out on a Bruker (Karlsruhe, Germany) DSX-400 spectrometer operating at a resonance frequency of 400.49 MHz for ^{1}H, 100.70 MHz for ^{13}C and 40.58 MHz for ^{15}N. A triple-resonance MAS probe equipped with a 4 mm spinning module was used for the experiments. Low temperature experiments were conducted by cooling the bearing air through a Kinetics Thermal Systems XR air-jet sample cooler (Stone Ridge, NY). The temperature was maintained within ±1 K of the desired value and the

spinning speed was regulated to within ±3 Hz. Typical 90°pulse lengths were 5 μs for ^{13}C and ^{15}N and 3.5-4.0 μs for ^{1}H. ^{1}H-^{13}C and ^{1}H-^{15}N cross-polarization (CP) contact times were 0.7 ms and 1 ms, respectively. Typical recycle delays were 2 s. ^{13}C and ^{15}N chemical shifts were referenced externally to the α-Gly ^{13}C' signal at 176.4 ppm on the TMS scale and the N-acetyl-valine ^{15}N signal at 122.0 ppm on the NH_3 scale, respectively. Secondary shifts were calculated after converting the random coil chemical shift values [20] onto the same scales.

2D ^{1}H-driven ^{13}C spin diffusion (PDSD) and ^{1}H spin diffusion (CHHC) experiments were carried out at a spinning speed of 5.4 kHz to minimize sideband overlap and to avoid rotational resonance effects [15] between directly bonded ^{13}C labels. A ω_1 spectral window of 20 kHz and a maximum t_1 evolution time of 11.2 ms were used. The mixing time τ_{SD} was 400 ms for ^{13}C spin diffusion and 200 μs for ^{1}H spin diffusion. For the CHHC experiment, a short ^{13}C-^{1}H CP contact time τ_{CP} of 120 μs was used before and after the ^{1}H mixing period to ensure site-specific detection of the ^{1}H-^{1}H distances. The short τ_{SD} for the CHHC experiment minimizes the relay mechanism for strong cross peaks [21].

The 2D wide-line separation (WISE) experiment [22] was used to measure ^{1}H–^{1}H dipolar couplings in various PG-1 samples. After ^{1}H evolution under ^{1}H–^{1}H and ^{1}H–^{13}C dipolar couplings for a maximum of 0.13 ms, the ^{1}H magnetization is transferred site-specifically to ^{13}C by a 200 μs Lee–Goldburg (LG) CP period [23,24].

^{13}C–^{1}H dipolar couplings between directly bonded C–H spins were measured using the 2D LG–CP experiment [25]. The evolution time (t_1) is the LG-CP contact time, during which ^{1}H spin diffusion is suppressed by the magic-angle spin lock. At short contact times (< 1 ms), only directly bonded ^{13}C–^{1}H dipolar couplings are observed. ^{13}C detection during t_2 resolves these ^{13}C-^{1}H couplings according to the ^{13}C isotropic chemical shifts. The spinning speed was 10 kHz and the maximum t_1 was 2.56 ms. To achieve polarization transfer, the first sideband matching condition, $\omega_{1C} = \omega_{eff,H} - \omega_r$, was used, where ω_{1C} is the ^{13}C spin-lock field strength and $\omega_{eff,H}$ is the ^{1}H effective spin-lock field strength. Due to the short ^{1}H $T_{1\rho}$ values, which make it difficult to measure small C–H couplings, we used a constant-time version of the experiment where a variable ^{1}H LG spin-lock period was added before CP to make the total ^{1}H spin-lock time constant [24,26].

^{1}H rotating-frame spin–lattice relaxation times ($T_{1\rho}$) were measured using a ^{13}C-detected ^{1}H LG spin-lock experiment. Again, the use of magic-angle spin lock suppresses ^{1}H spin diffusion so that only the $T_{1\rho}$ of protons directly attached to the ^{13}C is detected. The ^{1}H spin-lock field strength was 70 kHz.

Electron microscopy

Aliquots of incubated PG-1 solutions were applied to formvar coated nickel grids. After adsorption for ~2 minutes, the excess fluid was wicked off and the samples were negatively stained by applying a drop of 1% phosphotungstic acid (PTA; pH 6.2) for <1 minute. Excess fluid was wicked off, and grids were air-dried. TEM images were collected using a JEOL 1200EX II scanning and transmission electron microscope (Japan Electron Optics Laboratory, Peabody, MA) at 80 kV and digitally collected with a Megaview III camera and SIS Pro software (Soft Imaging Systems, Inc., Lakewood, CO).

Results

Figure 3.1 shows a schematic diagram of the possible modes of intermolecular packing of the β-hairpin PG-1. For simplicity, only two molecules are shown in each model, but the pattern is expected to repeat in a well-ordered aggregate on the tens of nanometer scale. In addition to the possibilities of parallel and antiparallel alignment, the β-hairpins can arrange themselves either with the like strand facing each other, NCCN, or with the unlike strands facing each other, NCNC. This results in four distinct packing motifs. These different modes of packing can be distinguished with suitably labeled peptides. If the peptide is labeled solely on one strand, then the presence of intermolecular cross peaks will prove the existence of the like-strand NCCN packing. If such cross peaks are absent, and NCNC packing is suspected, then a mixture of N-strand labeled and C-strand labeled peptide should give rise to intermolecular cross peaks. To determine whether the strands align in a parallel or antiparallel fashion, the labeling positions on each strand should include both ends. Figure 3.1 highlights the labeled residues in two PG-1 samples: one incorporates uniformly ^{13}C, ^{15}N-labeled F_{12}, V_{14} and G_{17} (red), while the other contains uniformly labeled G_3 and L_5 (green). The figure also shows the short intermolecular distances expected for each packing motif

(dashed lines): F_{12}-V_{14} for NCCN parallel packing (a), F_{12}-G_{17} for NCCN antiparallel packing (b), G_{17}-L_5 and possibly V_{14}-L_5 for NCNC parallel packing (c), and F_{12}-G_3, V_{14}-G_3 and V_{14}-L_5 for NCNC antiparallel packing (d).

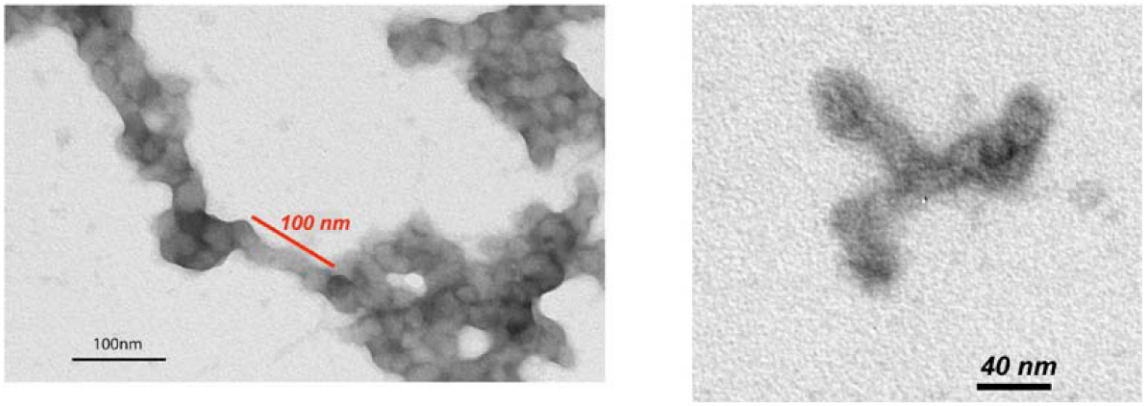

Figure 3.2. TEM images of PG-1 aggregates incubated from the PBS solution. The aggregates are ~100 nm long and ~10 nm wide.

Preparation and characterization of ordered PG-1 aggregates

To obtain well-ordered PG-1 aggregates, we incubated the peptide in PBS solution for an extended period of time with gentle agitation. Representative TEM images of the resulting aggregates (Figure 3.2) show a network of strands that are ~10 nm wide and ~100 nm long. These are shorter and thicker than the amyloid fibrils of Aβ peptides [10] and distinct in morphology. To assess the local order and secondary structure of the aggregates on the sub-nanometer length scale, we compared the ^{13}C and ^{15}N linewidths and chemical shifts of the incubated and untreated peptide. Figure 3.3(a-b) shows the ^{13}C CP-MAS spectra of [U-F_{12}, V_{14}, G_{17}] PG-1 in the two different states. Several changes are observed. First, the spectral resolution is much enhanced by incubation: for example, V_{14} Cα and F_{12} Cα became much better resolved, and the C' peak narrowed. Second, the Cα and C' peaks in the PG-1 aggregate shifted upfield compared to the untreated peptide, while the resolved Val Cβ shifted downfield. Based on the known ^{13}C secondary shifts of proteins [27,28], these indicate that the incubation procedure makes the β-strand conformation of PG-1 more ideal. In comparison, the N-strand labeled peptide, [U-G_3, L_5] PG-1, showed less pronounced

chemical shift and linewidth differences between the incubated and the untreated peptide, suggesting that incubation has less influence on the N-strand structure than the C-strand.

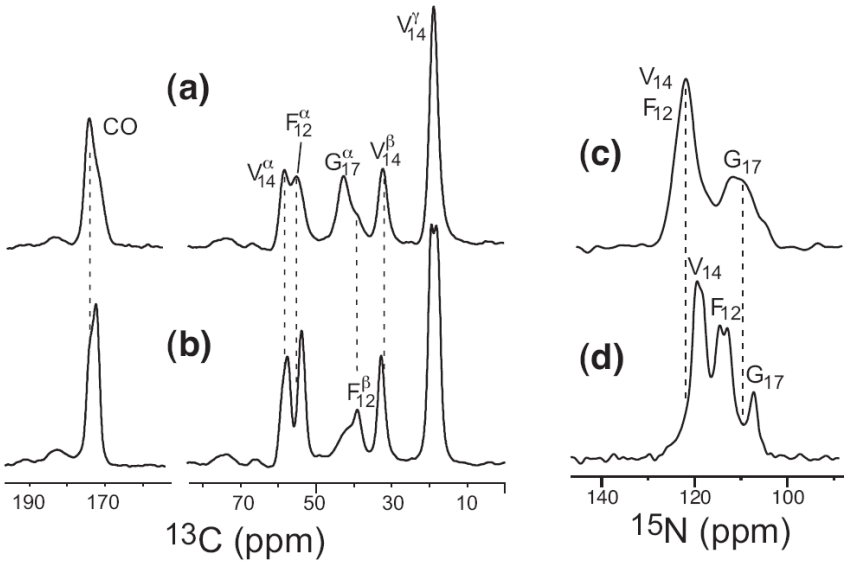

Figure 3.3. (a-b) ^{13}C MAS spectra of (a) untreated and (b) aggregated [U-F_{12}, V_{14}, G_{17}] PG-1. (c-d) ^{15}N MAS spectra of (c) untreated and (d) aggregated [U-F_{12}, V_{14}, G_{17}] PG-1.

Similar to the ^{13}C spectra, the ^{15}N CP-MAS spectra of [U-F_{12}, V_{14}, G_{17}] PG-1 show pronounced line narrowing and chemical shift changes for the aggregate sample. The most significant line narrowing occurs at G_{17} ^{15}N, while F_{12} undergoes the largest chemical shift change, ~8 ppm upfield compared to the untreated peptide. Since this change is larger than the typical ^{15}N secondary shift range of Phe [27], we suspect that it results from the location of Phe ^{15}N at the β-turn, whose chemical shift trend is not as well represented in the protein database as the canonical α-helix and β-sheet structures.

Figure 3.4 summarizes the linewidths (a) and ^{13}C isotropic shift (b) differences between the aggregated and untreated PG-1. The aggregate sample exhibits narrower linewidths and stronger β-sheet secondary shifts for most resolved sites, especially for the C-strand residues. For the untreated PG-1, residues in the middle of the strands such as V_{14} and L_5 have narrower lines than terminal residues such as G_{17}. The residue experiencing the most significant ordering is F_{12}, whose Cα and Cβ linewidths both decreased, while the terminal

G_{17} Cα showed slightly increased disorder in the aggregate. Thus, the β-turn region of the peptide is most strongly structured by incubation. Taken together, the NMR chemical shifts and the microscopy data indicate that the PG-1 aggregates prepared by solution incubation are well ordered on the tens of nanometer scale but do not have the micron-length order typical of amyloid fibrils. Since the purpose of this study is to determine the molecular-level packing and hydrogen bonding of PG-1, the nanometer-scale order evident from the NMR linewidths and chemical shifts is sufficient for further analysis using 2D ^{13}C correlation experiments.

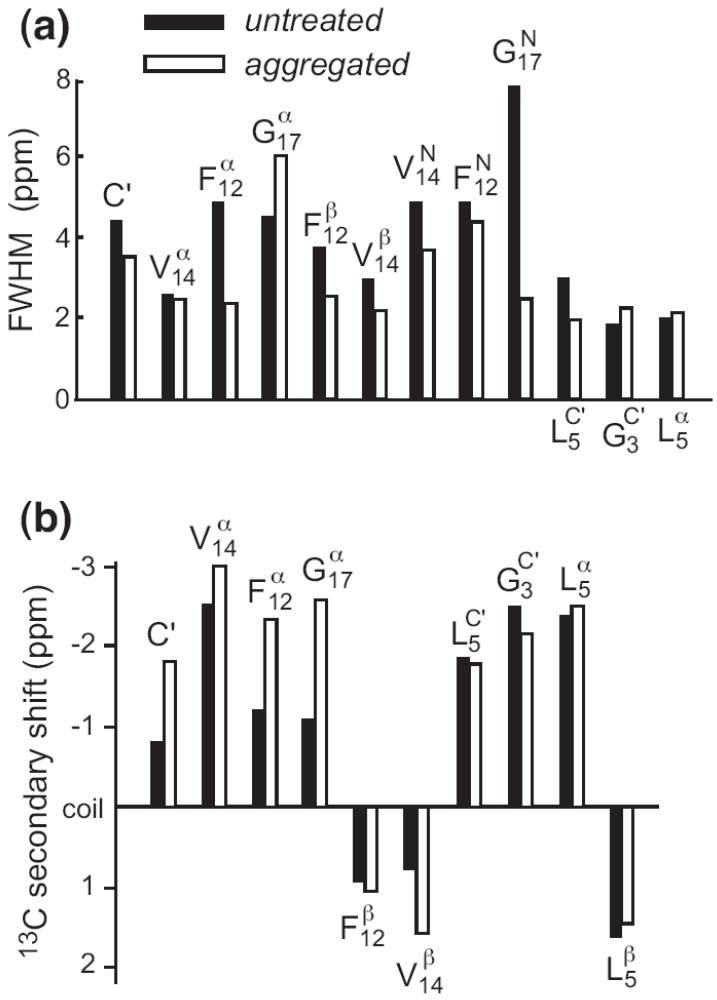

Figure 3.4. (a) ^{13}C and ^{15}N full widths at half maximum (FWHM) of untreated (filled) and aggregated (open) PG-1. Smaller linewidths indicate a more ordered conformation. (b) ^{13}C secondary shifts of untreated (filled)

and aggregated (open) PG-1, calculated as $\Delta_{obs} - \Delta_{rc}$, where Δ_{rc} are the random-coil chemical shifts. Negative Cα and C' secondary shifts and positive Cβ secondary shifts indicate a stronger β-sheet conformation.

Packing motif of PG-1 aggregates

To determine the packing of PG-1 β-hairpins in the ordered aggregate, we carried out 2D ^{1}H-driven ^{13}C spin diffusion (PDSD) experiments. Figure 3.5 shows the spectra of [U-F_{12}, V_{14}, G_{17}] PG-1 as 100% labeled aggregates (a), 20% diluted aggregates (b), and untreated 100% labeled peptide (c). A mixing time of 400 ms was used in all experiments to achieve complete exchange. The spectrum of the 100% PG-1 aggregate (Figure 3.5a) shows significant cross peaks between F_{12} and V_{14} such as α-α, α-β, and α-γ. These immediately suggest that the C-strand of one β-hairpin packs closely with another C-strand, causing intermolecular spin diffusion. There are no visible $V_{14} - G_{17}$ cross peaks and only a weak F_{12}-G_{17} α-α peak, suggesting that the two C-strands are mainly aligned in a parallel fashion. Since the G_{17}α signal is broad and partially overlaps with the F_{12}β peak at room temperature, we carried out the 2D PDSD experiment on the same sample at 253 K, when the G_{17}α intensity is stronger and better resolved. Under this condition, the F_{12}α-G_{17}α cross peak decrease even further, about half the intensity of the room-temperature peak (Table 3.1), confirming that the F_{12}-G_{17} α–α distance is long.

To rule out the possibility that the observed F_{12}-V_{14} cross peaks are intramolecular, we measured the 2D spectrum of a 20% diluted PG-1 aggregate sample, prepared by co-dissolving 20% labeled peptide with 80% unlabeled peptide in the incubation buffer. Dilution removes intermolecular ^{13}C-^{13}C spin diffusion, so that any inter-residue cross peaks in the spectra must result from intramolecular spin diffusion. Figure 3.5b shows the 2D spectrum of this diluted sample. Indeed, the F_{12}-V_{14} cross peaks are either significantly attenuated or disappeared. The only remaining strong cross peaks are intra-residue ones, confirming that the three labeled residues are sufficiently separated along the β-strand not to cause intramolecular ^{13}C spin diffusion within 400 ms.

To determine whether the NCCN parallel packing of the PG-1 aggregate is specifically caused by incubation, we measured the 2D spectrum of the untreated peptide. The spectrum (Figure 3.5c) shows much weaker F_{12}-V_{14} cross peaks but a stronger F_{12}-G_{17} α-

α peak. These indicate that in the absence of incubation, PG-1 does not adopt any preferential alignment in the solid state, but has a combination of parallel and antiparallel alignments. The fact that the F_{12}-G_{17} α-α peak is visible while V_{14}-G_{17} cross peaks are not suggests that it is easier for the two ends of the β-hairpin to contact each other than for the peptide to align in an out-of-registry fashion, which is necessary for forming V_{14}-G_{17} contacts.

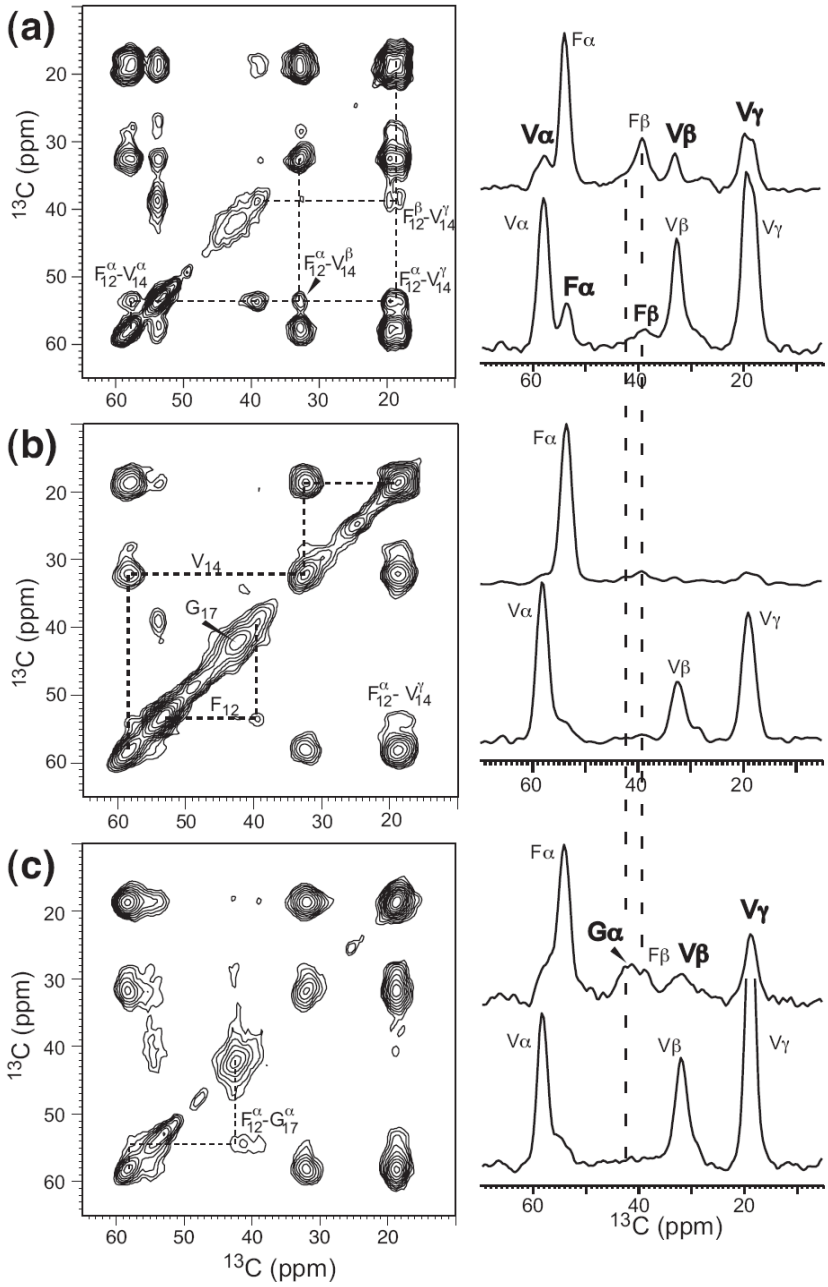

Figure 3.5. 2D ^{1}H-driven ^{13}C spin diffusion spectra of [U-F_{12}, V_{14}, G_{17}] PG-1. (a) 100% labeled aggregates. (b) 20% labeled aggregates. (c) 100% labeled but untreated peptide. For each 2D spectrum, the 1D cross sections through the $F_{12}\alpha$ (top row) and $V_{14}\alpha$ (bottom row) slices are shown on the right, where inter-residue cross peaks are indicated in bold.

Since cross peaks in the long-mixing-time PDSD experiment can arise from both direct and relay transfer, we carried out a ^{1}H spin diffusion experiment (CHHC) with a short τ_{SD} of 200 μs [18,21] to verify the direct nature of the intermolecular $F_{12}\alpha$-$V_{14}\alpha$ contact. It has been shown that within a τ_{SD} of ~200 μs, strong cross peaks in the CHHC spectrum reflect direct ^{1}H-^{1}H distances of within ~3 Å [18,21]. Figure 3.6 shows the CHHC spectra of aggregated (a) and untreated (b) PG-1. The F_{12}-V_{14} Hα-Hα cross peak is strong in the aggregate but is absent in the untreated peptide. In fact, the inter-residue α-α cross peak in the aggregate is higher than some of the intra-residue cross peaks such as Vα-Vγ (see 1D cross sections in Figure 3.6c). Compared to the highest intra-residue cross peak, Fα-Fβ, which has a distance of ~2.5 Å, the $F_{12}\alpha$-$V_{14}\alpha$ peak intensity is ~70%, strongly suggesting a direct $F_{12}\alpha$-$V_{14}\alpha$ distance of ~3 Å.

If the NCCN packing motif is correct, then there should be N-strand to N-strand interfaces in the PG-1 aggregate in addition to the C-strand to C-strand interfaces. To test this, we measured the 2D ^{13}C spin diffusion spectrum of the N-strand labeled aggregate, [U-G_3, L_5] PG-1 (Figure 3.7a). The spectrum shows well-resolved and clearly visible G_3-L_5 C'-α and C'-Cγ peaks, indicating the existence of short intermolecular distances. Again, the contribution of intramolecular spin diffusion is negligible based on the 2D spectrum of a 20% diluted sample (Supporting Information). Thus, the N-strand does form hydrogen bonds with another N-strand and in a parallel fashion. However, the cross peaks of the peptide aggregate are not significantly stronger than those of the untreated peptide (Table 3.1), suggesting that the N-strand is not as tightly packed as the C-strand, or that the N-terminus is more disordered than the C-terminus in the aggregate.

The presence of the NCCN packing does not in itself rule out the alternative NCNC packing. To determine if the ordered PG-1 aggregate contains a mixture of NCCN and NCNC packing motifs, we prepared an equimolar mixture of N- and C-strand labeled PG-1

aggregates. If NCNC packing is present, then cross peaks between the N-strand residues on one molecule and the C-strand residues on another molecule are expected. The 2D spectrum of this mixture is shown in Figure 3.7b. No N-strand to C-strand cross peaks such as V_{14}-L_5 (dashed circles) and V_{14}-G_3 are detected. The only visible intermolecular cross peaks are the F_{12}-V_{14} peaks due to NCCN parallel packing. These F_{12}-V_{14} peaks are about a factor of 2 weaker than the C-strand sample (Table 3.1), consistent with the 1:1 molar ratio of the two labeled peptides. Thus, NCCN parallel packing is the sole repeat motif in the ordered PG-1 sample.

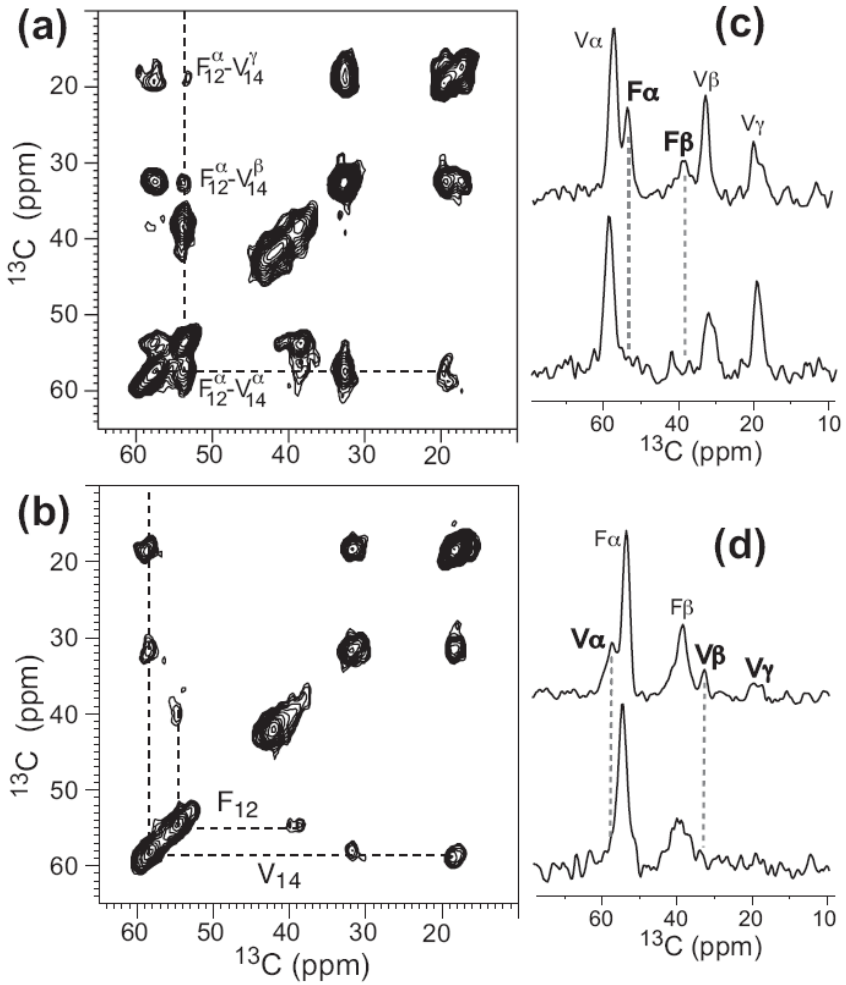

Figure 3.6. 2D CHHC spectra of (a) aggregated and (b) untreated [U-F_{12}, V_{14}, G_{17}] PG-1. (c) V_{14} Cα cross section for the aggregated (top) and untreated (bottom) peptide. (d) F_{12} Cα cross section for the aggregated (top) and untreated (bottom) peptide. Strong V_{14}-F_{12} cross peaks are observed only in the aggregate sample.

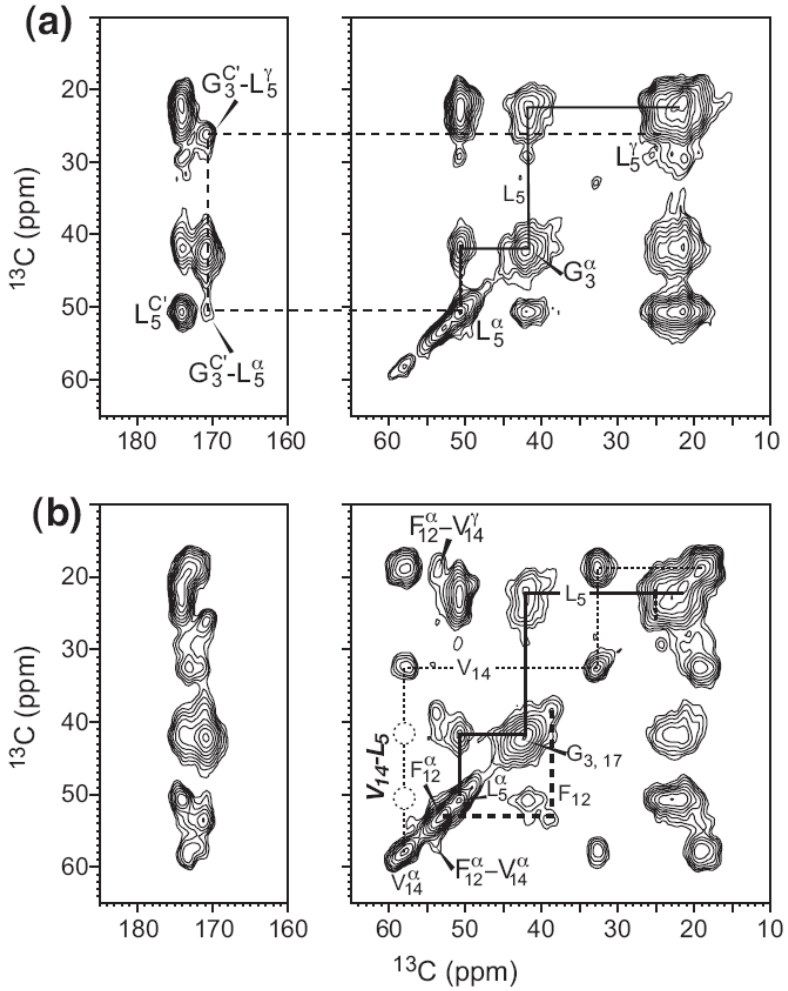

Figure 3.7. 2D ^{1}H-driven ^{13}C spin diffusion spectra of (a) 100% labeled [U-G_3, L_5] PG-1 aggregates, and (b) 1:1 mixture of [U-G_3, L_5] PG-1 and [U-F_{12}, V_{14}, G_{17}] PG-1 aggregates. Inter-strand cross peaks such as V_{14}-L_5 (dashed circles) are absent in (b).

Table 3.1 lists the normalized cross peak intensities of the 100% N- and C-strand labeled PG-1 aggregates and their untreated equivalents, and of the 1:1 mixture. The cross peak intensities (I_{AB} and I_{BA}) were normalized to the diagonal peaks (I_{AA} and I_{BB}) according to $I = (I_{AB} + I_{BA})/(I_{AA} + I_{BB})$, and the uncertainties were propagated accordingly from the noise of the 2D spectra. It can be seen that the ordered PG-1 aggregates show significantly stronger C-strand cross peaks than the untreated peptide in both the PDSD and CHHC spectra, while the N-strand cross peaks have more comparable intensities between the two samples. The F_{12}-V_{14} cross peak intensities in the mixed aggregate are about half the

intensities of the pure C-strand aggregate, consistent with the fact that only 50% of the C-strand labeled PG-1 is packed next to another C-strand labeled peptide.

Table 3.1. Cross peak intensities (I_{AB} and I_{BA}) of aggregated and untreated PG-1, normalized with respect to the diagonal peaks (I_{AA} and I_{BB}) according to $I = (I_{AB} + I_{BA})/(I_{AA} + I_{BB})$[a]. Uncertainties were propagated from the peak intensities and the noise of the 2D spectra.

Cross peaks		C-strand aggregate		N-strand aggregate	Untreated peptide		Mixed aggregate
		PDSD	CHHC	PDSD	PDSD	CHHC	PDSD
F_{12}-V_{14}	α–α	$0.256^{\pm0.012}$	$0.412^{\pm0.032}$	NA[b]	$0.212^{\pm0.018}$	$0.192^{\pm0.024}$	$0.146^{\pm0.010}$
	α–β	$0.270^{\pm0.014}$	$0.148^{\pm0.022}$	NA	$0.198^{\pm0.024}$	$0.062^{\pm0.026}$	$0.122^{\pm0.010}$
	α–γ	$0.290^{\pm0.010}$	$0.108^{\pm0.026}$	NA	$0.120^{\pm0.006}$	$0.050^{\pm0.014}$	$0.170^{\pm0.006}$
	β–α	$0.200^{\pm0.022}$	$0.256^{\pm0.046}$	NA	$0.088^{\pm0.028}$	$0.080^{\pm0.032}$	$0.190^{\pm0.020}$
	β–β	$0.254^{\pm0.026}$	$0.124^{\pm0.030}$	NA	$0.216^{\pm0.040}$	$0.084^{\pm0.038}$	$0.142^{\pm0.024}$
	β–γ	$0.182^{\pm0.012}$	$0.148^{\pm0.036}$	NA	$0.066^{\pm0.008}$	$0.038^{\pm0.016}$	$0.148^{\pm0.010}$
F_{12}	α–β	$0.506^{\pm0.020}$	$0.596^{\pm0.038}$	NA	$0.380^{\pm0.040}$	$0.460^{\pm0.036}$	$0.282^{\pm0.012}$
V_{14}	α–β	$0.782^{\pm0.022}$	$0.422^{\pm0.028}$	NA	$0.844^{\pm0.026}$	$0.412^{\pm0.028}$	$0.582^{\pm0.018}$
	α–γ	$0.730^{\pm0.012}$	$0.272^{\pm0.034}$	NA	$0.682^{\pm0.008}$	$0.320^{\pm0.014}$	$0.566^{\pm0.010}$
	β–γ	$0.798^{\pm0.014}$	$0.428^{\pm0.026}$	NA	$0.608^{\pm0.008}$	$0.428^{\pm0.016}$	$0.630^{\pm0.010}$
F_{12}-G_{17}	α–α	$0.186^{\pm0.018}$ ($0.108^{\pm0.022}$[c])	$0.158^{\pm0.028}$	NA	$0.238^{\pm0.022}$	$0.102^{\pm0.022}$	NA
G_3-L_5	C'–α	NA	NA	$0.086^{\pm0.010}$	$0.086^{\pm0.008}$	NA	NA
	C'–γ	NA	NA	$0.114^{\pm0.006}$	$0.134^{\pm0.008}$	NA	NA

[a]: For pure unmixed samples, intensities below ~0.200 are weak cross peaks reflecting long-range distances.

[b]: Not applicable.

[c]: Measured at 253 K.

Segmental mobility of PG-1 aggregates

The ^{13}C linewidths of the untreated and aggregated PG-1 samples (Figure 3.4) indicate that the F_{12} at the β-turn experiences the most significant line narrowing upon

aggregation, while the G_{17} Cα signal broadened rather than narrowed, suggesting chain-end disorder in the aggregate. To determine the origin of the order and disorder in the aggregate, we measured the ^{1}H-^{1}H dipolar coupling, ^{13}C-^{1}H dipolar coupling, and ^{1}H $T_{1\rho}$ of untreated and aggregated PG-1. These dynamic parameters are resolved by the ^{13}C isotropic shifts and the use of spin-diffusion free LGCP. Figure 3.8 shows the 2D ^{1}H WISE spectrum of the aggregate (a) and its Phe cross sections (solid lines, b), which are superimposed with the cross sections of the untreated peptide (dashed lines). The untreated PG-1 exhibits narrower ^{1}H widths than the aggregate, indicating larger amplitude motion. Moreover, the mobility difference increases down the Phe sidechain. Both PG-1 samples are more mobile than amino acid Phe: the latter has an aromatic ^{1}H-^{1}H coupling of 53 kHz, compared to 25 kHz for the aggregate sample and 9 kHz for the untreated peptide. Cooling the aggregated PG-1 to 253 K increased the ^{1}H-^{1}H couplings but did not completely immobilize the ring (Table 3.2). Consistently, the ^{13}C-^{1}H dipolar couplings also show that the Phe ring in the untreated peptide undergoes larger-amplitude motion than in the aggregate (Table 3.2). Compared to F_{12}, no substantial coupling differences are found at G_{17} and V_{14} between the untreated and aggregated samples. Taken together, these indicate that incubation immobilizes the hairpin tip more significantly than the C-terminus.

Table 3.2. ^{1}H FWHM of the WISE spectra, ^{13}C-^{1}H dipolar couplings and ^{1}H $T_{1\rho}$ values for aggregated and untreated PG-1.

		^{1}H FWHM (kHz)			^{13}C-^{1}H coupling (kHz)		$T_{1\rho}$ (ms)		
	Site	aggregated		untreated	aggregated	untreated	aggregated		untreated
		293 K	253 K	293 K	293 K	293 K	293 K	253 K	293 K
F_{12}	Cα	53	56	47	12	11	5.5	11	3.4
	Cβ	61	70	50	12	11	2.1	8.4	1.6
	Cδ	25	38	9	6.3	3.9	1.6	5.4	2.0
V_{14}	Cα	48	52	50	12	12	7.2	11	6.9
	Cβ	30	38	30	6.6	8.6	4.1	8.6	4.6
	Cγ	11	13	8	2.3	4.3	5.2	9.1	5.8
G_{17}	Cα	52	66	45	11	11	1.5	6.0	2.0

The ^{1}H $T_{1\rho}$ values of F_{12} Hα and Hβ increased in the aggregate (Table 3.2), while the $T_{1\rho}$ of G_{17} Hα decreased. These suggest that the broadening of G_{17} Cα signal in the aggregate (Figure 3.3) results from increased microsecond-timescale motions of the C-terminus, which interfere with CP, while the opposite occurs at F_{12} Cα and Cβ, making the β-turn more ordered and rigid in the aggregate.

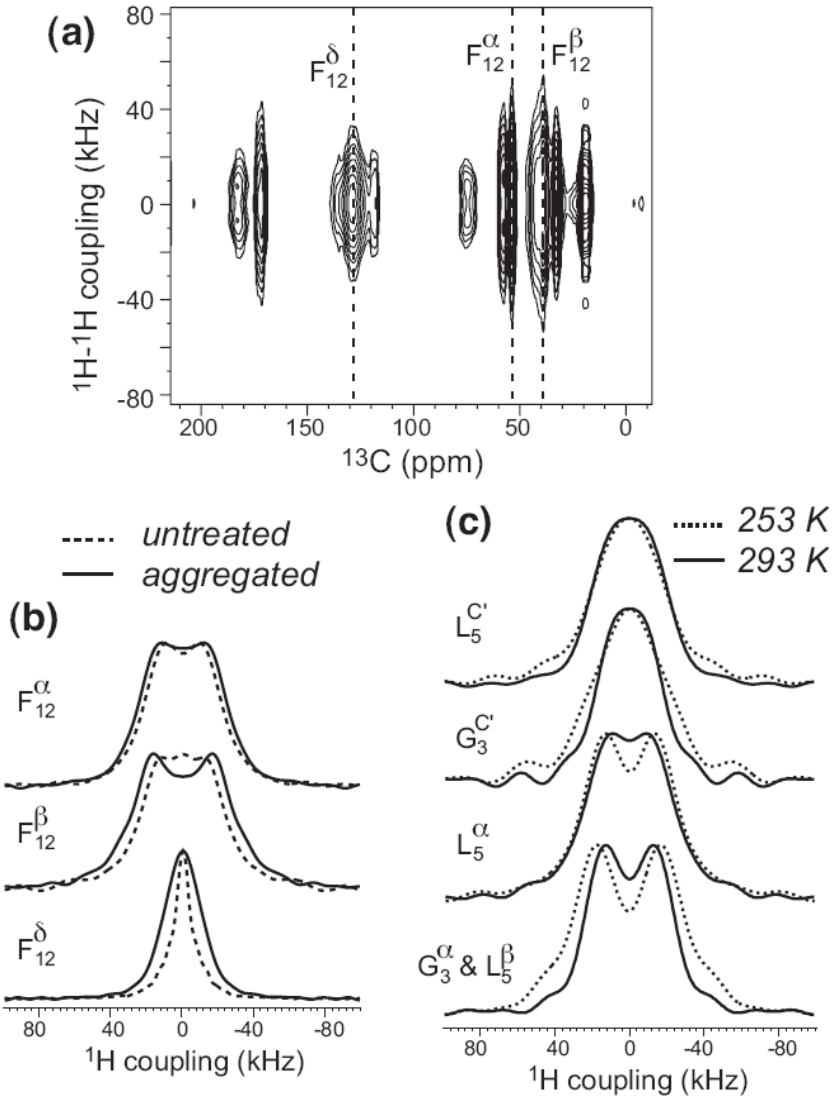

Figure 3.8. ^{1}H-^{1}H dipolar couplings of PG-1. (a) 2D WISE spectrum of [U-F_{12}, V_{14}, G_{17}] PG-1 aggregates. (b) 1D ^{1}H cross sections of untreated (dashed line) and aggregated (solid line) [U-F_{12}, V_{14}, G_{17}] PG-1. (c) 1D ^{1}H

cross sections of [U-G_3, L_5] PG-1 aggregates at 293 K (solid line) and 253 K (dotted line). The backbone dynamics are negligibly unaffected by the temperature, indicating that the N-terminal backbone is immobilized at room temperature.

Discussion

The NMR linewidths and chemical shifts and microscopy images indicate unambiguously that well-ordered PG-1 aggregates on the scale of at least tens of nanometers can be created by appropriate solution incubation. The fact that these aggregates do not show micron-length order may result from a combination of the highly charged nature of the peptide and the low aspect ratio of the molecule.

The cross peak patterns in the 2D ^{13}C correlation spectra indicate that the β-hairpins in the ordered aggregate pack and hydrogen-bond in a parallel fashion with like strands facing each other. Both ^{1}H-driven ^{13}C spin diffusion and direct ^{1}H spin diffusion support this conclusion. The ^{13}C spin diffusion experiment detects C-C distances up to ~7.5 Å within a mixing time of 500 ms, as shown by a recent study of α-spectrin SH3 domain [29], while the ^{1}H spin diffusion experiment can detect H-H distances of within ~3 Å in a short τ_{SD} of ~200 μs. Thus, the absence or weakness of ^{13}C spin-diffusion cross peaks such as F_{12}-G_{17} (Figure 3.5a) and V_{14}-L_5 (Figure 3.7b) in the peptide aggregates indicates C-C distances longer than 7.5 Å. These rule out the antiparallel packing and the alternate strand packing (NCNC) models. The strongest constraint in favor of NCCN parallel packing is the significant $F_{12}\alpha$-$V_{14}\alpha$ cross peak in the peptide aggregate. Although this cross peak in the ^{13}C spin diffusion spectrum could arise both from direct and relay transfer, the fact that in the ^{1}H spin diffusion spectrum this α–α peak is stronger than most inter- and intra-residue sidechain cross peaks (Table 3.1) rules out the possibility of sidechain-mediated relay transfer. In addition, the untreated peptide shows clear PDSD intra-residue sidechain cross peaks (Figure 3.5c) but negligible $F_{12}\alpha$-$V_{14}\alpha$ intensity, indicating that relay transfer alone is insufficient to produce backbone α–α cross peaks if the distance is large.

The fact that the N-strand G_3C'-$L_5\alpha$ peak is lower than the $F_{12}\alpha$-$V_{14}\alpha$ peak in the PDSD spectra is partly due to the larger isotropic shift difference between C' and Cα, which attenuates ^{13}C spin diffusion. It may also reflect a true looseness of the N-strand interface,

which is also manifested in the less dramatic line narrowing of the N-strand residues compared to the untreated peptide. This looseness may result from the more hydrophilic nature of the N-strand due to the presence of an additional Arg residue (R_4) in the middle of the strand (Figure 3.1). In comparison, the C-terminal strand is almost entirely hydrophobic, thus stabilizing the C-strand interface.

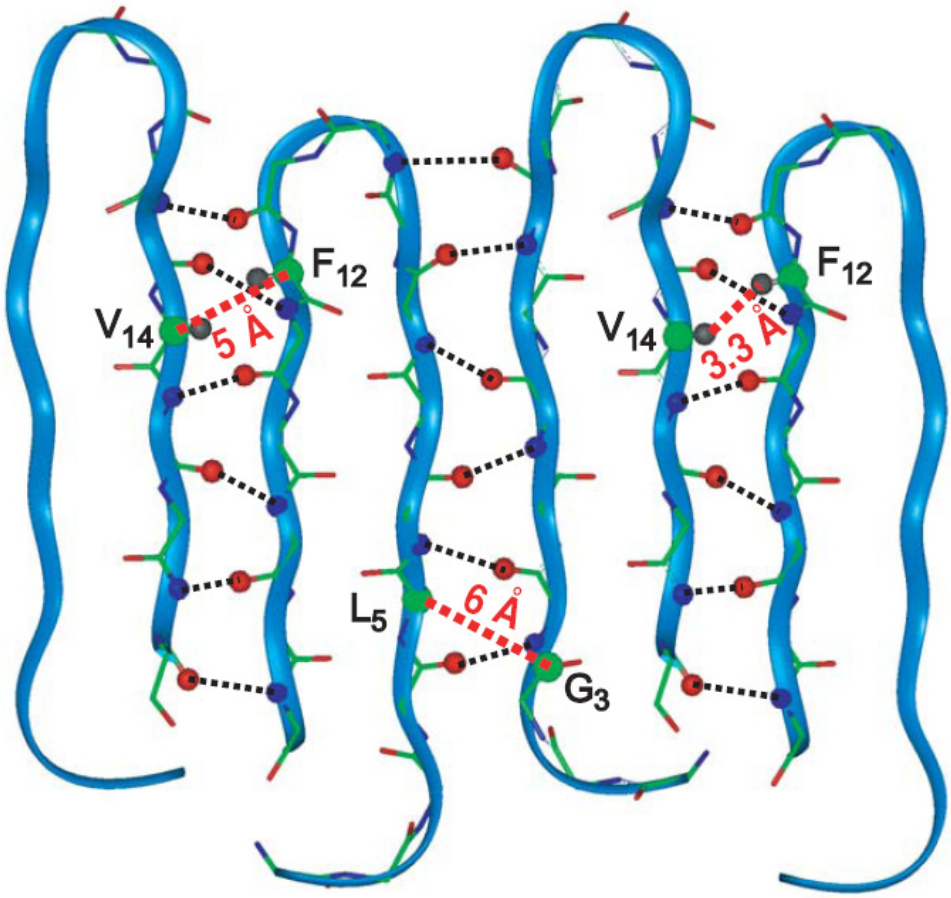

Figure 3.9. NCCN parallel packing model of PG-1 in the ordered aggregates. Short intermolecular F_{12}-V_{14} and G_3-L_5 Cα–Cα and Hα-Hα distances are highlighted in red. The N-O hydrogen bonds stabilizing the oligomeric structure are shown as black dashed lines.

Figure 3.9 illustrates the NCCN parallel packing model of PG-1, showing both a C-strand interface and an N-strand interface. The positions of the neighboring PG-1 molecules are adjusted to satisfy hydrogen bond lengths, $R_{N\text{-}O}$, of 2.4 – 3.6 Å [30,31]. Since parallel β-

strands do not have an inversion symmetry, each pair of residues has two different internuclear distances across the intermolecular interface. Based on this model, F_{12} and V_{14} have Cα-Cα distances of ~5 Å and 10 Å, the shorter of which is the main contributor to the cross peak in the PDSD spectra. Remarkably, a short F_{12}-V_{14} Hα-Hα distance of ~3.3 Å is found, confirming that the strong α–α cross peak in the CHHC spectrum (Figure 3.6a) is due to direct polarization transfer. At the N-strand interface, a G_3-L_5 C'-Cα distance of ~6 Å is found, also within the detection limit of ^{13}C spin diffusion. For the NCCN antiparallel packing motif yields F_{12} - V_{14} Cα-Cα distances of ~13 Å, well beyond the detection limit of ^{13}C spin diffusion.

This NCCN packing model shows the direction of the intermolecular contacts to be sideways in the β-hairpin plane rather than perpendicular to the plane. This reflects the fact that the sidechains occupy space above and below the β-hairpin plane, which makes it difficult to establish close inter-plane backbone contacts. In amyloid fibrils, the typical distances between adjacent β-sheet planes are 9 – 10 Å according to fiber diffraction studies [32,33]. Such a large distance is beyond the detection limit of ^{13}C spin diffusion. Moreover, since inter-plane packing is not driven by hydrogen bonding, any accidental close contact between β-sheet planes would be non-specific in nature; thus the untreated peptide should show similarly strong backbone cross peaks as the peptide aggregate if inter-sheet contact were the cause of these backbone cross peaks. This is inconsistent with the experimental data.

The NCCN parallel alignment of PG-1 in the ordered solid-state aggregate determined from these 2D experiments is consistent with the results obtained in the membrane [34]. There, intermolecular C-H, C-N, and C-F dipolar couplings between site-specifically labeled residues constrained the PG-1 dimer structure to be parallel with two C-strands lining the dimer interface. Thus, the PG-1 aggregate formed from solution incubation outside the membrane has similar packing and hydrogen bonding to the membrane-bound PG-1 oligomer. This suggests that the common driving force for the oligomerization of this β-hairpin peptide inside and outside the membrane is hydrogen bonding. This approach of preparing ordered aggregates may thus be useful for studying the oligomerization of other membrane-active β-sheet antimicrobial peptides whose crystal structures are not available.

It is interesting to note that a solution NMR study of PG-1 in DPC micelles [35] showed that the peptide forms antiparallel dimers with the C-strand lining the dimer interface. The reason for the different alignment between the micelle environment on the one hand, and the aggregate and lipid bilayer environments on the other, is presently unclear. However, since detergent micelles are well known to impose curvature strains onto peptides, one possible reason for the difference may be the different shape anisotropies of the parallel and antiparallel PG-1 dimers. The parallel NCCN packing observed in the aggregate and in the lipid bilayer puts six Arg residues at two adjacent β-turns in close proximity, forming a strongly amphipathic structure. The electrostatic repulsion between these β-turns may make the parallel dimer a bulkier structure than the antiparallel dimer, where the Arg-rich β-turns are spaced apart. The compact antiparallel dimer structure may thus be favored in the constrained micelle environment, while the parallel packing may be stabilized in the bilayer because the stronger amphipathic structure facilitates peptide insertion into the membrane.

Conclusion

We demonstrated the preparation and quaternary-structure determination of well-ordered aggregates of the β-hairpin antimicrobial peptide PG-1. 2D ^{13}C correlation experiments mediated by both ^{13}C and ^{1}H spin diffusion showed intermolecular backbone cross peaks that are consistent with parallel packing of the β-hairpins, with like strands lining the intermolecular interface. The C-strand interfaces in the aggregate are more tightly packed and ordered than the N-strand interfaces, which may result from the stronger hydrophobic nature of the C-strand. The ordered packing of the aggregate is supported by the reduced mobility of the Phe ring at the β-turn compared to the untreated peptide. This is the first time a β-hairpin peptide is shown to be able to form ordered aggregates on the length scale of tens of nanometers. The hydrogen-bonding propensity of PG-1 in the solid state determined from this study sheds light on the oligomerization of this peptide in lipid bilayers, which will be presented elsewhere [34].

Acknowledgement: We thank Dr. Tracey M. Pepper for help in the electron microscopy measurements. This work is supported by the National Institutes of Health grant GM-066976 to M. H. and grants AI-22839 and AI-37945 to A.J. W.

Supporting Information Available: The 2D ^{13}C correlation spectra of [U-F_{12}, V_{14}, G_{17}] PG-1 aggregates at 253 K and of 20% diluted [U-G_3, L_5] PG-1 are included.

References

(1) Bellm, L.; Lehrer, R. I.; Ganz, T. *Exp. Opin. Invest. Drugs* **2000**, *9*, 1731-1742.

(2) Muhle, S. A.; Tam, J. P. *Biochemistry* **2001**, *40*, 5777-5785.

(3) Epand, R. M.; Vogel, H. J. *Biochim. Biophys. Acta* **1999**, *1462*, 11-28.

(4) Buffy, J. J.; Waring, A. J.; Lehrer, R. I.; Hong, M. *Biochemistry* **2003**, *42*, 13725-13734.

(5) Buffy, J. J.; Waring, A. J.; Hong, M. *J. Am. Chem. Soc.* **2005**, *127*, 4477-4483.

(6) Hancock, R. E.; Lehrer, R. *Trends Biotechnol.* **1998**, *16*, 82-88.

(7) Hoover, D. M.; Rajashankar, K. R.; Blumenthal, R.; Puri, A.; Oppenheim, J. J.; Chertov, O.; Lubkowski, J. *J. Biol. Chem.* **2000**, *275*, 32911-32918.

(8) Hill, C. P.; Yee, J.; Selsted, M. E.; Eisenberg, D. *Science* **1991**, *251*, 1481-1485.

(9) Murphy, R. M. *Annu. Rev. Biomed. Eng.* **2002**, *4*, 155-174.

(10) Petkova, A. T.; Ishii, Y.; Balbach, J. J.; Antzutkin, O. N.; Leapman, R. D.; Delaglio, F.; Tycko, R. *Proc. Natl. Acad. Sci. USA* **2002**, *99*, 16742-16747.

(11) Balbach, J. J.; Petkova, A. T.; Oyler, N. A.; Antzutkin, O. N.; Gordon, D. J.; Meredith, S. C.; Tycko, R. *Biophys. J.* **2002**, *83*, 1205-1216.

(12) Yang, J.; Weliky, D. P. *Biochemistry* **2003**, *42*, 11879-11890.

(13) Toke, O.; O'Connor, R. D.; Weldeghiorghis, T. K.; Maloy, W. L.; Glaser, R. W.; Ulrich, A. S.; Schaefer, J. *Biophys. J.* **2004**, *87*, 675-687.

(14) Gullion, T.; Schaefer, J. *J. Magn. Reson.* **1989**, *81*, 196-200.

(15) Raleigh, D. P.; Levitt, M. H.; Griffin, R. G. *Chem. Phys. Lett.* **1988**, *146*, 71-76.

(16) Suter, D.; Ernst, R. R. *Phys. Rev. B* **1985**, *32*, 5608-5627.

(17) Tycko, R.; Ishii, Y. *J. Am. Chem. Soc.* **2003**, *125*, 6606-6607.

(18) Lange, A.; Luca, S.; Baldus, M. *J. Am. Chem. Soc.* **2002**, *124*, 9704-9705.

(19) Yamaguchi, S.; Hong, T.; Waring, A.; Lehrer, R. I.; Hong, M. *Biochemistry* **2002**, *41*, 9852-9862.

(20) Wishart, D. S.; Bigam, C. G.; Holm, A.; Hodges, R. S.; Sykes, B. D. *J. Biomol. NMR* **1995**, *5*, 67-81.

(21) Lange, A.; Seidel, K.; Verdier, L.; Luca, S.; Baldus, M. *J. Am. Chem. Soc.* **2003**, *125*, 12640-12648.

(22) Schmidt-Rohr, K.; Clauss, J.; Spiess, H. W. *Macromolecules* **1992**, *25*, 3273-3277.

(23) Lee, M.; Goldburg, W. I. *Phys. Rev.* **1965**, *140*, A1261-A1271.

(24) Yao, X. L.; Conticello, V. P.; Hong, M. *Magn. Reson. Chem.* **2004**, *42*, 267-275.

(25) vanRossum, B. J.; Forster, H.; deGroot, H. J. M. *J. Magn. Reson.* **1997**, *124*, 516-519.

(26) Tekely, P.; Gerardy, V.; Palmas, P.; Canet, D.; Retournard, A. *Solid State Nucl. Magn. Reson.* **1995**, *4*, 361-367.

(27) Wishart, D. S.; Sykes, B. D.; Richards, F. M. *J. Mol. Biol.* **1991**, *222*, 311-333.

(28) Spera, S.; Bax, A. *J. Am. Chem. Soc.* **1991**, *113*, 5490-5492.

(29) Castellani, F.; vanRossum, B.; Diehl, A.; Schubert, M.; Rehbein, K.; Oschkinat, H. *Nature* **2002**, *420*, 98-102.

(30) deDios, A. C.; Oldfield, E. *J. Am. Chem. Soc.* **1994**, *116*, 11485-11488.

(31) Creighton, T. E. *Proteins: Structures and molecular properties;* 2nd Ed. ed.; W.H. Freeman and Co.: New York, 1993.

(32) Jarvis, J. A.; Craik, D. J.; Wilce, M. C. *Biochem. Biophys. Res. Commun.* **1993**, *192*, 991-998.

(33) Malinchik, S. B.; Inouye, H.; Szumowski, K. E.; Kirschner, D. A. *Biophys. J.* **1998**, *74*, 537-545.

(34) Mani, R.; Tang, M.; Wu, X.; Buffy, J. J.; Waring, A.; Hong, M. *Biochemistry* **2005**, *45*, 8341-8349.

(35) Roumestand, C.; Louis, V.; Aumelas, A.; Grassy, G.; Calas, B.; Chavanieu, A. *FEBS Lett.* **1998**, *421*, 263-267.

Supporting Information

Intermolecular Packing and Alignment in an Ordered β-Hairpin Antimicrobial Peptide Aggregate from 2D Solid-State NMR

Ming Tang[a], Alan J. Waring [b], and Mei Hong [a]

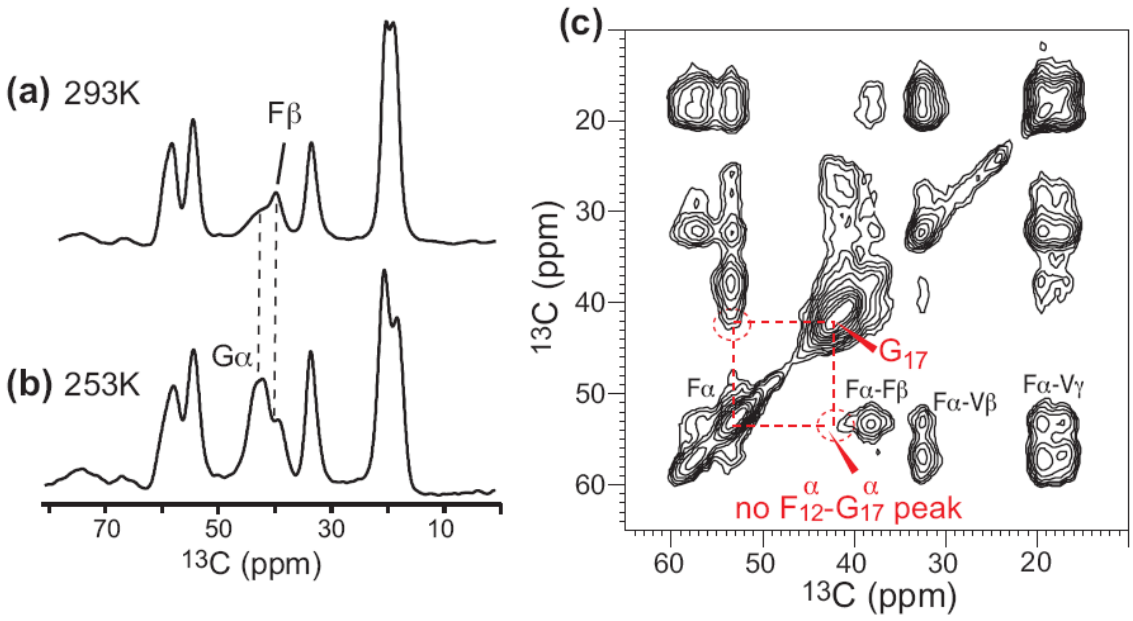

Figure S3.1. Lack of F_{12}-G_{17} α–α cross peak in the 100% [U-F_{12}, V_{14}, G_{17}] PG-1 aggregate at 253 K. (a) 1D ^{13}C spectrum of the peptide at 293 K. (b) 1D ^{13}C spectrum of the peptide at 253 K. The G_{17}α peak has higher intensity and is better resolved from the F_{12}β signal at 253 K. (c) 2D ^{13}C spin diffusion spectrum of the peptide aggregate at 253 K with a mixing time of 400 ms. Despite the prominent diagonal G_{17}α peak, the F_{12}-G_{17} α-α cross peak is negligible (dashed circles), confirming that the C-strands are aligned in a parallel fashion in the aggregate.

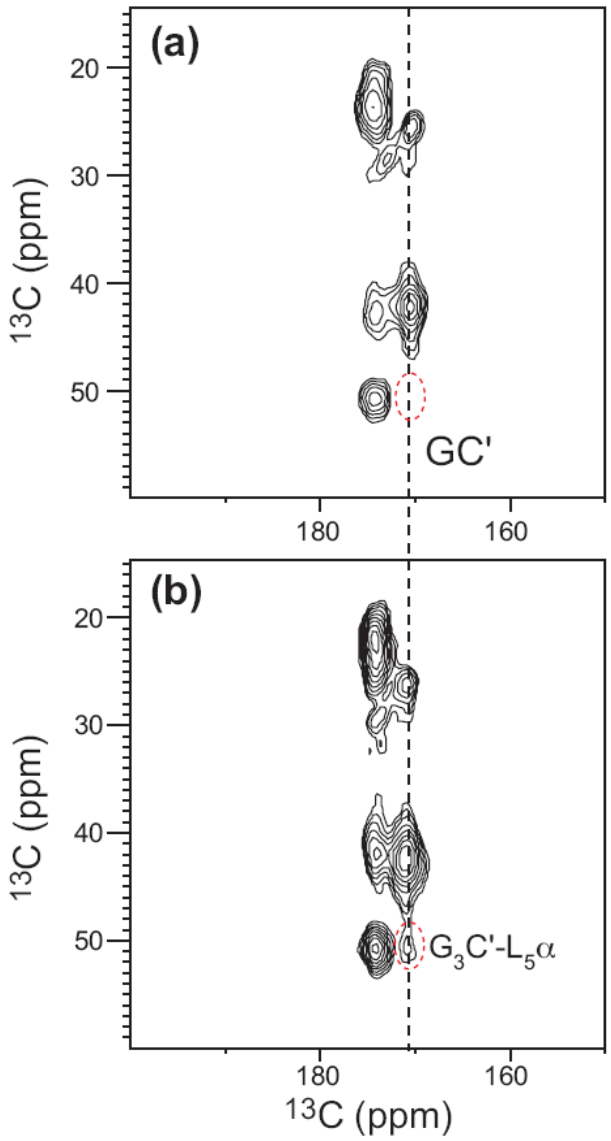

Figure S3.2. (a) 2D ^{13}C PDSD spectrum of 20% diluted and untreated [U-G_3, L_5] PG-1 at 293 K. Negligible G_3-L_5 C'-Cα cross peak is observed. (b) PDSD spectrum of the 100% [U-G_3, L_5] PG-1 aggregate is reproduced from Figure 3.7(a), where a clear G_3-L_5 C'-Cα cross peak is observed.

Chapter 4

Orientation of a β-hairpin Antimicrobial Peptide in Lipid Bilayers from 2D Dipolar Chemical-Shift Correlation NMR

Published in *Biophys. J.*

2006, 90, 3616-3624

Ming Tang [*], Alan J. Waring [#], Robert I. Lehrer [#], and Mei Hong [*]

[*] Department of Chemistry, Iowa State University, Ames, IA 50011

[#] Department of Medicine, University of California at Los Angeles School of Medicine, Los Angeles, CA 90095

Abbreviations:

DLPC: dilauroylphosphatidylcholine

POPC: palmitoyloleoylphosphatidylcholine

POPE: palmitoyloleoylphosphatidylethanolamine

POPG: palmitoyloleoylphosphatidylglycerol

MAS: magic angle spinning

CP: cross polarization

CSA: chemical shift anisotropy

Keywords: β-sheet peptides, orientation determination, tilt angle, dipolar coupling, ^{15}N NMR

Abstract

The orientation of a β-sheet membrane peptide in lipid bilayers is determined, for the first time, using 2D ^{15}N solid-state NMR. Retrocyclin-2 is a disulfide-stabilized cyclic β-hairpin peptide with antibacterial and antiviral activities. We used 2D separated-local-field spectroscopy correlating ^{15}N-^{1}H dipolar couplings with ^{15}N chemical shifts to determine the

orientation of multiply ^{15}N-labeled retrocyclin-2 in uniaxially aligned phosphocholine bilayers. Calculated 2D spectra exhibit characteristic resonance patterns that are sensitive to both the tilt of the β-strand axis and the rotation of the β-sheet plane from the bilayer normal, and that yield resonance assignment without the need for singly labeled samples. Retrocyclin-2 adopts a transmembrane orientation in DLPC bilayers, with the strand axis tilted at 20˚±10˚ from the bilayer normal, but changes to a more in-plane orientation in thicker POPC bilayers with a tilt angle of 65˚±15˚. These indicate that hydrophobic mismatch regulates the peptide orientation. The 2D spectra are sensitive not only to the peptide orientation but also to its backbone (ϕ, ψ) angles. Neither a bent hairpin conformation, which is populated in solution, nor an ideal β-hairpin with uniform (ϕ, ψ) angles and coplanar strands, agrees with the experimental spectrum. Thus, membrane binding orders the retrocyclin conformation by reducing the β-sheet curvature but does not make it ideal. ^{31}P NMR spectra of membranes with different compositions indicate that retrocyclin-2 selectively disrupts the orientational order of anionic membranes while leaving zwitteronic membranes intact. These structural results provide insights into the mechanism of action of this β-hairpin antimicrobial peptide.

Introduction

The orientation of membrane peptides in lipid bilayers is an important aspect of the three-dimensional structure of these molecules. Solid-state NMR spectroscopy is a well-established tool for determining the orientation of α-helical membrane peptides. The most common approach is to measure the ^{15}N chemical shift and ^{15}N-^{1}H dipolar couplings of macroscopically oriented peptides bound to lipid membranes (1). These two ^{15}N interaction tensors are approximately parallel to the helical axis, thus their frequencies reflect the orientation of the helical axis relative to the magnetic field. When the alignment axis is parallel to the magnetic field, this is also the helix orientation relative to the bilayer normal. To determine the peptide orientation with high angular resolution, 2D separated-local field (SLF) spectroscopy correlating the ^{15}N chemical shift with ^{15}N-^{1}H dipolar coupling is particularly powerful. Due to the small misalignment between the N-H bonds and the helical axis, the 2D SLF spectra of multiply ^{15}N-labeled helical peptides give characteristic wheel-

like patterns whose positions and sizes are exquisitely sensitive to the tilt angle of the helix from the membrane normal (2; 3). The peaks on these wheel patterns follow the helical wheel projection in a well-defined fashion, so that they can be assigned readily as long as one of the peaks is identified using a site-specifically labeled sample.

Compared to advances in the orientation determination of α-helical membrane peptides, knowledge about the orientation and insertion of β-sheet peptides in lipid bilayers is scarce. Although theoretical analyses of the 2D spectra of β-sheet peptides were given recently (4; 5), no experimental study of β-sheet peptide orientation using this 2D approach has been reported. The fact that the N-H bonds in β-sheet peptides are perpendicular rather than parallel to the strand axis further makes it unclear whether ^{15}N NMR is adequate for determining β-sheet peptide orientations.

Disulfide-stabilized β-hairpin antimicrobial peptides (6) are promising systems both for understanding β-sheet peptide binding to lipid membranes and for testing the applicability of the ^{15}N solid-state NMR method. These peptides are potent microbicidal molecules present in many animals and plants as part of their innate immune system (7-9). The most common mechanism of action of these small cationic peptides is the disruption of the microbial cell membrane. D-enantiomers of these peptides show similar activities as their L-counterparts, indicating that the targets of these peptides are the achiral lipids of the membrane rather than protein receptors in the membrane or inside the cell (10; 11).

Retrocyclin-2 is a circular 18-residue antimicrobial peptide encoded in the human genome by a θ-defensin pseudogene (12). It exhibits antibacterial activities and inhibits HIV entry into human cells (13-15). Similar to the monkey homolog, rhesus θ-defensin (RTD) (16), retrocyclin-2 has a β-hairpin structure stabilized by three cross-strand disulfide bonds. Its five Arg residues and the hydrophobic residues are distributed at nearly identical positions as in RTD-1 (Fig. 4.1). Thus, the solution NMR structure of RTD-1 to a good approximation is applicable to retrocyclin-2. Retrocyclin-2 has a high affinity to carbohydrate-containing cell surface molecules (17) and is localized on the cell membrane based on confocal microscopy images. However, the high-resolution structure of the peptide bound to the lipid bilayer is not yet known.

In this work, we report the orientation determination of multiply ^{15}N-labeled retrocyclin-2 using 2D ^{15}N dipolar-shift correlation NMR combined with macroscopic alignment of lipid membranes. We show that the 2D spectra of β-hairpin peptides are extremely sensitive to the orientations of the β-strand axis and β-sheet plane relative to the bilayer normal. Moreover, the spectral patterns yield non-degenerate values of the orientation angles, so that no site-specific-labeling-based assignment is necessary to resolve angular ambiguity. Experimental spectra indicate that retrocyclin-2 is transmembrane in DLPC bilayers but changes to a more in-plane orientation in POPC bilayers. Further, the 2D spectra are sensitive to the backbone (ϕ, ψ) angles. Neither a bent conformation present in solution nor an ideal cyclic conformation with coplanar strands agrees with the experimental data. These provide the first insights into the conformation and orientation of this class of cyclic β-hairpin peptides in the membrane.

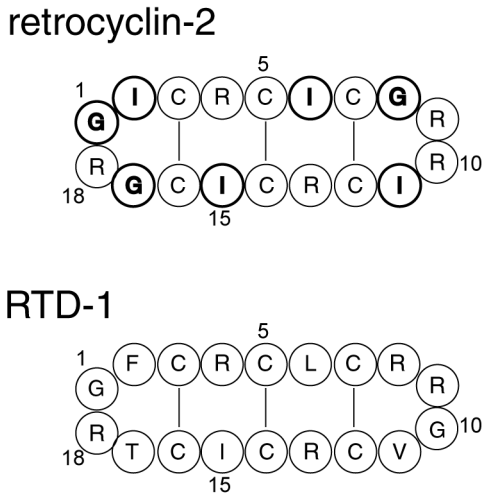

Figure 4.1. Amino acid sequences of retrocyclin-2 and RTD-1. The ^{15}N labeled residues in retrocyclin-2 are in bold.

Materials and Methods

Materials

All lipids, including DLPC, POPC, POPE, and POPG, were purchased from Avanti Polar Lipids (Alabaster, AL) and used without further purification. Retrocyclin-2 (GICRCICGRG ICRCICGR) was synthesized on a 0.25 mmol scale with an ABI 431A

peptide synthesizer using FastMoc™ chemistry (18). All residues were double coupled to insure optimal yield. Gly_1, Ile_2, Ile_6, Gly_8, Ile_{11}, Ile_{15}, Gly_{17} are ^{15}N labeled (Fig. 4.1). ^{15}N-labeled amino acids were purchased from Cambridge Isotope Lab (Andover, MA) and converted to the Fmoc derivatives by AnaSpec Inc. (San Jose, CA). The crude reduced peptide was purified by reverse-phase HPLC, oxidized with DMSO buffer, purified again to remove unreacted peptide, then cyclized (13). Glass cover slides with a thickness of 0.08 mm were obtained from Marienfeld Laboratory and cut to 6 x 12 mm^2 rectangles.

Membrane sample preparation

Glass-plate oriented membrane mixtures were prepared using a naphthalene-incorporated procedure described recently (19). The peptide was dissolved in TFE and mixed with a chloroform solution of the lipids with the desired molar ratio. The mixture was dried under a stream of N_2 gas and the dried film was redissolved in a 1:1 mixture of chloroform/TFE containing a two-fold excess of naphthalene with respect to the lipids. The solution was deposited on 10 – 30 glass plates with an area concentration of 0.01 – 0.02 mg/mm^2, air-dried for 2 hours and then vacuum dried for 5 hours to remove all solvents and naphthalene. About 1 μL of water was added directly to each glass plate, then the sample was hydrated indirectly at a relative humidity of 98% over a saturated solution of K_2SO_4 for 1 – 2 weeks. The glass plates were stacked, wrapped in parafilm and sealed in a polyethylene bag to prevent dehydration during the NMR experiments.

Solid-state NMR

NMR experiments were carried out on a Bruker DSX-400 spectrometer (Karlsruhe, Germany) operating at a resonance frequency of 162.12 MHz for ^{31}P and 40.58 MHz for ^{15}N. A static double-resonance probe with a home-built rectangular coil with the dimension of 6 x 12 x 5 mm^3 was used for the oriented membrane samples. The ^{15}N chemical shift was referenced to the isotropic signal of N-acetyl-valine at 122 ppm. The ^{31}P chemical shift was referenced to 85% phosphoric acid at 0 ppm. The 2D SLF experiments used MREV-8 (20; 21) to decouple the ^1H-^1H dipolar interaction during t_1, although other homonuclear decoupling schemes are also applicable. The MREV-8 90° pulse length was 3.8 μs. A ^1H decoupling

field strength of 50 kHz was used during ^{15}N detection. The ^{1}H-^{15}N CP contact time was 1 ms. The 2D spectra were acquired using 22-24 t_1 slices with a dwell time of 45.6 μs, resulting in a maximum evolution time of slightly over 1 ms. 1280 and 3072 scans were averaged for each t_1 time point for the DLPC and POPC-bound peptide samples, respectively.

Orientation simulations

2D ^{15}N-^{1}H/^{15}N correlation spectra were calculated using two FORTRAN programs. The first program defines a molecule-fixed coordinate system that reflects the β-strand axis and β-sheet plane geometry and calculates the anisotropic frequencies based on the orientation of the magnetic field ($\mathbf{B_0}$) in this coordinate system. The z-axis of this reference system, the β-strand axis, is defined and calculated as the average orientation of an even number of consecutive C'_{i-1}-N_i bonds (Fig. 4.2a). We used the six peptide bonds of residues 2-7 for this purpose. The y-z plane, the local β-sheet plane, is defined as the common plane containing the z-axis and a specific C=O vector. The C=O bond of residue 2 was used. The tilt angle τ is between the β-strand (z) axis and the $\mathbf{B_0}$ field, while the rotation angle ρ is defined as between the y-axis and the projection of $\mathbf{B_0}$ onto the x-y plane. ρ = 0° indicates that $\mathbf{B_0}$ is parallel to the β-sheet (y-z) plane. The molecular bonds necessary for defining the orientations of the ^{15}N chemical shift and N-H dipolar tensors, including the N-H^N, C'-N, and N-Cα bonds, were extracted from the PDB coordinates of RTD-1 (1HVZ). The chemical shift and dipolar coupling frequencies were calculated from the scalar products between $\mathbf{B_0}$ and the respective tensors as $\mathbf{B_0}$ is rotated through all combinations of (τ, ρ) angles. The unique angular range of τ is 0° to 90°, while ρ is sampled over the entire 360° range. We refer to this β-sheet based program as the relative orientation program.

To accurately visualize the results of the orientation calculation, and to determine the orientation of non-ideal β-hairpins, whose sheet axis and sheet plane are ill defined, a second Fortran program without an internal β-sheet reference system was used. The program defines the $\mathbf{B_0}$ orientation by a polar angle β and an azimuthal angle α in the default PDB coordinate system (22). This program is referred to as the absolute orientation program. The best-fit (α, β) angles were converted into the Cartesian coordinates (sinβcosα, sinβsinα, cosβ) of a

vector from the origin and added to the PDB file. This vector, the bilayer normal, was rotated together with the molecule until it was vertical on the screen, thus giving the exact orientation of the β-sheet peptide (22).

The two FORTRAN programs were checked for consistency by calculating the spectra for a transmembrane ($\tau = 0^\circ$, $\rho = 0^\circ$) and an in-plane ($\tau = 90^\circ$, $\rho = 90^\circ$) extended strand ($\phi = \psi = 180^\circ$) using the relative orientation program, then fitting these spectra using the absolute orientation program. The best-fit (α, β) angles were then visualized in Insight II to confirm that the molecules have the desired orientations.

Input ^{15}N chemical shift and N-H dipolar tensors for the simulations were as follows. The z-axis of the ^{15}N chemical shift tensor is 17° from the N-H bond (23) while the x-axis is 25° from the peptide plane (24). The rigid-limit N-H dipolar coupling was 10 kHz, corresponding to a bond length of 1.07 Å. Literature ^{15}N chemical shift principal values of (64, 77, 217) ppm (23) were used to simulate the general orientation-dependent spectra of Fig. 4.2 and Fig. 4.3. To fit the experimental 2D spectra of retrocyclin-2, the chemical shift difference between Ile and Gly was taken into account. The principal values were estimated from the ^{15}N MAS sideband intensities of unoriented retrocyclin-2 in DLPC bilayers. For Ile, the ^{15}N principal values were (75, 76, 221) ppm, while for Gly, the principal values were (42, 86, 202) ppm. These were used for most of the simulations in Figs. 4, 6, 7, and 8. Calculations show that the use of literature ^{15}N chemical shift tensor values did not change the best-fit (τ, ρ) angles, but the fit to the experimental spectra is actually somewhat better using the standard ^{15}N tensor values.

The solution NMR structure of RTD-1 (PDB code: 1HVZ) was used to represent the retrocyclin-2 structure. The RTD-1 structure has a significant backbone RMSD of 1.55 Å due to dynamic disorder in the middle of the strands (25). As a result, some of the minimum-energy structures show a substantial curvature of the β-sheet plane. We chose structure 15 to represent the straight β-hairpin population and structure 13 to represent the bent hairpin. The average (ϕ, ψ) angles for the strand residues (2-8 and 11-17) in structure 15 are (–103°, 99°), while the average (ϕ, ψ) angles for the strand residues in structure 13 are (-66°, 63°), which deviate significantly from the ideal β-strand geometry.

An "ideal" 18-residue β-hairpin was generated to further assess the sensitivity of the 2D spectra to backbone conformation. This ideal β-hairpin has uniform torsion angles of (ϕ = -137˚, ψ = 135˚) for the strand residues and (ϕ_i = -45˚, ψ_i = 85˚) and (ϕ_{i+1} = 155˚, ψ_{i+1} = -20˚) for the turn residues. The turn-residue torsion angles were optimized to make the two strands coplanar.

Best fits to the experimental spectrum were determined by finding the minimum root-mean squared deviation (RMSD) between the experiment and the simulations:

$$\mathrm{RMSD} = \sqrt{\sum_i \left(\frac{\omega_{d,i}^{exp} - \omega_{d,i}^{sim}}{\delta_d} \right)^2 + \sum_i \left(\frac{\omega_{CS,i}^{exp} - \omega_{CS,i}^{sim}}{\delta_{CS}} \right)^2} \quad . \qquad (1)$$

Here $\omega_{d,i}^{sim}$ and $\omega_{CS,i}^{sim}$ are the calculated dipolar coupling and chemical shift of residue *i*, respectively, while $\omega_{d,i}^{exp}$ and $\omega_{CS,i}^{exp}$ represent the frequencies of an experimental peak closest to the calculated frequencies of residue *i*. The frequency differences were normalized by the rigid-limit anisotropy, δ_d and δ_{CS}, of the interactions. The goodness of fit was assessed by comparing the RMSD with the experimental RMS noise, which was obtained by replacing $\omega_{d,i}^{sim}$ and $\omega_{CS,i}^{sim}$ in eq. (1) with frequencies that reflect the read-out uncertainty of each peak. Resonance assignment was made after the best fit was found and an experiment peak with the frequencies closest to the calculated frequencies of residue *i* was assigned to residue *i*.

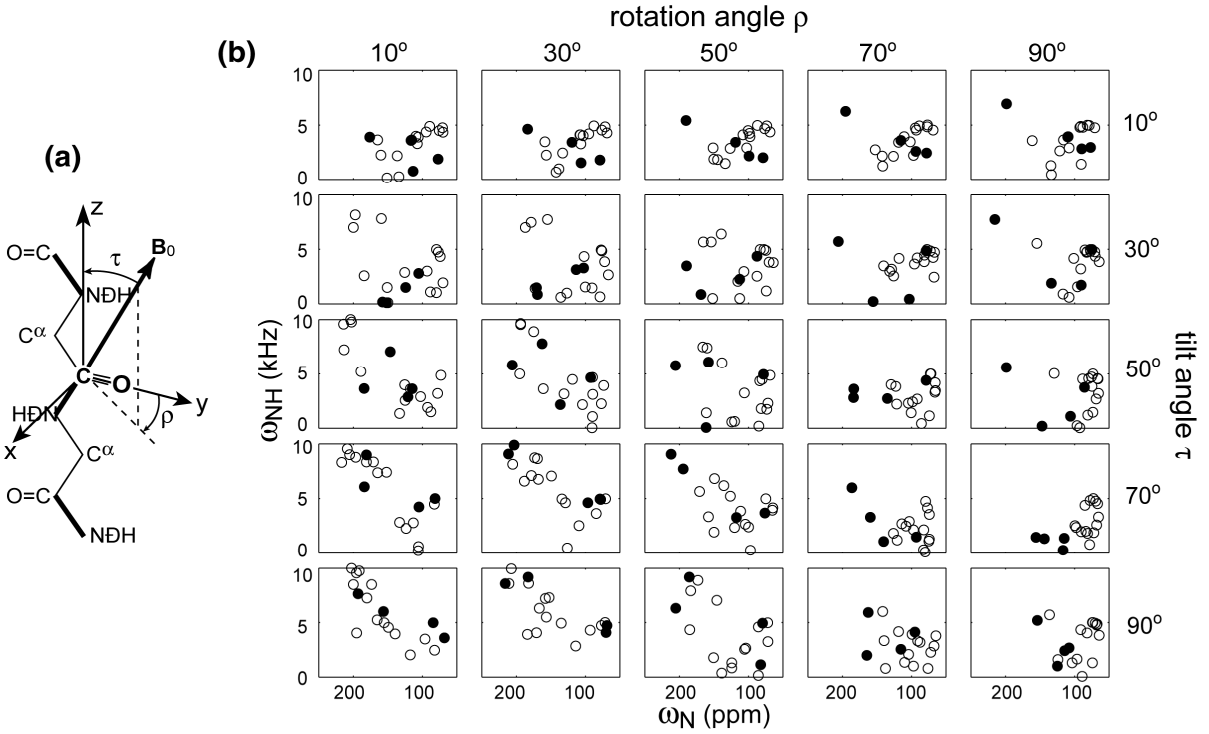

Figure 4.2. (a) Definition of the tilt angle τ and rotation angle ρ in a β-strand peptide. (b) Calculated 2D ^{15}N-^{1}H/^{15}N correlation spectra as a function of τ and ρ for an 18-residue β-hairpin molecule, using structure 15 of RTD-1. The resonances of all 18 residues are shown. Filled and open circles represent the resonances of turn and strand residues, respectively.

Results

Fig. 4.2b shows the calculated spectra for a range of τ and ρ angles based on the RTD-1 structure 15. All 18 resonances are shown. The strand and turn residues are shown as unfilled and filled circles, respectively. As expected, the turn residues often give rise to outlier peaks in the 2D spectra due to their distinct N-H bond orientations from the strand residues, thus they serve as useful identifiers of the peptide orientation. The unique range of the ρ angle is 360˚; but for clarity only a 90˚ range is shown. Significant peak dispersion is observed in these spectra, both when the strand axis is nearly parallel (e.g. τ = 10˚, ρ = 10˚) and when it is perpendicular (e.g. τ = 90˚, ρ = 10˚) to $\mathbf{B_0}$. This differs from α-helical peptides, which have no dispersion when the helical axis is parallel to the bilayer normal (τ = 0˚) and very limited spectral dispersion when τ = 90˚. The frequency dispersion in Fig. 4.2 results from both the inherent twist of the β-strand and the presence of the turn residues. The largest

spectral dispersion is obtained when (τ, ρ) approach (90˚, 0˚), which corresponds to the case where the strand axis is perpendicular to the bilayer normal while the β-sheet plane is parallel to the membrane normal. This orientation is unlikely for a small monomeric β-strand peptide but possible as part of a β-barrel protein. Fig. 4.2 shows that the transmembrane (τ–>0˚) and in-plane orientations (τ = 90˚, ρ = 90˚) have sufficient frequency differences to be distinguishable, even though in theory both their N-H bonds are perpendicular to $\mathbf{B_0}$. The in-plane orientation has more limited spectral dispersion, with the peaks clustered at the 90˚ edge of both dimensions. Fig. 4.3 shows the calculated spectra for the seven ^{15}N-labeled residues in retrocyclin-2. For this subset of signals, the transmembrane (e.g. τ = 10˚, ρ = 10˚) and in-plane (τ = 90˚, ρ = 90˚) spectra are even more distinguishable.

Fig. 4.2 indicates that the 2D spectra of β-hairpin peptides depend sensitively on both the τ and ρ angles. The resonance patterns are much less symmetric than the PISA wheels of α-helices, whose shape and position depend primarily on τ but not on ρ. The ρ-angle of a β-sheet peptide can be uniquely determined without resonance assignment, as long as the number of residues is smaller than the periodicity dictated by the β-sheet twist. Such periodicity can range from 25 to 108 residues depending on the β-sheet (ϕ, ψ) angles (4). Since typical β-strands have less than 15 residues, this condition is usually satisfied. Therefore, from the 2D ^{15}N-^{1}H/^{15}N correlation spectra of β-sheet peptides, non-degenerate values of (τ, ρ) angles can be obtained without the need for singly labeled samples for resonance assignment, in contrast to α-helices. For β-hairpin peptides, the presence of the turn residues further facilitates orientation determination and resonance assignment.

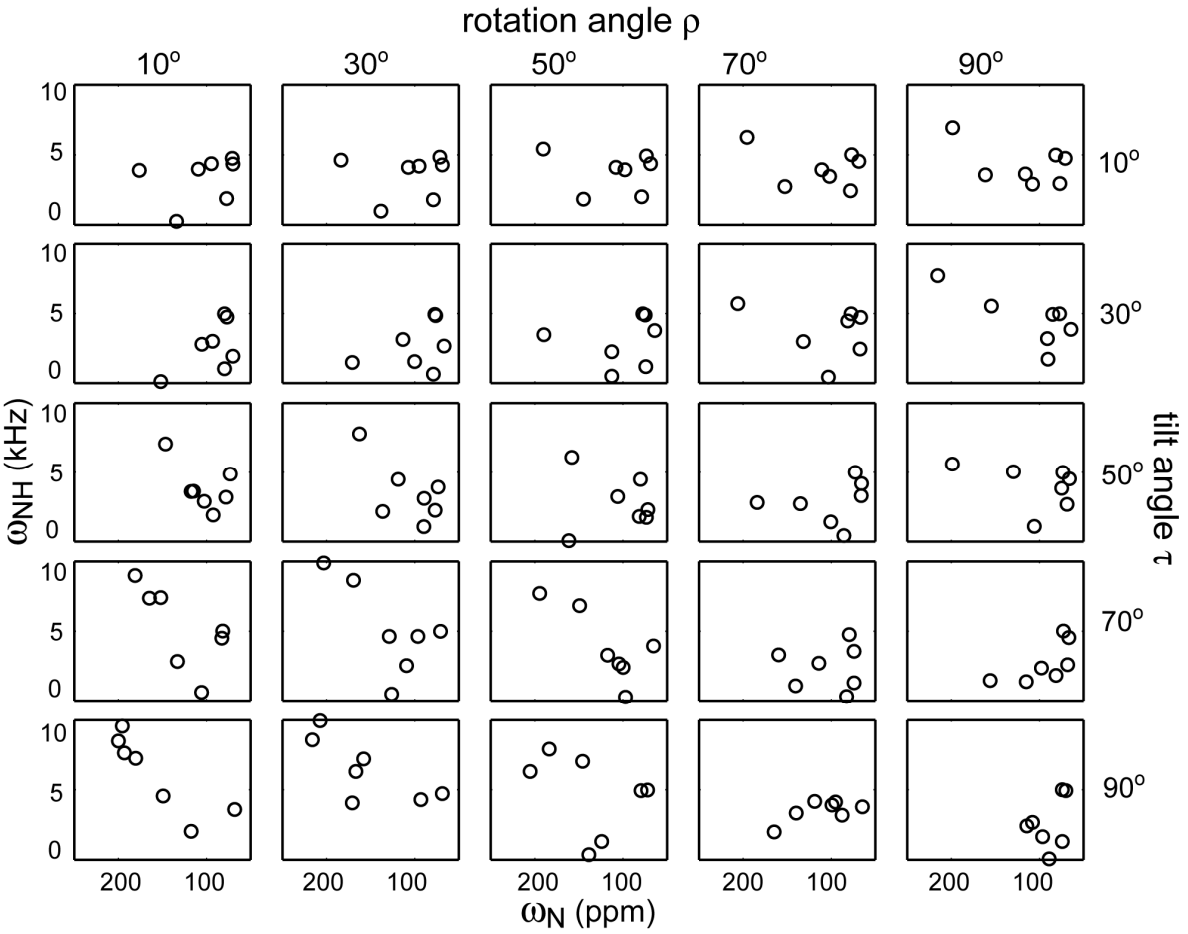

Figure 4.3. Calculated 2D ^{15}N-^{1}H/^{15}N correlation spectra for the seven ^{15}N labeled residues in retrocyclin-2. The spectra are subsets of those in Figure 4.2. Note the clear difference between the transmembrane ($\tau = 10^{\circ}$, $\rho = 10^{\circ}$) and in-plane ($\tau = 90^{\circ}$, $\rho = 90^{\circ}$) orientations.

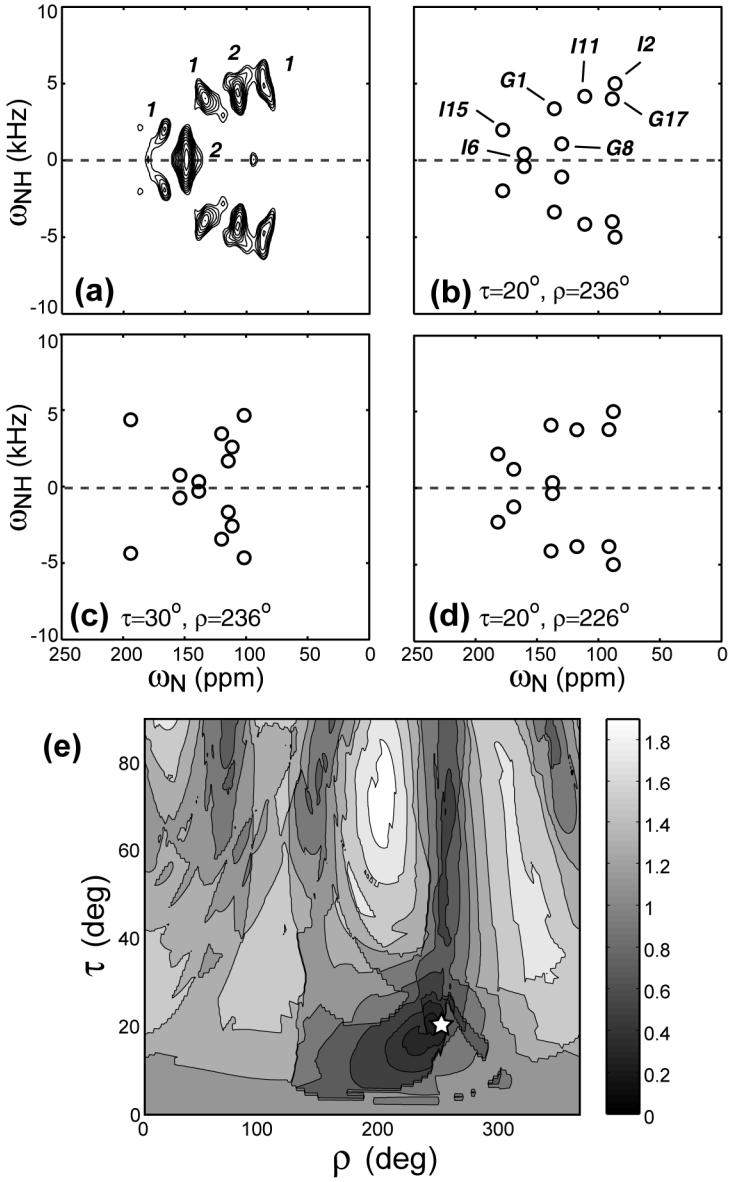

Figure 4.4. (a) Experimental 2D ^{15}N-^{1}H/^{15}N correlation spectrum of retrocyclin-2 in DLPC bilayers (P:L=1:25). The relative volumes of the resolved peaks are indicated. (b) Best-fit spectrum using the measured ^{15}N chemical shift principal values of the peptide, which are (42, 86, 202) ppm for Gly and (75, 76, 221) ppm for Ile. Best-fit angles: $\tau = 20^{\circ}$, $\rho = 236^{\circ}$. Resonance assignment is indicated. (c) Best-fit spectrum using standard ^{15}N chemical shift tensor values of (64, 77, 217) ppm (23) for all sites. The same best-fit angles as (b) are obtained, but the agreement with the experimental spectrum is better than (c), especially in the Gly8 position. (d) Simulated 2D spectrum with $\tau = 30^{\circ}$, $\rho = 236^{\circ}$. (e) Simulated 2D spectrum for $\tau = 20^{\circ}$, $\rho = 226^{\circ}$. (f) RMSDs between the experiment and simulations as a function of (τ, ρ) angles. The minimum RMSD occurs at $\tau = 20^{\circ}$, $\rho = 236^{\circ}$ (star).

The experimental 2D spectrum of retrocyclin-2 bound to DLPC bilayers (1 : 25 molar ratio) is shown in Fig. 4.4a. The spectrum shows five resolved peaks, two of which contain overlapping resonances based on the peak volumes. The best-fit spectrum was obtained at ($\tau = 20^\circ$, $\rho = 236^\circ$) and shown in Fig. 4.4b along with the assignment. The simulated spectrum, calculated using ^{15}N chemical shift principal values estimated from the MAS sideband spectrum of the peptide, agrees well with the experimental pattern for all peaks except for Gly8, whose chemical shift deviates by ~10 ppm between the two. However, it is well known that the Gly ^{15}N chemical shift tensor values are less well defined than the other amino acids. Indeed, when standard literature ^{15}N chemical shift tensor values of (64, 77, 217) ppm (23) were used in the simulation, much better agreement in the Gly8 position was obtained (Fig. 4.4c) while the best-fit angles remain unchanged at ($\tau = 20^\circ$, $\rho = 236^\circ$).

To assess the angular uncertainty of the measured orientation angles, we show two simulated spectra near the best fit, with τ and ρ each differing by 10°. Both give spectral patterns distinctly different from the experimental spectrum (Fig. 4.4d, e). Fig. 4.4f shows the 2D RMSD map as a function of (τ, ρ) at 1° increments. The global minimum at ($\tau = 20^\circ$, $\rho = 236^\circ$) has an RMSD value of 0.26, comparable to the experimental RMS noise (0.20), while the two alternative simulations in Fig. 4.4(d-e) have much higher RMSD values of 0.63 and 0.40, confirming that the (τ, ρ) uncertainties are within $\pm 10^\circ$. Moreover, the 2D RMSD contour plot shows a single global minimum, indicating the uniqueness of the angles determined due to the multiple frequency constraints available in the spectrum.

Fig. 4.5 shows the orientation of retrocyclin-2 in DLPC bilayers. Since the peptide is almost completely transmembrane, the plane of the β-sheet is roughly parallel to the bilayer normal despite the large ρ angle of 236°. In other words, the peptide inserts into the membrane in a way that encounters low resistance.

Since the twenty minimum-energy structures of RTD-1 show considerable variations in the curvature of the β-sheet, to assess whether the orientation solution depends on the peptide backbone conformation, we carried out further simulations using a bent hairpin structure (Fig. 4.6c). Since it was not possible to define a meaningful strand axis and sheet plane for this structure, the simulation was carried out using the absolute orientation program. The resulting RMSD map between the simulated and the experimental spectra is shown in

Fig. 4.6a. The best-fit orientation occurs at ($\beta = 88^\circ$, $\alpha = 347^\circ$) and has an RMSD value (0.47) that is more than twice the experimental uncertainty (0.20), indicating a poor fit. This can be seen clearly in the superposition of the experimental and best-fit simulated spectra in Fig. 4.6b. The lack of a good fit rules out the bent hairpin conformation of retrocyclin-2 in the membrane.

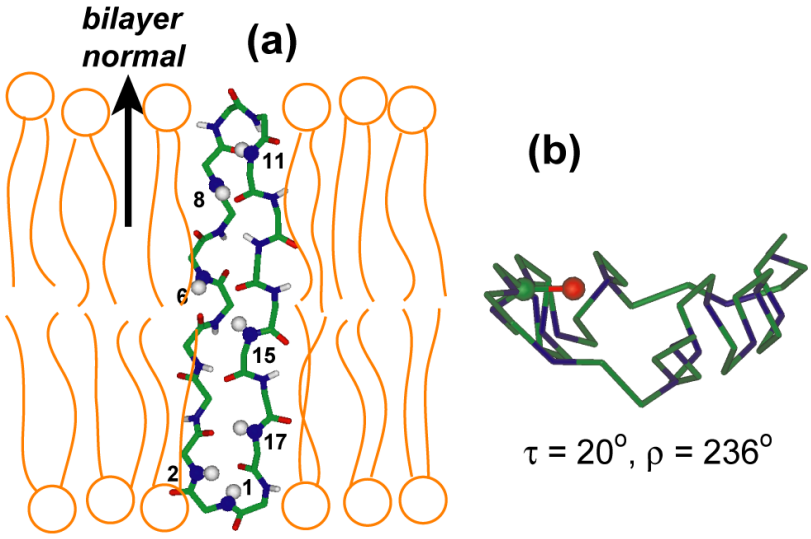

Figure 4.5. Retrocyclin-2 orientation in DLPC bilayers. (a) Viewed from the side of the DLPC bilayer. The end-to-end backbone length of the β-hairpin is ~27 Å, comparable to the P-P distance of 31 Å for liquid-crystalline DLPC bilayers. (b) Viewed from the top of the lipid bilayer. The C=O bond of residue 2 used for defining the ρ angle is highlighted. The β-sheet plane is relatively straight.

The possibility of overall fast libration of the peptide between the straight and the bent β-hairpin conformations can be reasonably ruled out, because the ^{15}N chemical shift anisotropies of the peptide in DLPC bilayers are close to the rigid limit values, and because five out of seven ^{15}N-labeled residues are located at the rigid β-turns of the peptide.

The solution structure that reproduced the experiment (Fig. 4.5) has strand (ϕ, ψ) angles that span a large range: the ϕ angles range from -155° to -67° and ψ angles from 59° to 158°. The turn residues in this structure have torsion angles close to those of a type-II β-turn: ($\phi_{18} = -60^\circ$, $\psi_{18} = 94^\circ$), ($\phi_1 = 131^\circ$, $\psi_1 = -25^\circ$); and ($\phi_9 = -67^\circ$, $\psi_9 = 80^\circ$), ($\phi_{10} = 128^\circ$, $\psi_{10} = -18^\circ$). To test if the peptide exists as a more ideal β-hairpin in the membrane, we simulated the 2D spectra for a model β-hairpin structure (Fig. 4.7a) with uniform (ϕ, ψ) angles. The strand

torsion angles correspond to those of the classical antiparallel β-sheet. The turn residues' torsion angles were modified from those of the RTD-1 structure so that the two strands are coplanar. As expected, the calculated spectra for this ideal hairpin show much less frequency dispersion than the spectra of the actual RTD-1 structure in Fig. 4.3, and the resonances fall on predictable elliptical patterns indicated as gray lines in Fig. 4.7 (4). The global best fit using this ideal β-hairpin, near ($\tau = 70^{\circ}$, $\rho = 220^{\circ}$), disagrees noticeably with the experimental data (filled circles). The minimum RMSD is 0.43, again significantly higher than the experimental RMS noise. Thus, the 2D data rule out this ideal β-hairpin structure for the membrane-bound retrocyclin-2.

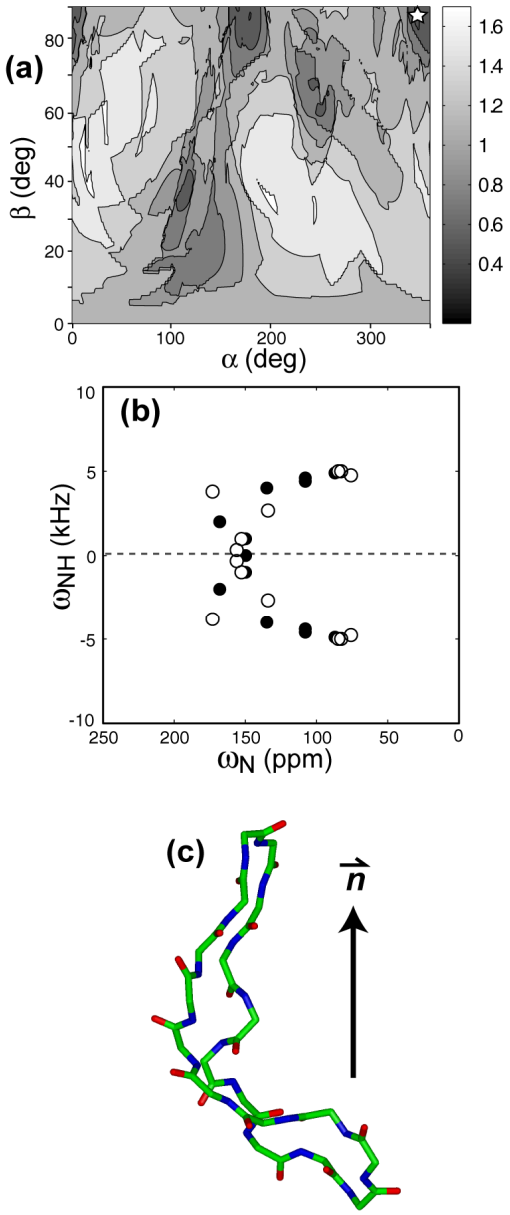

Figure 4.6. (a) RMSD between the experiment and simulations using a bent hairpin structure of RTD-1. The minimum RMSD of 0.47, which is significantly higher than the experimental RMS noise of 0.20, occurs at $\beta = 88^{\circ}$, $\alpha = 347^{\circ}$ (star). (b) Best-fit simulation (open circles) superimposed with the experimental spectrum (filled circles). The two differ significantly. (c) RTD-1 structure 13 used for the simulations, showing significant curvature in the β-hairpin. The peptide is shown in its best-fit orientation, which happens to be transmembrane.

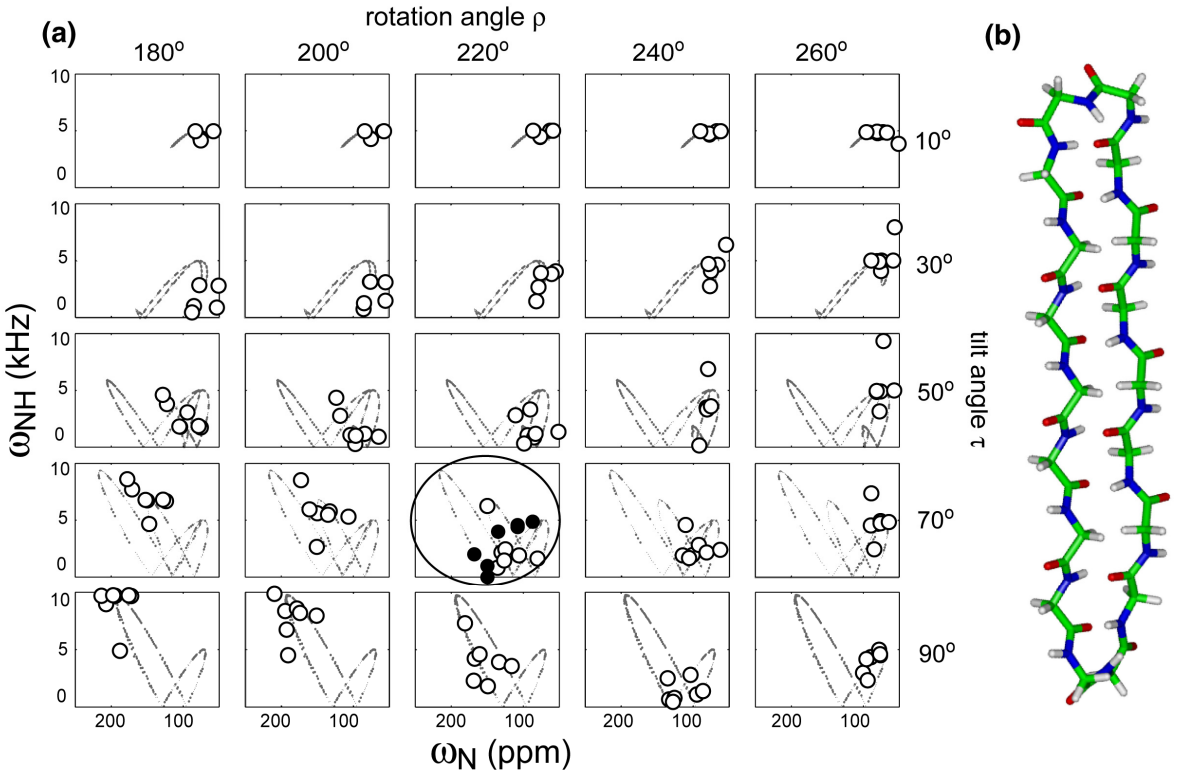

Figure 4.7. (a) Simulated 2D ^{15}N-^{1}H/^{15}N correlation spectra of an ideal β-hairpin as a function of (τ, ρ) angles. Only the frequencies of the seven labeled residues are shown. Gray lines illustrate the orientation-dependent elliptical patterns on which the strand resonances fall. The best-fit spectrum, near (τ = 70˚, ρ = 220˚), does not fit the experimental spectrum well (filled circles). (b) The ideal hairpin conformation.

To investigate the orientation dependence of retrocyclin-2 on membrane thickness, we performed the 2D ^{15}N-^{1}H/^{15}N correlation experiment on retrocyclin-2 oriented in POPC bilayers, which have a P-P distance of ~45 Å. The experimental spectrum (Fig. 4.8a) shows smaller ^{15}N chemical shifts and lower spectral resolution than those of the DLPC/retrocyclin-2 membrane, suggesting that the peptide has changed to a more in-plane orientation. Indeed, simulations yield best-fit angles of (τ = 65±15˚, ρ = 278±20˚) (Fig. 4.8b-c), which differ substantially from the peptide orientation in DLPC bilayers. Thus, the β-hairpin orientation becomes more parallel to the membrane plane in POPC bilayers (Fig. 4.8d) due to the increase of the membrane thickness.

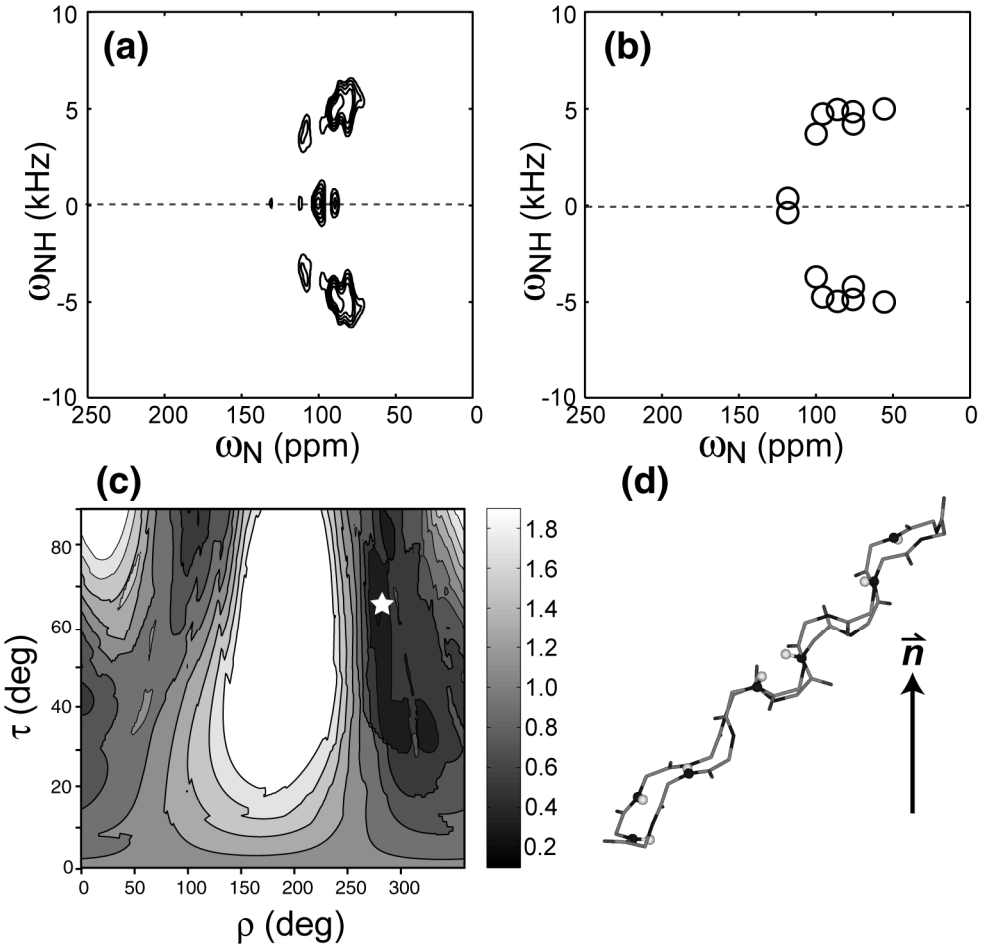

Figure 4.8. (a) Experimental 2D ^{15}N-^{1}H/^{15}N correlation spectrum of retrocyclin-2 in POPC bilayers (P:L=1:25). The peak shift to lower chemical shifts compared to the DLPC spectrum (Fig. 4.4a) and the strong overlap both indicate a more in-plane orientation of the peptide. (b) Best-fit spectrum with $\tau = 65^{\circ}$ and $\rho = 278^{\circ}$. (c) RMSD between the experiment and simulations as a function of (τ, ρ). The minimum RMSD position is indicated by a star. (d) Orientation of retrocyclin-2 in POPC bilayers.

To investigate the selective disruption of microbial membranes by retrocyclin-2, we measured the ^{31}P spectra of oriented membranes of different compositions in the presence of 4% peptide. The zwitterionic POPC membrane retained good orientational order at this peptide concentration, while the mixed anionic membrane, POPC/POPG and POPE/POPG (3:1 molar ratio), showed significant powder intensities, indicating that retrocyclin-2 preferentially destroys the orientational order of anionic membranes. This resembles the behavior of RTD-1 (26). Since bacterial membranes are rich in phosphatidylglycerol lipids

while eukaryotic membranes are not, this indicates that an important mechanism of retrocyclin action is electrostatic in origin.

Discussion

The above data show that ^{15}N 2D dipolar-shift correlation NMR is a sensitive technique for determining the orientation and restraining the secondary structure of β-sheet and β-hairpin peptides in lipid bilayers. Several aspects of this orientation determination differ from the case of α-helical peptides. First, because β-strands lack cylindrical symmetry around the main molecular axis, their 2D spectra depend characteristically on both the tilt angle of the strand axis and the rotation angle of the sheet plane. In contrast, the PISA wheel patterns of α-helical peptides are distinguished mostly by the tilt of the helical axis and not by the helix rotation angle (2). The unique dependence of the β-sheet spectra on both τ and ρ, or the lack of angular degeneracy, means that resonance assignment is not necessary for orientation determination, but can be obtained, if desired, from spectral fitting directly without additional singly labeled samples. The second aspect unique to β-hairpin peptides is the presence of outlier resonances of the turn residues because of their different N-H bond orientations from the strand residues. These peaks further enhance the spectral differences between different (τ, ρ) angles and facilitate orientation determination. Third, although both transmembrane and in-plane β-hairpin peptides have N-H bonds approximately perpendicular to the bilayer normal, in practice they give distinguishable spectra. This is a result of the inherent twist of the β-sheet, the non-ideality of the β-hairpin, and the unique orientations of the turn residues. For α-helical peptides, the situation is quite different: the transmembrane and in-plane orientations resonate at completely different frequencies, but both show much less spectral dispersion than β-hairpin peptides.

The 2D ^{15}N-^{1}H/^{15}N correlation technique employed here can be conducted in a number of ways: for example, the ^{1}H-^{15}N polarization transfer can be achieved using the PISEMA sequence (27), and ^{1}H homonuclear decoupling can be carried out using alternative sequences such as FSLG (28). These should improve the resolution in the dipolar dimension but do not change the orientation-dependent spectral patterns. The fact that both the DLPC and POPC-bound peptide spectra have a single global best fit (Figs. 4f, 8c) indicates the

uniqueness of the orientation determination due to the multiple frequency constraints brought about by the multiple ^{15}N labels. Thus, the combination of extensive ^{15}N labeling, uniaxial membrane alignment, and 2D SLF NMR, is a powerful approach for determining β-sheet peptide orientations with high precision.

The transmembrane orientation of retrocyclin-2 in DLPC bilayers determined from this study has several implications. First, how does the peptide satisfy hydrogen bonding to reduce the number of polar backbone groups exposed to the hydrophobic membrane? About half the residues in retrocyclin-2 form cross-strand intramolecular hydrogen bonds, leaving ten residues with remaining polar N-H and C=O groups exposed to the lipid bilayer. One possibility is that retrocyclin-2 may be oligomerized so that the number of polar groups per molecule is reduced. This could be tested by a recently developed spin diffusion experiment that determines the aggregation number of peptides in lipid membranes (29). Second, the transmembrane orientation of retrocyclin-2 in DLPC bilayers is stabilized by the hydrophobic matching between the peptide backbone length and the membrane thickness. The end-to-end length of the straight hairpin is ~27 Å, while the P-P distance of DLPC bilayers is 31 Å (30; 31). The similar hydrophobic length supports the transmembrane orientation. Moreover, the transmembrane orientation allows the three cationic Arg sidechains at the two β-turns (residues 9, 10, 18) to interact favorably with the anionic phosphate headgroups. These favorable hydrophobic and electrostatic interactions may help to overcome the energetic cost of inserting the remaining non-hydrogen-bonded polar groups into the membrane.

When the thicker POPC bilayer is used, retrocyclin-2 changes its tilt angle to ~65˚, much closer to the in-plane orientation. Similar dependences of peptide orientations on the membrane thickness have been reported in the literature (30; 32-34). For peptides much shorter than the membrane thickness, an in-plane orientation is expected. For example, the ten-residue cyclic β-hairpin peptide gramicidin S was found to be oriented parallel to the plane of DMPC bilayers (35). The change of retrocyclin-2 orientation from transmembrane in 12:0 DLPC bilayers to nearly surface-bound in 16:0-18:1 POPC bilayers indicates that retrocyclin-2 structure depends on the lipid environment. In principle, the headgroup structure and charge can also affect the peptide orientation. Since retrocyclin-2 disrupts the

orientational order of bacteria-mimicking anionic membranes (Fig. 4.9), it is difficult to determine its orientation in these lipid bilayers using the aligned-membrane approach. It is also possible that retrocyclin-2, like the lipids in these anionic membranes, may adopt a distribution of orientations in these environments.

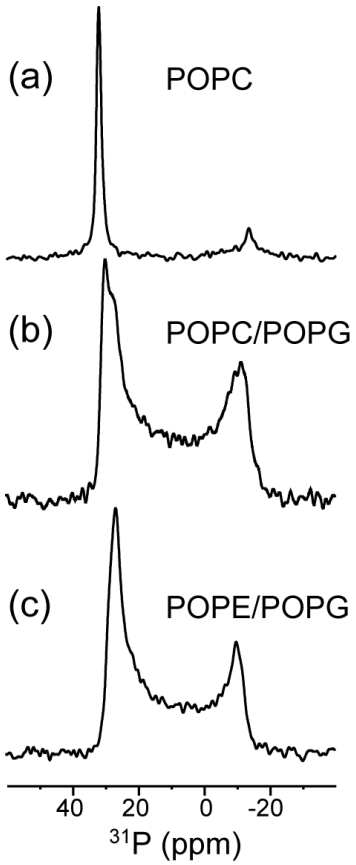

Figure 4.9. ^{31}P spectra of retrocyclin-2 bound to various oriented lipid bilayers at a peptide concentration of 4%. (a) POPC. (b) POPC/POPG. (c) POPE/POPG.

Acknowledgement: This work is supported by the National Institutes of Health grant GM-066976 to M. Hong and grants AI-22839 and AI-37945 to A.J. Waring and R.I. Lehrer.

References

1. Opella, S.J., A. Nevzorov, M.F. Mesleb, and F.M. Marassi. 2002. Structure determination of membrane proteins by NMR spectroscopy. Biochem. Cell Biol. 80:597-604.

2. Marassi, F.M., and S.J. Opella. 2000. A solid-state NMR index of helical membrane protein structure and topology. J. Magn. Reson. 144:150-155.

3. Wang, J., J. Denny, C. Tian, S. Kim, Y. Mo, F. Kovacs, Z. Song, K. Nishimura, Z. Gan, R. Fu, J.R. Quine, and T.A. Cross. 2000. Imaging membrane protein helical wheels. J. Magn. Reson. 144:162-167.

4. Marassi, F.M. 2001. A simple approach to membrane protein secondary structure and topology based on NMR spectroscopy. Biophys. J. 80:994-1003.

5. Vosegaard, T., and N.C. Nielsen. 2002. Towards high-resolution solid-state NMR on large uniformly 15N- and [13C,15N]-labeled membrane proteins in oriented lipid bilayers. J. Biomol. NMR 22:225-247.

6. Lehrer, R.I., and T. Ganz. 2002. Defensins of vertebrate animals. Curr. Opin. Immunol. 14:96-102.

7. Epand, R.M., and H.J. Vogel. 1999. Diversity of antimicrobial peptides and their mechanisms of action. Biochim. Biophys. Acta 1462:11-28.

8. Hancock, R.E., and M.G. Scott. 2000. The role of antimicrobial peptides in animal defenses. Proc. Natl. Acad. Sci. USA 97:8856-8861.

9. Bechinger, B. 1999. The structure, dynamics, and orientation of antimicrobial peptides in membranes by multidimensional solid-state NMR spectroscopy. Biochim. Biophys. Acta 1462:157-183.

10. Wade, D., A. Boman, B. Wahlin, C.M. Drain, D. Andreu, H.G. Boman, and R.B. Merrifield. 1990. All D-amino acid containing channel forming antibiotic peptides. Proc. Natl. Acad. Sci. USA 87:4761-4765.

11. Owen, S.M., D. Rudolph, W. Wang, A.M. Cole, M.A. Sherman, A.J. Waring, R.I. Lehrer, and R.B. Lal. 2004. A theta-defensin composed exclusively of D-amino acids is active against HIV-1. J. Peptide Res. 63:469-476.

12. Cole, A.M., W. Wang, A.J. Waring, and R.I. Lehrer. 2004. Retrocyclins: using past as prologue. Curr. Protein Pept. Sci. 5:373-381.

13. Cole, A.M., T. Hong, K.M. Boo, T. Nguyen, C. Zhao, G. Bristol, J.A. Zack, A.J. Waring, O.O. Yang, and R.I. Lehrer. 2002. Retrocyclin: a novel primate peptide that protects cells from infection by T- and M-tropic strains of HIV-1. Proc. Natl. Acad. Sci. U.S.A. 99:1813-1818.

14. Munk, C., G. Wei, O.O. Yang, A.J. Waring, W. Wang, T. Hong, R.I. Lehrer, N.R. Landau, and A.M. Cole. 2003. The theta-defensin, retrocyclin, inhibits HIV-1 entry. AIDS Res. Hum. Retroviruses 19:875-881.

15. Yasin, B., W. Wang, M. Pang, N. Cheshenko, T. Hong, A.J. Waring, B.C. Herold, E.A. Wagar, and R.I. Lehrer. 2004. Theta defensins protect cells from infection by herpes simplex virus by inhibiting viral adhesion and entry. J. Virology 78:5147-5156.

16. Tang, Y.Q., J. Yuan, G. Osapay, K. Osapay, D. Tran, C.J. Miller, A.J. Ouellette, and M.E. Selsted. 1999. A cyclic antimicrobial peptide produced in primate leukocytes by the ligation of two truncated alpha-defensins. Science 286(5439):498-502.

17. Wang, W., A.M. Cole, T. Hong, A.J. Waring, and R.I. Lehrer. 2003. Retrocyclin, an antiretroviral theta-defensin, is a lectin. J. Immunol. 170:4708-4716.

18. Fields, C.G., D.H. Lloyd, R.L. Macdonald, K.M. Ottenson, and R.L. Nobel. 1991. HBTU activation for automated Fmoc solid-phase peptide synthesis. Peptide Res. 4:95-101.

19. Hallock, K.J., K. Henzler Wildman, D.K. Lee, and A. Ramamoorthy. 2002. An innovative procedure using a sublimable solid to align lipid bilayers for solid-state NMR studies. Biophys. J. 82(5):2499-2503.

20. Rhim, W.-K., D.D. Elleman, and R.W. Vaughan. 1973. Analysis of multiple-pulse NMR in solids. J. Chem. Phys. 59:3740-3749.

21. Mansfield, P. 1971. Symmetrized pulse sequences in high resolution NMR in solids. J. Phys. C Solid State Phys. 4(11):1444.

22. Yamaguchi, S., T. Hong, A. Waring, R.I. Lehrer, and M. Hong. 2002. Solid-state NMR investigations of peptide-lipid interaction and orientation of a beta-sheet antimicrobial peptide, protegrin. Biochemistry 41(31):9852-9862.

23. Wu, C.H., A. Ramamoorthy, L.M. Gierasch, and S.J. Opella. 1995. Simultaneous characterization of the amide 1H chemical shift, 1H-15N dipolar, and 15N chemical shift

interaction tensors in a peptide bond by three-dimensional solid-state NMR. J. Am. Chem. Soc. 117:6148-6149.

24. Hong, M., J.D. Gross, W. Hu, and R.G. Griffin. 1998. Determination of the peptide torsion angle phi by 15N chemical shift and 13Ca-1Ha dipolar tensor correlation in solid-state MAS NMR. J. Magn. Reson. 135:169-177.

25. Trabi, M., H.J. Schirra, and D.J. Craik. 2001. Three-dimensional structure of RTD-1, a cyclic antimicrobial defensin from rhesus macaque leukocytes. Biochemistry 40:4211-4221.

26. Buffy, J.J., M.J. McCormick, S. Wi, A. Waring, R.I. Lehrer, and M. Hong. 2004. Solid-State NMR Investigation of the Selective Perturbation of Lipid Bilayers by the Cyclic Antimicrobial Peptide RTD-1. Biochemistry 43:9800-9812.

27. Wu, C.H., A. Ramamoorthy, and S.J. Opella. 1994. High-resolution heteronuclear dipolar solid-state NMR spectroscopy. J. Magn. Reson. Ser A 109:270-272.

28. Bielecki, A., A.C. Kolbert, H.J.M. de Groot, R.G. Griffin, and M.H. Levitt. 1990. Frequency-switched Lee-Goldburg sequences in solids. Adv. Magn. Reson. 14:111-124.

29. Buffy, J.J., A.J. Waring, and M. Hong. 2005. Determination of Peptide Oligomerization in Lipid Membranes with Magic-Angle Spinning Spin Diffusion NMR. J. Am. Chem. Soc. in press.

30. Harroun, T.A., W.T. Heller, T.M. Weiss, L. Yang, and H.W. Huang. 1999. Experimental evidence for hydrophobic matching and membrane-mediated interactions in lipid bilayers containing gramicidin. Biophys. J. 76:937-945.

31. Kucerka, N., Y. Liu, N. Chu, H.I. Petrache, S.A. Tristram-Nagle, and J.F. Nagle. 2005. Structure of fully hydrated fluid phase DMPC and DLPC lipid bilayers using X-ray scattering from oriented multilamellar arrays and from unilamellar vesicles. Biophys J. ASAP article.

32. Harzer, U., and B. Bechinger. 2000. Alignment of lysine-anchored membrane peptides under conditions of hydrophobic mismatch: a CD, 15N and 31P solid-state NMR spectroscopy investigation. Biochemistry 39:13106-13114.

33. de Planque, M.R., and J.A. Killian. 2003. Protein-lipid interactions studied with designed transmembrane peptides: role of hydrophobic matching and interfacial anchoring. Mol. Membr. Biol. 20:271-284.

34. Park, S.H., and S.J. Opella. 2005. Tilt angle of a trans-membrane helix is determined by hydrophobic mismatch. J. Mol. Biol. 350:310-318.

35. Salgado, J., S.L. Grage, L.H. Kondejewski, R.S. Hodges, R.N. McElhaney, and A.S. Ulrich. 2001. Membrane-bound structure and alignment of the antimicrobial b-sheet peptide gramicidin S derived from angular and distance constraints by solid-state 19F-NMR. J. Biomol. NMR 21:191-208.

Chapter 5

Trehalose-Protected Lipid Membranes for Determining Membrane Protein Structure and Insertion

Published in J. Magn. Reson.

2007, 184, 222-227

Ming Tang [a], Alan J. Waring [b], and Mei Hong [a]

[a] Department of Chemistry, Iowa State University, Ames, IA 50011

[b] Department of Medicine, University of California at Los Angeles School of Medicine, Los Angeles, California 90095

Abstract

Trehalose preserves lipid bilayers during dehydration and rehydration by replacing water to form hydrogen bonds between its own OH groups and lipid headgroups. We compare the lipid conformation and dynamics between trehalose-protected lyophilized membranes and hydrated membranes, to assess the suitability of the trehalose-containing membrane as a matrix for membrane protein structure determination. ^{31}P spectra indicate that the lipid headgroup of trehalose-protected dry POPC membrane (TRE-POPC) have an effective phase transition temperature that is ~50 K higher than that of the hydrated POPC membrane. In contrast, the acyl chains have similar transition temperatures in the two membranes. Intramolecular lipid ^{13}C'-^{31}P distances are the same in TRE-POPC and crystalline POPC, indicating that the lipid headgroup and glycerol backbone conformation is unaffected by trehalose incorporation. Intermolecular ^{13}C-^{31}P distances between a membrane peptide and the lipid headgroups are 10% longer in the hydrated membrane at 226 K than in the trehalose-protected dry membrane at 253 K. This is attributed to residual motions in the hydrated membrane, manifested by the reduced ^{31}P chemical shift anisotropy, even at the low temperature of 226 K. Thus, trehalose lyoprotection facilitates the study of membrane protein

structure by allowing experiments to be conducted at higher temperatures than possible with the hydrated membranes.

Keywords: trehalose, lipid bilayers, ^{13}C-^{31}P distances, membrane peptide structure, solid-state NMR

1. Introduction

Trehalose (TRE), a non-reducing disaccharide of glucose, is known to stabilize lipid bilayers and proteins during dehydration and rehydration. It is found at concentrations as much as 20 wt% of the dry weight of anhydrobiotic organisms [1]. Generally, the protection efficiency is proportional to the concentration of trehalose, but the full protection can be achieved when the concentration of trehalose reaches a threshold, which is ~100 mM in the preservation of proteins and 0.3 g/g of lipid in the preservation of phospholipid bilayers during drying [2, 3]. The mechanism of trehalose stabilization of cell membranes is proposed to be a depression of the gel to liquid-crystalline (LC) phase transition temperature (T_m) of the dry membrane, so that membrane disruption, which normally occurs during phase transition, is prevented during rehydration [4]. On a molecular level, trehalose is believed to replace the hydrogen bonds between water and the lipid phosphate group with hydrogen bonds between its own OH groups and the phosphate, thus maintaining membrane integrity in the absence of water. This "lyoprotecting" property of trehalose can be, and indeed has been [5], exploited in solid-state NMR studies of the depth of insertion of membrane proteins. The depth information can be obtained from distance measurements between ^{13}C labels in the protein and the ^{31}P spin of the lipid headgroup. This requires the motions that are abundant in hydrated lipid bilayers to be frozen to yield rigid-limit distance-dependent dipolar couplings. Freezing lipid motions requires temperatures of at least 40 K below T_m, often over an extended period of time to allow signal averaging of the lipid-diluted peptides. These are challenging conditions for NMR experiments. We show here that trehalose-containing dry lipid membranes preserve the lipid bilayer structure while removing the headgroup and glycerol backbone motions at higher temperatures than the hydrated membranes, thus facilitating the measurement of protein-lipid distances. While the phase properties of

trehalose-DPPC mixtures had been investigated by NMR before [6, 7], a comparison of the conformation of the hydrated and trehalose-containing membranes for protein structure determination has not been reported.

2. Results and discussion

We first characterize the dynamic structure of trehalose-containing lipid membranes by static ^{31}P and ^{2}H NMR. POPC is chosen as a model system because its chain lengths (16 and 18 carbons) are dominant in biological membranes and the choline headgroup is common in eukaryotic cell membranes. Hydrated POPC bilayers have a relatively low T_m of 271 K, thus necessitating low temperatures of ~220 K or below to freeze the lipid motion. We compared the mobility of the lipid headgroup and the acyl chain between the hydrated POPC and trehalose-protected lyophilized POPC membrane (TRE-POPC) at various temperatures. Fig. 5.1 shows the ^{31}P spectra of hydrated POPC bilayers with 35 wt% water (a) and lyophilized POPC membrane containing 20 wt% trehalose (b). The transition temperature for the headgroup region of the TRE-POPC membrane is ~323 K, which is ~50 K higher than that of the hydrated POPC membrane. At 273 K, the ^{31}P spectrum of hydrated POPC (a) shows a small chemical shift anisotropy (CSA), $\delta = \delta_{ZZ}-\delta_{iso}$, of 30 ppm and an asymmetry parameter η of 0, characteristic of uniaxially mobile lipids in L_α-phase membrane. In contrast, TRE-POPC reaches a similarly narrow CSA and uniaxial lineshape only at ~323 K. To obtain the rigid-limit ^{31}P CSA of ~110 ppm [8], a low temperature of 233 K is required for hydrated POPC while T = 263 K is sufficient for TRE-POPC. Fig. 5.1(c, d) plots ^{31}P CSA δ and η as a function of temperature for the two samples. Compared to the hydrated POPC membrane, trehalose increases the lipid-headgroup phase transition temperature by ~50 K. This does not contradict the fact that trehalose suppresses the T_m of dry POPC, which is ~340 K [9]. Based on the observed temperature at which ^{31}P CSA is motionally narrowed (323 K), the addition of 20% trehalose decreased the T_m of dry POPC by ~15 K.

In comparison, the acyl chain region exhibits a much smaller difference between the transition temperatures of the hydrated POPC membrane and TRE-POPC membrane. The ^{2}H quadrupolar couplings of d_{31}-POPC (Fig. 5.2) indicate that at the highest temperature at which the lipid headgroups are rigid, the chains in the hydrated membrane are frozen (233 K)

while the chains in the TRE-POPC membrane remain partly mobile (263 K). The deferred freezing of the acyl chains compared to the headgroup was also observed in TRE-DPPC membrane [6]. At the same temperature, the lipid chain dynamics is similar between the hydrated and the trehalose-protected POPC membranes, as seen, for example, in the ^{2}H spectra at 263 K (Fig. 5.2). Thus, trehalose specifically restricts the motion of the lipid headgroups while largely preserving the acyl chain mobility. For the peptide-lipid headgroup distance measurement, it is sufficient that the headgroup is rigid.

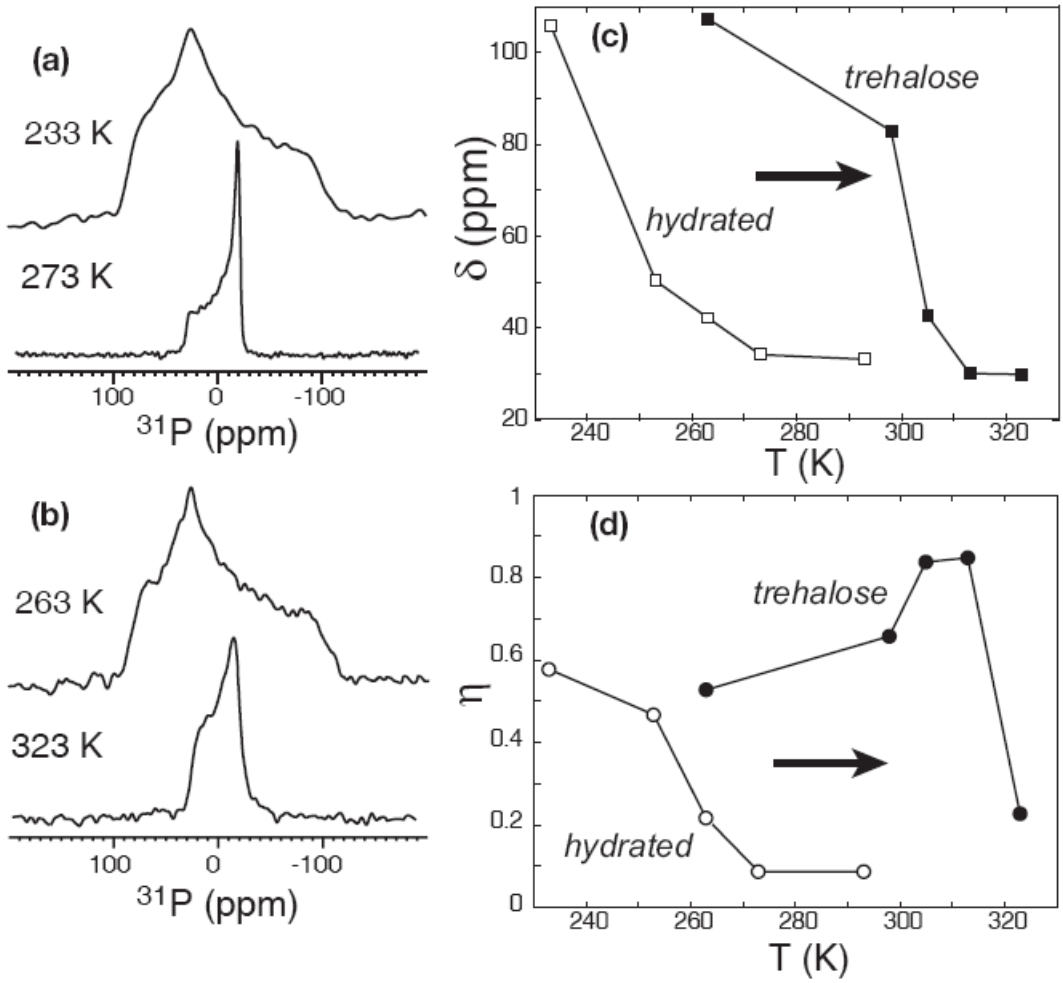

Fig. 5.1. Static ^{31}P spectra of (a) hydrated POPC and (b) lyophilized POPC with 20% trehalose. (c) Temperature dependence of the ^{31}P chemical shift anisotropy parameter δ for hydrated POPC (open squares) and TRE-POPC (filled squares). (d) Temperature dependence of the ^{31}P chemical shift asymmetry parameter η for hydrated POPC (open circles) and TRE-POPC (filled circles).

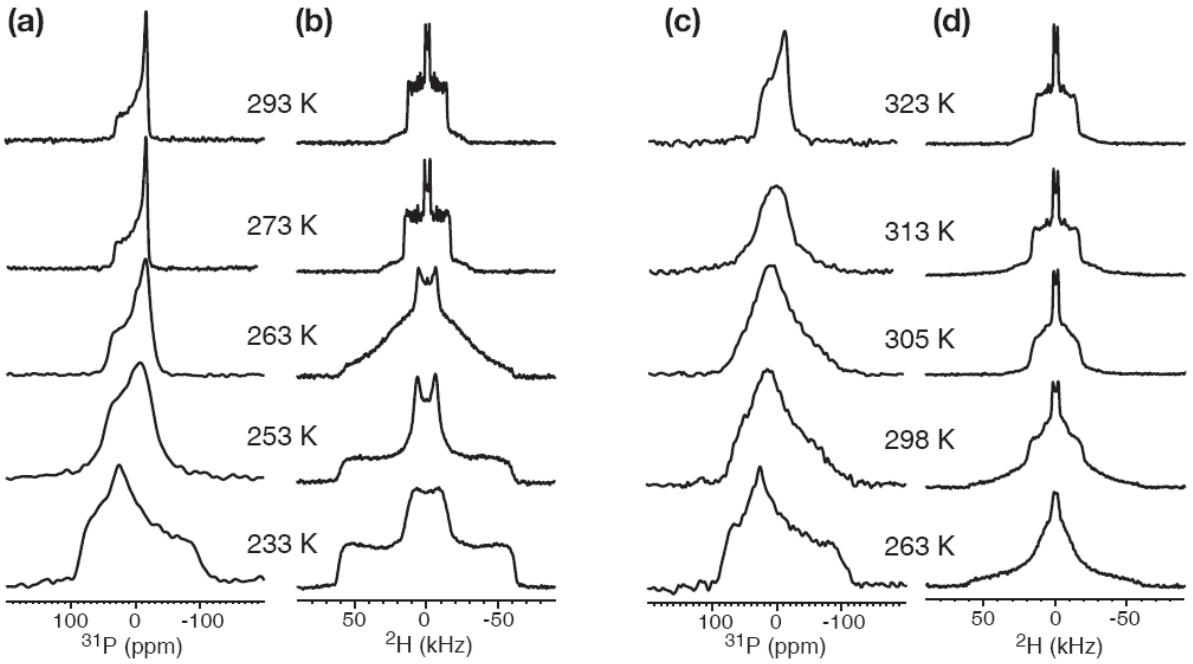

Fig. 5.2. Static ^{31}P (a, c) and ^{2}H (b, d) spectra of d_{31}-POPC in the hydrated membrane (a, b) and in the lyophilized membrane with 20% trehalose (c, d). The lipid headgroup transition temperature is ~273 K for the hydrated POPC but ~323 K for TRE-POPC. However, the acyl chain mobilities are similar between the two membranes.

To assess if the addition of trehalose affects the headgroup and glycerol backbone conformation of the lipid, we measured the intramolecular distances between the two carboxyl (C') carbons and ^{31}P in the ^{13}C'-labeled crystalline POPC and TRE-POPC. The rotational-echo double resonance (REDOR) experiment [10] was used to measure the heteronuclear distance. Crystalline POPC was used to represent the structure of frozen hydrated POPC, since crystal structures of other phosphocholine lipids show well-defined lamellar structures in which the headgroup and backbone conformation of the molecules is believed to represent the main conformation of the hydrated lipid [11]. Fig. 5.3a shows ^{13}C'-^{31}P REDOR S/S_0 values of ^{13}C'-labeled crystalline POPC obtained at room temperature. Four ^{13}C' peaks are resolved, indicating the high degree of order of the sample. These are assigned to two unique molecules in the unit cell, each with two distinct ^{13}C' sites, *sn*-1 and *sn*-2 C'. The presence of two inequivalent molecules in the unit cell is inferred from the crystal structure of the analogous DMPC lipid [11], since the POPC crystal structure is not known.

The two downfield $^{13}C'$ peaks exhibit faster REDOR decays indicative of a distance of 5.3 Å, while the two upfield peaks give longer distances of 6.2 Å and 6.7 Å (Fig. 5.3a). The crystal structure of DMPC [11] shows that the *sn*-2 $^{13}C'$-^{31}P distances are shorter than the *sn*-1 $^{13}C'$-^{31}P distances by 1.4 Å and 2.4 Å (Table 5.1). Thus, we assigned the downfield peaks to *sn*-2 $^{13}C'$. Fig. 5.3b shows the REDOR data of TRE-POPC acquired at 263 K. While the resolution is reduced compared to the crystalline sample, the differential dephasing remains clear (inset). TRE-POPC also exhibits a short distance, 5.3 ± 0.6 Å, for the downfield signal and longer distances, 5.8 ± 1.0 Å and 6.8 ± 1.2 Å, for the two upfield peaks. The distances have significant distributions, reflected by the need for a Gaussian distribution function to simulate the REDOR curves, with the half-width-at-half-maximum of the Gaussian reported as the uncertainty. This distance distribution is consistent with the observed peak broadening, indicating increased conformational heterogeneity of the lyophilized TRE-POPC membrane compared to the crystalline POPC lipid. Despite this heterogeneity, the average distances are similar between the crystalline POPC and TRE-POPC, indicating that trehalose preserves the lipid headgroup and glycerol backbone conformation. To emphasize the innate disorder and distance distribution in lipid bilayers, we also show the $^{13}C'$-^{31}P distances from MD simulations of hydrated POPC bilayers (Fig. 5.3c-d). The average distances and their standard deviations are 5.5 ± 0.5 Å (*sn*-2) and 6.2 ± 0.5 Å (*sn*-1) for the L_α phase (http://persweb.wabash.edu/facstaff/fellers/), and 4.7 ± 0.6 Å (*sn*-2) and 6.7 ± 0.6 Å (*sn*-1) for the gel phase [12]. The measured REDOR distances agree well with these values within experimental uncertainty, except for the 5.8 Å distance in the TRE-POPC sample.

Table 5.1. Comparison of intramolecular $^{13}C'$-^{31}P distances in crystalline and trehalose-protected POPC lipids from REDOR, MD simulations and X-ray crystallography.

Sites	Chemical shift (ppm)	$^{13}C'$-^{31}P distances (Å)				
		Crystalline POPC	TRE-POPC	MD		DMPC crystal structure
				L_α phase [a]	Gel phase [b]	
sn-1	172.0	6.2	6.8 ± 1.2	6.2 ± 0.5	6.7 ± 0.6	6.8
	173.5	6.7	5.8 ± 1.0			7.0
sn-2	174.6	5.3	5.3 ± 0.6	5.5 ± 0.5	4.7 ± 0.6	5.4
	175.5	5.3	5.3 ± 0.6			4.6

[a] Obtained from: http://persweb.wabash.edu/facstaff/fellers/coordinates/popc.pdb.

[b] Obtained from http://www.lrz-muenchen.de/~heller/membrane/gel.pdb [12].

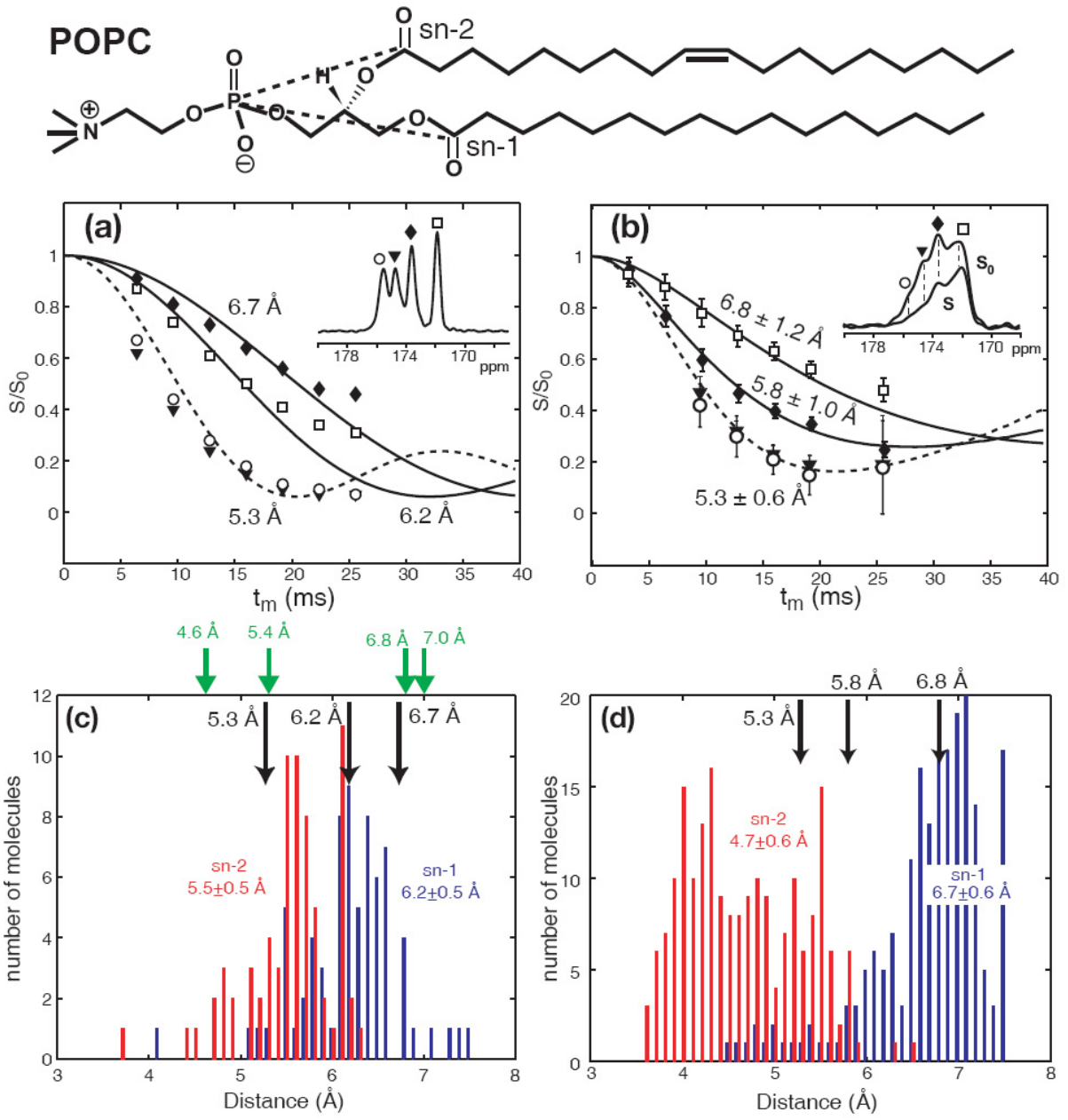

Fig. 5.3. $^{13}C'\{^{31}P\}$ REDOR data of (a) crystalline POPC at 293 K and (b) TRE-POPC at 263 K. The chemical structure of POPC is shown at the top, with the dashed lines indicating the distances measured here. (a) Best-fit distances for crystalline POPC, whose $^{13}C'$ spectrum is shown in the inset, are 5.3 Å (dashed line) for the two downfield peaks, and 6.2 Å and 6.7 Å (solid lines) for the two upfield peaks. (b) Inset is the S_0 (solid line) and S (dashed line) spectra of TRE-POPC at t_m = 12.8 ms. Best-fit distances are 5.3 ± 0.6 Å for the downfield peaks

and 5.8 ± 1.0 Å and 6.8 ± 1.2 Å for the upfield peaks. Simulations in (a, b) used an intensity scaling factor of 90% to account for the effects of pulse imperfection [15]. (c) ^{13}C'-^{31}P distance distribution in liquid-crystalline POPC bilayers from MD simulations. The average *sn*-1 ^{13}C' - ^{31}P distance (blue) is 6.2 Å with a standard deviation of 0.5 Å. The average *sn*-2 ^{13}C'-^{31}P distance (red) is 5.5 ± 0.5 Å. Black arrows: REDOR-extracted ^{13}C'-^{31}P distances in crystalline POPC. Green arrows: ^{13}C'-^{31}P distances in the DMPC crystal structure [11]. (d) ^{13}C'-^{31}P distance distribution in gel-phase POPC bilayers from MD simulations [12]. The average *sn*-1 ^{13}C'-^{31}P distance (blue) is 6.7 ± 0.6 Å. The average *sn*-2 ^{13}C'-^{31}P distance (red bars) is 4.7 ± 0.6 Å. Black arrows: measured ^{13}C'-^{31}P distances in the TRE-POPC membrane.

We show an example of trehalose lyoprotection for facilitating structural investigation of membrane proteins using protegrin-1 (PG-1). PG-1 is a disulfide-stabilized 18-residue β-hairpin antimicrobial peptide that kills microbial cells by disrupting their cell membranes [13]. To determine the depth of insertion of PG-1 in the lipid bilayer, we measured the distance between ^{13}C'-labeled Val$_{16}$ of PG-1 and the lipid ^{31}P. Fig. 5.4a shows ^{13}C{^{31}P} REDOR decays of Val$_{16}$ ^{13}C' in the dry TRE-POPE/POPG membrane (filled squares), acquired at 253 K, and in the hydrated POPE/POPG membrane (open circles), acquired at 226 K. The former gave a distance of 6.5 Å while the latter gave a longer distance of 7.2 Å. Although we cannot rule out the possibility of subtle differences in the PG-1 depth of insertion between the two membranes, the ^{13}CO linewidth (3.5 ppm) and chemical shift (172 ppm) of Val$_{16}$ are the same between the frozen hydrated membrane and the trehalose-protected membrane, indicating that the peptide conformation, and by inference its binding, is unchanged. At the same time, ^{31}P NMR spectra show that there is residual motion in the hydrated membrane even at the low temperature of 226 K. The ^{31}P CSA principle values are (82.9 ppm, 21.4 ppm, -110.0 ppm) for the TRE-POPE/POPG membrane (black) at 253 K (Fig. 5.4b), giving δ = 108.1 ppm, while the hydrated POPE/POPG membrane (red) has a smaller CSA of δ = 104.7 ppm (80.1 ppm, 21.1 ppm, -106.4 ppm). Thus, the hydrated lipid bilayer exhibits small-amplitude motion of the headgroups even at 226 K [8]. This motion is faster than the ^{31}P CSA interaction of ~18 kHz. Since the measured ^{13}C-^{31}P dipolar coupling is about 35 Hz, there are likely additional slower headgroup motions on the 10^{-5} – 10^{-2} s timescale that further average the peptide-lipid dipolar coupling. Thus, we attribute the

observed 0.7 Å longer distance or a dipolar order parameter of 0.74 ($S = \bar{\omega}_d / \omega_d$) to this residual motion.

The above REDOR distances were extracted using two-spin simulations (one ^{13}C and one ^{31}P). Geometric constraints indicate that at most two ^{31}P spins can be simultaneously close to any carbon in the middle of the peptide chains. Using 3-spin simulations changes the individual distances by up to 20% for short distances of < 4.5 Å and up to 10% for distances longer than 6.5 Å, and thus does not affect the structural conclusion significantly. A full report of the PG-1 peptide-lipid distance study will be given elsewhere.

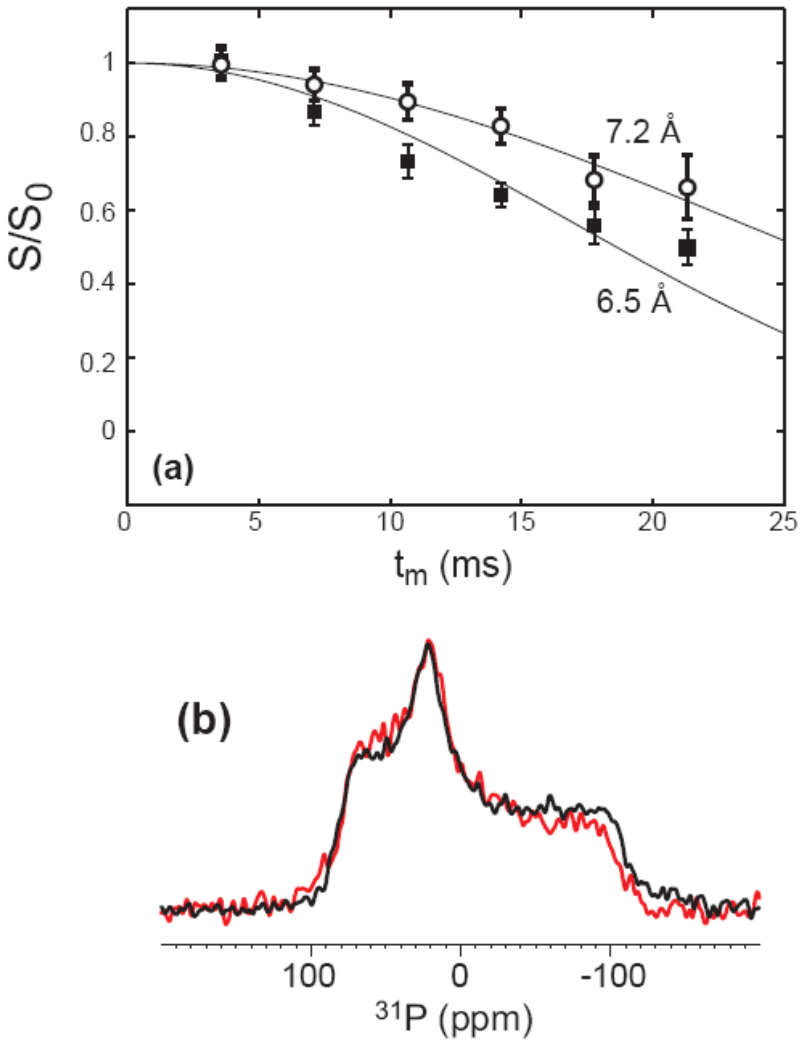

Fig. 5.4. (a) REDOR curves of PG-1 Val_{16} ^{13}CO after natural abundance correction in the TRE-POPE/POPG membrane (filled squares) and in hydrated POPE/POPG membrane (open circles). The experiments were conducted at 253 K for the lyophilized sample and 226 K for the hydrated sample. Best-fit distances are 6.5 Å for the former and 7.2 Å for the latter. (b) ^{31}P static spectra of the TRE-POPE/POPG membrane (black) at 253 K and the hydrated POPE/POPG membrane (red) at 226 K. Both contain PG-1 at P/L (mole) = 1:12.5.

3. Conclusion

In conclusion, we find that trehalose-protected dry lipid membrane gives rise to a more immobilized matrix in the headgroup and glycerol backbone region, while not significantly affecting the lipid chain mobility compared to the hydrated membrane. Importantly, the membrane interface immobilization by trehalose occurs without changing

the lipid headgroup and backbone conformation, as shown by intramolecular $^{13}C'$-^{31}P distances. This suggests that the rigid-limit membrane-bound structure of proteins should be very similar between hydrated and trehalose-protected dry membranes. A peptide-lipid ^{13}C-^{31}P distance measurement shows that the hydrated membrane sample gives a motionally averaged coupling even at 226 K while the trehalose-protected dry sample gives rigid-limit dipolar coupling already at 253 K. Thus, trehalose lyoprotection should facilitate the determination of membrane protein distances to lipid headgroups as well as membrane protein conformation itself by enabling these experiments at conveniently accessible mild low temperatures.

4. Materials and methods

Unlabeled and $^{13}C'$ labeled 1-palmitoyl-2-oleoyl-*sn*-glycerol-3-phosphatidylcholine (POPC), 1-palmitoyl-2-oleoyl-*sn*-glycero-3-phosphatidylethanolamine (POPE), and 1-palmitoyl-2-oleoyl-*sn*-glycero-3-phosphatidylglycerol (POPG) were purchased from Avanti Polar Lipids (Alabaster, AL). PG-1 (NH_2-RGGRLCYCRRRFCVCVGR-$CONH_2$) was synthesized using Fmoc solid-phase protocols as previously described [14].

Membrane sample preparation

Six different membrane samples were prepared. Hydrated POPC and trehalose-protected dry POPC were used to measure the ^{31}P chemical shift anisotropy and ^{2}H quadrupolar couplings of the perdeuterated palmitoyl chains. $^{13}C'$-labeled POPC in the crystalline form and the trehalose-mixed form was used to measure intramolecular $^{13}C'$-^{31}P distances. Two PG-1 containing membrane samples were compared with respect to their intermolecular ^{13}C-^{31}P distances: a trehalose-containing dry POPE/POPG membrane, and a hydrated POPE/POPG membrane.

Crystalline $^{13}C'$-labeled POPC was taken directly from the Avanti bottle. The high degree of structural order is evident from the fact that the ^{31}P spectrum gives the rigid-limit CSA at ambient temperatures (not shown), and that four ^{13}CO peaks are well resolved in a 4 ppm range, with linewidths (FWHM) of 0.4-0.6 ppm.

Hydrated POPC membrane was prepared by adding 35 wt% water directly to the dry lipid powder. The trehalose-containing dry POPC membrane was prepared by mixing trehalose (20% of dry lipid mass) and POPC in water, freeze-thawing the suspension three times, then lyophilizing the mixture. The dried mixture was packed into a 4 mm MAS rotor, then further lyophilized in the rotor to remove the moisture from packing.

To prepare the PG-1-containing membrane sample, POPE and POPG (3:1 molar ratio) were mixed in chloroform and blown dry, then redissolved in cyclohexane and lyophilized. The lipids were redissolved in water and subjected to five cycles of freeze-thawing to form homogeneous vesicles. The peptide and lipid solutions were mixed, incubated at 303 K for 12 hours, then ultracentrifuged at 55,000 rpm for 2 hours. For the hydrated POPE/POPG membrane sample, the pellet was directly packed into a 4 mm MAS rotor. For the trehalose-protected dry membrane sample, the pellet was resuspended in water, and an amount of trehalose equivalent to 20% of the dry weight of the lipids and peptide was added. The suspension was subjected to three more cycles of freeze-thawing, lyophilized, packed into a 4 mm MAS rotor, then lyophilized again to remove residual moisture from packing.

Solid-state NMR experiments

NMR experiments were carried out on a Bruker DSX-400 spectrometer operating at a resonance frequency of 400.49 MHz for ^{1}H, 162.12 MHz for ^{31}P, 61.48 MHz for ^{2}H and 100.70 MHz for ^{13}C. A double-resonance static probe equipped with a 5-mm diameter solenoid coil was used for static ^{2}H and ^{31}P experiments. A triple-resonance MAS probe with a 4 mm spinning module was used for the ^{13}C{^{31}P} REDOR experiments. Low temperatures were achieved using a Kinetics Thermal Systems XR air-jet sample cooler (Stone Ridge, NY). The temperature was maintained within ±1 K of the reported value, and the spinning speed was regulated to within ±3 Hz. Typical 90° pulse lengths were 4 - 5 μs for all nuclei. ^{1}H decoupling field strengths of 50-80 kHz were used. ^{1}H-^{13}C cross-polarization (CP) contact times were 0.5 ms. ^{13}C chemical shifts were referenced externally to the α-Gly ^{13}C' signal at 176.49 ppm on the TMS scale. The ^{31}P chemical shift was referenced externally to 85% phosphoric acid at 0 ppm.

A modified REDOR pulse sequence containing composite ^{31}P π pulses, 90°180°90°, and exorcycled ^{13}C π pulse was used [15]. This composite-pulse sequence reduces the effect of the pulse flip angle errors, thus improving the distance accuracy. Two experiments were conducted for each t_m, a control experiment (S_0) where all the ^{31}P pulses are turned off, and a dephasing experiment (S) where the ^{31}P pulses are on. The normalized dephasing, S/S_0, as a function of t_m gives the dipolar coupling without the T_2 relaxation effect of the ^{13}C spin. Typical 180˚ pulse lengths were 10 μs for ^{13}C and 8-10 μs for ^{31}P. The spinning speed was 5 kHz for the pure lipid samples and 4.5 kHz for the peptide-containing membrane samples. REDOR data were simulated using an in-house Fortran program.

Acknowledgments

This work is supported by NIH grants GM-066976 to M. H. and AI-22839 and AI-37945 to A.J.W.

References

[1] J.H. Crowe, L.M. Crowe, D. Chapman, Preservation of Membranes in Anhydrobiotic Organisms - the Role of Trehalose, Science 223 (1984) 701-703.

[2] J.H. Crowe, L.M. Crowe, J.F. Carpenter, C.A. Wistrom, Stabilization of Dry Phospholipid-Bilayers and Proteins by Sugars, Biochem. J. 242 (1987) 1-10.

[3] T.J. Anchordoquy, K.I. Izutsu, T.W. Randolph, J.F. Carpenter, Maintenance of quaternary structure in the frozen state stabilizes lactate dehydrogenase during freeze-drying, Arch. Biochem. Biophys. 390 (2001) 35-41.

[4] J.H. Crowe, J.F. Carpenter, L.M. Crowe, The role of vitrification in anhydrobiosis, Annu. Rev. Physiol. 60 (1998) 73-103.

[5] O. Toke, W.L. Maloy, S.J. Kim, J. Blazyk, J. Schaefer, Secondary structure and lipid contact of a peptide antibiotic in phospholipid bilayers by REDOR, Biophys. J. 87 (2004) 662-674.

[6] C.W. Lee, S.K. Das Gupta, J. Mattai, G.G. Shipley, O.H. Abdel-Mageed, A. Makriyannis, R.G. Griffin, Characterization of the L lambda phase in trehalose-stabilized dry membranes by solid-state NMR and X-ray diffraction, Biochemistry 28 (1989) 5000-5009.

[7] C.W. Lee, J.S. Waugh, R.G. Griffin, Solid-state NMR study of trehalose/1,2-dipalmitoyl-sn-phosphatidylcholine interactions, Biochemistry 25 (1986) 3737-3742.

[8] S.J. Kohler, M.P. Klein, Orientation and Dynamics of Phospholipid Head Groups in Bilayers and Membranes Determined from P-31 Nuclear Magnetic-Resonance Chemical Shielding Tensors, Biochemistry 16 (1977) 519-526.

[9] K.L. Koster, M.S. Webb, G. Bryant, D.V. Lynch, Interactions between soluble sugars and POPC (1-palmitoyl-2-oleoylphosphatidylcholine) during dehydration: vitrification of sugars alters the phase behavior of the phospholipid, Biochim. Biophys. Acta 1193 (1994) 143-150.

[10] T. Gullion, J. Schaefer, Rotational echo double resonance NMR, J. Magn. Reson. 81 (1989) 196-200.

[11] R.H. Pearson, I. Pascher, The molecular structure of lecithin dihydrate, Nature 281 (1979) 499-501.

[12] H. Heller, M. Schaefer, K. Schulten, Molecular-Dynamics Simulation of a Bilayer of 200 Lipids in the Gel and in the Liquid-Crystal Phases, J. Phys. Chem. 97 (1993) 8343-8360.

[13] L. Bellm, R.I. Lehrer, T. Ganz, Protegrins: new antibiotics of mammalian origin., Exp. Opin. Invest. Drugs 9 (2000) 1731-1742.

[14] S. Yamaguchi, T. Hong, A. Waring, R.I. Lehrer, M. Hong, Solid-state NMR investigations of peptide-lipid interaction and orientation of a beta-sheet antimicrobial peptide, protegrin, Biochemistry 41 (2002) 9852-9862.

[15] N. Sinha, K. Schmidt-Rohr, M. Hong, Compensation for pulse imperfections in rotational-echo double-resonance NMR by composite pulses and EXORCYCLE, J. Magn. Reson. 168 (2004) 358-365.

Chapter 6

Phosphate-Mediated Arginine Insertion into Lipid Membranes and Pore Formation by a Cationic Membrane Peptide from Solid-State NMR

Published in J. Am. Chem. Soc.

2007, 129, 11438-11446

Ming Tang[1], Alan J. Waring[2], and Mei Hong[1]

[1] Department of Chemistry, Iowa State University, Ames, IA 50011

[2] Department of Medicine, University of California at Los Angeles School of Medicine, Los Angeles, California 90095

Keywords: toroidal pores, REDOR, Arg-rich peptides, guanidinium-phosphate complexation, cationic residues.

Abstract

The insertion of charged amino acid residues into the hydrophobic part of lipid bilayers is energetically unfavorable yet found in many cationic membrane peptides and protein domains. To understand the mechanism of this translocation, we measured the ^{13}C-^{31}P distances for an Arg-rich β-hairpin antimicrobial peptide, PG-1, in the lipid membrane using solid-state NMR. Four residues, including two Arg's, scattered through the peptide were chosen for the distance measurements. Surprisingly, all residues show short distances to the lipid ^{31}P: 4.0 – 6.5 Å in anionic POPE/POPG membranes and 6.5 – 8.0 Å in zwitterionic POPC membranes. The shortest distance of 4.0 Å, found for a guanidinium Cζ at the β-turn, suggests $N-H\cdots O-P$ hydrogen bond formation. Torsion angle measurements of the two Arg's quantitatively confirm that the peptide adopts a β-hairpin conformation in the lipid

bilayer, and gel-phase ^{1}H spin diffusion from water to the peptide indicates that PG-1 remains transmembrane in the gel phase of the membrane. For this transmembrane β-hairpin peptide to have short ^{13}C-^{31}P distances for multiple residues in the molecule, some phosphate groups must be embedded in the hydrophobic part of the membrane, with the local ^{31}P plane parallel to the β-strand. This provides direct evidence for toroidal pores, where some lipid molecules change their orientation to merge the two monolayers. We propose that the driving force for this toroidal pore formation is guanidinium-phosphate complexation, where the cationic Arg residues drag the anionic phosphate groups along as they insert into the hydrophobic part of the membrane. This phosphate-mediated translocation of guanidinium ions may underlie the activity of other Arg-rich antimicrobial peptides and may be common among cationic membrane proteins.

Introduction

Charged and polar residues are surprisingly common in a diverse range of membrane proteins. For instance, cationic antimicrobial peptides (AMPs) such as protegrin-1 (PG-1: **R**GG**R**LCYC**RRR**FCVCVG**R**) permeabilize the lipid membranes of microbes to cause cell death [1,2]. Cell-penetrating peptides such as the HIV TAT peptide (48-60: G**RKKRR**Q**RRR**PPQ) are rich in Arg and Lys and yet translocate across cell membranes with ease [3,4]. Voltage-gated potassium channels contain voltage-sensing domains (e.g. KvAP S4 helix: LGLF**R**LV**R**LL**R**FL**R**ILLII) rich in Arg [5]. Polar residues such as Asn and Glu play important functional and stabilizing roles in the folding of membrane proteins by forming interhelical hydrogen bonds [6-8]. Generally, the insertion of the charged and polar residues into the hydrophobic part of the bilayer is energetically unfavorable. This has been studied in detail by measuring, for example, the free energies of transferring peptides from water to octanol [9]. However, this view is recently modified by the finding that hydrophobic residues compensate for the energy cost of incorporating charged and polar residues into the lipid bilayer and that the free energy of insertion also depends sensitively on the position of the polar residues in the membrane [10]. Using an *in vitro* endoplasmic reticulum translocon system, von Heijne, White, and coworkers measured the equilibrium constant of membrane insertion of designed polypeptides containing the amino acid of interest at various positions

[10]. The resulting biological hydrophobicity scale for the twenty amino acids was found to be position-dependent as well as charge- and polarity- dependent. It was found that the S4 helix of the voltage-gated potassium channel KvAP inserts into the membrane despite the presence of four Arg's [11], and the fraction of insertion increases when two Arg residues moved one step closer to the C-terminus. Molecular dynamics simulations showed that the effective lipid bilayer thickness was reduced to an astonishingly small ~10 Å near the inserted S4 helix so that water and phosphate groups stabilize the Arg residues in the middle of the helix through hydrogen bonding [12]. However, such a dramatic accommodation of the Arg residues by the lipid bilayer has not been directly observed experimentally.

PG-1 is a broad-spectrum AMP found in porcine leukocytes [1,13]. It is a β-hairpin molecule stabilized by two disulfide bonds and contains six Arg residues (Figure 6.1a). Its Arg-rich sequence and β-sheet conformation [14] are characteristic of many AMPs such as human defensins and tachyplesin [15,16]. PG-1 carries out its antimicrobial function by forming pores in the microbial cell membrane, thus disrupting the membrane's barrier function. These pores were observed from lipid vesicle leakage assays [17,18] and neutron diffraction [19]. Recently, ^{1}H and ^{19}F spin diffusion NMR data showed that PG-1 self-assembles into a transmembrane oligomeric β-barrel in bacteria-mimetic POPE/POPG membranes [20], providing the first high-resolution structure of PG-1 at the pores. However, the depths of insertion of the Arg residues in these β-barrels relative to the lipid bilayer remain elusive. According to the hydrophobicity scale of White and Von Heijne, the insertion of a single Arg into the center of the bilayer costs a free energy of 2.58 kcal/mol [10], one of the highest ΔG values among the twenty amino acids. Yet PG-1, with six Arg residues distributed both in the middle of the β-strand and at the two ends of the β-hairpin, has been shown to insert well into the hydrophobic part of most lipid membranes except for cholesterol-containing POPC bilayers at high peptide concentrations [20-23]. To solve this puzzle, we have now measured the distances between Arg residues in PG-1 and ^{31}P of the lipid headgroups using rotational-echo double resonance (REDOR) experiments. Surprisingly, we found that both Arg's at the β-turn and in the middle of the β-strand have short distances of less than 6.5 Å to ^{31}P. This is true for both the backbone and the sidechain of the Arg residues, thus sidechain snorkeling to the membrane surface [24] cannot account for the observation. Instead, the data indicate that

PG-1 causes some of the phosphate groups to insert into the hydrophobic part of the membrane so that the local ^{31}P plane is parallel to the β-strands. Thus, some lipid molecules must change their orientations and merge the two monolayers, as proposed in the toroidal pore model. These results, which represent the first high-resolution distance constraints of Arg residues in proteins with respect to lipid membranes, suggest that the molecular mechanism for toroidal pore formation is guanidinium-phosphate complexation, which neutralizes the guanidinium ions before they insert into the membrane.

Materials and Methods

All lipids were purchased from Avanti Polar Lipids (Alabaster, AL). PG-1 was synthesized using Fmoc chemistry as previously described [25]. Four PG-1 samples were synthesized, containing U-^{13}C, ^{15}N-Arg_4 and ^{15}N-Leu_5, U-^{13}C, ^{15}N-Arg_{11} and ^{15}N-Phe_{12}, $^{13}C\alpha$-Leu_5, and ^{13}CO-Val_{16}. U-^{13}C, ^{15}N-labeled Arg was obtained from Spectra Stable Isotopes (Columbia, MD) as Fmoc-Arg(MTR)-OH.

POPE and POPG lipids were mixed in chloroform at a 3:1 molar ratio and blown dry under N_2 gas. The mixture was then redissolved in cyclohexane and lyophilized. The dry lipid powder was dissolved in water and subjected to five cycles of freeze-thawing to form uniform vesicles. An appropriate amount of PG-1 to reach a peptide-lipid molar ratio of 1 : 12.5 was dissolved in water and mixed with the lipid vesicle solution, incubated at 303 K overnight, then centrifuged at 55,000 rpm for 2.5 hours. The pellet was packed into a MAS rotor, giving a hydrated membrane sample. For the trehalose-protected membrane samples, the pellet was resuspended in water, and an amount of trehalose equivalent to 20% of the dry mass of the lipid and peptide was added [26]. The suspension was subject to three freeze-thawing cycles, then lyophilized and packed into a rotor. A further lyophilization step was applied to the sample in the rotor to remove moisture gained during packing. The POPC samples were prepared similarly. The sugar-protected dry membranes have the same lamellar structure as hydrated membranes, but have reduced lipid headgroup motion, thus enabling distance experiments to be conducted at mild temperatures [27].

NMR experiments were carried out on a Bruker DSX-400 (9.4 Tesla) spectrometer (Karlsruhe, Germany) and an AVANCE II 600 MHz (14.1 Tesla) spectrometer. Triple-

resonance magic-angle spinning (MAS) probes with a 4 mm spinning module was used. Low temperatures were reached using a Kinetics Thermal Systems XR air-jet sample cooler (Stone Ridge, NY) on the 400 MHz system and a Bruker BCU-Xtreme unit on the 600 MHz spectrometer. Typical 90° pulse lengths were 4 – 5 μs for ^{13}C and ^{31}P, and ^{1}H decoupling fields of 50-80 kHz were used. ^{13}C chemical shifts were referenced externally to the α-Gly $^{13}C'$ signal at 176.49 ppm on the TMS scale.

^{13}C-^{31}P distances were measured using a selective REDOR experiment [28] for the uniformly ^{13}C, ^{15}N-labeled Arg residues and non-selective REDOR [29] for the site-specifically labeled Leu_5 $^{13}C\alpha$ and Val_{16} ^{13}CO samples. Composite 90°180°90° pulses were applied on the ^{31}P channel to reduce the effect of flip angle errors and enhance the distance accuracy [30]. For the selective REDOR experiment, the central ^{13}C π pulse is a rotor-synchronized Gaussian pulse of 444 or 888 μs centered at the ^{13}C frequency of interest. This soft pulse recouples the desired ^{13}C-^{31}P dipolar coupling, but removes the ^{13}C-^{13}C J-coupling between the ^{13}C on resonance and its directly bonded ^{13}C. For the specifically labeled samples, a hard ^{13}C π pulse was used. At each REDOR mixing time (t_m), a control experiment (S_0) with the ^{31}P pulses off and a dephasing experiment (S) with the ^{31}P pulses on were carried out. The normalized dephasing, S/S_0, as a function of t_m gives the ^{13}C-^{31}P dipolar coupling. The CO data were corrected for the lipid natural-abundance CO signal. The experiments were conducted under 4.5 kHz MAS at 253 K for the TRE-POPE/POPG membranes, and under 5 kHz MAS and 263 K for the TRE-POPC membranes. ^{31}P 180° pulse lengths of 8-9 μs were used to achieve complete inversion of the broad ^{31}P resonance.

The ψ angles of Arg_4 and Arg_{11} were measured using the NCCN technique, which correlates the $^{15}N_i$-$^{13}C\alpha_i$ and $^{13}CO_i$- $^{15}N_{i+1}$ dipolar couplings to obtain the relative orientation of the two bonds [31,32]. $^{13}C\alpha$-^{13}CO double quantum coherence was excited using the SPC-5 sequence [33], and evolves under the REDOR-recoupled ^{13}C-^{15}N dipolar interaction [29]. A pair of ^{13}C spectra were collected at each C-N mixing time, and the S/S_0 values of the CO and Cα signals were averaged and plotted as a function of mixing time to yield the ψ-angle dependent curve. The ϕ angles were measured using the HNCH technique, which correlates the $^{1}H^{N}$-^{15}N and $^{13}C\alpha$-$^{1}H\alpha$ dipolar couplings [34]. The experiment yields H^{N}-N-Cα-Hα angle

(ϕ_H), which is related to the ϕ-angle according to $\phi = \phi_H + 60°$. The NCCN and HNCH experiments were conducted at 253 K on the trehalose-protected membrane samples under 5.5 kHz and 4.44 kHz MAS, respectively.

The 2D ^{31}P-^{1}H correlation experiment with ^{1}H spin diffusion [35] was conducted on hydrated POPE/POPG membranes with and without PG-1 at 303 K under 5 kHz MAS. The ^{1}H spin diffusion mixing time was 64 ms, and a pre-evolution ^{1}H T_2 filter of 800 μs was used to select the mobile component. The ^{1}H-^{31}P CP contact time was 4 ms. The ^{1}H chemical shifts of the POPE/POPG membrane were assigned via the well-known ^{13}C chemical shifts by a ^{13}C-^{1}H 2D correlation experiment.

The gel-phase ^{1}H spin diffusion experiment [36] from water to peptide was carried out on DLPC-bound PG-1 samples, which were used previously to measure the depths of PG-1 residues in the liquid-crystalline (LC) phase by Mn^{2+} paramagnetic relaxation enhancement [22]. The experiments were performed between 230 K and 243 K, such that the water ^{1}H linewidth after a 200 μs T_2 filter is 330 Hz [37]. After the T_2 filter, only the water ^{1}H magnetization and a small amount of headgroup γ proton signal remains, so that without spin diffusion, the ^{13}C spectrum suppresses all peptide and lipid signals except for the lipid Cγ signal. ^{1}H mixing times of 0.25 – 49 ms were then used to detect peptide signals that result from spin diffusion from the membrane surface water.

Results

^{13}C-^{31}P distances between PG-1 and lipid headgroups

We measured the distances from two Arg residues, Arg_4 and Arg_{11}, and two hydrophobic residues, Leu_5 and Val_{16}, to the lipid phosphate groups. Arg_{11} represents the β-turn, which contains three consecutive Arg's, whereas Arg_4 lies in the middle of the N-terminal β-strand (Figure 6.1a). Two types of lipid membranes were used to bind the peptide: the anionic POPE/POPG mixture mimics the bacterial membrane, whereas the zwitterionic POPC bilayer allows the electrostatic effect on distances to be examined. Figure 6.1(b) shows a representative ^{13}C spectrum of Arg_4 in trehalose-protected POPE/POPG (TRE-POPE/POPG) membrane. Both Arg_4 and Arg_{11} exhibit β-sheet secondary shifts for Cα and CO (Table 6.1), but the Arg_4 Cα chemical shift is smaller than Arg_{11} Cα, indicating a more

ideal β-sheet conformation. The Arg Cβ peak overlaps with Cγ (Figure S6.1) and thus cannot be used for secondary structure analysis. Arg_{11} Cα shows two peaks that are 1.0 ppm apart, which we attribute to small conformational differences due to binding to two different lipid headgroups. Overall, the Arg chemical shifts are similar between the POPE/POPG membrane and the POPC membrane, indicating that the conformation is unchanged by the membrane composition.

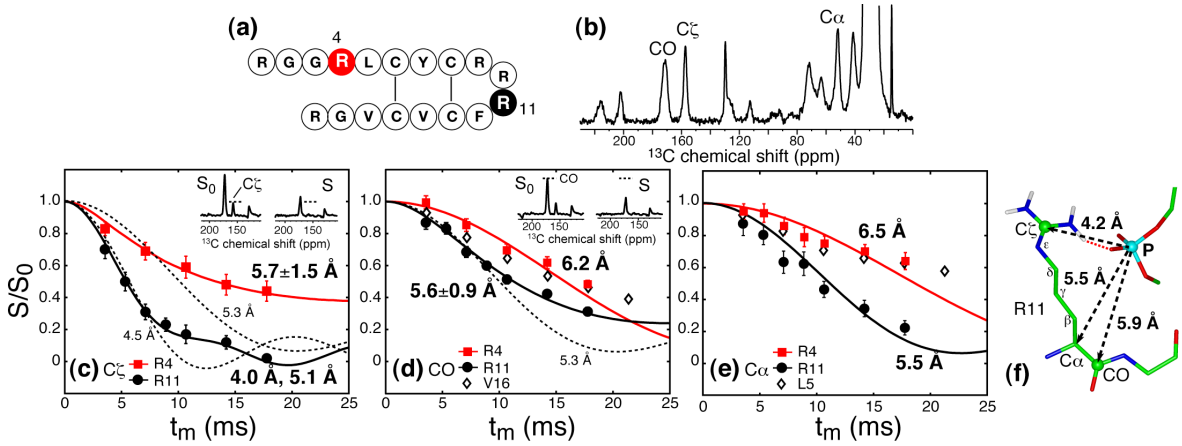

Figure 6.1. ^{13}C-^{31}P REDOR data of Arg_4 (red squares), Arg_{11} (black circles), Leu_5 and Val_{16} (open diamonds) of PG-1 in POPE/POPG membranes. (a) Amino acid sequence of PG-1. The labeled Arg_4 and Arg_{11} are shaded. (b) ^{13}C spectrum of Arg_4 in the TRE-POPE/POPG membrane. The assigned Arg peaks are resolved from the lipid ^{13}C signals. (c) $^{13}C\zeta$-^{31}P distances of Arg_4 and Arg_{11}. Best-fit distances are 5.7 ± 1.5 Å for Arg_4 and 4.0 Å and 5.1 Å (1 : 1) for Arg_{11}. The single-distance best-fit curves of 5.3 Å and 4.5 Å (dashed lines) disagree with the experiment, indicating a distance distribution for Arg_{11}. A pair of REDOR spectra of Arg_{11} Cζ is shown in the inset. (d) ^{13}CO-^{31}P distances. Best-fit distances are 6.2 Å for Arg_4 and Val_{16} and 5.6 ± 0.9 Å for Arg_{11}. The single-distance curve of 5.3 Å (dashed line) does not fit the Arg_{11} data. A pair of Arg_{11} REDOR spectra is shown in the inset. (e) $^{13}C\alpha$-^{31}P distances. Best-fit distances are 6.3 Å for Arg_4 and Leu_5 and 5.5 Å for Arg_{11}. (f) Model of the guanidinium-phosphate complex for Arg_{11} with the measured ^{13}C-^{31}P distances. A putative hydrogen bond between the guanidinium and phosphate groups is indicated as red dotted line.

Figure 6.1(c-e) shows the $^{13}C\{^{31}P\}$ REDOR data of various ^{13}C sites in the POPE/POPG membrane. At 253 K, the trehalose-protected membrane [27] has fully immobilized lipid headgroups, as manifested by the rigid-limit ^{31}P chemical shift span (193 ppm). A selective ^{13}C π pulse was used during the REDOR period for the Arg-labeled samples to remove the ^{13}C-^{13}C J-couplings [28]. Intriguingly, all backbone sites of the four

residues as well as the sidechain of both Arg residues gave short distances of 4.0 – 6.5 Å, with Arg_{11} Cζ exhibiting the shortest distances of 4.0 Å and 5.1 Å at a 1:1 ratio (Figure 6.1c). The backbone of the two hydrophobic residues has distances of 6.2 Å and 6.5 Å. These distances have estimated uncertainties of ±0.2 Å. In addition to the short distances, all REDOR curves show nearly quantitative (90%) decay, with the remaining 10% due to pulse imperfections [30]. This means that all peptides, rather than just a fraction, lie close to the lipid headgroups. To verify that the experiment can detect longer ^{13}C-^{31}P distances, we measured the intramolecular ^{13}C-^{31}P distances of POPE bilayers at 226 K. Indeed long distances of 8 Å and greater than 12 Å, which gave no detectable dephasing within a mixing time of 20 ms, were found for the lipid chain carbons far away from ^{31}P (supporting information Figure S6.2).

Table 6.1. ^{13}C isotropic chemical shifts (δ) and full-width-half-maximum (FWHM) linewidths of Arg_4 and Arg_{11} in trehalose-protected POPE/POPG and POPC membranes.

residue	site	POPE/POPG		POPC	
		δ (ppm)	FWHM (ppm)	δ (ppm)	FWHM (ppm)
Arg_4	CO	171.0	4.5	171.1	5.1
	Cα	51.7	3.5	51.7	4.2
	Cζ	157.2	2.6	157.2	2.9
Arg_{11}	CO	172.1	3.8	173.1	4.2
	Cα	53.3, 54.3	6.6	53.8	5.8
	Cζ	157.4	2.5	157.3	2.6

The above distances were extracted by fitting the experimental REDOR dephasing using a two-spin model. While in principle each ^{13}C spin can couple to multiple ^{31}P spins in the plane of the lipid bilayer, the large ^{31}P-^{31}P separation of ~10 Å due to the size of the headgroups, combined with the strong ^{13}C-^{31}P dephasing observed for the PG-1 residues, result in a situation where the vertical distance from the ^{13}C to the multi-^{31}P plane is either the same as or slightly shorter than the two-spin distance. Thus, it is sufficient to analyze the measured REDOR data using the two-spin model. Importantly, the *relative* proximity of various ^{13}C labels to the ^{31}P spins are independent of whether two-spin or multi-spin models

are used in the simulation. Detailed geometric consideration and numerical simulations for up to five-spin systems are given in the supporting information and Figure S6.3.

While the distances between PG-1 and the lipid ^{31}P are overall short, there are residue-specific differences. Arg_{11} is closer to the ^{31}P than Arg_4 by 0.6 – 1.7 Å (Table 6.2). In particular, the short Arg_{11} Cζ-P distances (4.0 Å and 5.1 Å) suggest the formation of a guanidinium-phosphate complex through electrostatic interaction and hydrogen bonding. Figure 6.1f shows a model of this complex. The presence of two Arg_{11} Cζ-P distances is attributed to differential binding of the peptide to the zwitterionic POPE and anionic POPG lipids: the shorter 4.0 Å distance is most likely associated with the POPG fraction. This hypothesis is consistent with the presence of two slightly different Cα chemical shifts of Arg_{11} in the POPE/POPG membrane. Figure 6.1 also shows that the Arg_4 Cζ and Arg_{11} CO data do not match single-distance REDOR curves but require fitting by a Gaussian distance distribution, with half-width at half maximum of 1.5 Å and 0.9 Å, respectively, suggesting conformational heterogeneity at these sites.

To further determine whether the Arg_4 and Arg_{11} distances to ^{31}P depend on the nature of the lipid headgroup, we measured the ^{13}C-^{31}P distances in the zwitterionic POPC membrane. Figure 6.2 shows that the distances are 1.0 – 2.5 Å longer in the POPC membrane than in the POPE/POPG membrane (Table 6.2). Thus, electrostatic attraction plays a significant role in the Arg-phosphate distances. Similar to the trend observed in the POPE/POPG membrane, Arg_4 is ~1.0 Å further away from ^{31}P than Arg_{11} in the POPC membrane.

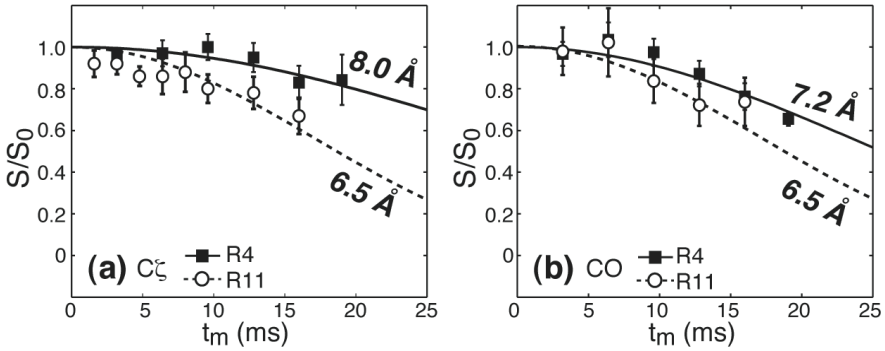

Figure 6.2. ^{13}C-^{31}P REDOR data of (a) Cζ and (b) CO of Arg_4 (squares) and Arg_{11} (circles) in POPC membrane, acquired at 263 K. (a) Best-fit Cζ-P distances are 8.0 Å for Arg_4 (solid line) and 6.5 Å for Arg_{11} (dashed line). (b) Best-fit CO-P distances are 7.2 Å for Arg_4, and 6.5 Å for Arg_{11}.

The peptide-lipid ^{13}C-^{31}P distances measured in the dry TRE-POPE/POPG membrane show only small differences from those in the hydrated POPE/POPG membrane. As shown in Figure S6.4, the Arg_4 Cζ-P distance increased from 5.7±1.5 Å in the dry membrane to 6.8 Å in the hydrated membrane, whereas the Arg_{11} Cζ-P distance remained unchanged. The CO-P distances of both Arg's are 0.3–0.6 Å longer in the hydrated membrane. We attribute the small increase in ^{13}CO-^{31}P distances to residual motions in the hydrated membrane. This is confirmed by the slightly smaller ^{31}P chemical shift span of the hydrated membrane (184 ppm) at 226 K than that of the dry membrane at 253 K (193 ppm).

Figure 6.3 summarizes the ^{13}C-^{31}P distances in the POPE/POPG and POPC membranes. Arg_{11} is the closest residue to the lipid headgroups, and the sidechain guanidinium Cζ are closer to ^{31}P than the backbone atoms. Both Arg residues lie closer to the phosphates in the anionic membrane than in the zwitterionic membrane.

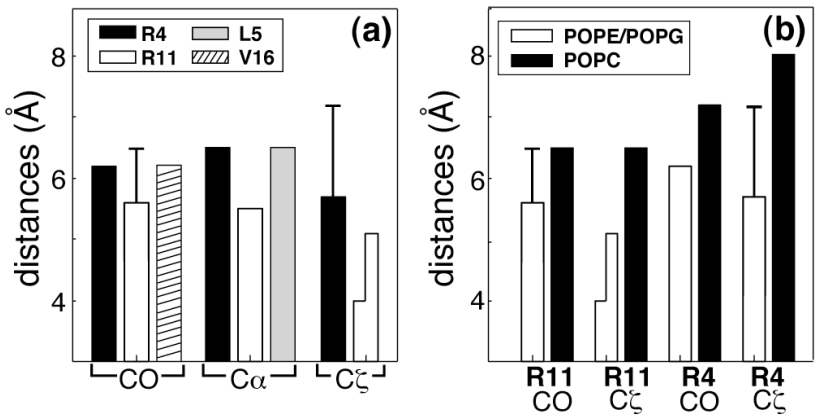

Figure 6.3. Summary of site-specific ^{13}C-^{31}P distances between PG-1 and lipid ^{31}P. (a) Distance comparison for various sites in the POPE/POPG membrane. (b) Comparison of distances between the POPE/POPG membrane (open) and the POPC membrane (filled). "Error" bars indicate distance distributions.

Arg_4 and Arg_{11} conformation

To confirm the β-hairpin conformation of PG-1 in the lipid membrane, we determined the backbone (ϕ, ψ) torsion angles of Arg_4 and Arg_{11} using the dipolar correlation experiments HNCH [34] and NCCN [31,32]. Figure 6.4 shows the HNCH (ϕ angle) and NCCN (ψ angle) data of the two residues in POPC (a, b) and POPE/POPG (c) membranes at 253 K. Both experiments give doubly degenerate angles due to the intrinsically uniaxial nature of the dipolar interaction. This gives rise to $2^4 = 16$ combinations of backbone conformations for each residue. However, using the conformation-dependent Arg Cα and CO chemical shifts (Table 6.1) and the disulfide bond constraints, we can eliminate most solutions, leaving a single solution of (-120°, 159°) for Arg_4 and (-90°, -75°) for Arg_{11} in the POPC membrane. Root mean-square deviation (RMSD) analysis (Figure S6.5) gives angular uncertainties of 5˚–15˚. Thus, Arg_4 adopts a nearly ideal β-strand conformation while Arg_{11} has a β-turn conformation. Changing the membrane to POPE/POPG did not affect the Arg_4 ϕ angle (Figure 6.4c), but altered the Arg_{11} ϕ angle from -90° to -60°. The larger impact of the lipid headgroup on Arg_{11} conformation than Arg_4 is consistent with the shorter distances of Arg_{11} to the phosphate groups. Figure 6.5 summarizes the (ϕ, ψ) angles of Arg_4 and Arg_{11} in POPC membranes.

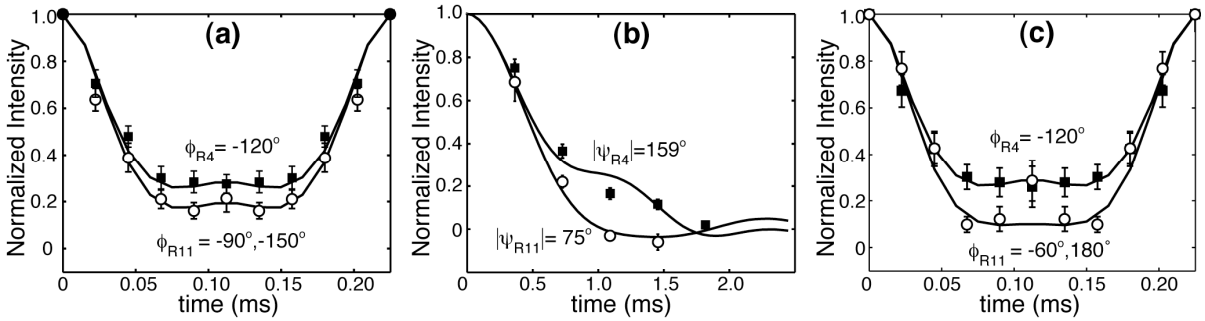

Figure 6.4. HNCH (a, c) and NCCN (b) data and best-fit simulations of Arg_4 (squares) and Arg_{11} (circles) in the POPC membrane (a, b) and POPE/POPG membrane (c). (a) The best-fit ϕ angles are -120 ± 15° for Arg_4 and -90 ± 10° for Arg_{11} in the POPC membrane. (b) The best-fit ψ angles are 159 ± 5° for Arg_4 and -75 ± 15° for Arg_{11} in the POPC membrane. (c) The best-fit ϕ angles are -120 ± 15° for Arg_4 and -60 ± 10° for Arg_{11} in the POPE/POPG membrane. The angular uncertainty was estimated from RMSD analyses (Figure S6.5).

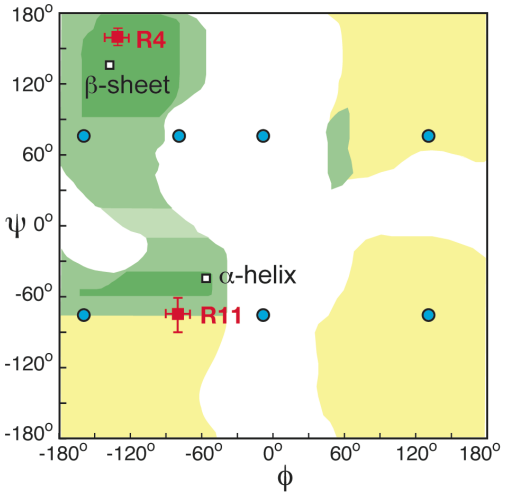

Figure 6.5. Ramachandran diagram of Arg_4 and Arg_{11} in PG-1. Experimental (ϕ, ψ) torsion angles are shown in red squares. Blue circles indicate other (ϕ, ψ) angle solutions for Arg_{11} that are ruled out by chemical-shift and disulfide-bond constraints. The classical α-helix and β-sheet positions are indicated as open squares.

^{1}H spin diffusion from the lipid chain to the headgroup in the liquid-crystalline phase

To provide further constraints to the membrane morphology and PG-1 topology in the POPE/POPG membrane, we measured the ^{1}H spin diffusion rates from the lipid chains to the headgroups in the absence and presence of PG-1. A ^{31}P-^{1}H 2D correlation experiment was used, where the chain $(CH_2)_n$ to ^{31}P cross peak results from distance-dependent ^{1}H spin diffusion. In the LC phase where the lipid ^{1}H-^{1}H dipolar coupling is weakened by motion, a lamellar bilayer free of the peptide requires several hundred milliseconds for the $(CH_2)_n$-P cross peak to develop [35]. If PG-1 inserts into the hydrophobic part of the membrane, or if PG-1 binding shortens the headgroup-chain distance through chain upturns [38,39], then spin diffusion will be faster, giving rise to a stronger $(CH_2)_n$-P cross peak.

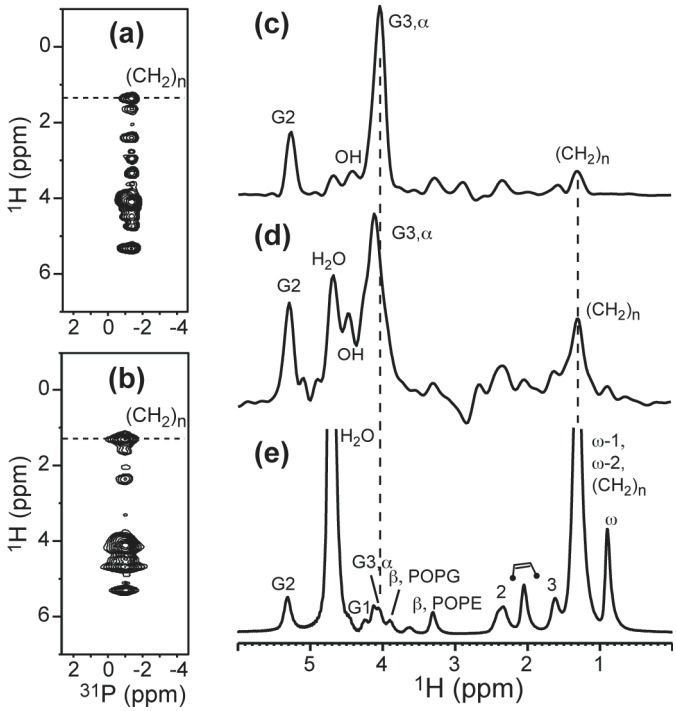

Figure 6.6. ^{31}P-^{1}H correlation spectra of hydrated POPE/POPG membranes with and without PG-1 after a ^{1}H spin diffusion mixing time of 64 ms. (a, b) 2D spectra of POPE/POPG bilayers without and with PG-1, respectively. ^{1}H cross sections are shown in (c) for the peptide-free membrane and (d) for the peptide-bound membrane. (e) Direct-excitation ^{1}H spectrum of the POPE/POPG membrane for comparison. Assignment is obtained from ^{13}C-^{1}H 2D correlation (Figure S6.6). The $(CH_2)_n$ cross peak in (d) is much higher than in (c). The low H_2O cross peak in (c) is attributed to strong hydrogen bonding between the lipid headgroups and water, which immobilizes water and prevents their detection by the ^{1}H T_2 filter. PG-1 likely disrupts some of the lipid-water hydrogen bonds, increasing the H_2O peak intensity in (d).

Figure 6.6 compares the ^{31}P-^{1}H 2D spectra of POPE/POPG membranes without (a, c) and with (b, d) PG-1, measured with a ^{1}H mixing time of 64 ms. Both spectra show the strongest cross peak from the glycerol G3 and α protons, which are closest to the phosphate group. The ^{1}H chemical shift assignment is obtained from a ^{13}C-^{1}H 2D correlation spectrum shown in the supporting information Figure S6.6. Relative to the largest G3/α cross peak, the $(CH_2)_n$ cross peak of the peptide-bound membrane is three-fold higher than that of the peptide-free sample. Thus, either the chain-headgroup distance is shortened in the presence of PG-1, or PG-1 inserts into the acyl chain region, providing a faster spin diffusion route to the headgroup.

^{1}H spin diffusion from water to peptide in the gel phase

Previous experiments on PG-1 bound to DLPC [22,25], POPC [21], and POPE/POPG bilayers [20] showed that the peptide is well inserted into these membranes in the LC phase. To verify that in the gel phase PG-1 remains inserted, we carried out a gel-phase ^{1}H spin diffusion experiment that transfers the water ^{1}H magnetization on the membrane surface to the peptide [36,37]. The depth of individual residues is estimated from the rate of the spin diffusion buildup curves. The experiment was carried out at ~ 240 K on DLPC-bound PG-1 samples, which had been previously used to measure the insertion state of the peptide in the LC phase [22]. Figure 6.7 shows the ^{13}C-detected water-to-peptide ^{1}H spin diffusion curves for four residues. Gly_2 Cα and Phe_{12} CO exhibit the fastest buildup curves (a, b), indicating binding to the headgroup and glycerol backbone regions close to the water molecules. Leu_5 Cα and Val_{16} CO show significantly slower initial buildup rates (c, d), which are consistent with insertion to the beginning of the acyl chains. The relative depths are $Gly_2 < Phe_{12} < Leu_5 \approx Val_{16}$. This profile is identical to that measured in the LC phase [22]. Thus, freezing the bilayer to the gel phase does not change the insertion state of PG-1.

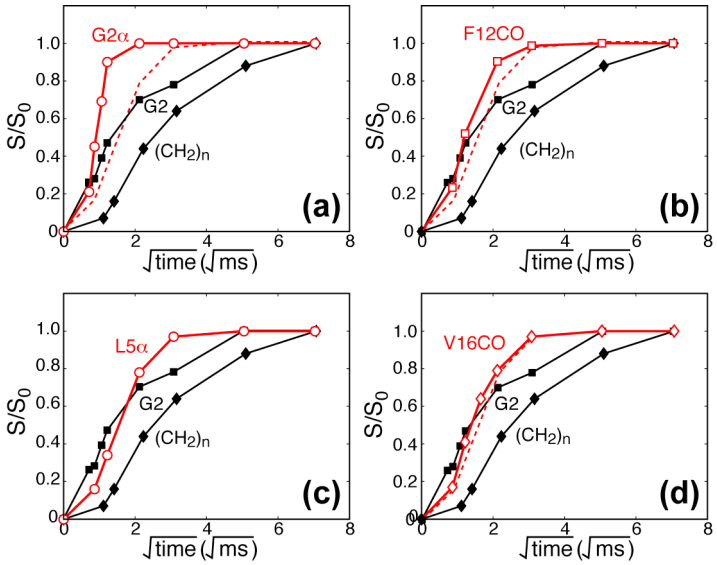

Figure 6.7. Gel-phase ^{1}H spin diffusion from water to PG-1 in DLPC bilayers at 240 K. Red symbols: Data of ^{13}C-labeled residues in PG-1. Black symbols: data of lipid glycerol G2 and $(CH_2)_n$ signals. The Leu_5 Cα curve is reproduced as dashed lines in (a, b, d) for comparison. The fast buildup of Gly_2 Cα and Phe_{12} CO and the slower buildup curves of Leu_5 Cα and Val_{16} CO are consistent with the paramagnetic relaxation enhancement data on the same samples in the LC phase [22].

Discussion

The (ϕ, ψ) torsion angle data shown here indicate that PG-1 adopts an ideal β-strand conformation at Arg_4 and β-turn torsion angles at Arg_{11}, confirming that the peptide has a β-hairpin fold under the solid-state NMR experimental conditions. This rigid disulfide-linked β-hairpin is ~30 Å long based on solution NMR structure of the peptide [14].

The ^{13}C-^{31}P REDOR distance data indicates that no measured residues in PG-1 are far from the ^{31}P atoms. The distances are 4.0 – 6.5 Å in the POPE/POPG membrane and 6.5 – 8.0 Å in the POPC membrane. This close proximity contrasts with the much longer ^{13}C-^{31}P distances between the lipid chains and the headgroups. What membrane morphology and peptide topology can give rise to similarly short ^{13}C-^{31}P distances for four widely dispersed residues in a β-hairpin?

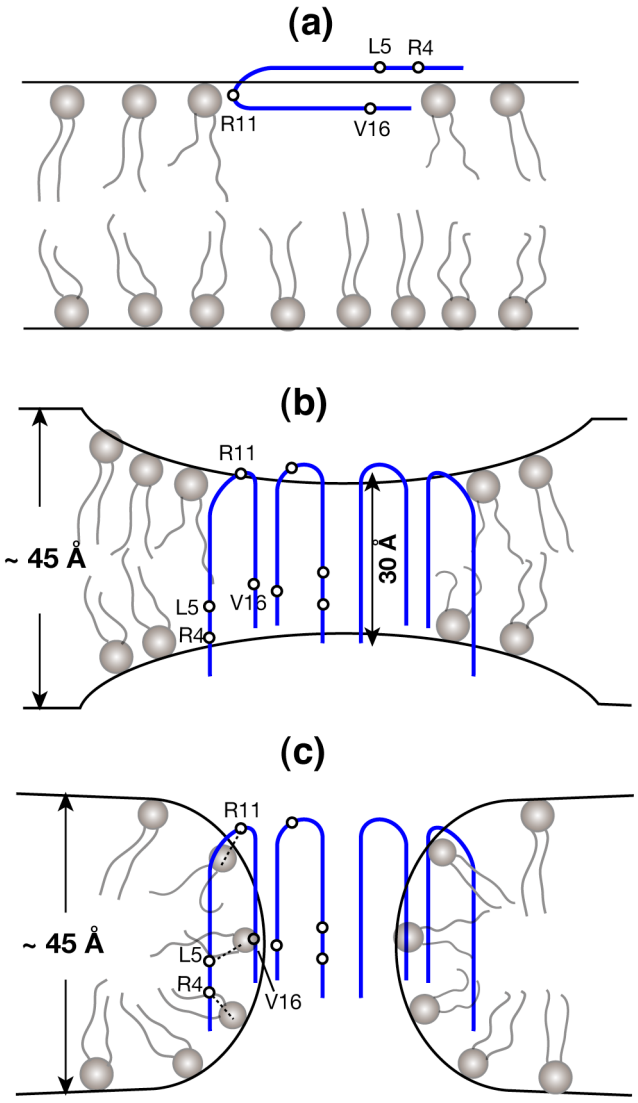

Figure 6.8. Schematic structural models of PG-1 in the POPE/POPG membrane. (a) PG-1 is bound to the membrane surface. This model can be ruled out by absolute orientation measurements and ^{1}H spin diffusion data. (b) Peptide oligomers thin the membrane without changing the lipid orientation. Leu_5 Cα and Arg_4 Cα should differ in their ^{13}C-^{31}P distances by 3.6 Å, which disagrees with the REDOR data. (c) Peptide oligomers cause toroidal pores in the membrane, so that the local ^{31}P plane is roughly parallel to the β-strands, giving rise to similar ^{13}C-^{31}P distances to Leu_5 Cα and Arg_4 Cα. In models (b) and (c), only part of the β-barrel is drawn for clarity.

Figure 6.8 illustrates three possible scenarios of membrane morphology and peptide insertion states that satisfy the distance data. First, the short distances could result from PG-1 being bound to the lipid bilayer surface (Figure 6.8a). However, this is inconsistent with

various orientation and depth data acquired on a number of lipid membranes. In LC-phase DLPC (12:0) bilayers PG-1 β-strands were found to be tilted by ~55˚ from the bilayer normal based on ^{13}C and ^{15}N anisotropic chemical shifts on glass-plate oriented samples [25]. In the longer-chain lipid diphytanoylphosphatidylcholine (DPhPC, 16:0 [$(CH_3)_4$]), oriented circular dichroism experiments by Huang and coworkers indicated that PG-1 is also transmembrane at peptide-lipid molar ratios larger than ~1:30 [23,40]. Since these orientation data were obtained on macroscopically aligned samples, the transmembrane orientation is referenced to the external plane of glass plates, independent of the local curvature of the lipid membrane. In addition to orientation constraints, ^{1}H spin diffusion from the lipid chains to the peptide indicated that PG-1 is in close contact with the acyl chains in both POPC membranes [21] and POPE/POPG membranes [20] in the LC phase, thus the peptide cannot exclusively lie on the membrane surface. The 2D ^{31}P-^{1}H spin diffusion spectra shown here confirm the participation of PG-1 in the hydrophobic part of the membrane. Finally, cooling the membrane to the gel phase does not change the depth of insertion of PG-1, since the gel-phase water-to-peptide ^{1}H spin diffusion data gave the same depth profile as the LC-phase Mn^{2+} paramagnetic relaxation enhancement data [22]. Thus, at the peptide-lipid molar ratios used here, PG-1 adopts a stable inserted state in lipid bilayers with varying thicknesses and phases.

Can the distance data be explained by membrane thinning, where lipid bilayers thin sufficiently to give short distances to all four residues in the peptide (Figure 6.8b)? This possibility can also be ruled out. Since the thinned membrane remains lamellar, the ^{31}P plane would still be roughly perpendicular to the transmembrane β-strands. This would require Leu_5 Cα and Arg_4 Cα to differ in their ^{13}C-^{31}P distances by ~3.6 Å, because the distance between two consecutive α carbons in a β-strand is fixed by the covalent geometry to be 3.6 Å along the β-strand axis. Instead, we measured identical distances of 6.5 Å for Leu_5 Cα and Arg_4 Cα to ^{31}P. Moreover, the fact that short distances are found for backbone as well as the sidechain carbons rules out snorkeling of the Arg sidechain to the membrane surface [24,41].

These considerations lead to the conclusion that, for Arg_4 and Leu_5 to have equal Cα-P distances, the local ^{31}P plane must be roughly parallel instead of perpendicular to the β-strand axis. Since the PG-1 β-strands have an externally referenced transmembrane

orientation, this parallelity means some lipid molecules must turn their orientation to embed their headgroups in the hydrophobic region of the membrane, thus establishing equidistant contacts to Arg_4 and Leu_5 Cα (Figure 6.8c). The presence of rotated lipid molecules that merge the two leaflets of lamellar bilayers is the key signature of the toroidal pore [42,43].

This toroidal pore model is strongly supported by static ^{31}P lineshapes of POPC/POPG, POPE/POPG, and POPC membranes in the presence of PG-1. Both glass-plate aligned samples [44,45] and unoriented liposome samples [25] give rise to spectra with a prominent broad peak centered at the isotropic shift, indicating the presence of non-lamellar lipids with near isotropic morphology. On the other hand, the remaining aligned peak or powder intensity in these spectra indicates that residual lamellar bilayer remains in these samples, as required by the toroidal pore model, thus complete micelle formation is unlikely.

How can the β-strands lie close to both the headgroups and the acyl chains, as constrained by the ^{13}C-^{31}P distances and the lipid-to-peptide ^{1}H spin diffusion data? We hypothesize that the rotated lipid molecules may partially intercalate between the β-strands, such that both the headgroups and the acyl chains are in close contact to the β-strands (Figure 6.8c). 2D ^{13}C-^{13}C correlation spectra of fibrilized PG-1 indicate that the N-strand - N-strand interface is more loosely packed than the C-strand - C-strand interface [46,47], which may allow lipid intercalation.

Similar to PG-1, short peptide-headgroup distances, short peptide-lipid chain distances, and enhanced lipid headgroup-chain contacts, were reported for an α-helical magainin analog, K3, which contains no Arg but only Lys as its cationic residues [48]. Intriguingly, the short peptide – headgroup distances occur only for ~30% of K3, as manifested by the plateau value of the REDOR curves. This contrasts with the 100% REDOR dephasing of PG-1. The ^{31}P lineshapes of the K3-containing membrane also do not exhibit disorder. Thus, the Arg-cationic PG-1 has stronger membrane-disruptive ability and shorter distances to lipids than the Lys-cationic K3.

The ^{13}C-^{31}P distance data of PG-1 not only point to the toroidal pore as the only possible lipid organization near the peptide, but also suggests that guanidinium-phosphate association may be the driving force for toroidal pore formation: the Arg residues may drag the phosphate groups along to overcome the free energy barrier of inserting into the

hydrophobic part of the membrane. This anion-mediated translocation of guanidinium groups has been reported for oligoarginines from water to chloroform and from water to anionic lipid bilayers [49]. Comparisons of different counterions' abilities for polyarginine translocation revealed that a combination of amphiphilic phosphate anions such as the phosphatidylglycerol lipids and hydrophilic phosphates maximize the translocation across the membrane [50].

The nature of the guanidinium - phosphate interaction is ionic. This is supported by the 1.0 – 2.5 Å shorter C-P distances in the anionic POPE/POPG membrane than in the zwitterionic POPC membrane. The cationic trimethylamine group in the POPC headgroup should repel the guanidinium cation, weakening the guanidinium-phosphate complex. The ionic interaction is also supported by the 1.0 – 2.0 Å shorter distances of Arg_{11} to ^{31}P than Arg_4. Arg_{11} is one of three consecutive Arg's at the β-turn and thus belongs to a much larger charge cluster than Arg_4, which is surrounded by hydrophobic residues. Thus, electrostatic attraction between guanidinium cations and phosphate anions play an important role in peptide insertion and membrane defect formation.

A second possible contribution to stable guanidinium-phosphate complexation is hydrogen bonding. In the absence of steric hindrance, the guanidinium ion can form as many as four hydrogen bonds with two phosphate groups [51]. This bidentate complex is unstable for the basic lysine, which may explain the relative abundance of Arg over Lys in cationic AMPs. The short Arg_{11} Cζ-P distances of 4.0 Å and 5.1 Å strongly suggest the existence of such a bidentate complex.

We hypothesize that this ionic and hydrogen-bond-stabilized guanidinium-phosphate complexation may be a general mechanism for the translocation of Arg residues in membrane peptides and proteins, and the resulting membrane defect may be quite common. For example, the Arg-rich TAT(48-60) peptide induces rod-shaped lipid micelles in DMPC membranes [52]. The Arg-rich cyclic defensin RTD-1 causes micron-diameter lipid cylinders [53]. In KvAP potassium channel, the Arg-rich S4 segment is reported to move by ~20 Å across the membrane during channel opening [54]. MD simulations of the S4 helix suggests that the organization of POPC bilayers is highly perturbed in the vicinity of the helix, with a hydrogen-bonded network of water and phosphate groups formed around the guanidinium

ions [12]. Such lipid counterions are shown experimentally here for PG-1. They shield the guanidinium ion from the lipid acyl chains, thus reducing the free energy of membrane insertion [11].

One difference between PG-1 and other transmembrane cationic proteins is its β-sheet conformation, which promotes oligomerization through backbone $N-H\cdots O=C$ hydrogen bonds [20,47]. This self-assembly may further facilitate the insertion of multiple Arg's by reducing the lipid chain-peptide interface.

Conclusion

The first measurement of the distances between Arg residues in a cationic membrane peptide and the ^{31}P of lipid headgroups is presented. The uniformly short ^{13}C-^{31}P distances for multiple sites in PG-1 indicate that the β-hairpin peptide induces toroidal pores in the membrane, where some lipid headgroups become embedded in the hydrophobic region of the bilayer. Comparison of distances in anionic membranes and zwitterionic membranes suggest that the driving force for the toroidal pore formation is guanidinium-phosphate association, which neutralizes the guanidinium ions to facilitate their insertion into the hydrophobic part of the membrane. Thus, PG-1 may pull the phosphate groups along as it inserts, causing toroidal pores. We propose that this guanidinium-phosphate complexation may be a general phenomenon among membrane-lytic Arg-rich antimicrobial peptides.

Acknowledgement: This work is supported by the National Institutes of Health grants GM-066976 to M. H. and AI-37945 to A. J. W.

Supporting Information: Description of the multi-spin simulations, additional spectra and control distance data, RMSD analysis for the torsion angle data, and 2D ^{1}H-^{13}C spectrum of lipids for assignment, are provided.

References

(1) Bellm, L.; Lehrer, R. I.; Ganz, T. *Exp. Opin. Invest. Drugs* **2000**, *9*, 1731-1742.

(2) Hancock, R. E.; Lehrer, R. *Trends Biotechnol.* **1998**, *16*, 82-8.

(3) Vives, E.; Brodin, P.; Lebleu, B. *J. Biol. Chem.* **1997**, *272*, 16010-7.

(4) Jarver, P.; Langel, U. *Biochim. Biophys. Acta* **2006**, *1758*, 260-3.

(5) Long, S. B.; Campbell, E. B.; Mackinnon, R. *Science* **2005**, *309*, 897-903.

(6) DeGrado, W. F.; Gratkowski, H.; Lear, J. D. *Protein Sci.* **2003**, *12*, 647-65.

(7) Choma, C.; Gratkowski, H.; Lear, J. D.; DeGrado, W. F. *Nat. Struc. Biol.* **2000**, *7*, 161-166.

(8) Lear, J. D.; Gratkowski, H.; Adamian, L.; Liang, J.; DeGrado, W. F. *Biochemistry* **2003**, *42*, 6400-7.

(9) White, S. H.; Wimley, W. C. *Annu. Rev. Biophys. Biomol. Struct.* **1999**, *28*, 319-365.

(10) Hessa, T.; Kim, H.; Bihlmaier, K.; Lundin, C.; Boekel, J.; Andersson, H.; Nilsson, I.; White, S. H.; von Heijne, G. *Nature* **2005**, *433*, 377-81.

(11) Hessa, T.; White, S. H.; von Heijne, G. *Science* **2005**, *307*, 1427.

(12) Freites, J. A.; Tobias, D. J.; von Heijne, G.; White, S. H. *Proc. Natl. Acad. Sci. U. S. A.* **2005**, *102*, 15059-64.

(13) Kokryakov, V. N.; Harwig, S. S.; Panyutich, E. A.; Shevchenko, A. A.; Aleshina, G. M.; Shamova, O. V.; Korneva, H. A.; Lehrer, R. I. *FEBS Lett.* **1993**, *327*, 231-6.

(14) Fahrner, R. L.; Dieckmann, T.; Harwig, S. S.; Lehrer, R. I.; Eisenberg, D.; Feigon, J. *Chem. & Biol.* **1996**, *3*, 543-550.

(15) Hancock, R. E.; Scott, M. G. *Proc. Natl. Acad. Sci. USA* **2000**, *97*, 8856-8861.

(16) Zasloff, M. *Nature* **2002**, *415*, 389-395.

(17) Ternovsky, V. I.; Okada, Y.; Sabirov, R. Z. *FEBS Lett.* **2004**, *576*, 433-6.

(18) Lehrer, R. I.; Barton, A.; Ganz, T. *J. Immunol. Methods* **1988**, *108*, 153-8.

(19) Yang, L.; Weiss, T. M.; Lehrer, R. I.; Huang, H. W. *Biophys. J.* **2000**, *79*, 2002-9.

(20) Mani, R.; Cady, S. D.; Tang, M.; Waring, A. J.; Lehrer, R. I.; Hong, M. *Proc. Natl. Acad. Sci. U.S.A.* **2006**, *103*, 16242-16247.

(21) Buffy, J. J.; Waring, A. J.; Lehrer, R. I.; Hong, M. *Biochemistry* **2003**, *42*, 13725-13734.

(22) Buffy, J. J.; Hong, T.; Yamaguchi, S.; Waring, A.; Lehrer, R. I.; Hong, M. *Biophys. J.* **2003**, *85*, 2363-2373.

(23) Heller, W. T.; Waring, A. J.; Lehrer, R. I.; Huang, H. W. *Biochemistry* **1998**, *37*, 17331-8.

(24) Segrest, J. P.; De Loof, H.; Dohlman, J. G.; Brouillette, C. G.; Anantharamaiah, G. M. *Proteins* **1990**, *8*, 103-17.

(25) Yamaguchi, S.; Hong, T.; Waring, A.; Lehrer, R. I.; Hong, M. *Biochemistry* **2002**, *41*, 9852-9862.

(26) Crowe, J. H.; Crowe, L. M.; Chapman, D. *Science* **1984**, *223*, 701-703.

(27) Tang, M.; Waring, A. J.; Hong, M. *J. Magn. Reson.* **2007**, *184*, 222-227.

(28) Jaroniec, C. P.; Tounge, B. A.; Rienstra, C. M.; Herzfeld, J.; Griffin, R. G. *J. Am. Chem. Soc.* **1999**, *121*, 10237-10238.

(29) Gullion, T.; Schaefer, J. *J. Magn. Reson.* **1989**, *81*, 196-200.

(30) Sinha, N.; Schmidt-Rohr, K.; Hong, M. *J. Magn. Reson.* **2004**, *168*, 358-65.

(31) Costa, P. R.; Gross, J. D.; Hong, M.; Griffin, R. G. *Chem. Phys. Lett.* **1997**, *280*, 95-103.

(32) Feng, X.; Lee, Y. K.; Sandstroem, D.; Eden, M.; Maisel, H.; Sebald, A.; Levitt, M. H. *Chem. Phys. Lett.* **1996**, *257*, 314-320.

(33) Hohwy, M.; Rienstra, C. M.; Jaroniec, C. P.; Griffin, R. G. *J. Chem. Phys.* **1999**, *110*, 7983-7992.

(34) Hong, M.; Gross, J. D.; Griffin, R. G. *J. Phys. Chem. B* **1997**, *101*, 5869-5874.

(35) Huster, D.; Yao, X. L.; Hong, M. *J. Am. Chem. Soc.* **2002**, *124*, 874-883.

(36) Kumashiro, K. K.; Schmidt-Rohr, K.; Murphy, O. J.; Ouellette, K. L.; Cramer, W. A.; Thompson, L. K. *J. Am. Chem. Soc.* **1998**, *120*, 5043-5051.

(37) Gallagher, G. J.; Hong, M.; Thompson, L. K. *Biochemistry* **2004**, *43*, 7899-7906.

(38) Huster, D.; Arnold, K.; Gawrisch, K. *J. Phys. Chem.* **1999**, *103*, 243-251.

(39) Huster, D.; Gawrisch, K. *J. Am. Chem. Soc.* **1999**, *121*, 1992-1993.

(40) Heller, W. T.; Waring, A. J.; Lehrer, R. I.; Harroun, T. A.; Weiss, T. M.; Yang, L.; Huang, H. W. *Biochemistry* **2000**, *39*, 139-145.

(41) Strandberg, E.; Morein, S.; Rijkers, D. T. S.; Liskamp, R. M. J.; vanderWel, P. C. A.; Killian, J. A. *Biochemistry* **2002**, *41*, 7190-7198.

(42) Matsuzaki, K. *Biochim. Biophys. Acta* **1998**, *1376*, 391-400.

(43) Ludtke, S. J.; He, K.; Heller, W. T.; Harroun, T. A.; Yang, L.; Huang, H. W. *Biochemistry* **1996**, *35*, 13723-13728.

(44) Mani, R.; Buffy, J. J.; Waring, A. J.; Lehrer, R. I.; Hong, M. *Biochemistry* **2004**, *43*, 13839-48.

(45) Mani, R.; Waring, A. J.; Lehrer, R. I.; Hong, M. *Biochim. Biophys. Acta* **2005**, *1716*, 11-18.

(46) Tang, M.; Waring, A. J.; Hong, M. *J. Am. Chem. Soc.* **2005**, *127*, 13919-13927.

(47) Mani, R.; Tang, M.; Wu, X.; Buffy, J. J.; Waring, A. J.; Sherman, M. A.; Hong, M. *Biochemistry* **2006**, *45*, 8341-9.

(48) Toke, O.; Maloy, W. L.; Kim, S. J.; Blazyk, J.; Schaefer, J. *Biophys. J.* **2004**, *87*, 662-74.

(49) Sakai, N.; Takeuchi, T.; Futaki, S.; Matile, S. *Chembiochem.* **2005**, *6*, 114-122.

(50) Sakai, N.; Matile, S. *J. Am. Chem. Soc.* **2003**, *125*, 14348-14356.

(51) Schug, K. A.; Lindner, W. *Chem. Rev.* **2005**, *105*, 67-114.

(52) Afonin, S.; Frey, A.; Bayerl, S.; Fischer, D.; Wadhwani, P.; Weinkauf, S.; Ulrich, A. S. *Chemphyschem* **2006**, *7*, 2134-2142.

(53) Buffy, J. J.; McCormick, M. J.; Wi, S.; Waring, A.; Lehrer, R. I.; Hong, M. *Biochemistry* **2004**, *43*, 9800-9812.

(54) Jiang, Y.; Ruta, V.; Chen, J.; Lee, A.; MacKinnon, R. *Nature* **2003**, *423*, 42-48.

Supporting Information
Phosphate-Mediated Arginine Insertion into Lipid Membranes and Pore Formation by a Cationic Membrane Peptide from Solid-State NMR

Ming Tang[1], Alan J. Waring[2], and Mei Hong[1]

[1] Department of Chemistry, Iowa State University, Ames, IA 50011

[2] Department of Medicine, University of California at Los Angeles School of Medicine, Los Angeles, California 90095

Multi-spin consideration of the ^{13}C-^{31}P REDOR data

The experimental ^{13}C-^{31}P REDOR data were simulated using a two-spin model to give the distances. It is relevant to consider how inclusion of multiple ^{31}P spins coupled to each ^{13}C affects the distance results. The typical lipid headgroup area is ~65 $Å^2$. This corresponds to an average ^{31}P-^{31}P distance of ~9 Å in the plane of the membrane. With the presence of 20% trehalose, which can partially intercalate between the headgroups, we approximate the P-P separation as 10 Å. Under this geometric constraint, we constructed multi-^{31}P-spin and single ^{13}C spin networks and calculated their heteronuclear REDOR curves using the SIMPSON program [1]. Figure S6.3(a-d) shows the best-fit REDOR curves for the Arg_{11} Cζ data in POPE/POPG membrane assuming one, two, and three ^{31}P spins. In the simple two-spin case (one ^{13}C and one ^{31}P), single-distance calculations do not fit the data well, as shown by the best-fit curve of 4.5 Å (a, dashed line). Instead, a 1:1 mixture of 4.0 Å and 5.1 Å is necessary.

For a three-spin system containing one ^{13}C and two ^{31}P atoms, the ^{13}C can be close to one ^{31}P spin and far from the other. This geometry gives a short ^{13}C-^{31}P distance of 4.5 Å and a long distance of ~8.9 Å while still maintaining the ^{31}P-^{31}P separation of 10 Å (Figure S6.3b). The resulting three-spin REDOR curve is very similar to the unsatisfactory single-distance two-spin fit (a), indicating that in the presence of a short distance, longer distances have negligible effects on the REDOR dephasing. Having more than three ^{31}P spins does not change this conclusion, as long as a single short distance dominates the dipolar coupling.

Alternatively, a three-spin geometry may contain two similar ^{13}C-^{31}P distances (Figure S6.3c). In this case, we find that two equal distances of 5.2 Å fit the data similarly well as the mixed distance two-spin fit (a). Thus, an equilateral three-spin geometry is a possible solution. This, however, only increases the reported ^{13}C-^{31}P distances by an average of 0.6 Å compared to the two-spin simulation.

When four spins with three equal ^{13}C-^{31}P distances are considered (Figure S6.3d), the minimum ^{13}C-^{31}P distance allowed by the ^{31}P-^{31}P constraint is 5.8 Å, which is obtained when the ^{13}C spin lies in the plane of the ^{31}P atoms. This is a sterically unfavorable situation, but even with these shortest distances, the simulated REDOR curve still decays more slowly than the experimental data, indicating that the more physical and longer distances will only deviate further from the data. Therefore, for strong observed dipolar couplings, the inclusion of multiple ^{31}P spins in the simulation either minimally affects the distance results compared to the two-spin simulation or is unphysical.

When the observed REDOR dipolar dephasing is slow, indicating overall longer distances, ^{13}C coupling to multiple ^{31}P spins is more likely and increases the individual ^{13}C-^{31}P distances more significantly compared to the two-spin distance result. Figure S6.3e plots the individual ^{13}C-^{31}P distances as a function of the total number of spins in the simulation. From now on we only consider the geometry where all ^{13}C-^{31}P distances are equal in the multi-spin network. For example, a five-spin simulation of an apparent two-spin distance of 8.0 Å increases the individual ^{13}C-^{31}P distances to 10 Å. However, in the presence of multiple ^{31}P spins the real distance of interest is not the individual ^{13}C-^{31}P distances but the vertical distance from the ^{13}C to the ^{31}P plane (Figure S6.3g). This vertical distance is shorter than the individual ^{13}C-^{31}P distances, and can be exactly calculated from the simulation results of Figure S6.3e. Figure S6.3f shows that this vertical distance decreases as the number of spins increases, and reaches a plateau at long distances. Moreover, this plateau value for the vertical distance is similar to or slightly shorter than the apparent two-spin distance. For example, a two-spin distance of 8.0 Å is fit by a vertical distance of 7.0 Å in a five-spin geometry. Figure S6.3f also confirms that for short two-spin distances such as 5.0 Å, the multi-spin consideration is invalid due to steric conflict, as unphysically short vertical distance is obtained.

The average ^{31}P-^{31}P separation of 10 Å gives a ^{31}P-^{31}P dipolar coupling of ~20 Hz, which is spun out by MAS. Simulation of the REDOR curve for a ^{13}C-^{31}P distance of 7.4 Å in a four-spin system (one ^{13}C and three ^{31}P spins) confirms that the ^{31}P-^{31}P homonuclear coupling does not influence the REDOR dephasing.

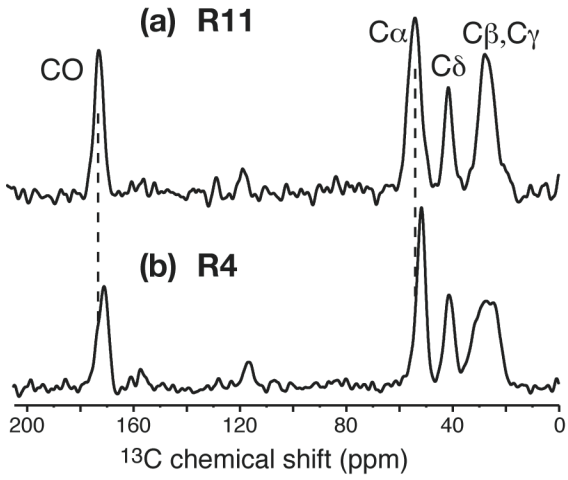

Figure S6.1. ^{13}C double-quantum filtered spectra of Arg-labeled PG-1 in the POPC/trehalose membrane. (a) Arg_{11} labeled PG-1. (b) Arg_4 labeled PG-1. Note the difference in the Cα and CO chemical shifts between the two residues. The Arg Cβ signal is not resolved from Cγ and thus cannot be used for secondary structure analysis. The spectra were measured at 253 K under 5.5 kHz MAS.

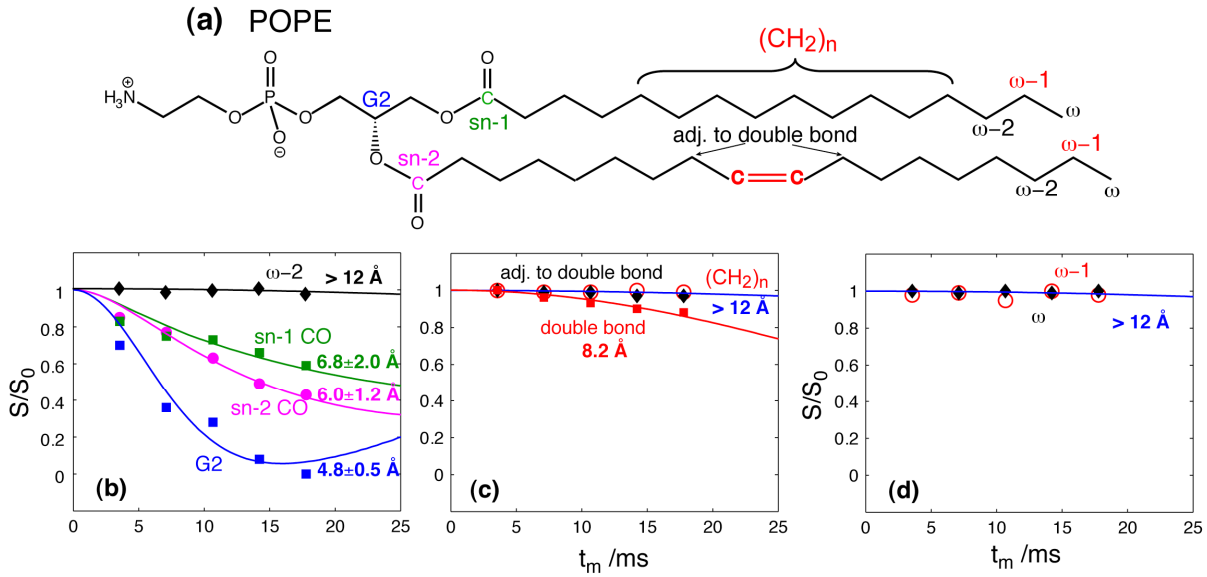

Figure S6.2. $^{13}C\{^{31}P\}$ REDOR data of hydrated POPE bilayers at 226 K. (a) POPE chemical structure and nomenclature. (b) REDOR decays of the ω-2 (black), *sn*-1 CO (green), *sn*-2 CO (magenta) and glycerol G2 (blue) carbons. (c) REDOR decays of $(CH_2)_n$ (open red circles) carbons, the double bond carbon (filled red squares) and the carbons next to the double bond (black diamond). (d) REDOR decays of ω-1 carbons (red) and the ω CH_3 carbon (black).

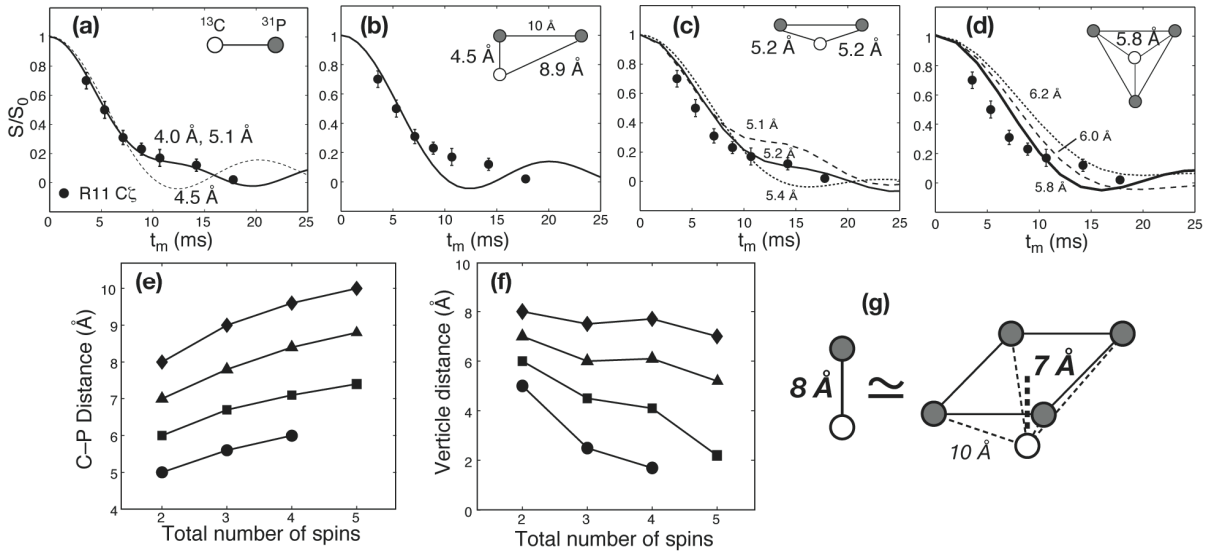

Figure S6.3. Simulated ^{13}C-^{31}P REDOR curves for one ^{13}C and multiple ^{31}P spins. (a) Two-spin simulations. (b) Three-spin simulation. (c) Four-spin simulations. (d) Five-spin simulations. The Arg_{11} Cζ data is shown. The geometry of the spin systems is shown in each panel in (a-d). (e) Individual ^{13}C-^{31}P distances as a function of

the total number of spins when all ^{13}C-^{31}P distances in each cluster are equal. (f) The vertical distance between the ^{13}C and the ^{31}P plane as a function of the total number of spins. The vertical distance approaches the two-spin distance with increasing number of spins and with increasing distances.

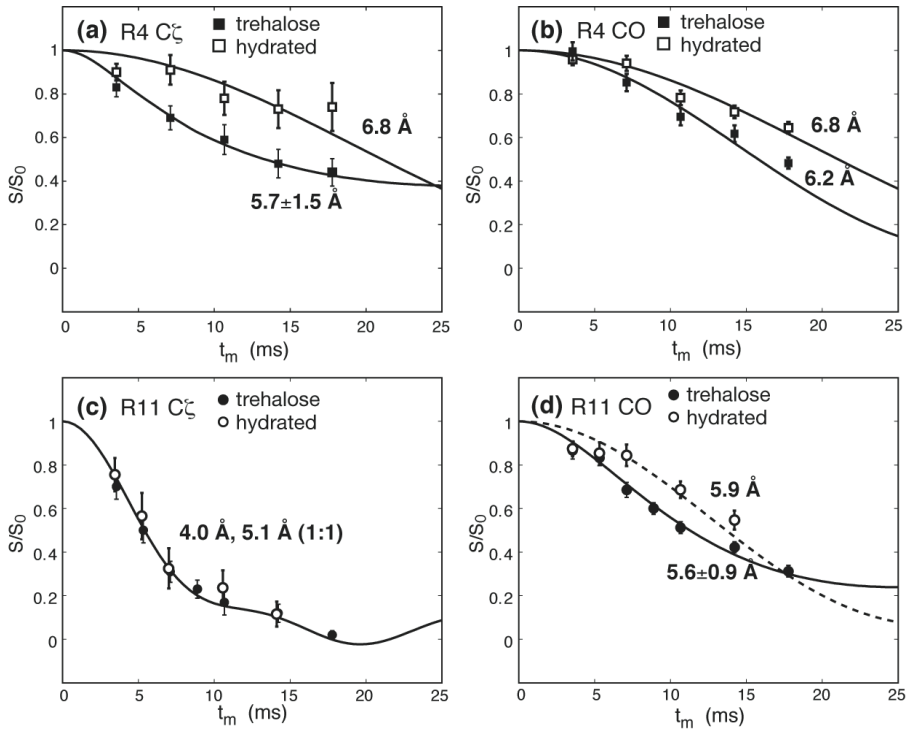

Figure S6.4. Comparison of $^{13}C\{^{31}P\}$ REDOR data for TRE-POPE/POPG membranes (filled symbols) and hydrated POPE/POPG membranes (open symbols). (a) REDOR decays of Arg_4 Cζ. The best fit is 5.7 ± 1.5 Å (Gaussian distribution) for the dry membrane and 6.8 Å for the hydrated membrane. (b) REDOR decays of Arg_4 CO. The best fit is 6.2 Å for the dry membrane and 6.8 Å for the hydrated membrane. (c) REDOR decays of Arg_{11} Cζ. The best fits for both the dry and hydrated membranes are a 1 : 1 mixture of 4.0 Å and 5.1 Å. (d) REDOR decays of Arg_{11} CO. The best fit is 5.6 ± 0.9 Å (Gaussian distribution) for the dry membrane and 5.9 Å for the hydrated membrane.

The larger difference in the Arg_4 $^{13}C\zeta$-^{31}P distance between the hydrated and dry membranes compared to Arg_{11} may be due to hydrogen bonding differences. In the hydrated membrane Arg_4 - ^{31}P hydrogen bonding may be mediated by water molecules whereas in the trehalose-protected membrane hydrogen bond may be direct, since the bulky trehalose cannot easily intercalate between the peptide and the lipid headgroup. In comparison, Arg_{11} at the β-turn has less steric conflict than Arg_4 in the middle of the β-strand, and thus may be able to

form direct hydrogen bonds with the phosphate in both membranes, giving identical $^{13}C\zeta$-^{31}P distances.

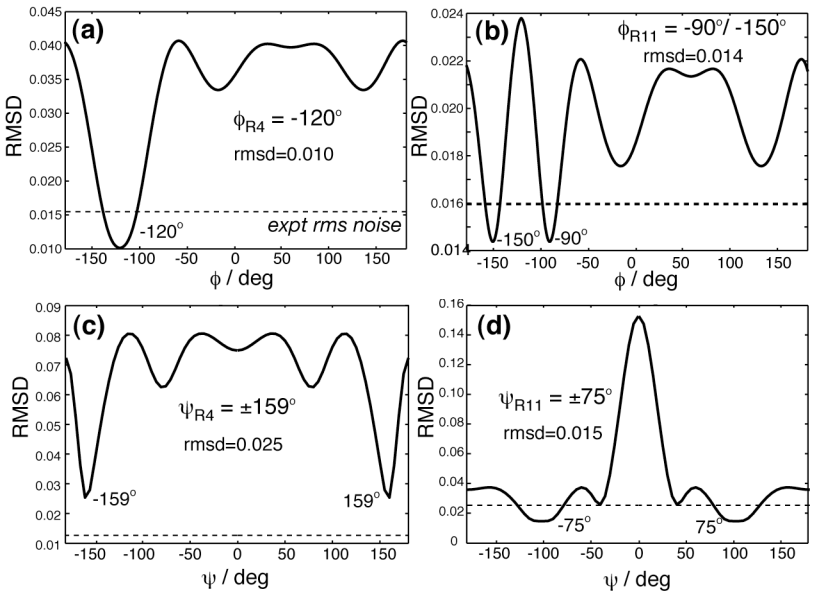

Figure S6.5. Root mean-square deviation (RMSD) of the (ϕ, ψ) angle data for Arg_4 and Arg_{11}. (a) RMSD of the Arg_4 HNCH data in the TRE-POPC membrane. The minimum occurs at ϕ = 120° with an uncertainty of 15°. (b) RMSD of the Arg_{11} HNCH data in the TRE-POPC membrane. Two minima were found at ϕ = -90° and ϕ = -150° with an uncertainty of 10°. (c) RMSD of Arg_4 NCCN data in the TRE-POPC membrane. Two minima were found at ϕ = ±159° with an uncertainty of 5°. (d) RMSD of the Arg_{11} NCCN data in the TRE-POPC membrane. Two minima were found at ϕ = ±75° with an uncertainty of 15°. Dashed lines indicate the experimental RMS noise.

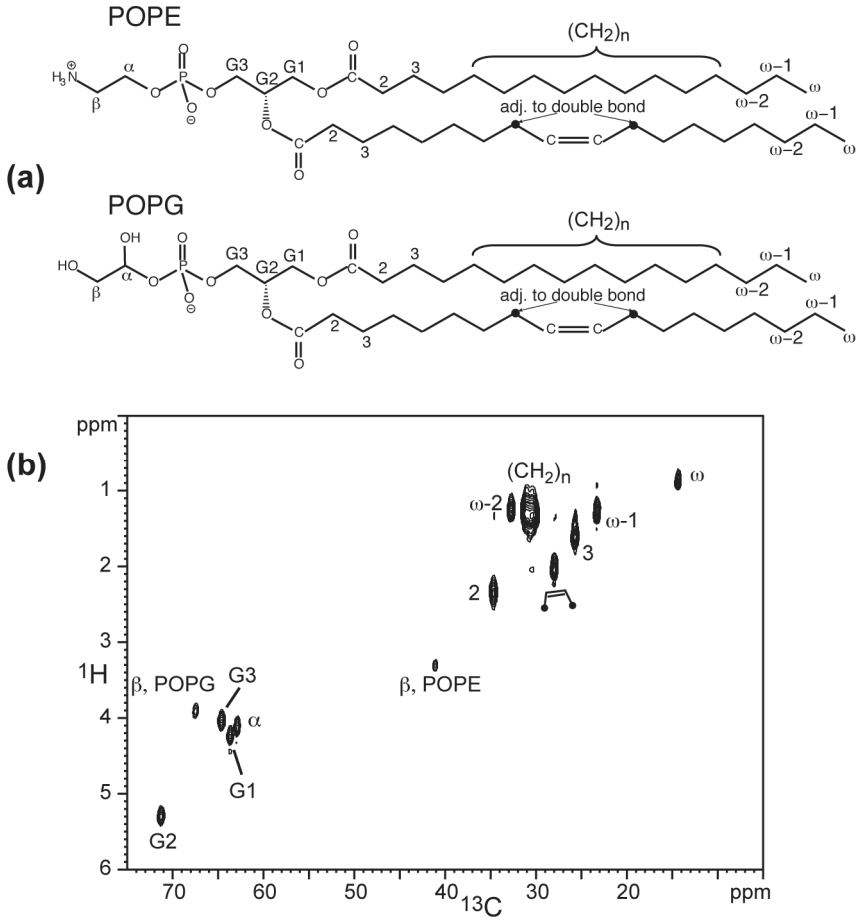

Figure S6.6. ^{1}H chemical shift assignment of POPE/POPG membranes by ^{13}C-^{1}H 2D correlation. (a) POPE and POPG chemical structures and the nomenclature for the various functional groups. (b) ^{13}C-^{1}H heteronuclear correlation spectrum of the membrane, measured at 303 K under 5 kHz MAS. The ^{13}C chemical shift assignment is based on the literature [2]. Due to the fast uniaxial mobility of the lipid molecules, MAS alone is sufficient to give a high-resolution ^{1}H dimension, without the need for ^{1}H homonuclear decoupling.

Reference

1. Bak, M.; Rasmussen, J. T.; Nielsen, N. C., *J. Magn. Reson.* **2000**, *147*, (2), 296-330.

2. Husted, C.; Montez, B.; Le, C.; Moscarello, M. A.; Oldfield, E., *Magn. Res. Med* **1993**, *29*, 168-178.

Chapter 7

Arginine Dynamics in a Membrane-Bound Cationic Beta-Hairpin Peptide from Solid-State NMR

Published in ChemBioChem

2008, 9, 1487-1492

Ming Tang[a], Alan J. Waring[b], and Mei Hong[a]

[a] Department of Chemistry, Iowa State University, Ames, IA 50011

[b] Department of Medicine, University of California at Los Angeles School of Medicine, Los Angeles, California 90095

This chapter is modified from the manuscript in its pre-publication form, but not the article in its final version.

Abstract

The site-specific motion of Arg residues in a membrane-bound disulfide-linked antimicrobial peptide, protegrin-1 (PG-1), is investigated using magic-angle spinning solid-state NMR, to better understand the membrane insertion and lipid interaction of this cationic membrane-disruptive peptide. C-H and N-H dipolar couplings and ^{13}C chemical shift anisotropies were measured in the anionic POPE/POPG membrane and found to be reduced from the rigid-limit values by varying extents, indicating the presence of segmental motion. An Arg residue at the β-turn region of the peptide shows much weaker spin interactions, indicating larger amplitudes of motion, than an Arg residue in the β-strand region of the peptide. This is consistent with the exposure of the β-turn to the membrane surface and the immersion of the β-strand in the hydrophobic middle of the membrane, and supports the

previously proposed oligomerization of the peptide into β-barrels in the anionic membrane. ^{13}C T_2 and ^{1}H $T_{1\rho}$ relaxation times indicate that the β-turn backbone undergoes large-amplitude intermediate-timescale motion in the fluid phase of the membrane, causing significant line broadening and loss of spectral intensity. This study illustrates the strong correlation between the dynamics and the structure of membrane proteins and the capability of solid-state NMR spectroscopy for providing detailed information on site-specific dynamics in complex membrane protein assemblies.

Keywords: membrane proteins, molecular dynamics, antimicrobial peptides, solid-state NMR, arginine.

Introduction

Molecular motion is common in membrane proteins and is often intimately related to the function and lipid-interaction of these molecules. Solid-state NMR (SSNMR) spectroscopy is a versatile tool to characterize molecular dynamics on a wide range of timescales (picoseconds to seconds) and to determine the amplitude of anisotropic motion. Large-amplitude segmental motion has been reported, for example, for a bacterial toxin that spontaneously inserts into the lipid membrane as a result of its intrinsic conformational plasticity [1], a lipidated Ras signaling protein [2], the catalytic domain of a membrane-bound enzyme [3], and the loops of the seven-transmembrane-helix protein rhodopsin [4]. In addition to internal segmental motion, whole-body reorientation has been discovered for many small membrane peptides of both β-sheet and α-helical secondary structures [5-7].

Protegrin-1 (PG-1) is a broad-spectrum antimicrobial peptide found in porcine leukocytes [8, 9]. It is a β-hairpin molecule stabilized by two disulfide bonds and contains six Arg residues (RGGRLCYCRRRFCVCVGR). PG-1 achieves its antimicrobial function by forming non-selective pores in the microbial cell membrane that disrupt the membrane's barrier function [10, 11]. Recently, the high-resolution oligomeric structure of PG-1 at the pores was determined using ^{1}H and ^{19}F spin diffusion NMR techniques [12]. The peptide was found to self-assemble into a transmembrane β-barrel in bacteria-mimetic anionic POPE/POPG membranes. ^{13}C-^{31}P distance constraints indicate that the Arg residues in these transmembrane β-barrels are complexed with lipid phosphates [13], suggesting that the charge

neutralization by ion pairing reduces the free energy of peptide insertion into the hydrophobic part of the membrane, and the consequent tethering of lipid headgroups may be the cause for toroidal pore formation.

The experiments that yielded the equilibrium oligomeric structure of PG-1 and the toroidal pore morphology of the lipid membrane were carried out at low temperatures of about –40˚C, in the gel phase of the membrane, to eliminate any motion that would average the distance-dependent dipolar couplings. On the other hand, PG-1 carries out its antimicrobial action in the liquid-crystalline (LC) phase of the membrane, where it is expected to be more mobile. How the dynamics of PG-1 and its Arg sidechains affect toroidal pore formation has not yet been studied. If Arg-phosphate complex formation is true, then the functional groups involved in the complex – the guanidinium ions, the lipid phosphates, and possibly water – should be less mobile than in their respective bulk environments. Thus, understanding Arg motion in PG-1 in the lipid membrane may provide additional insight into guanidinium-phosphate interaction. More generally, although the motion of long-chain amino acid residues has begun to be investigated in microcrystalline proteins [14-16], motion of the same residues in membrane proteins is still scarcely studied by NMR. Arg is particularly common in many medically important membrane peptides and proteins such as antimicrobial peptides (AMPs) [17], cell-penetrating peptides [18, 19], and voltage-sensing domains of ion channels [20].

In this work we report the amplitudes of microsecond timescale motions of Arg and other residues in PG-1 bound to the POPE/POPG membrane. We found that an Arg in the β-strand part of the molecule, which is embedded in the hydrophobic interior of the membrane, is much less mobile than an Arg in the β-turn part of the molecule, which is exposed to the membrane surface. This is consistent with the oligomeric structure and lipid interaction of this antimicrobial peptide.

Results

We first characterized the dynamic structure of PG-1 in POPE/POPG bilayers by variable-temperature ^{13}C and ^{15}N CP-MAS experiments. A series of CP spectra were collected between 243 K and 308 K for PG-1 containing U-^{13}C, ^{15}N-labeled Arg_4, Leu_5, and

Arg_{11}, and ^{15}N-labeled Phe_{12}. As shown in Figure 7.1, the Cα peaks of Arg_4 and Leu_5 are much sharper and higher than the Cα peak of Arg_{11}. At 295 K, the full widths at half-maximum (FWHM) of Arg_4 and Leu_5 Cα's are ~3 ppm, compared to 6 ppm for Arg_{11} Cα. As the temperature decreases, the Arg_{11} Cα intensity increases significantly. This suggests that in the liquid-crystalline phase of the membrane Arg_{11} backbone undergoes large-amplitude intermediate-timescale motion that becomes frozen in the gel phase of the membrane, while the Arg_4 and Leu_5 Cα sites are more rigid. In other words, the β-turn backbone is more mobile than the β-strand backbone. A similar trend is observed in the ^{15}N CP-MAS spectra (Figure 7.2). The backbone Nα peaks of Arg_4 and Leu_5 are sharp and well resolved, with FWHM of 2 – 3 ppm at 283 K, while the Arg_{11} Nα peak is broad and overlaps with Phe_{12} Nα, giving a FWHM of 9 ppm for the combined peak at 283 K. Only at 243 K do the Arg_{11} Nα and Phe_{12} Nα peaks become resolved. We assigned the Nα peaks by ^{13}C-^{15}N 2D correlation experiments (data not shown) [21].

Table 7.1. ^{13}C apparent linewidths (Δ*) and homogeneous linewidths (Δ) of PG-1 in POPE/POPG membrane at 283 K and 243 K. The apparent linewidths are read off from 1D CP spectra. The homogeneous linewidths are obtained from T_2 measurements as $\Delta = 1/\pi T_2$. The linewidths were measured at a ^{13}C Larmor frequency of 100 MHz.

Residue	Sites	283 K		243 K	
		Δ* / Hz	Δ / Hz	Δ* / Hz	Δ / Hz
Arg_4	Cα	272	199	222	118
	Cδ	222	187	493	289
	Cζ	111	84	201	80
Arg_{11}	Cα	473	289	604	133
	Cδ	161	106	534	265
	Cζ	81	53	222	94

To distinguish the contribution of static structural heterogeneity versus dynamic disorder to the linewidths, we measured the ^{13}C T_2 of Arg_4 and Arg_{11} at two different temperatures, 283 K and 243 K, using the Hahn echo experiment. Table 7.1 shows the ^{13}C apparent linewidths, Δ^*, read off from the CP spectra, and the ^{13}C homogeneous linewidths, Δ, obtained from the T_2 values according to $\Delta = 1/\pi T_2$. At 243 K, the homogeneous linewidths of Arg_4 and Arg_{11} are similar, indicating that motion is largely frozen. However, the apparent linewidth of Arg_{11} backbone Cα (604 Hz, or 6.0 ppm) is much larger than Arg_4 Cα (222 Hz, or 2.2 ppm), indicating that there is much larger conformational disorder at the β-turn backbone than at the β-strand. In comparison, the sidechains of Arg_4 and Arg_{11} at 243 K exhibit similar homogeneous linewidths as well as similar apparent linewidths, indicating that both the static and dynamic heterogeneities are comparable for the two sidechains. At 283 K, Arg_{11} Cα exhibits both larger Δ and larger Δ^* than Arg_4 Cα, indicating that the β-turn backbone has greater dynamic as well as static disorder than the β-strand backbone. In contrast, the sidechain of Arg_{11} has narrower Δ and Δ^* than the Arg_4 sidechain, indicating that Arg_{11} sidechain undergoes faster motions than Arg_4.

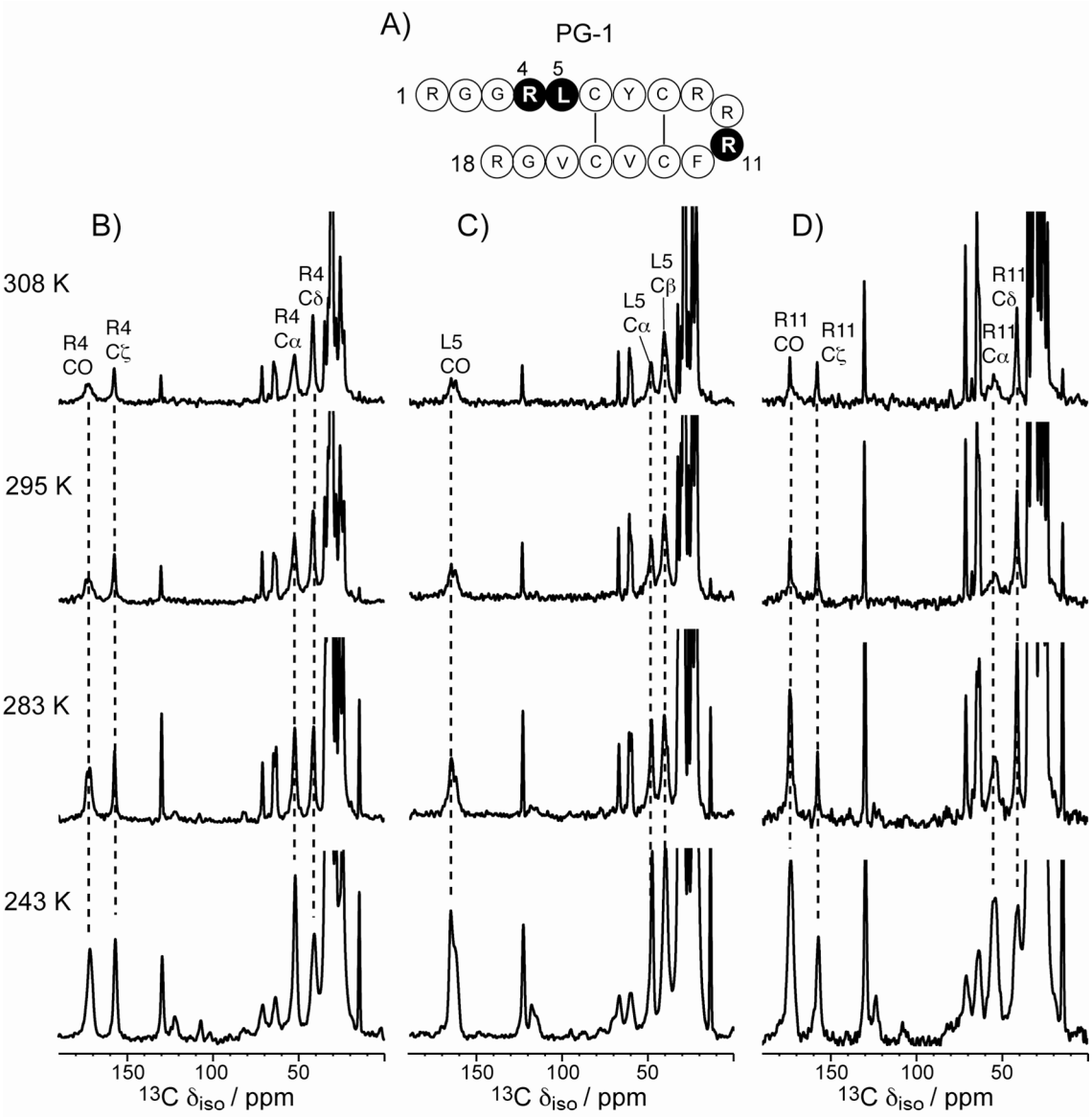

Figure 7.1. ^{13}C CP-MAS spectra in PG-1 bound to the POPE/POPG membrane (P/L = 1:12.5) from 243 K to 308 K. A) Amino acid sequence of PG-1. Labeled residues are shaded. B) ^{13}C CP-MAS spectra of Arg_4, C) ^{13}C CP-MAS spectra of Leu_5, D) ^{13}C CP-MAS spectra of Arg_{11}. Peptide peaks are assigned and annotated.

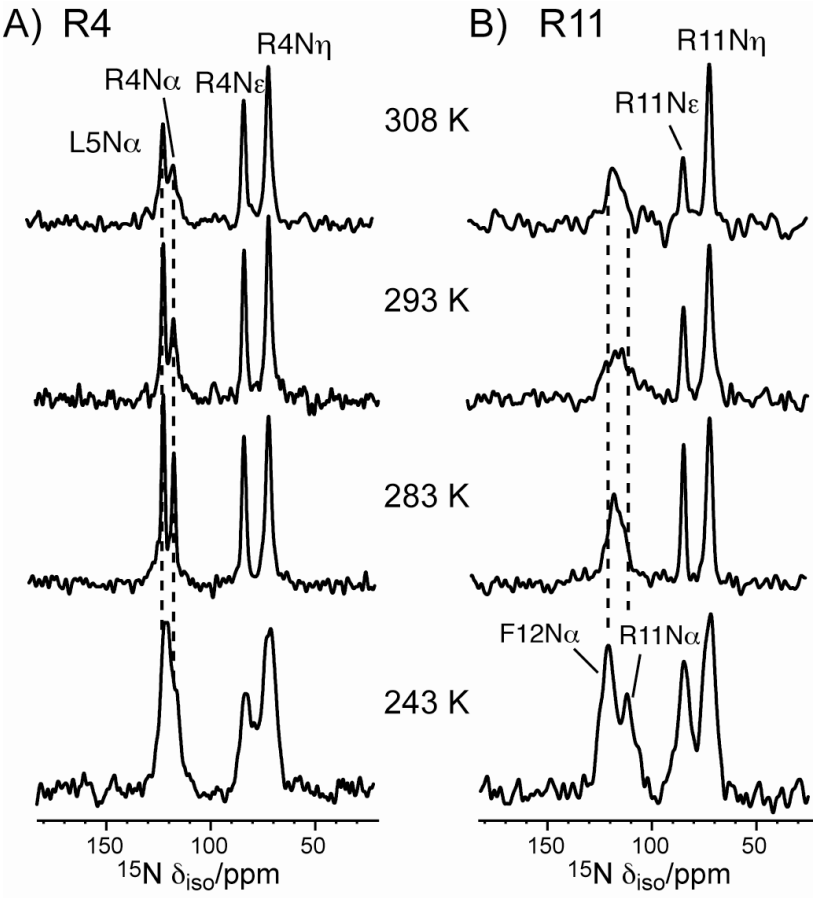

Figure 7.2. ^{15}N CP-MAS spectra of PG-1 in the POPE/POPG membrane at various temperatures. A) Arg_4, Leu_5. B) Arg_{11} and Phe_{12}. Assignments were obtained from ^{13}C-^{15}N 2D correlation spectra (not shown).

To obtain information on the motional amplitudes of the Arg sidechains, especially the guanidinium group, we measured the ^{13}C chemical shift anisotropy (CSA) of Cζ, the center of the guanidinium ion. We chose the intermediate temperature of 283 K for the CSA and the subsequent dipolar coupling experiments, since at this temperature the spectra have the best overall combination of resolution and sensitivity. The theoretical phase transition temperature of the POPE/POPG (3:1) membrane is 291 K, thus the spectra theoretically correspond to the gel-phase membrane, but the phase transition is likely broadened by the peptide. The peptide mobility closer to the physiological temperature may be extrapolated from the 283 K data and is expected to be higher, but the differences between residues should be similar. We used the 2D separation of undistorted powder patterns by effortless recoupling (SUPER) experiment [22] to recouple the CSA interaction and correlate it with the isotropic

^{13}C chemical shift. Figure 7.3 shows the 2D SUPER spectra and 1D cross sections of the model compound Fmoc-Arg(MTR)-OH, and Arg_4 and Arg_{11} in PG-1 bound to the POPE/POPG membrane. For the dry powder sample Fmoc-Arg(MTR)-OH, the Cζ cross section yielded a CSA anisotropy parameter δ, defined as the difference between the largest principal value δ_{zz} and the isotropic shift δ_{iso}, of 78 ppm. This CSA is the rigid-limit value, since C-H dipolar couplings of the sidechain carbons in this model compound have nearly rigid-limit values (Table 7.2). In comparison, PG-1 Arg_4 and Arg_{11} Cζ both give reduced CSA's: the Arg_4 Cζ $\bar{\delta}$ is 47.3 ppm whereas the Arg_{11} Cζ CSA is much smaller, 10.3 ppm. These correspond to a motional scaling factor of 0.13 for Arg_{11} and 0.61 for Arg_4. Thus, the Arg_{11} sidechain has larger-amplitude motion than Arg_4. Since T_2 data indicate narrower homogeneous linewidths of Arg_{11} Cδ and Cζ than Arg_4, the Arg_{11} sidechain motion is both faster and larger in amplitude than the Arg_4 sidechain.

Table 7.2. Dipolar order parameters and CSA motional scaling factors [a] of PG-1 residues at 283 K and of three crystalline model compounds at 295 K.

Sites	Arg_4	Arg_{11}	Fmoc-Arg	Arg-HCl	Leu_5	Leu
Nα	1.05	0.70	-	-	0.95	-
Cα	0.93	0.70	0.91	0.91	0.93	0.95
Cβ	0.61	-	0.86	0.91	0.56	0.93
Cγ	0.63	-	0.91	0.91	0.44	-
Cδ	0.48	0.21	0.91	1.02	0.43	0.34
Nε	0.48	0.24	-	-	-	-
Cζ[a]	0.61	0.13	-	-	-	-
Nη	0.36	0.28	-	-	-	-

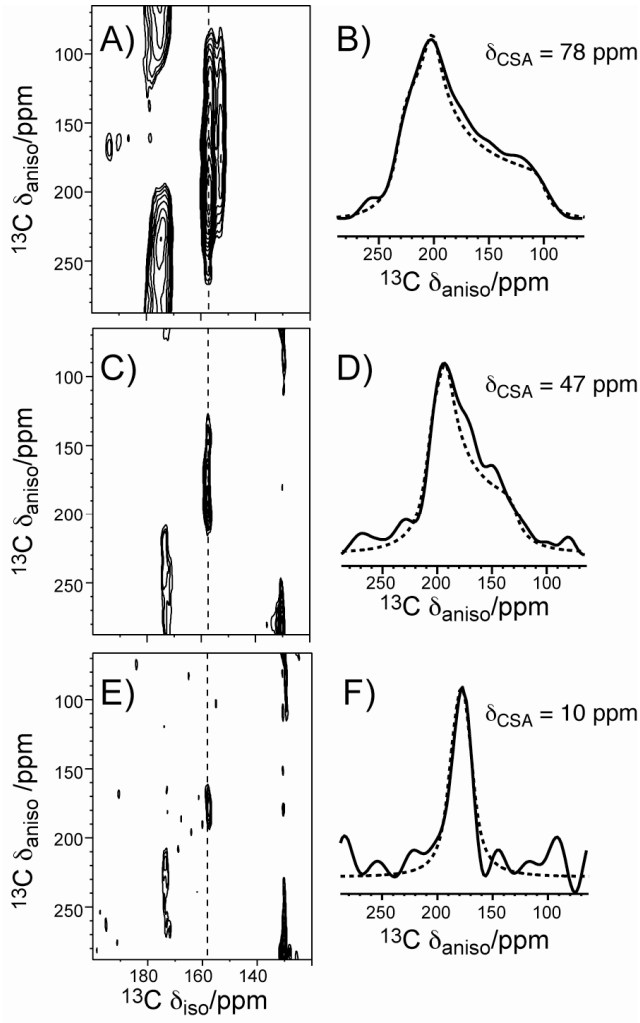

Figure 7.3. Arg Cζ chemical shift anisotropies from the SUPER experiment. The 2D SUPER spectra are shown in A), C), E) and the corresponding Cζ 1D cross sections are shown in B), D), F). A, B) Fmoc-Arg(MTR)-OH. C, D) PG-1 Arg_4. E, F) PG-1 Arg_{11}. The PG-1 data were measured at 283 K in the POPE/POPG membrane.

To obtain more quantitative information on the motional amplitude, we measured C-H and N-H dipolar couplings, whose tensor orientation and rigid-limit coupling strength are exactly known. The dipolar couplings were readily measured using the 2D dipolar-chemical shift correlation (DIPSHIFT) experiment to yield the bond order parameter, $S = \overline{\delta}/\delta$. Figure 7.4 shows representative DIPSHIFT curves of Arg_4 and Arg_{11} in POPE/POPG-bound PG-1. Cα-H represents the backbone, while Cδ-H_2, Nε-H and Nη-H_2 represent the sidechains. The order parameters are compiled in Table 7.2. Both the backbone Nα and Cα of Arg_4 and Leu_5 exhibit nearly rigid-limit couplings, with order parameters of 0.93-1.00. In contrast, the Arg_{11}

Cα and Nα have significantly lower order parameters of 0.70. Thus, the β-strand backbone of the peptide is immobilized in the POPE/POPG membrane at this temperature, while the Arg_{11} backbone retains significant local segmental motion. For resolved sites (Cδ, Nε, and Nη) in the sidechains, Arg_4 and Leu_5 also have stronger dipolar couplings than those of Arg_{11}, indicating that the β-strand sidechains have smaller amplitudes of motion, consistent with the variable-temperature spectra and the CSA results. Some ^{13}C sites in the sidechain, such as Arg Cβ, Cγ, Leu Cγ and Cδ, overlap with the lipid peaks, so we used a double-quantum (DQ) filtered DIPSHIFT experiment to suppress the lipid signals and measure the C-H couplings of these Arg sites [1]. Figure 7.5 shows representative 1D DQ spectra and DQ-DIPSHIFT dephasing curves of Arg_4 and Leu_5. Arg_{11} has prohibitively low sensitivity in the DQ-DIPSHIFT experiment due to unfavorable motional rates at this temperature and is thus not measured. Table 7.2 shows that in general, the sidechain order parameters decrease with increasing distance from the backbone. Arg_{11} at the β-turn, which is close to the membrane surface, has much higher amplitudes of motion, or much lower order parameters, than Arg_4 and Leu_5 in the β-strand part of the peptide, which is embedded in the membrane [12].

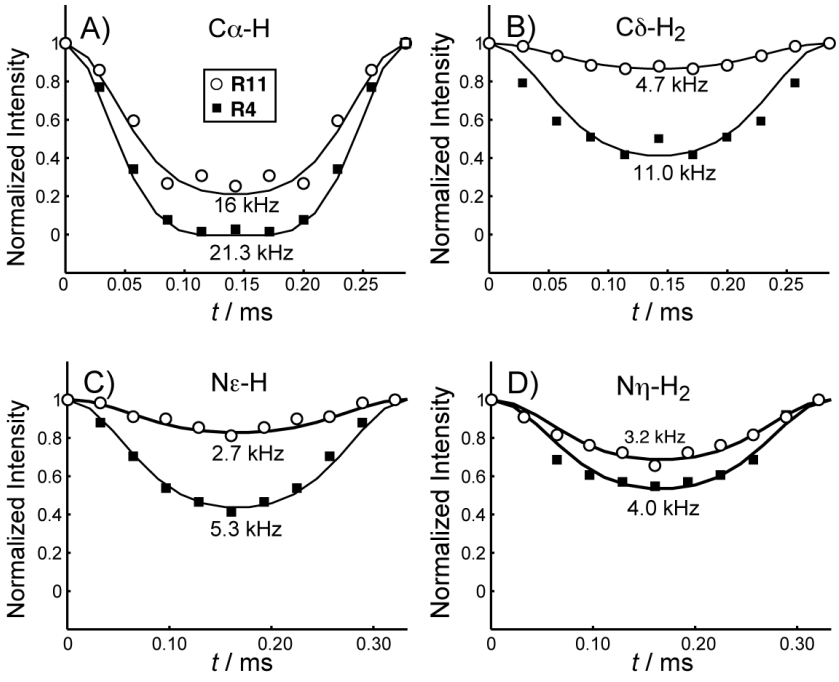

Figure 7.4. ^{13}C-^{1}H and ^{15}N-^{1}H DIPSHIFT curves of several sites of Arg_4 (closed squares) and Arg_{11} (open circles) in PG-1 at 283 K. A) Cα-H. B) Cδ-H_2. C) Nε-H. D) Nη-H_2. Arg_{11} gives weaker couplings than Arg_4, indicating larger motional amplitudes.

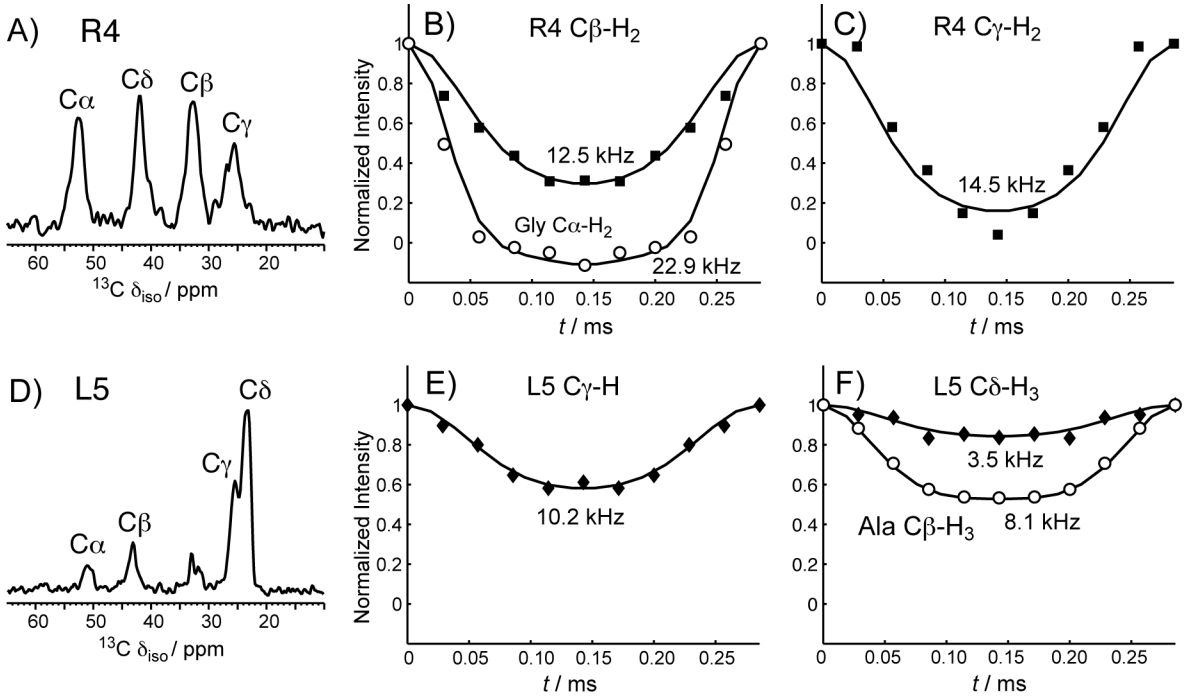

Figure 7.5. 1D ^{13}C DQ filtered spectra and DQ-DIPSHIFT curves of Arg_4 and Leu_5 in PG-1 in the POPE/POPG membrane. A) 1D DQ spectrum of Arg_4. The Cβ and Cγ peaks no longer overlap with the lipid peaks. B) DIPSHIFT curves of Arg_4 Cβ (squares) and the crystalline amino acid Gly Cα (circles). The Gly Cα data give the rigid-limit coupling for CH_2 groups, which is 22.9 kHz. C) DIPSHIFT curve of Arg_4 Cγ. D) 1D DQ spectrum of Leu_5. The Cγ and Cδ peaks no longer overlap with the lipid peaks. E) DIPSHIFT curve of Leu_5 Cγ. F) DIPSHIFT curves of Leu_5 Cδ (diamonds) and the crystalline amino acid Ala Cβ (circles). The Ala Cβ data give the rigid-limit coupling for methyl groups, which is 8.1 kHz. This is one-third of the one bond C-H coupling due to the three-site jump of the CH_3 group.

To obtain further information on the rates of motions of these residues, we measured the ^{1}H $T_{1\rho}$ relaxation times, listed in Table 7.3. Most sites in Arg_4, Leu_5 and Arg_{11} have similar ^{1}H $T_{1\rho}$ values (1.6 – 2.6 ms), except for Arg_{11} Hα, which has a much shorter $T_{1\rho}$ (0.83 ms) than Arg_4 Hα (2 ms). This is consistent with the ^{13}C T_2 data indicating more pronounced intermediate-timescale motion of the β-turn backbone compared to the β-strand backbone.

Table 7.3. ^{1}H $T_{1\rho}$ (ms) of POPE/POPG-bound PG-1 at 283 K and of crystalline Arg·HCl at 295 K. Experimental uncertainties are given in the parentheses. The ^{1}H spin-lock field strengths were 50 kHz in the ^{15}N-detected experiment and 62.5 kHz in the ^{13}C-detected experiments.

Sites	Arg_4	Arg_{11}	Arg · HCl
H^N	2.6 (0.2)	2.2 (0.3)	-
Hα	2.0 (0.1)	0.8 (0.1)	8.8
Hδ	1.6 (0.1)	1.9 (0.1)	9.5
Hε	2.2 (0.2)	2.6 (0.2)	8.8
Hη	1.9 (0.2)	1.8 (0.1)	8.8

Discussion

The solid-state NMR data shown here indicate that the β-turn backbone undergoes large-amplitude segmental motion on the microsecond timescale, while the β-strand backbone is mostly immobilized in the POPE/POPG membrane in the liquid-crystalline phase. The latter is consistent with the previously reported immobilization of PG-1 strand residues in POPC/POPG membranes [23]. Concomitant with the backbone mobility difference, the sidechains also exhibit dynamic differences: Arg_{11} has much lower order parameters than Arg_4 (Table 7.2), indicating large motional amplitudes. Both membrane-associated Arg's are much more mobile than the crystalline compound Arg · HCl.

The dynamic difference between Arg_4 and Arg_{11} can be understood in terms of the self-assembly of PG-1 and the peptide-lipid interactions. The β-strands containing Arg_4 and Leu_5 are involved in intermolecular association with other PG-1 molecules through N–H···O=C hydrogen bonds to form β-barrels [12, 24], thus these residues should experience hindered motion. The strand aggregation is important to PG-1 antimicrobial activity. Mutation of Val_{14} to *N*-methyl-Val, which disrupted hydrogen bonding of the Val_{14} backbone to its intermolecular partner, resulted in much lower antimicrobial activity [25]. In contrast, the β-turn Arg_{11} is not involved in intermolecular hydrogen bonding and is located near the membrane surface, thus has more motional freedom.

A second contributing factor to the different sidechain dynamics of Arg_{11} and Arg_4 may be the guanidinium-phosphate interaction. ^{13}C-^{31}P distance data indicated that both sidechains lie within hydrogen-bonding distance to lipid phosphates [13]. However, while the Arg_4 guanidinium group interacts with the phosphate groups that have moved to the middle of the membrane as part of the toroidal pore, the Arg_{11} guanidinium ion interacts with phosphates at the membrane surface with much higher mobility. Thus, the motional restriction caused by the lipid phosphate groups is more severe for Arg_4 than for Arg_{11}. We note that at the temperature of 283 K where most dynamics data were obtained, the lipid molecules are much more mobile than at ~230 K where the ^{13}C-^{31}P distances were measured. Thus, the guanidinium-phosphate association at 283 K is likely to be transient rather than permanent.

The high mobility of the β-hairpin tip of PG-1 dovetails the observation of an analogous β-hairpin antimicrobial peptide, TP-I [26]. There, G10 at the β-turn exhibited an order of magnitude shorter ^1H $T_{1\rho}$ than the β-strand residues. Field-dependent $T_{1\rho}$ analysis indicated that the shorter $T_{1\rho}$ of G10 results from larger motional amplitudes of the β-turn and not to rate differences from the rest of the peptide [26].

Molecular dynamics simulations of the S4 helix of the voltage-gated potassium channel KvAP [27] suggested that lipid headgroups and water stabilize Arg insertion by forming a hydrogen-bonded network. The effective lipid bilayer thickness was reduced to a remarkably small 10 Å near the inserted S4 helix so that water and phosphate groups can stabilize the Arg's in the middle of the S4 helix by hydrogen bonds [28]. Based on the comparison of the mean-square displacement of phosphate groups near the peptide with those far away from the peptide and the analysis of the survival function of water molecules in the system, it was found that both phosphate groups and water molecules are much less mobile in the vicinity of the guanidinium groups than in their respective bulk environments. In particular, the mean residence times for water molecules hydrogen-bonded to Arg_9 and Arg_{12} in the S4 helix, which are close to the bilayer surface, are much shorter than those hydrogen-bonded to Arg_{15} and Arg_{18}, which lie in the hydrophobic core of the membrane (90-300 ps versus 1000-2000 ps). This different residence time suggests that the water molecules near Arg in the hydrophobic core are less mobile than those near Arg at the membrane surface.

This in turn suggests that Arg's in the hydrophobic part of the membrane are less mobile than those close to the bilayer surface. These are consistent with the different mobility observed between Arg_4 and Arg_{11} in PG-1.

In summary, we have measured the dipolar couplings, CSA's, and T_2 and $T_{1\rho}$ relaxation times of key Arg residues in PG-1 in the bacteria-mimetic anionic POPE/POPG membrane. The linewidths and motional scaling factors show that the β-turn Arg_{11} near the membrane surface is significantly more mobile than the β-strand Arg_4 and Leu_5 in the hydrophobic part of the membrane. The different mobility is consistent with the location of the residues with respect to the membrane, the intermolecular aggregation of this peptide, and the strong Arg-phosphate interaction. Thus, the site-specific dynamics of PG-1 correlate well with its topological and oligomeric structure. Solid-state NMR is shown to be a useful tool for elucidating the relation between membrane protein dynamics and its structure.

Experimental section

1-palmitoyl-2-oleoyl-*sn*-glycero-3-phosphatidylethanolamine (POPE), and 1-palmitoyl-2-oleoyl-*sn*-glycero-3-phosphatidylglycerol (POPG) were purchased from Avanti Polar Lipids (Alabaster, AL). PG-1 (NH_2-RGGRLCYCRRRFCVCVGR-$CONH_2$) was synthesized using Fmoc chemistry as previously described [7]. Three PG-1 samples were synthesized, containing U-^{13}C, ^{15}N-Arg_4 and ^{15}N-Leu_5, U-^{13}C, ^{15}N-Arg_{11} and ^{15}N-Phe_{12}, U-^{13}C, ^{15}N-Leu_5. U-^{13}C, ^{15}N-labeled Arg was obtained from Spectra Stable Isotopes (Columbia, MD) as Fmoc-Arg(MTR)-OH.

POPE and POPG lipids (3:1) were mixed in chloroform and blown dry under N_2 gas. The mixture was then redissolved in cyclohexane and lyophilized. The dry lipid powder was dissolved in water and subjected to five cycles of freeze-thawing to form uniform vesicles. An appropriate amount of PG-1 to reach a peptide-lipid molar ratio (P/L) of 1 : 12.5 was dissolved in water and mixed with the lipid vesicle solution, incubated at 303 K overnight, then centrifuged at 55,000 rpm for 2.5 hours. The pellet was packed into a MAS rotor, giving a fully hydrated membrane sample.

NMR experiments were carried out on a Bruker DSX-400 (9.4 Tesla) spectrometer (Karlsruhe, Germany). Triple-resonance magic-angle spinning (MAS) probes with a 4 mm

spinning module was used. Temperatures were controlled by a Kinetics Thermal Systems XR air-jet sample cooler (Stone Ridge, NY) on the 400 MHz system. Typical 90° pulse lengths were 5 – 6 μs for ^{13}C and ^{15}N, and ^{1}H decoupling fields of 50-80 kHz were used. ^{13}C chemical shifts were referenced externally to the α-Gly $^{13}C'$ signal at 176.49 ppm on the TMS scale. ^{15}N chemical shifts were referenced externally to the *N*-acetyl-Val $^{15}N\alpha$ signal at 121.72 ppm.

^{13}C-^{1}H and ^{15}N-^{1}H dipolar couplings were measured using the 2D DIPSHIFT experiment [29] at 3.0–3.5 kHz MAS with MREV-8 for ^{1}H homonuclear decoupling. Pulse lengths of 3.5 μs were used in the MREV-8 pulse train. The N-H DIPSHIFT experiments were performed with dipolar doubling [30, 31] to increase the precision of the measured couplings. Some ^{13}C sites overlap with lipid peaks, so the double-quantum-filtered (DQ) DIPSHIFT experiments [1] were used to measure these dipolar couplings. The DQ filter used SPC5 homonuclear dipolar recoupling sequence [32]. The ^{13}C CSA was measured using the 2D SUPER experiment [22] under 3.5 kHz MAS. The corresponding ^{13}C field strength was 42 kHz. ^{1}H rotating-frame spin-lattice relaxation times ($T_{1\rho}$) was measured using spin-lock field strengths of 50–62.5 kHz. The ^{13}C and ^{15}N 1D spectra were measured between 243 and 308 K. All DIPSHIFT, SUPER and $T_{1\rho}$ experiments were carried out at 283 K.

Acknowledgement

This work is supported by the National Institutes of Health grant GM-066976 to M. H.

References

[1] D. Huster, L. S. Xiao, M. Hong, *Biochemistry*. **2001**, *40*, 7662-7674.

[2] G. Reuther, K. T. Tan, A. Vogel, C. Nowak, K. Arnold, J. Kuhlmann, H. Waldmann, D. Huster, *J. Am. Chem. Soc.* **2006**, *128*, 13840-13846.

[3] J. C. Williams, A. E. McDermott, *Biochemistry*. **1995**, *34*, 8309-8319.

[4] M. Etzkorn, S. Martell, O. C. Andronesi, K. Seidel, M. Engelhard, M. Baldus, *Angew. Chem. Int. Ed.* **2007**, *46*, 459-462.

[5] S. D. Cady, C. Goodman, W. F. DeGrado, M. Hong, *J. Am. Chem. Soc.* **2007**, *129*, 5719-5729.

[6] S. H. Park, A. A. Mrse, A. A. Nevzorov, A. A. De Angelis, S. J. Opella, *J. Magn. Reson.* **2006**, *178*, 162-165.

[7] S. Yamaguchi, T. Hong, A. Waring, R. I. Lehrer, M. Hong, *Biochemistry*. **2002**, *41*, 9852-9862.

[8] L. Bellm, R. I. Lehrer, T. Ganz, *Exp. Opin. Invest. Drugs*. **2000**, *9*, 1731-1742.

[9] V. N. Kokryakov, S. S. Harwig, E. A. Panyutich, A. A. Shevchenko, G. M. Aleshina, O. V. Shamova, H. A. Korneva, R. I. Lehrer, *FEBS Lett.* **1993**, *327*, 231-236.

[10] M. E. Mangoni, A. Aumelas, P. Charnet, C. Roumestand, L. Chiche, E. Despaux, G. Grassy, B. Calas, A. Chavanieu, *FEBS Lett.* **1996**, *383*, 93-98.

[11] Y. Sokolov, T. Mirzabekov, D. W. Martin, R. I. Lehrer, B. L. Kagan, *Biochim. Biophys. Acta.* **1999**, *1420*, 23-29.

[12] R. Mani, S. D. Cady, M. Tang, A. J. Waring, R. I. Lehrer, M. Hong, *Proc. Natl. Acad. Sci. U.S.A.* **2006**, *103*, 16242-16247.

[13] M. Tang, A. J. Waring, M. Hong, *J. Am. Chem. Soc.* **2007**, *129*, 11438-11446.

[14] J. Lorieau, A. E. McDermott, *Magn. Reson. Chem.* **2006**, *44*, 334-347.

[15] J. L. Lorieau, A. E. McDermott, *J. Am. Chem. Soc.* **2006**, *128*, 11505-11512.

[16] B. J. Wylie, W. T. Franks, D. T. Graesser, C. M. Rienstra, *J. Am. Chem. Soc.* **2005**, *127*, 11946-11947.

[17] R. E. Hancock, R. Lehrer, *Trends Biotechnol.* **1998**, *16*, 82-88.

[18] E. Vives, P. Brodin, B. Lebleu, *J. Biol. Chem.* **1997**, *272*, 16010-16017.

[19] P. Jarver, U. Langel, *Biochim. Biophys. Acta*. **2006**, *1758*, 260-263.

[20] S. B. Long, E. B. Campbell, R. Mackinnon, *Science*. **2005**, *309*, 897-903.

[21] M. Hong, R. G. Griffin, *J. Am. Chem. Soc.* **1998**, *120*, 7113-7114.

[22] S. F. Liu, J. D. Mao, K. Schmidt-Rohr, *J. Magn. Reson.* **2002**, *155*, 15-28.

[23] J. J. Buffy, A. J. Waring, R. I. Lehrer, M. Hong, *Biochemistry*. **2003**, *42*, 13725-13734.

[24] R. Mani, M. Tang, X. Wu, J. J. Buffy, A. J. Waring, M. A. Sherman, M. Hong, *Biochemistry*. **2006**, *45*, 8341-8349.

[25] J. Chen, T. J. Falla, H. J. Liu, M. A. Hurst, C. A. Fujii, D. A. Mosca, J. R. Embree, D. J. Loury, P. A. Radel, C. C. Chang, L. Gu, J. C. Fiddes, *Biopolymers*. **2000**, *55*, 88-98.

[26] T. Doherty, A. J. Waring, M. Hong, *Biochemistry*. **2008**, *47*, 1105-1116.

[27] T. Hessa, S. H. White, G. von Heijne, *Science*. **2005**, *307*, 1427.

[28] J. A. Freites, D. J. Tobias, G. von Heijne, S. H. White, *Proc. Natl. Acad. Sci. U. S. A.* **2005**, *102*, 15059-15064.

[29] M. G. Munowitz, R. G. Griffin, G. Bodenhausen, T. H. Huang, *J. Am. Chem. Soc.* **1981**, *103*, 2529-2533.

[30] M. Hong, J. D. Gross, C. M. Rienstra, R. G. Griffin, K. K. Kumashiro, K. Schmidt-Rohr, *J. Magn. Reson.* **1997**, *129*, 85-92.

[31] D. Huster, S. Yamaguchi, M. Hong, *J. Am. Chem. Soc.* **2000**, *122*, 11320-11327.

[32] M. Hohwy, C. M. Rienstra, C. P. Jaroniec, R. G. Griffin, *J. Chem. Phys.* **1999**, *110*, 7983-7992.

Chapter 8

Effects of Guanidinium-Phosphate Hydrogen Bonding on the Membrane-Bound Structure and Activity of an Arginine-Rich Membrane Peptide from Solid-State NMR

Published in Angew. Chem. Int. Ed.

2008, 47, 3202-3205

Ming Tang, Alan J. Waring, Robert I. Lehrer, and Mei Hong*

(*) M. Tang, Dr. M. Hong
Department of Chemistry
Iowa State University
Ames, IA 50011 (USA)
Fax: (+1) 515-294-0105
E-mail: mhong@iastate.edu
Homepage: http://www.public.iastate.edu/~hongweb

Dr. A. J. Waring, Dr. R. I. Lehrer
Department of Medicine
University of California at Los Angeles
Los Angeles, CA 90095 (USA)

This chapter is modified from the manuscript in its pre-publication form, but not the article in its final version.

Keywords

Membrane proteins, solid-state NMR, guanidinium-phosphate complex, Arg-rich proteins, structure determination, antimicrobial peptides.

Arginine- (Arg) and lysine-rich cationic peptides and protein domains are found in a wide range of membrane-active proteins such as antimicrobial peptides,[1] cell-penetrating peptides,[2] and voltage-sensing domains of potassium channels.[3] Yet what three-dimensional structures these proteins adopt to enable translocation of the charged residues into the low dielectric milieu of the hydrophobic part of the lipid membrane against the free-energy barrier[4] remain poorly understood. An increasing number of molecular dynamics simulations and experimental studies has suggested the importance of Arg interaction with lipids in membrane protein function.[5, 6] Magic-angle spinning (MAS) solid-state NMR (SSNMR) spectroscopy can provide direct experimental insights into this intriguing energetic and structural question.

We have recently reported SSNMR distance-constrained guanidinium-phosphate ($\mathrm{Gdn\text{-}PO_4^-}$) complex formation between the Arg's of a β-hairpin antimicrobial peptide, PG-1, and the lipid phosphates.[7] The existence of these complexes suggests that the Arg's are neutralized by the phosphates to enable transmembrane insertion of the peptide. We hypothesized that the peptide-associated phosphate headgroups transferred to the hydrophobic part of the membrane are responsible for the toroidal pore defects.[8] Such Gdn-$\mathrm{PO_4^-}$ complexes should be stabilized by $\mathrm{N-H\cdots O=P}$ hydrogen bonds and electrostatic attraction.[9]

Here we test the importance of $\mathrm{Gdn\text{-}PO_4^-}$ hydrogen bonding to the structure and activity of PG-1 by dimethylating each guanidinium, thus reducing the number of N-H hydrogen bond donors (Figure 8.1).[10] We show that this Arg dimethylation significantly alters the membrane insertion and activity of PG-1. Figure 8.2 shows oriented ^{31}P spectra of POPC/POPG membranes containing 0-4% of the mutant, $\mathrm{Arg^{mm}}$-PG-1. Without the peptide, membranes uniaxially aligned on glass plates exhibit the expected single peak at ~30 ppm without other intensities in the anisotropic chemical shift range. With increasing $\mathrm{Arg^{mm}}$-PG-1, residual powder intensities indicative of misalignment and a small 0-ppm isotropic peak

indicative of toroidal pores are created. Lineshape simulations indicate that the isotropic component in the 4% Arg^{mm}-PG-1 sample is 20% of the total intensity, much less than the 39% caused by PG-1. Thus Arg dimethylation reduces membrane disruption.

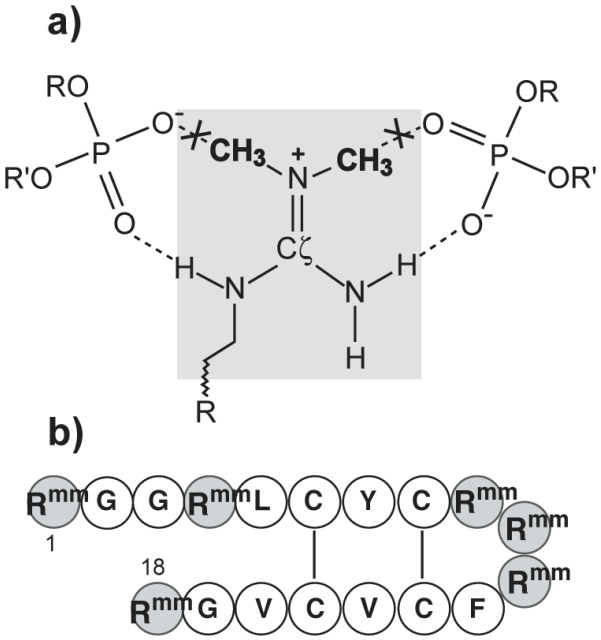

Figure 8.1. a) Structure of dimethylated Arg and its bidentate complex with phosphate ions. b) Arg^{mm}-PG-1 amino acid sequence.

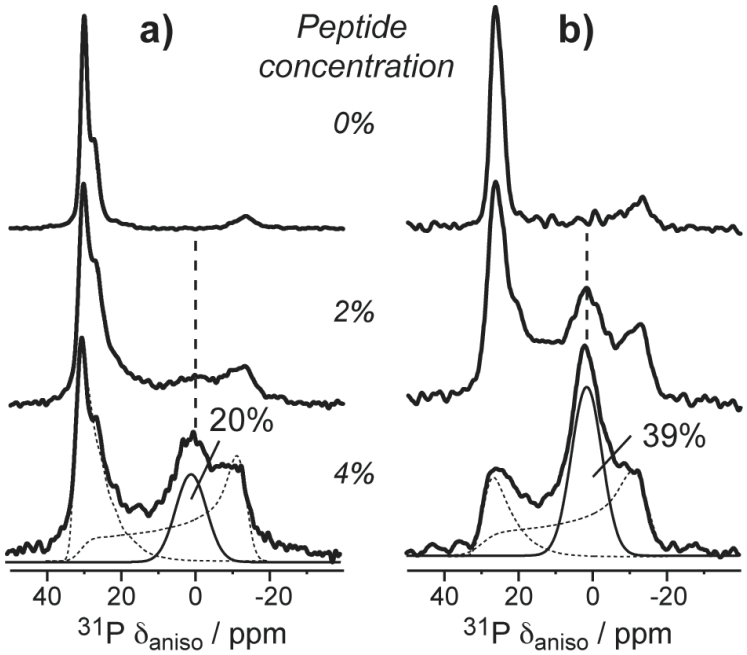

Figure 8.2. Oriented ^{31}P spectra of POPC/POPG membranes with 0-4% a) Arg^{mm}-PG-1 and b) PG-1. The 4% samples spectra are simulated with an aligned peak, an isotropic peak, and a powder pattern, to yield the fraction of the isotropic peak.

Corroborating the ^{31}P NMR data are the minimal effective concentrations (MECs) of Arg^{mm}-PG-1 and PG-1 against a number of bacteria. In a physiological amount of salt, the average MEC of Arg^{mm}-PG-1 is 3.4-fold higher than PG-1, indicating that the mutant is 3.4-fold less potent (Table S8.1). At low salt, Arg^{mm}-PG-1 is still 1.4-fold less potent. The weaker activity supports the lower membrane disorder of Arg^{mm}-PG-1 in the ^{31}P spectra. The different salt-concentration dependence of the two peptides suggests different mechanisms are involved in their antimicrobial action (Supporting Information).

To determine the topological structure of Arg^{mm}-PG-1 in the lipid membrane, we measured peptide-lipid ^{13}C-^{31}P distances. Figure 8.3 shows REDOR distance curves of several ^{13}C-labeled sites. L5 Cα, next to the most hydrophobic Arg, R4, increased its distance from 6.9±1.6 Å in PG-1 to 8.5 Å in Arg^{mm}-PG-1, suggesting that R4 mutation weakened the Gdn-PO_4^- complex. All measured distances are within 5.7 – 8.5 Å. Since the membrane has much less isotropic defects in the presence of Arg^{mm}-PG-1, the distance similarity suggests that Arg^{mm}-PG-1 binds at the membrane-water interface, with the strand axis roughly parallel to the membrane plane.

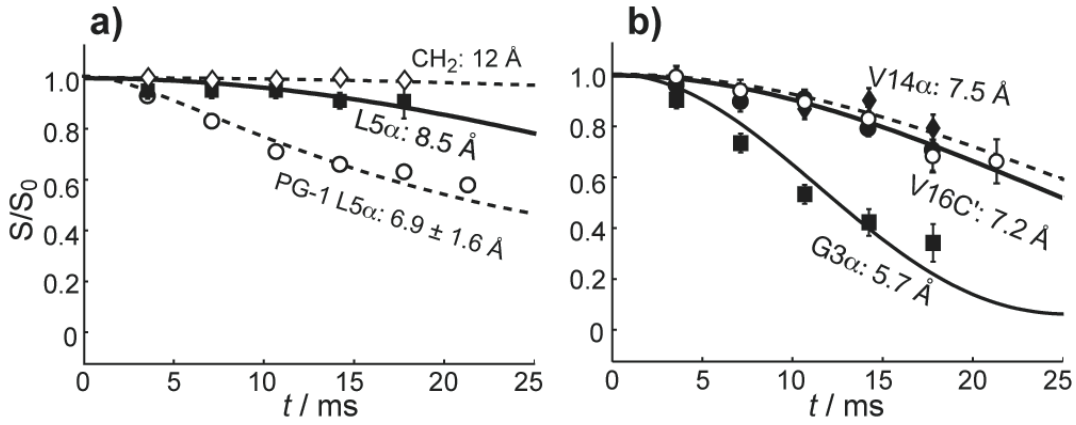

Figure 8.3. ^{13}C-^{31}P distances of Arg^{mm}-PG-1 in hydrated POPE/POPG membranes. a) L5α (squares) in Arg^{mm}-PG-1, compared with PG-1 (circles). Lipid CH_2 data (diamonds) give the long distance limit. b) G3α (squares) and V14α (diamonds) in Arg^{mm}-PG-1, and V16C' in Arg^{mm}-PG-1 (filled circles) and in PG-1 (open circles).

To verify the interfacial hypothesis, we measured the distance between Arg^{mm}-PG-1 and the lipid chains using a 2D ^{31}P-detected ^{1}H spin diffusion experiment.[11] In a peptide-free membrane, the lipid chain $(CH_2)_n$ cross peak with ^{31}P is very weak due to the long distance and high mobility of the lipids. A rigid transmembrane (TM) peptide facilitates spin diffusion via its strongly coupled ^{1}H network, giving high CH_2-P intensity. In contrast, a surface-bound peptide or a TM peptide with large-amplitude motion are ineffective spin-diffusion conduits, thus giving low CH_2-P intensities.

Figure 8.4a shows the 2D spectrum of Arg^{mm}-PG-1 in POPE/POPG membrane at a mixing time of 64 ms. In the 1D cross sections, the Arg^{mm}-PG-1 CH_2 intensity is higher than the pure membrane and lower than PG-1 (b-d). The CH_2 buildup curves (e) confirm that PG-1 has the fastest rise, as expected for the TM peptide; Arg^{mm}-PG-1 has slower buildup, while the peptide-free bilayer has the slowest rise. These support the interfacial binding of Arg^{mm}-PG-1.

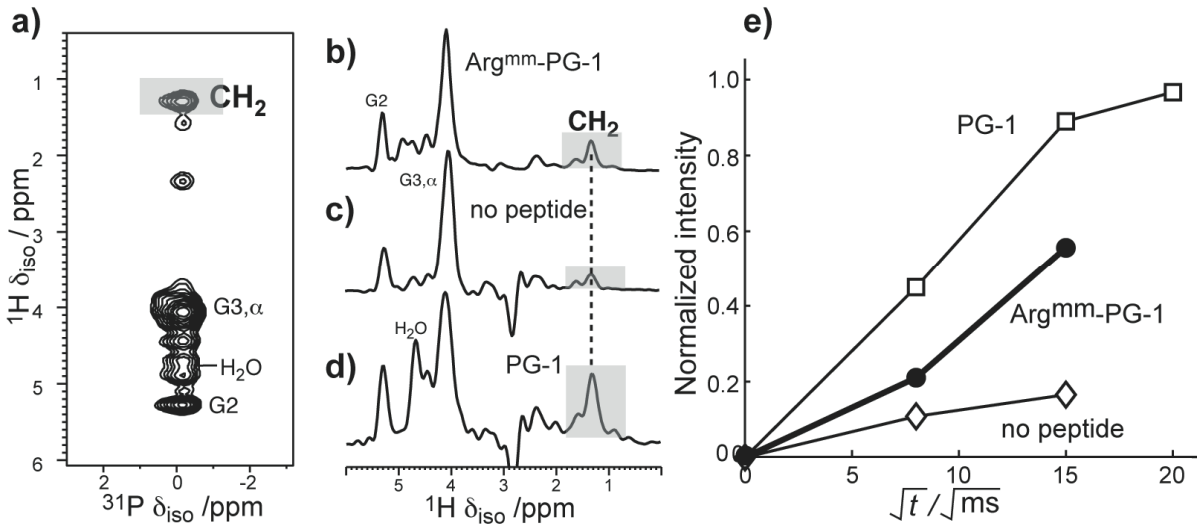

Figure 8.4. ^{31}P-detected ^{1}H spin diffusion spectra of POPE/POPG membranes at 303 K. a) 64 ms 2D spectrum of Arg^{mm}-PG-1-containing membrane. b-d) 64 ms 1D cross sections of membranes containing b) Arg^{mm}-PG-1, c) no peptide, and d) PG-1. e) CH_2 buildup curves for the three samples.

To assess if Arg^{mm}-PG-1 is TM but highly mobile, which could still satisfy the ^{1}H spin diffusion data, we measured C-H dipolar couplings of two Cα sites. Both L5 and V14 give Cα-Hα couplings that are 60-70% of the rigid-limit value in the POPC/POPG

membrane (Table 8.1), shown in 2D LG-CP[12] spectra (Figures S8.1), indicating that the peptide is mobile. This contrasts with the fully immobilized PG-1 backbone in anionic membranes.[13, 14] L5 and V14 are next to the disulfide bonds, thus backbone segmental motion is unlikely, and the reduced couplings are most likely due to rigid-body rotation of Arg^{mm}-PG-1 around the bilayer normal, $\vec{n}$. Indeed, recoupled Cα chemical shift anisotropies (CSA) of L5 and V14 show uniaxial lineshapes (Figures S8.2), confirming the uniaxiality of the backbone motion. Under this rotation, S_{CH} depends on the C-H bond orientation with $\vec{n}$ as $S_{CH}=\left\langle\left(3\cos^2\theta-1\right)/2\right\rangle$, so the L5 and V14 S_{CH}'s must be related by the orientations of the two bonds to each other and to $\vec{n}$, and the S_{CH} should indicate the peptide orientation.[15, 16]

Table 8.1. Cα S_{CH} of Arg^{mm}-PG-1 in two anionic lipid membranes.

S_{CH}	POPC/POPG	POPE/POPG
L5	0.69	0.84
V14	0.62	0.37

Figures 8.5, S3 and S4 show calculated S_{CH}'s for strand residues in an ideal antiparallel β-hairpin as a function of (τ, ρ) angles [17]: τ is the tilt angle between the strand axis and $\vec{n}$, and ρ is the rotation angle of the β-hairpin plane from $\vec{n}$. ρ = 0° when $\vec{n}$ lies in the β-sheet plane. For the TM case $\tau \approx 180^\circ$, S_{CH} is generally less than 0.5 due to the near perpendicularity of the Cα-Hα bonds to $\vec{n}$. For τ of 130°–180°, the measured S_{CH} > 0.6 for L5 and V14 in the POPC/POPG membrane cannot be both satisfied. As the strands become more parallel to the bilayer plane ($\tau \to 90^\circ$), S_{CH} adopts larger values and varies over the entire range of 0–1. The best fit is (τ, ρ) = (116°, 179°), indicating that the strand axis is roughly orthogonal to $\vec{n}$ and the hairpin plane is parallel to $\vec{n}$. The latter is reasonable as the peptide meets the least resistance at this orientation when inserting into the membrane. Three other symmetry-related (τ, ρ) solutions exist, but they agree less well with the ^{13}C-^{31}P distance data (Table S8.2).

If residual segmental motion had remained at L5 and V14 Cα, it would mean the whole-body S_{CH} is larger than 0.6-0.7, which would require τ to be even closer to 90°. Thus, the strand axis must be parallel to the membrane plane. In the POPE/POPG membrane, the

L5 and V14 S_{CH}'s change to 0.84 and 0.37 (Table 1). But due to the high angular resolution of S_{CH} in this regime (Figures S8.5), the difference translates to only small (τ, ρ) changes, with the best fit at (113˚, 164˚). Thus, Arg^{mm}-PG-1 is interfacial in both anionic membranes. We also considered the effect of the backbone structure on the orientation calculation. Figures S8.6 and Table S8.2 show that even with the non-ideal PG-1 solution structure, the C-H dipolar couplings still constrain the strand axis to be perpendicular to $\vec{n}$.

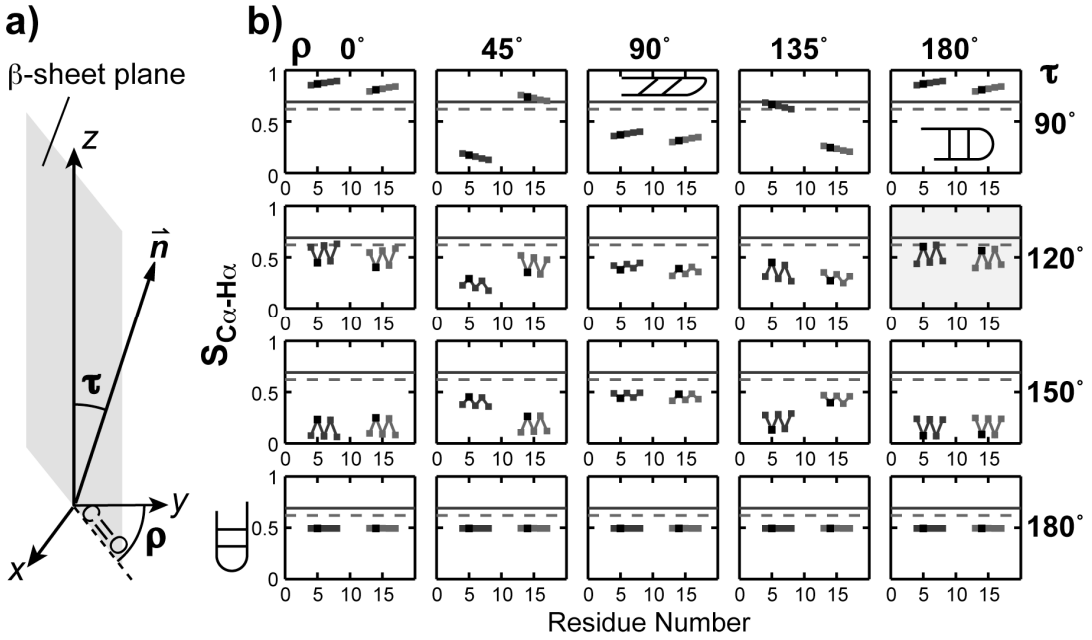

Figure 8.5. a) Definition of (τ, ρ) angles. τ is the angle between the strand axis z and the bilayer normal $\vec{n}$, and ρ is the angle between the C=O bond of residue 6 and the common plane of z and $\vec{n}$. b) Calculated $S_{C\alpha-H\alpha}$ of the strand residues (4-8 and 13-17) in an ideal β-hairpin as a function of (τ, ρ). The measured $S_{C\alpha-H\alpha}$ of L5 and V14 are drawn as solid and dashed lines, respectively. The best-fit (τ, ρ) panel, near (120˚, 180˚), is shaded.

Figure 8.6 summarizes the dramatic topology difference of Arg^{mm}-PG-1 and PG-1 in the lipid membrane. The hydrogen-bond-deficient mutant is no longer TM but is inserted to the membrane-water interface, 5.7-8.5 Å from the ^{31}P plane and further from the hydrophobic center of the membrane than PG-1. The mutant is uniaxially mobile and thus not oligomerized, while PG-1 forms immobile multimeric β-barrels in the anionic membrane, possibly promoted by high salt concentration. Thus, hydrogen-bond deficiency caused by

Arg-dimethylation in this antimicrobial peptide weakens Gdn-PO_4^- complexation, prevents peptide insertion and oligomerization, and reduces the membrane disruptive activity. The data here suggest that the remaining activity of Arg^{mm}-PG-1 is achieved by a different mechanism, most likely in-plane diffusion, which still gives rise to isotropic lipid morphologies but at a lower amount than the toroidal pore mechanism employed by wild-type PG-1 [18]. Gdn-PO_4^- hydrogen bonding may also affect the structure and function of other Arg-rich membrane proteins, as suggested by recent molecular dynamics simulations of a potassium channel and a cell-penetrating peptide.[3, 5, 6]

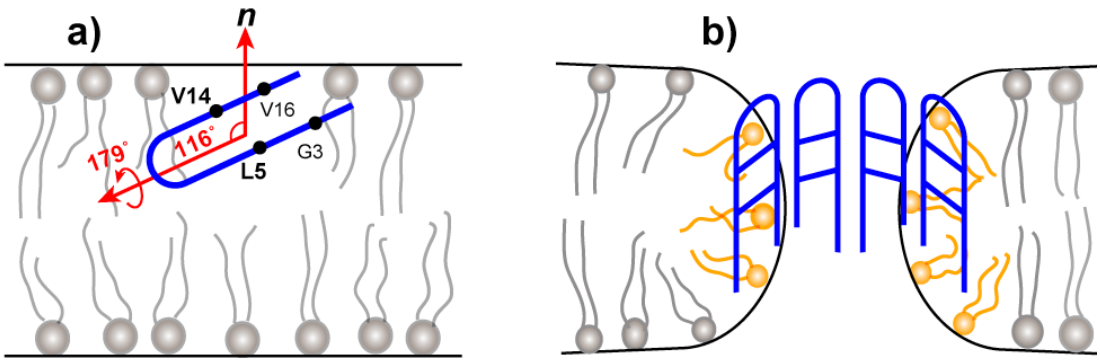

Figure 8.6. Topological structure of a) Arg^{mm}-PG-1 and b) PG-1 in anionic lipid membranes.

Experimental section

Arg^{mm}-PG-1 is synthesized by Fmoc chemistry and purified to >95%. The peptides were reconstituted into lipid vesicles at P/L (mole) = 1:15. All NMR data were obtained at 9.4 Tesla using a triple-resonance 4 mm MAS probe and a static probe. ^{13}C-^{31}P REDOR experiments were conducted at 225 K under 4.5 kHz MAS. 2D LG-CP and DIPSHIFT experiments were used to measure C-H dipolar couplings and the ROCSA experiment was used to measure the ^{13}C CSA. Further details of orientation simulations are given in the supporting information.

References

[1] M. Zasloff, *Nature* **2002**, *415*, 389.

[2] R. Fischer, M. Fotin-Mleczek, H. Hufnagel, R. Brock, *Chembiochem.* **2005**, *6*, 2126.

[3] Y. Jiang, V. Ruta, J. Chen, A. Lee, R. MacKinnon, *Nature* **2003**, *423*, 42.

[4] T. Hessa, H. Kim, K. Bihlmaier, C. Lundin, J. Boekel, H. Andersson, I. Nilsson, S. H. White, G. von Heijne, *Nature* **2005**, *433*, 377.

[5] J. A. Freites, D. J. Tobias, G. von Heijne, S. H. White, *Proc. Natl. Acad. Sci. U.S.A.* **2005**, *102*, 15059.

[6] H. D. Herce, A. E. Garcia, *Proc. Natl. Acad. Sci. U.S.A.* **2007**, *104*, 20805.

[7] M. Tang, A. J. Waring, M. Hong, *J. Am. Chem. Soc.* **2007**, *129*, 11438.

[8] K. Matsuzaki, O. Murase, N. Fujii, K. Miyajima, *Biochemistry* **1996**, *35*, 11361.

[9] K. A. Schug, W. Lindner, *Chem. Rev.* **2005**, *105*, 67.

[10] J. B. Rothbard, T. C. Jessop, R. S. Lewis, B. A. Murray, P. A. Wender, *J. Am. Chem. Soc.* **2004**, *126*, 9506.

[11] D. Huster, X. L. Yao, M. Hong, *J. Am. Chem. Soc.* **2002**, *124*, 874.

[12] B. J. vanRossum, C. P. deGroot, V. Ladizhansky, S. Vega, H. J. M. deGroot, *J. Am. Chem. Soc.* **2000**, *122*, 3465.

[13] J. J. Buffy, A. J. Waring, R. I. Lehrer, M. Hong, *Biochemistry* **2003**, *42*, 13725.

[14] R. Mani, S. D. Cady, M. Tang, A. J. Waring, R. I. Lehrer, M. Hong, *Proc. Natl. Acad. Sci. U.S.A.* **2006**, *103*, 16242.

[15] M. Hong, T. Doherty, *Chem. Phys. Lett.* **2006**, *432*, 296.

[16] S. D. Cady, C. Goodman, C.Tatko, W. F. DeGrado, M. Hong, *J. Am. Chem. Soc.* **2007**, *129*, 5719.

[17] M. Tang, A. J. Waring, R. I. Lehrer, M. Hong, *Biophys. J.* **2006**, *90*, 3616.

[18] T. Doherty, A. J. Waring, M. Hong, *Biochemistry* **2008**, *47*, 1105.

Supporting Information

Effects of Guanidinium-Phosphate Hydrogen Bonding on the Membrane-Bound Structure and Activity of an Arginine-Rich Membrane Peptide from Solid-State NMR

Ming Tang[1], Alan J. Waring[2], Robert I. Lehrer[2], and Mei Hong[1]

[1] Department of Chemistry, Iowa State University, Ames, IA 50011

[2] Department of Medicine, University of California at Los Angeles, Los Angeles, CA 90095

Antimicrobial assays

Radial diffusion assays were performed in media supplemented with 100 mM NaCl or in low salt media. Both assay media contained 10 mM sodium phosphate buffer, 1% agarose, and 0.3 mg/ml of trypticase soy broth powder to allow the organisms to grow until the underlay assay gel was covered with a nutrient-rich overlay gel that allowed surviving microbes to form colonies. The high-salt results are more predictive of activity in physiological fluids.

Table S8.1. Minimum effective concentrations (MEC) of PG-1 and Arg^{mm}-PG-1 against various bacteria at high and low salt conditions.

MEC (μg/ml)	100 mM NaCl		Low NaCl	
	PG-1	Arg^{mm}-PG-1	PG-1	Arg^{mm}-PG-1
Gram-negative bacteria				
E. coli	1.09	3.00	1.55	1.58
P. aeruginosa	1.39	3.41	1.90	1.62
K. pneumoniae	1.93	8.76	4.47	7.9
Gram-positive bacteria				
S. epidermidis	1.07	1.90	4.19	4.29
E. faecalis	1.54	3.10	4.10	3.17
B. subtilis	1.22	3.91	1.79	3.58
S. aureus	1.66	10.4	5.10	9.35
mean (n=7)	**1.41**	**4.92**	**3.30**	**4.50**

The mean activities of PG-1 and Arg^{mm}-PG-1 in 100 mM NaCl differ significantly ($p<0.001$ by the Mann-Whitney Rank Sum test).

Table 8.1 shows that higher salt concentration increases the activity of PG-1, but does not affect the activity of Arg^{mm}-PG-1. We hypothesize that higher salt concentration promotes PG-1 aggregation, which is essential for its toroidal-pore mechanism of action [2]. In our previous study of the structure of PG-1 fibrils outside the lipid membrane,[1] high salt concentration was used to promote fibril formation. The fact that salt level does not affect the activity of Arg^{mm}-PG-1 suggests that the mutant adopts a different mechanism of action that does not require peptide aggregation. This is consistent with the large-amplitude dynamics observed for the mutant.

Motionally averaged dipolar couplings and chemical shift anisotropies

C-H dipolar couplings of Arg^{mm}-PG-1 were measured using the 2D LG-CP experiment [3] for the POPC/POPG sample and the DIPSHIFT experiment [4] for the POPE/POPG sample. The LG-CP experiment was conducted under 10 kHz spinning at 295 K. The DIPSHIFT experiment was performed under 3.5 kHz MAS at 303 K, the higher temperature due to the higher phase transition temperature of the POPE/POPG membrane. The MREV-8 sequence was used for ^{1}H homonuclear decoupling. The scaling factors for the LG-CP sequence and the MREV-8 sequence are 0.57 and 0.47, respectively.

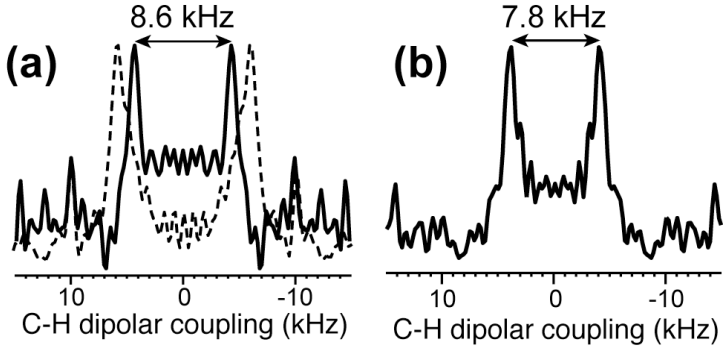

Fig. S8.1. ^{13}C-^{1}H LG-CP cross sections of Arg^{mm}-PG-1 in the POPC/POPG membrane at 295 K. (a) L5 Cα. (b) V14 Cα. Dashed line in (a) indicates the rigid-limit coupling of 12.5 kHz, measured at 233 K. The experimental uncertainty is ±0.2 kHz.

In addition to C-H dipolar couplings, we measured the Cα chemical shift anisotropy (CSA) of L5 and V14 using the ROCSA experiment [5] to assess if the backbone motion is uniaxial. The experiment was carried out at 303 K on the POPE/POPG membrane samples under 6 kHz MAS. Fig. S8.2 shows the ROCSA spectra and the relevant peptide and lipid cross sections. The lipid cross sections (Fig. S8.2c) give a control of the expected uniaxial lineshapes due to the known uniaxial rotation of lipids around the bilayer normal. It can be seen that the peptide L5 and V14 Cα sites also have uniaxial lineshapes (Fig. S8.2b), with motionally narrowed anisotropy parameter $\bar{\delta}$ of 17 ppm for L5 and 11 ppm for V14. The rigid-limit anisotropy parameter δ for β-sheet Val is known from previous experimental studies to be 25 ppm [6], while the rigid-limit δ for the β-sheet conformation of Leu has been obtained from *ab initio* calculations to be 19.5 ppm [7]. Thus, the CSA order parameter $S_{CSA} = \bar{\delta}/\delta$ is 0.89 for L5 and 0.44 for V14. These values are consistent with the C-H order parameters measured for these two sites in the POPE/POPG membrane. Most importantly, the uniaxial CSA lineshapes confirm the presence of uniaxial rotation of the Arg^{mm}-PG-1 backbone around the membrane normal.

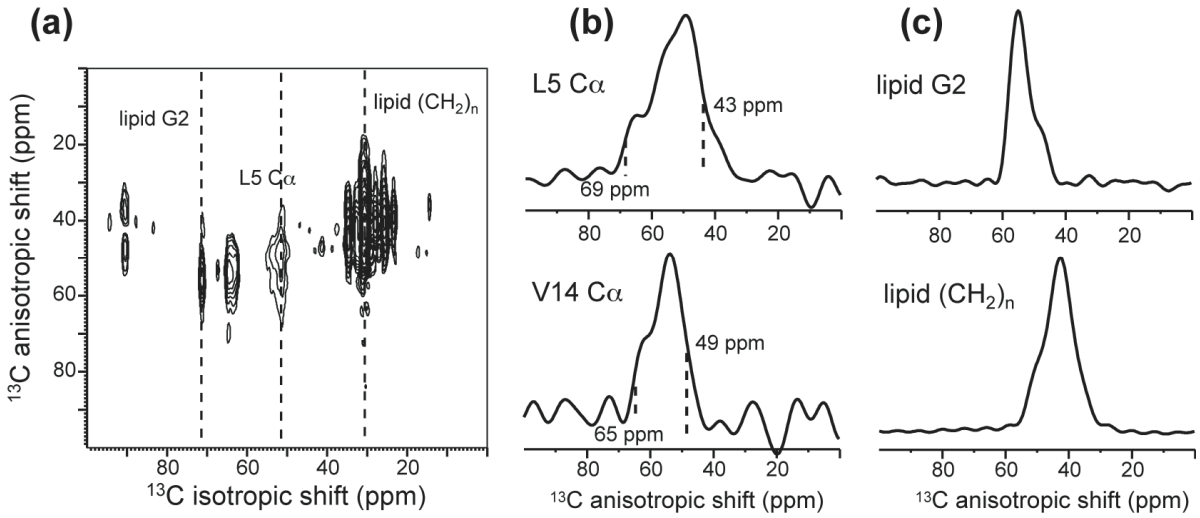

Fig. S8.2. ^{13}Cα CSA of Arg^{mm}-PG-1. (a) 2D ROCSA spectra of Arg^{mm}-PG-1 in POPE/POPG membranes at 303 K. (b) 1D cross sections of the peptide L5 and V14 Cα sites. (c) 1D cross sections of two lipid peaks, glycerol G2 and acyl chain $(CH_2)_n$. The lipid lineshapes are uniaxial as expected. The peptide lineshapes are similarly uniaxial, indicating uniaxial rotation around the membrane normal.

Orientation calculations

The ideal antiparallel β-hairpin structure was constructed using (ϕ, ψ) torsion angles of (-137˚, +135˚) for the strand residues, and (-45˚, +85˚) and (+155˚, -20˚) for the *i*+1 and *i*+2 residues of the β-turn [8]. The turn torsion angles were modified from the classical β-turn conformations to make the two strands approximately parallel. The strand axis was chosen to be the average orientation of six consecutive C'-N bonds from residue 4 to residue 9. The tilt angle τ is the angle between this strand axis and the bilayer normal. The ρ angle was defined as the angle between the C=O bond of residue 6 and the common plane of the strand axis and the bilayer normal. The peptide was rotated through all combinations of (τ, ρ) angles and the C-H dipolar couplings of the N-strand residues 4 - 8 and C-strand residues 13 - 17 were calculated and converted to the order parameter according to $S_{CH} = \omega(\tau,\rho)/\omega_{rigid}$.

Fig. S8.3 shows a more extended set of S_{CH} values for (τ, ρ) angles in the range (10-90˚, 0˚-180˚), which complements the simulations in Fig. 5. The best fit (τ, ρ) in this range for the POPC/POPG bound Arg^{mm}-PG-1 is (64˚, 359˚), and is related to the global best fit (116˚, 179˚) by symmetry.

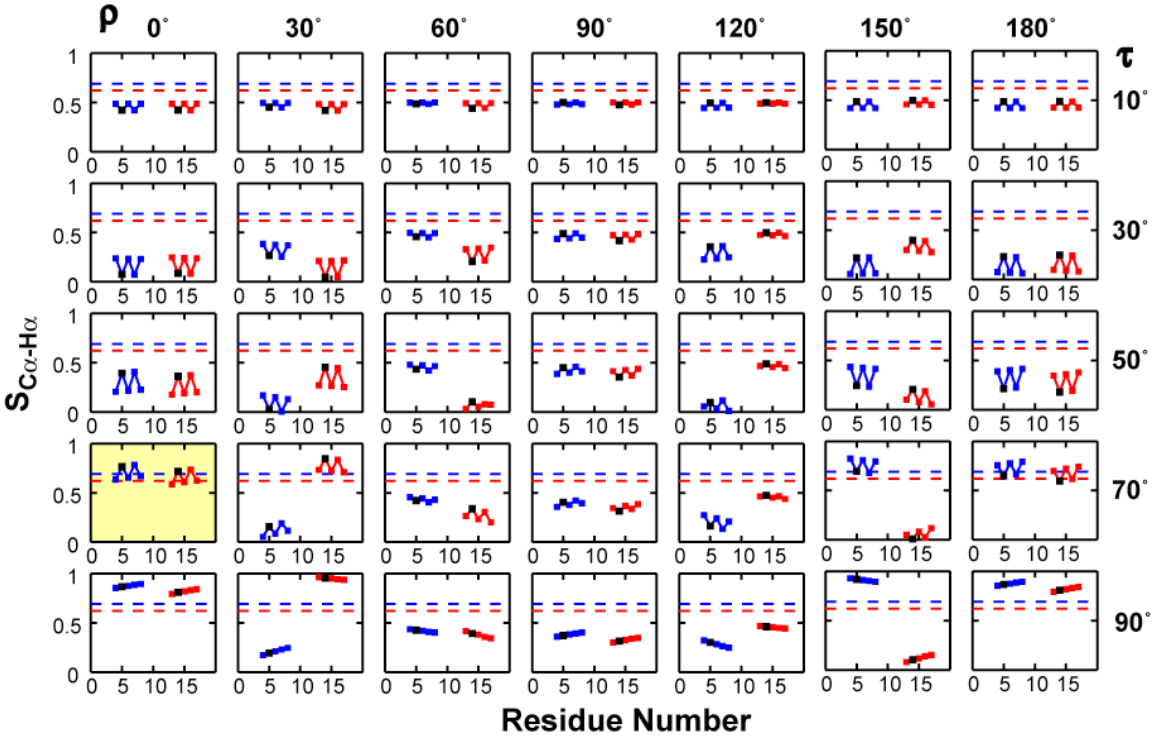

Fig. S8.3. S_{CH} of an ideal β-hairpin as a function of (τ, ρ). The N- and C-strand S_{CH}'s are plotted as blue and red squares, respectively, with the L5 and V14 values in black. The experimental S_{CH}'s for L5 and V14 in the POPC/POPG membrane are drawn as blue and red dashed lines. The yellow highlighted panel indicates the approximate position of one of the four best-fit orientations.

Fig. S8.4 shows the RMSD between the calculated S_{CH} and the experimental S_{CH}'s of L5 and V14 in the POPC/POPG membrane. The RMSD is calculated as

$$\mathrm{RMSD} = \sqrt{\left(S_{CH,calc}^{L5} - S_{CH,expt}^{L5}\right)^2 + \left(S_{CH,calc}^{V14} - S_{CH,expt}^{V14}\right)^2}.$$

From the RMSD, four symmetry-related best-fit orientations are identified and listed in Table S8.2. Taking into account the ^{13}C-^{31}P distance constraints, the global best-fit (τ, ρ) angles are orientation A, (116°, 179°).

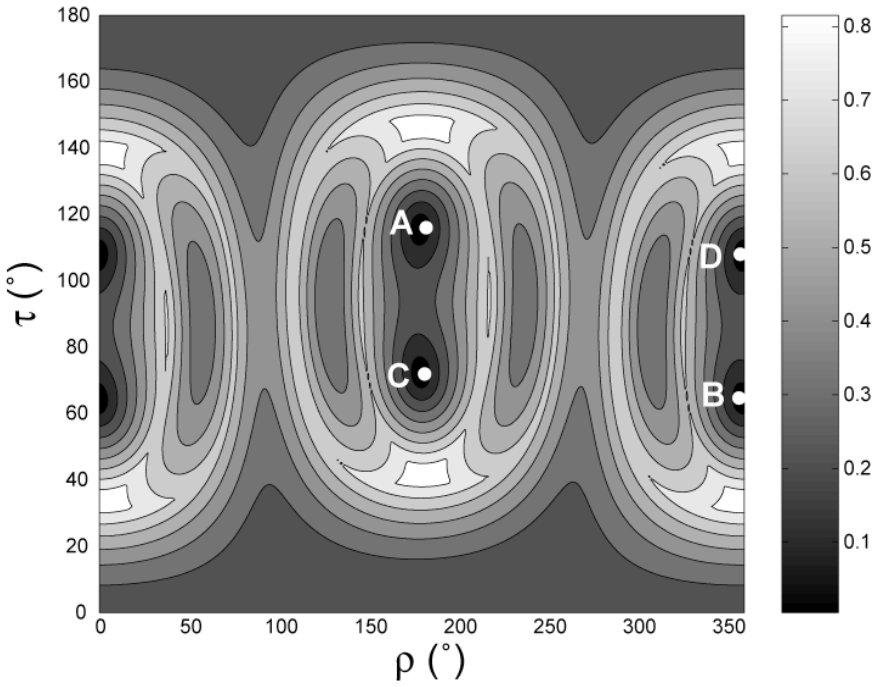

Fig. S8.4. RMSD between the calculated and experimental Cα-Hα order parameters of Arg^{mm}-PG-1 in the POPC/POPG membrane as a function of (τ, ρ). The four lowest RMSD positions are related by symmetry and are indicated as A, B, C, D.

To obtain the peptide orientation in the POPE/POPG membrane, we carried out the same S_{CH} calculation but compared these with the POPE/POPG experimental data. Fig. S8.5a shows S_{CH} for (τ, ρ) of (50-130˚, 160˚-340˚). The ideal β-hairpin structure is used in the calculation. Again, four symmetry-related best-fit orientations are found according to the RMSD analysis (Fig. S8.5b). The orientation (τ, ρ) = (113˚, 164˚) is chosen as the global best fit because it agrees best with the ^{13}C-^{31}P distance data. This orientation is quite similar to that found in POPC/POPG membranes, as shown by the schematic representation in Fig. S8.5c, indicating that the composition change from POPC to POPE lipids does not affect the Arg^{mm}-PG-1 orientation significantly.

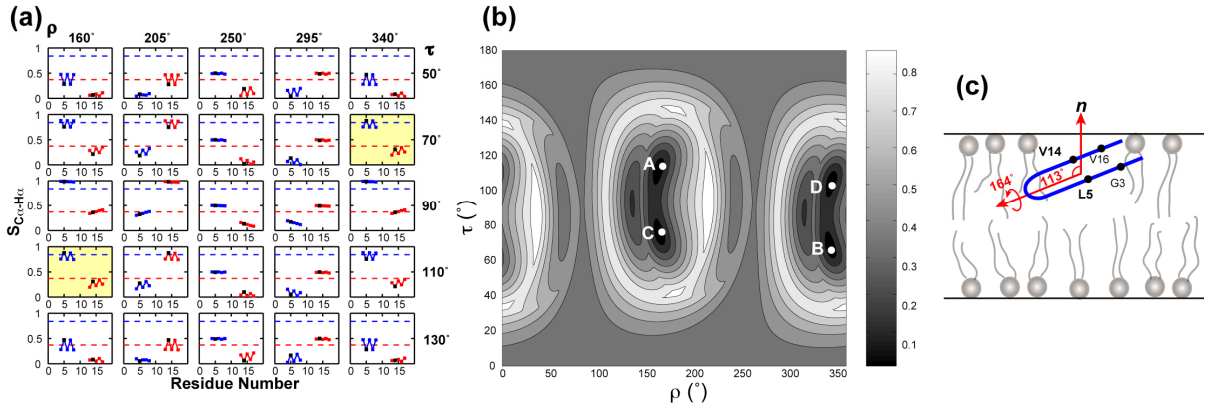

Fig. S8.5. Orientation of Arg^{mm}-PG-1 in the POPE/POPG membrane. (a) S_{CH} of an ideal β-hairpin for various (τ, ρ) angles. The N- and C-strand S_{CH}'s are plotted as blue and red squares, respectively, with L5 and V14 values in black. The experimental Cα S_{CH}'s for L5 and V14 in the POPE/POPG membrane are drawn as blue and red dashed lines, respectively. Some of the approximate best-fit orientations are highlighted in yellow to indicate the agreement with the experimental data. (b) RMSD between the calculated and experimental Cα-Hα order parameters of Arg^{mm}-PG-1 in the POPE/POPG membrane as a function of (τ, ρ). (c) Topological structure of Arg^{mm}-PG-1 in the POPE/POPG membrane.

To assess if the structure used in the S_{CH} calculation affects the orientation result significantly, we also calculated S_{CH} using the solution NMR structure of PG-1 (PDB: 1PG1) [9]. In the 20 energy-minimized structures, the backbone conformations of the β-strand residues 5-9 and 12-17 have relatively small variations. We chose the representative structure #10 as the input for the orientation calculation. Fig. S8.6 shows that the best-fit τ angles fall in the same range as the ideal hairpin simulations, close to 90˚, thus the conclusion that the strand axis is roughly parallel to the membrane plane is unchanged. However, for the POPC/POPG membrane, even the best-fit (τ, ρ) angles of (100˚, 152˚) does not agree with the experimental data very well (Fig. S8.6a), suggesting that the solution structure of PG-1 may deviate non-negligibly from the membrane-bound peptide structure. Nevertheless, the best-fit (τ, ρ) range of (60˚-90˚, 150˚-180˚) is in general good agreement with the ideal hairpin simulations (Table S8.2). In conclusion, Arg^{mm}-PG-1 has the strand axis perpendicular to the membrane normal and has the hairpin plane roughly parallel to the membrane normal, regardless of the input structure.

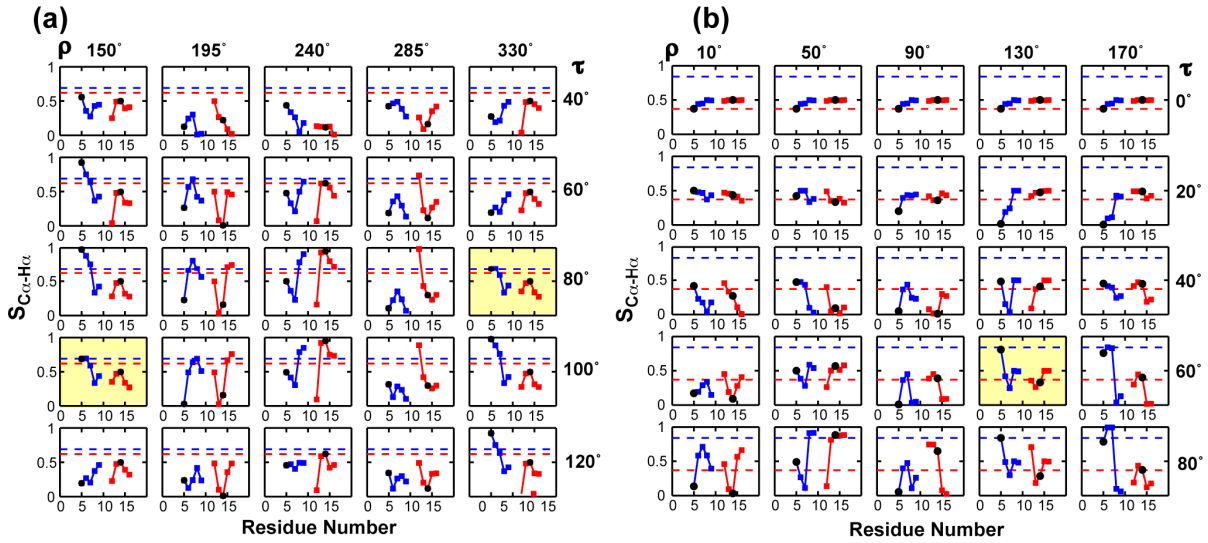

Fig. S8.6. Calculated S_{CH}'s using the PG-1 solution structure #10. Values of residues 5-9 and 12-17 are shown in blue and red squares, respectively, with the L5 and V14 S_{CH}'s in black. The experimental S_{CH}'s for L5 and V14 are drawn as blue and red dashed lines, respectively. (a) Experimental data is that of the POPC/POPG membrane. (b) Experimental data is that of the POPE/POPG membrane. The approximate best-fit orientations are highlighted in yellow to indicate the agreement with the experimental data.

The somewhat different quality of fit between the PG-1 solution NMR structure and the ideal β-hairpin structure can be explained by the distorted backbone conformation of the PG-1 solution structure, shown in Fig. S8.7. The Cα-Hα vectors are along the same direction in the ideal β-hairpin, but point to a range of directions in the solution NMR structure #10.

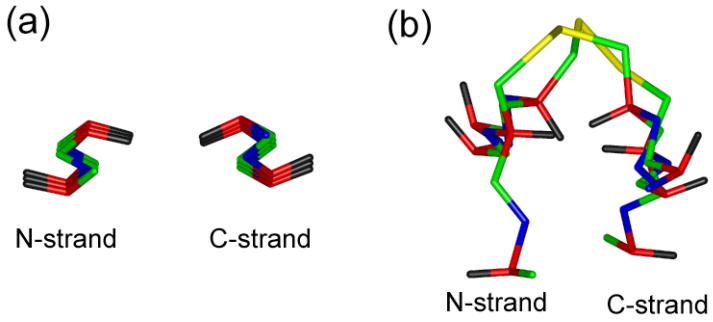

Fig. S8.7. Comparison of the structures of (a) the ideal β-hairpin and (b) PG-1 solution NMR structure #10 (PDB: 1PG1). Cα and Hα atoms are highlighted in red and black, respectively. The β-strand axis is perpendicular to the view plane. Residues 5-9 and 12-17 are shown in sticks.

Table S8.2 summarizes the best-fit orientations of Arg^{mm}-PG-1 in POPC/POPG and POPE/POPG membranes from simulations using the ideal β-hairpin structure and the solution NMR structure #10. The global best-fit angles in each case after taking into account the ^{13}C-^{31}P distance constraints is listed in column A. All global best-fit orientations fall into a relatively narrow range of (τ, ρ) = (85-120˚, 130-180˚), indicating that Arg^{mm}-PG-1 strand axis is perpendicular to the bilayer normal. This is distinctively different from the transmembrane orientation of PG-1 [2].

Table S8.2. Best-fit (τ, ρ) angles for Arg^{mm}-PG-1 in POPC/POPG and POPE/POPG membranes. Solution A is the global best-fit based on agreement with the ^{13}C-^{31}P distance constraints.

Structure	Membrane	**A**	B	C	D	Error
Ideal hairpin	POPC/POPG	**(116˚, 179˚)**	(64˚, 359˚)	(72˚, 179˚)	(108˚, 359˚)	± 3˚
Ideal hairpin	POPE/POPG	**(113˚, 164˚)**	(67˚, 344˚)	(76˚, 164˚)	(104˚, 344˚)	± 3˚
PG-1 #10	POPC/POPG	**(100˚, 152˚)**	(80˚, 332˚)	(46˚, 153˚)	(134˚, 333˚)	—
PG-1 #10	POPE/POPG	**(89˚, 137˚)**	(91˚, 317˚)	(60˚, 133˚)	(120˚, 313˚)	± 6˚

^{1}H spin diffusion

2D ^{31}P-detected ^{1}H spin-diffusion experiments were conducted at 303 K under 5 kHz MAS. After ^{1}H evolution, a mixing time (t_m) of 64 – 400 ms was applied to transfer ^{1}H polarization from the mobile lipids and water to the final destination of lipid headgroup ^{31}P for detection. In the absence of transmembrane proteins, the lipid chain CH_2 to ^{31}P cross peak is very slow to develop due to the extremely weak dipolar coupling. The presence of transmembrane peptides significantly facilitates the spin diffusion via the pathway CH_2 –> peptide –> ^{31}P. To ensure that only the mobile lipid and water polarization served as the source of spin diffusion, we suppressed the rigid peptide polarization by a ^{1}H T_2 relaxation filter of 0.8 ms before ^{1}H chemical-shift evolution and spin diffusion.

^{13}C-^{31}P distance measurement

^{13}C-^{31}P distances were measured using the rotational-echo double resonance (REDOR) experiment. Composite 90°180°90° pulses were applied on the ^{31}P channel to reduce the

effect of flip angle errors and enhance the distance accuracy. At each REDOR mixing time (t_m), a control experiment (S_0) with the ^{31}P pulses off and a dephasing experiment (S) with the ^{31}P pulses on were carried out. The normalized dephasing, S/S_0, as a function of t_m gives the ^{13}C-^{31}P dipolar coupling. The ^{13}CO dephasing was corrected for the lipid natural-abundance CO contribution. The experiments were conducted under 4.5 kHz MAS at 225 K. ^{31}P 180° pulse lengths of 9 μs were used to achieve complete inversion of the broad ^{31}P resonance.

References

[1] M. Tang, A. J. Waring, M. Hong, *J. Am. Chem. Soc.* **2005**, *127*, 13919.

[2] R. Mani, S. D. Cady, M. Tang, A. J. Waring, R. I. Lehrer, M. Hong, *Proc. Natl. Acad. Sci. U.S.A.* **2006**, *103*, 16242.

[3] B. J. vanRossum, C. P. deGroot, V. Ladizhansky, S. Vega, H. J. M. deGroot, *J. Am. Chem. Soc.* **2000**, *122*, 3465.

[4] M. Munowitz, W. P. Aue, R. G. Griffin, *J. Chem. Phys.* **1982**, *77*, 1686.

[5] J. C. C. Chan, R. Tycko, *J. Chem. Phys.* **2003**, *118*, 8378.

[6] X. L. Yao, M. Hong, *J. Am. Chem. Soc.* **2002**, *124*, 2730.

[7] H. Sun, L. K. Sanders, E. Oldfield, *J. Am. Chem. Soc.* **2002**, *124*, 5486.

[8] M. Tang, A. J. Waring, R. I. Lehrer, M. Hong, *Biophys. J.* **2006**, *90*, 3616.

[9] R. L. Fahrner, T. Dieckmann, S. S. Harwig, R. I. Lehrer, D. Eisenberg, J. Feigon, *Chem. & Biol.* **1996**, *3*, 543.

Appendix A

Input code for multispin simulation using SIMPSON:

```
spinsys {
  channels 13C 31P
  nuclei   13C 31P 31P 31P 31P
  dipole   1 2 -12.24 0 45 0

  dipole   1 3 -12.24 0 45 90

  dipole   1 4 -12.24 0 45 180
  dipole   1 5 -12.24 0 45 270
}

par {
  proton_frequency 400e6
  spin_rate        1000
  sw               spin_rate/2.0
  np               13
  crystal_file     rep168
  gamma_angles     18
  start_operator   I1x
  detect_operator  I1p
  verbose          1101
  variable rf      150000
  use_cluster      0
}

proc pulseq {} {
  global par

  maxdt 1.0

  set t180 [expr 0.5e6/$par(rf)]
  set tr2 [expr
0.5e6/$par(spin_rate)]

  reset
  delay $tr2
  pulseid $t180 0 x $par(rf) x
  delay $tr2
  pulseid $t180 0 x $par(rf) y
  store 1

  reset
  acq
  delay $tr2
  pulseid $t180 0 x $par(rf) x
  delay $tr2
  pulseid $t180 $par(rf) x 0 x
  prop 1
  store 2
  acq

  for {set i 2} {$i < $par(np)}
{incr i} {
    reset
    prop 1
    prop 2
    prop 1
    store 2
    acq
  }
}

proc main {} {
  global par

  set f [fsimpson]
  fsave $f $par(name).fid -xreim
#  fzerofill $f 8192
#  faddlb $f 100 0
#  fft  $f
#  fsave $f $par(name).spe -binary
}
```

Appendix B

Input codes for DIPSHIFT simulation:

For X-H tensors:

```
120 180 60                  mintorsion, maxtorsion,ktorsionstep
60                          nalpha
60                          nbeta
60                          ngamma
15                          ntd
3.5                         omigar (NOT angular frequency)
1                           idipcsyn -- both(2)/cs(1)/dip(0)
0                           idqyn -- dq factor yes(1)/no(0)
-w/2 -w/2 w                 N csa principal values
5.8                         C-H dipolar coupling, 1-bond
0.  60.  0.                 alpha,beta,gamma of N-C in NH CSA system
0.  109.5  0.               alpha and beta of N-C in C-H  system
0.                          T2 widening width kHz
```

For $X-H_2$ tensors:

```
120 180 60                  mintorsion, maxtorsion,ktorsionstep
60                          nalpha
60                          nbeta
60                          ngamma
15                          ntd
3.5                         omigar (NOT angular frequency)
1                           idipcsyn -- both(2)/cs(1)/dip(0)
0                           idqyn -- dq factor yes(1)/no(0)
-w 0 w                      N csa principal values
5.8                         C-H dipolar coupling, 1-bond
0.  60.  0.                 alpha,beta,gamma of N-C in NH CSA system
0.  109.5  0.               alpha and beta of N-C in C-H  system
0.                          T2 widening width kHz
```

Appendix C

Input code for HNCH simulation:

```
120 180 60                  mintorsion, maxtorsion,ktorsionstep
60                          nalpha
60                          nbeta
60                          ngamma
15                          ntd
4.444                       omigar (NOT angular frequency)
2                           idipcsyn -- both(2)/cs(1)/dip(0)
1                           idqyn -- dq factor yes(1)/no(0)
-2.614 -2.614 5.228         N csa principal values
10.92                       C-H dipolar coupling, 1-bond
0.  60.  0.                 alpha,beta,gamma of N-C in NH CSA system
0.  109.5  0.               alpha and beta of N-C in C-H  system
0.                          T2 widening width kHz
```

Appendix D

Program code for SLF simulation using Fortran:

```
c    program calc Pisa wheel pattern

      parameter      (nmaxx=256,nmaxy=256)
      real    redat(0:nmaxx,0:nmaxy),b0(3),aleng(100)
            real
reNH(0:nmaxx,0:nmaxy),reCSA(0:nmaxx,0:nmaxy)
            real  rePISA(0:nmaxx,0:nmaxy)
            real  vNH(100,3),uNH(100,3),uCO(100,3),
betax(3),ubetax(3)
            real
vCN(100,3),uCN(100,3),aCNleng(100),uNH2(100,3)
            real  vNC(100,3),uNC(100,3),aNCleng(100)
           real  testbetax(3),omegNH(100),omegCSA(100)
            real
uniNH(3),uniNC(3),vs11(3),vs22(3),vs33(3)
            real uniCO(3),testCO2(3),
vCO(100,3),uniCO1(3),uniCO2(3)
            real v1s11(3),v2s11(3),v1s22(3),v2s22(3)
            real uniNH1(3),uniNH2(3),aCOleng(100)
            real v1s33(3),v2s33(3),vs22intopl(3)
            real cols11(100,3),cols22(100,3),cols33(100,3)
            real
col2s11(100,3),col2s22(100,3),col2s33(100,3)
            integer num(100)
            real beB0betax,gammabetax
            integer int1, outnumt, tcount, inr,outnumr,
rcount,t,r,b,p
            character*32 outfile,outb,outp
      common redat,nx,ny,outfile
            real testperp(3), testperp2(3)

c.....................Input.....................

      write(6,*)'Calculation of 2 series of 1D spectra'
      write(6,*)'(1) CO CSA spectra'
            write(6,*)'(2) N csa spectra'
            write(6,*)'from given N-H, C=O, and CO-N
vectors'
            write(6,*)'and the resulting 2D spectrum'

            write(6,*)'delta NH coupling (kHz, ca. 10) -->'
            write(6,*)'10'
            delta=10.0

            write(6,*)'Width of NH range (kHz, ca. 20.2) -
->'
            write(6,*)'20.2'
            swNH=20.2
c           read(5,*)swNH

            write(6,*)'15N CSA:'
      write(6,*)'s11= 64, s22= 77, s33= 217 (order
matters!)'
            s11=64
            s22=77
            s33=217
c           write(6,*)'chem. shift s11,s22,s33 -->'
c      read(5,*) s11,s22,s33

      write(6,*)'ppm range of w2 axis (e.g. 300, 0) -->'
            ppmmin=300
            ppmmax=0
c      read(5,*)ppmmin,ppmmax

      write(6,*)'# of frequency points (e.g. 100) -->'
      read(5,*)nx
            nxd2=nx/2
            wNHscal=(nx-1)/swNH
            wCSAscal=(nx-1)/(ppmmax-ppmmin)


            ny0=18                        !number of NH
bonds
            ny=ny0

c.....................................................
c.............RTD structure 15.....................
c.....................................................
```

c Add molecular coordinates here!

```
c           Definition Ni-Hi=vNH(i,#)

c            Definition Ci-1Ni=vCN(i, #)

c           Definition CiOi=vCO(i, #)

c           Definition NiCi=vNC(i, #)

c-----------------------------------------------------
c calculate unit vectors
c-----------------------------------------------------

            write(6,*)'lengths of N-H vectors:'
            do j=1,ny

              aleng(j)=0.
              do i=1,3
                aleng(j)=aleng(j)+vNH(j,i)*vNH(j,i)
              enddo
              aleng(j)=sqrt(aleng(j))
            write(6,*)j,aleng(j)
              do i=1,3
```

```
              uNH(j,i)=vNH(j,i)/aleng(j)
             enddo
            enddo !j residue number


            write(6,*)'lengths of CO-N vectors:'
            do j=1,ny
             aCNleng(j)=0.
             do i=1,3
              aCNleng(j)=aCNleng(j)+vCN(j,i)*vCN(j,i)
             enddo
             aCNleng(j)=sqrt(aCNleng(j))
            write(6,*)j,aCNleng(j)
             do i=1,3
              uCN(j,i)=vCN(j,i)/aCNleng(j)
             enddo
            enddo                              !j residue
number

            write(6,*)'lengths of C=O vectors:'
            do j=1,ny
             aCOleng(j)=0.
             do i=1,3
              aCOleng(j)=aCOleng(j)+vCO(j,i)*vCO(j,i)
             enddo
             aCOleng(j)=sqrt(aCOleng(j))
            write(6,*)j,aCOleng(j)
             do i=1,3
              uCO(j,i)=vCO(j,i)/aCOleng(j)
             enddo
            enddo                              !j residue
number

            write(6,*)'lengths of N-Ca vectors:'
            do j=1,ny
             aNCleng(j)=0.
             do i=1,3
              aNCleng(j)=aNCleng(j)+vNC(j,i)*vNC(j,i)
             enddo
             aNCleng(j)=sqrt(aNCleng(j))
            write(6,*)j,aNCleng(j)
             do i=1,3
              uNC(j,i)=vNC(j,i)/aNCleng(j)
             enddo
            enddo !j residue number

c-------------------------------------------------------
c determine principal axes of 15N CSAs
c-------------------------------------------------------

            ochiNHs33=-17
            write(6,*)'angle of N-H & s33 (e.g. -17) -->'
            write(6,*)'-17'
c           read(5,*)ochiNHs33

            alphoutofplane=25
            write(6,*)'out-of-plane angle of s22 (e.g. 25)'
     write(6,*)'25'
c           read(5,*)alphoutofplane

            do j=1,ny

             do i=1,3
              uniNH(i)=uNH(j,i)
              uniNC(i)=uNC(j,i)
             enddo

            chiNHs33=ochiNHs33

c for geometry see Hong et al., JMR 135, p. 169, Fig. 2
c cross product of N-Ca and N-H yields s22(into-plane)
axis
             call crossprodU(uniNH,uniNC,vs22intopl)

c rotate N-H around s22(into-plane) axis to give s33 axis
            call rotaxis(vs22intopl,chiNHs33,uniNH,vs33)

c rotate s22(into-plane) around s33 axis to give s22 axis
(tilted)
             call
rotaxis(vs33,alphoutofplane,vs22intopl,vs22)

c cross product of s22 and s33 gives s11
             call crossprodU(vs22,vs33,vs11)

            do i=1,3
             cols11(j,i)=vs11(i)
             cols22(j,i)=vs22(i)
             cols33(j,i)=vs33(i)
            enddo

            enddo                              !j residue
number

            goto 20  !skip CO calculation (needs to be
renamed, otherwise functional)

c-------------------------------------------------------
c determine principal axes of 13CO CSAs
c-------------------------------------------------------

c           ochiCOs22=0
c           write(6,*)'angle of C-O bond & s22 (e.g. 10) --
>'
c           read(5,*)ochiCOs22
c
c           do j=1,ny
c
c            do i=1,3
c             uniCO(i)=uCO(j,i)
c             uniCN(i)=uCN(j,i)
c            enddo
c
c           if(j.eq.1) then                    !1st
residue has only Calpha
c            chiCOs22=-ochiCOs22
c           else
c            chiCOs22=ochiCOs22
c           endif
```

```
c for geometry see Hartzell et al, JACS, 1987, 109, 5968,
Fig2.
c cross product of C-N and C-O yields s33 (out-of-plane)
axis

c               call crossprodU(uniCN,uniCO,vCs33)

c rotate C=O bond (in the plane) around s33 axis to give
s22 axis

c               call rotaxis(vCs33,chiCOs22,uniCO,vCs22)

c cross product of s22 and s33 gives s11

c               call crossprodU(vCs22,vs33,vCs11)

c             do i=1,3
c               cols11(j,i)=vCs11(i)
c               cols22(j,i)=vCs22(i)
c               cols33(j,i)=vCs33(i)
c             enddo

c             enddo                                 !j residue
number

c end of skipped CO section
c-----------------------------------------------------
c determine the orientation of the b-strand axis
c-----------------------------------------------------

20      write(6,*)'define b-strand axis and antiparallel b-
sheet plane'
        write(6,*)'starting residue for b-sheet axis (e.g.13)--
>'
              write(6,*)'start from #2-7 residue'
              nstart=2
c             read(5,*) nstart

              betax(1)=0.
              betax(2)=0.
              betax(3)=0.
              betaxlen=0.

              do j=nstart,nstart+5

                do i=1,3
                 betax(i)=betax(i)+vCN(j,i)
                enddo

              enddo


              do i=1,3
                betaxlen=betaxlen+betax(i)*betax(i)
              enddo
              betaxlen=sqrt(betaxlen)
              do i=1,3
                ubetax(i)=betax(i)/betaxlen
              enddo
              write(6,*)ubetax(1),ubetax(2),ubetax(3)
              write(6,*)betaxlen

              thebetax=acosd(ubetax(3))
              if(sind(thebetax).ne.0) then
                sinphi=ubetax(2)/sind(thebetax)
                cosphi=ubetax(1)/sind(thebetax)
                if(sinphi.gt.0) then
                  phibetax=acosd(cosphi)
                else
                  phibetax=360.-acosd(cosphi)
                endif
              else
                phibetax=0.
              endif
              write(6,*)'b-strand axis (theta,phi)=
',thebetax,phibetax

c-----------------------------------------------------
c restrict to the labeled residues of interest
c-----------------------------------------------------

c             k=1
              write(6,*)'15N-labeled residue numbers (end: -
1, all:-99)-->'
              write(6,*)'18, -1'
c             write(6,*)'1,2,6,8,11,15,17'

c             num(1)=1
c             num(2)=2
c             num(3)=6
c             num(4)=8
c             num(5)=11
c             num(6)=15
c             num(7)=17
c 50          read(5,*)num(k)
c             if(num(k).gt.0) then
c               k=k+1
c               goto 50
c             endif

c             if(num(k).eq.-99) then
               do k=1,ny
                num(k)=k
               enddo
               numresi=ny
c              goto 2001  !jump out
c             endif

c             numresi=k-1
c             numresi=7
c now renumber residues 1..numresi

              do k=1,numresi
                do i=1,3
                  uNH(k,i)=uNH(num(k),i)
                  cols11(k,i)=cols11(num(k),i)
                  cols22(k,i)=cols22(num(k),i)
                  cols33(k,i)=cols33(num(k),i)
                enddo
              enddo
```

```
            write(6,*)'Number of residues = ',numresi

c           define start of rotation angle
2001        write(6,*)'define betaplane using which CO
vector?'
            read(5,*) pstart

c           auto ouput many results
            write(6,*)'angle range and incre between B0
and b-strand axis -->'
            read(5,*)beB0betax0, beB0betax1, int1
            write(6,*)'rotation angle range and incre along
b-strand axis -->'
            read(5,*) gammabetax0, gammabetax1, inr

c           cal cycle
            outnumt=(beB0betax1-beB0betax0)/int1+1
            tcount=0
100         beB0betax=beB0betax0+tcount*int1
            b0(1)=0
            b0(2)=sind(beB0betax)                    !B0 in
the y-z plane, same as sheet plane
            b0(3)=cosd(beB0betax)
            tcount=tcount+1
            outnumr=(gammabetax1-gammabetax0)/inr+1
            rcount=0
200         gammabetax=gammabetax0+rcount*inr

c           remove r is r-1 problem
            r=gammabetax

c           write(6,*)'rotation angle around b-strand axis -
->'
c           read(5,*) gammabetax

c-------------------------------------------------------
c now transform to make the b-strand axis the z axis
c-------------------------------------------------------
            gammabet0=0
      call rotvect(phibetax,thebetax,0,
     &            ubetax,testbetax)
      write(6,*)'b-strand axis, should be 0 0 1:'
      write(6,*)testbetax(1),testbetax(2),testbetax(3)
      write(6,*)

c calculate plane of sheet to determine gammabetax
(angle betw)

      do i=1,3
            uniCO1(i)=uCO(pstart,i)
      enddo

            gammabetold=0

      call rotvect(phibetax,thebetax,0,
     &            uniCO1,uniCO2)
      gammabetold=acosd(uniCO2(2))    !uniCO2(2) is
the dot product between
c           uniCO2 and the y-axis (0 1 0).

            call crossprodU(uniCO2,testbetax,testperp)

            gammabet0=acosd(testperp(1))
            !testperp(1) is the dot product between
c           testperp and the x-axis (1 0 0).

            if(testperp(2).lt.0) then
        gammabet0=-gammabet0
      endif

      call rotvect(0,0,gammabet0,
     &            testperp,testperp2)
        write(6,*)'b-sheet plane, new CO axis, should be 1 0
0:'
       write(6,*)testperp2(1),testperp2(2),testperp2(3)
c         write(6,*)

            gammabetax=gammabetax+gammabet0


c-------------------------------------------------------
c now calculate frequencies
c-------------------------------------------------------

c apply rotation to all selected residues


            do j=1,numresi

              do i=1,3
                uniNH1(i)=uNH(j,i)
                v1s11(i)=cols11(j,i)
                v1s22(i)=cols22(j,i)
                v1s33(i)=cols33(j,i)
              enddo

      call rotvect(phibetax,thebetax,gammabetax,
     &            uniNH1,uniNH2)

       call rotvect(phibetax,thebetax,gammabetax,
     &            v1s11,v2s11)
        call rotvect(phibetax,thebetax,gammabetax,
     &            v1s22,v2s22)
        call rotvect(phibetax,thebetax,gammabetax,
     &            v1s33,v2s33)
              do i=1,3
                uNH2(j,i)=uniNH2(i)         !N-H bond of
residue j in new frame
                col2s11(j,i)=v2s11(i)       !s11 axis of
residue j in new frame
                col2s22(j,i)=v2s22(i)       !s22 axis of
residue j in new frame
                col2s33(j,i)=v2s33(i)       !s33 axis of
residue j in new frame
c             write(6,*)'col2s11',col2s11(j,i)
              enddo
```

```
            enddo      !j residue number

            do j=1,numresi
            do iw=1,nx
              reNH(iw,j)=0.
              reCSA(iw,j)=0.
            enddo
            enddo

            do jw=1,nx
            do iw=1,nx
              rePISA(iw,jw)=0.
              redat(iw,jw)=0.
            enddo
            enddo

            do j=1,numresi

c cos(theta)=B0*NH dot product
             costheta=0.
             cosgam1=0.          !direction cosine
             cosgam2=0.
             cosgam3=0.
             do i=1,3
              costheta=costheta+b0(i)*uNH2(j,i)
              cosgam1=cosgam1+b0(i)*col2s11(j,i)
            !direction cosine
              cosgam2=cosgam2+b0(i)*col2s22(j,i)
              cosgam3=cosgam3+b0(i)*col2s33(j,i)
            enddo

c calculate frequencies

             wNH=0.5*delta*(3*costheta**2-1)

wCSA=s11*cosgam1**2+s22*cosgam2**2+s33*cosga
m3**2
             omegNH(j)=wNH
             omegCSA(j)=wCSA
             iwNHp=nx/2+wNH*wNHscal
             iwNHm=nx/2-wNH*wNHscal
            !2nd transition
       iwCSA=(ppmmax-wCSA)*wCSAscal+1

             write(6,*)'residue number: ', num(j)
             write(6,*)'NH dipolar coupl., kHz & pts:
',wNH,iwNHp,iwNHm
             write(6,*)'N chemical shift, ppm & pts: ',
wCSA, iwCSA

c save PISA wheel

             redat(j,1)=abs(wNH)
             redat(j,2)=wCSA

c put unit intensity into spectrum at the frequencies

             reNH(iwNHp,j)=reNH(iwNHp,j)+1.    !slice j
is spectrum of NH bond j
             reNH(iwNHm,j)=reNH(iwNHm,j)+1.  !slice j
is spectrum of NH bond j

             reCSA(iwCSA,j)=reCSA(iwCSA,j)+1.


rePISA(iwNHp,iwCSA)=rePISA(iwNHp,iwCSA)+1.  !2
D corr. spectrum

rePISA(iwNHm,iwCSA)=rePISA(iwNHm,iwCSA)+1.  !
2D corr. spectrum

            enddo  ! j residue number

       write(6,*)'write 2D NH/CSA (PISA wheel) to the
disk'
            write(6,*)'read with read2dbin (100) in
Matlab'

             WRITE(6,*) 'Name of output file -->'

             b=int(beB0betax)
             p=r
c            p=int(gammabetax-gammabet0)

             WRITE(6,*) 'Name of output file -->'
             if (b .lt. 100) then
               outb=char(int(b/10)+48)//char(b-
int(b/10)*10+48)
             else
               outb=char(int(b/100)+48)//char(int((b-
int(b/100)*100)/10)+48)
    &        //char(b-int(b/10)*10+48)
             endif
             if (p .lt. 100) then
               outp=char(int(p/10)+48)//char(p-
int(p/10)*10+48)
             else
               outp=char(int(p/100)+48)//char(int((p-
int(p/100)*100)/10)+48)
    &        //char(p-int(p/10)*10+48)
             endif
             outfile='t'//trim(outb)//'r'//trim(outp)

             write(6,*)outfile
435          format(a32)
       open(unit=12,file=outfile,form='unformatted')
       write(12) ((redat(i,j),i=1,numresi),j=1,2)
       close(12)
c            ny=ny0

             rcount=rcount+1
             if (rcount.lt.outnumr) goto 200
             if (tcount.lt.outnumt) goto 100

             write(6,*)'re-run b-strand orientation (0//1) -->'
             read(5,*)irerun
             if(irerun.eq.1) goto 2001
```

```
            write(6,*)'re-run b-strand orientation (0//1) -->'
            read(5,*)irerun
            if(irerun.eq.1) goto 2001
c
      stop
      end
```

```
c ****************** end main program
****************************
```

c Add subroutines and functions here!